# Effects of Mechanical Forces on the Biological Properties of Porcine Aortic Valve Leaflets

A Thesis
Presented to
The Academic Faculty

by

**Yun Xing**

In Partial Fulfillment
of the Requirements for the Degree
Doctor of Philosophy in Bioengineering

School of Chemical and Biomolecular Engineering
Georgia Institute of Technology
November 2004

# Effects of Mechanical Forces on the Biological Properties of Porcine Aortic Valve Leaflets

Approved by:


Dr Ajit P. Yoganathan
Department of Biomedical Engineering
Georgia Institute of Technology, Advisor

Dr Robert M. Nerem
School of Mechanical Engineering
Georgia Institute of Technology

Dr Steve L. Hilbert
Center for Devices & Radiological Research
Food and Drug Administration

Dr Timothy M. Wick
School of Chemical & Biomolecular Engineering
Georgia Institute of Technology

Dr Hanjoong Jo
Department of Biomedical Engineering
Georgia Institute of Technology



Date Approved: 7 January 2005

# ACKNOWLEDGEMENTS

I am grateful to many people at Georgia Tech for their guidance and support during this project. First and foremost, I wish to thank my advisor, Ajit Yoganathan, for his counsel. My colleagues in the Cardiovascular Fluid Mechanics Laboratory were great friends and often provided technical advice. I especially want to thank Dr Zhaoming He, who had been a great help in designing the experimental systems; and Dr James Warnock, who proofread my thesis and many other writings and provided very insightful comments in our discussions about my data, he has indeed been a tremendous help in completing this project on time. Several undergraduate students contributed to this project, and I thank Kanika Chawla, Daniel Conway, and David Chu for their efforts. I also wish to thank the faculty members on my thesis committee -Steve Hilbert, Hanjoong Jo, Bob Nerem, and Tim Wick - for their help in shaping this project and in reviewing the final dissertation. Finally, I wish to thank the administrative staff in both biomedical and chemical engineering for their assistance through the years.

Most of the biological research in this thesis would not be possible if not for the kindness and generosity of the various GTEC faculty members. I wish to thank Dr Tim Wick for allowing me to work in his lab and use his tissue culture facilities for the past five years. The Wick lab members provided great support to get me started and have been so throughout the whole project. I also would like to thank Dr Marc Levenston's lab for their help with my radiolabeling experiments; Dr Hanjoong Jo's lab, Manu Platt in particular, for the Western blotting and Zymography studies. Last but not least, I am truly thankful for the many advices and valuable input from Dr Stephen Hilbert throughout the past five years. In addition to that, Dr Hilbert's lab, Mr Howard Lukoff in particular, has also supported me with the actual immunostaining experiments as well as initiating the oxyblot studies.

Two other people deserve special thanks. Aortic valves for these experiments were donated by Greer Holifield of Holifield's Farm in Covington. Mr. Holifield allowed me to work inside the plant so I could place the valves in saline immediately, allowing me to better preserve their

viability. His plant provides tissues to many experimental groups at Georgia Tech as well as grade schools throughout the area. His generosity in supporting research is greatly appreciated. The pressure chamber used in these experiments were constructed by Jim McEntee of J.M. Machining in Lawrenceville. Jim reviewed my designs and suggested improvements to make them easier to machine and ultimately use. He often made small prototypes at no charge so that certain aspects of the design could be tested. I am grateful for his efforts. Financial support for this project came primarily from the ERC Program of the National Science Foundation under Award Number EEC-9731643.

I am also grateful for the emotional support and encouragement provided by my family as well as the friends we made in Atlanta, particularly those from Atlanta Chinese Christian Church - Campus Fellowship. Most of all, I am indebted to my husband, Keke, for his love, encouragement, and confidence in me kept me going on this project when it seemed like things would never work out.

# TABLE OF CONTENTS

# LIST OF TABLES

# LIST OF FIGURES

# SUMMARY

Cardiac valves are dynamic, sophisticated structures which interact closely with the surrounding hemodynamic environment. Altered mechanical stresses, including pressure, shear and bending stresses, are believed to cause changes in valve biology, but the cellular and molecular events involved in these processes are not well characterized. Therefore, the overall goal of this project was to determine the biological effects of pressure and shear stress, each as an individual mechanical factor, on cultured porcine aortic valve leaflets. Chosen biological properties include collagen synthesis, sGAG synthesis, cell proliferation, tissue morphology, cell phenotypical markers, and protease activity.

The first aim of this project was to determine the effects of pressure on valve biology. Two pressure regimes including both constant and cyclic pressure were studied. In the constant pressure study, three pressure levels were examined: physiological (100 mmHg), hypertensive (140 mmHg) and severe hypertesnive (170 mmHg). Collagen synthesis was significantly enhanced under pressure as compared to atmospheric controls. This increase was not statistically significant at 100 mmHg. At 140 mmHg and 170 mmHg collagen synthesis increased significantly by 37.5% and 90%, respectively. No significant differences in DNA and sGAG synthesis were observed with the exception that DNA synthesis at 100 mmHg was slightly lower than its atmospheric control. In the cyclic pressure study, the effects of both pressure magnitude and pulse frequency were studied. With the frequency fixed at 1.167 Hz, collagen and sGAG synthesis increased proportionally with mean pressure level. At a fixed pressure level (80-120 mmHg), there was no linear dependence on pulse frequency (0.5, 1.167, and 2 hz), except that at 0.5 Hz, collagen and sGAG synthesis were slightly increased by 25% and 14%, respectively. DNA synthesis did not vary much pressure magnitude, but was significantly increased by 72% at 2 Hz. Additionally, an experiment combining high magnitude (150-190 mmHg) and high frequency (2 Hz) was performed. Results showed significant increases in collagen and sGAG synthesis(collagen: 74%, sGAG: 56%), but cell proliferation was low and not different from the controls. Under both the constant and cyclic pressure conditions, the

amount of $\alpha$-SMC actin was not significantly different from the controls, but was lower than fresh valves.

The second aim of the project was to determine the effects of steady laminar shear stress on the biology of aortic valve leaflets. Shear levels ranging from 1 dyne/cm$^2$ to 80 dyne/cm$^2$ were studied. Collagen synthesis, sGAG content, endothelial cell alignment and tissue morphology was analyzed afterwards. Scanning electron microscopy (SEM) results showed that 48 hrs′ exposure to shear did not alter the circumferential alignment of endothelial cells on the ventricularis surface. Collagen synthesis was significantly enhanced at both 9 and 25 dyne/cm$^2$, but not different from static controls under other shear conditions. sGAG content in the leaflets was slightly lower than the controls, but the differences were not statistically significant. The second sub-aim of the shear stress was to identify the role of the endothelium in valvular responses to shear. Leaflets were first denuded of the endothelium and then exposed to shear. The absence of endothelium was confirmed by SEM and routine H $\&$ E. Results showed that denuded leaflets had different responses to shear from the intact leaflets. Collagen synthesis was not affected at any shear levels, but sGAG content was increased at shear of 9, 25 and 40 dyne/cm$^2$. There was no clear pattern between the changes and shear level, though. Under both conditions, the amount of $\alpha$-SMC actin was not significantly different from the controls, but was lower than fresh valves.

Molecular biology studies showed that the observed increases in collagen synthesis under pressure/shear stress were concurrent with decreases in cathepsin activity and expression. Particularly, cathepsin S and L expression and activity were declined, cathepsin B was present but not affected by either mechanical force. This converse relationship between collagen synthesis and cathepsin activity indicated that cathepsins might be involved in valvular extracellular matrix remodeling. Immunohistochemistry results showed that endothelial cells were major contributors for valvular cathepsin production, although interstitial cells also showed cathepsin production. MMP-2 and MMP-9 activity was not affected by either pressure or steady shear stress.

In summary, the results showed that valve leaflets responded to elevated pressure or steady laminar shear stress by increases in matrix synthesis and changes in cell proliferation, but not by changes in contractile proteins. These process might involve participation of lysosomal protease.

# CHAPTER I

# INTRODUCTION

In the United States, about five million people are diagnosed with heart valve disease each year. According to the American Heart Association statistics, heart valve disease is responsible for nearly 20,000 deaths per year and is a contributing factor in about 42,000 deaths [3]. Heart valve disease most commonly results from valve degeneration caused by calcification or weakened supportive structures in the valve. Other causes are pathologies such as rheumatic valve disease or bacterial infections, congenital abnormalities or damage from medications such as Phen-Fen [1].

Treatment for heart valve disease depends on the type and severity of the diagnosis. In some cases, only careful monitoring is needed; in others, medication can control the symptoms and slow or halt the progression of the disease. However, more serious cases require surgery to repair or replace defective valves. Every year, surgeons perform more than 225,000 heart valve operations worldwide [1]. The success rate for heart valve surgery is excellent. Heart valve repair and replacement can relieve symptoms and prolong life. Currently, there are four options for aortic valve (AV) replacement: mechanical valves, bioprosthetic valves, allograft (human valves from cadaver) and autograft valves.

Mechanical heart valves (MHV) account for nearly half of the replacements valves. Since its first clinical use in 1952, more than 50 different designs of MHVs have been developed so far [176]. Currently, the bileaflet valve constitutes the majority of modern valve designs. These valves are distinguished mainly for providing the closest approximation to central flow achieved in a natural heart valve. The main advantage of mechanical heart valves is their lifelong durability. Therefore they are suitable for people who do not want additional valve surgery in the future. The foremost drawback of mechanical valves is their blood clotting potential, which makes it necessary for the recipient to be on lifelong anti-coagulant therapy. Bioprosthetic valves are made of either porcine valve or bovine pericardium. These valves have superior hemodynamics and do not require anti-coagulant

therapy. A major drawback of bioprosthetic valves is their durability, which is quite limited as compared with mechanical valves, with an average longevity of only about 7-15 years. Currently there are two types of human valves that are being used in clinical practice. Allografts are human valves obtained from a cadaver. These valves are generally cryopreserved immediately following removal from a donor prior to implantation into the recipient. Allografts have superior hemodynamics, minimal immunogenic potential, and no need for anticoagulation and other advantages. The use of allografts is severely limited by its inadequate supply. Alternatively, an autograft may be used. The use of autograft valves was pioneered through the Ross procedure. The Ross procedure is a type of specialized aortic valve surgery where the patient's diseased aortic valve is replaced with his or her own pulmonary valve. The pulmonary valve is then replaced with a cryopreserved cadaveric pulmonary valve. A drawback of this procedure is that it is highly demanding on the surgeon's skillfulness and some patients' conditions may not allow a two-valve surgery. Although the various replacement valves seem to differ in their advantages and disadvantages, they do share one common weakness: the lack of growth potential. The growth potential problem is extremely important for the pediatric population. As the child grows their heart becomes bigger and will need a bigger valve, too. This calls for a need for a living valve, which is capable of adapting to the surrounding hemodynamics and remodel accordingly.

Recent advances in tissue engineering have spurred the development of a tissue engineered (TE) valve. The ideal TE valve should be free of all the problems encountered by other types of valves. They should be non-immunogenic, since the cells will be harvested from the recipient. There would be no concerns about supply, since eventually the TE valves will be manufactured on a factory scale and have off-the-shelf availability. Most importantly, they will have the ability to grow, since they are made of living cells. There are currently two major approaches towards making a TE valve. The synthetic material approach, in which a scaffold made of synthetic material, is used as an initial support for cell attachment and growth. The constructs may be preconditioned in a bioreactor before implantation into the body. The second strategy is the decellularization-recellurazition strategy. Here, heart valves are first decellularized by chemical or mechanical means (e.g.high pressure) to remove the allogenic cells; the remaining extra-cellular matrix (ECM) is then recellularized with autologous cells, followed by precondioning and finally implantation.

It is commonly accepted that preconditioning in a bioreactor is critical for the development of a TE valve. Although it is not clear yet what the ideal tissue valve would be like, it is believed that resemblance to the native valve in structure and material properties would also lead to similarities in function. *In vitro* preconditioning has been shown to be beneficial for this purpose. For instance, a TE blood vessel preconditioned under pulsatile flow showed superior properties than simple static incubation [96]. However, there is still a scarcity of knowledge as regards to the optimal preconditioning conditions for a TEAV. In order to determine the optimal *in vitro* preconditioning conditions for a TEAV, an understanding of the native hemodynamics and the corresponding biological response is critical. The benefits will be two-folded: firstly, understanding how a native valve responds to these mechanical factors will help predict the responses of a TE valve; secondly, this will provide insight into the physiological development and pathological remodeling processes of a native valve.

The environment of the AV will be examined since aortic valve replacements account for nearly 50% of all valve replacement procedures [52]. Under normal physiological conditions, the AV is exposed to a harsh and complex flow environment, experiencing back pressure, shear stress and bending stresses during each cardiac cycle. This thesis will be focused on the effects of the first two factors; pressure and shear stress. AV pressure load during diastole is 80-120 mmHg, and about zero during systole. This pressure generates two mechanical effects: the normal stress which is in line with the pressure and tensile stress in the transverse direction. As a result, the leaflets become thinner during diastole and are stretched in the transverse direction. Although the pressure load and its hemodynamic function on the AV has been well characterized, little is known about its biological effects on valvular cells. To study the effect of pressure on valve leaflets, a system is needed to generate pressure covering both physiological and pathophysiological pressure ranges. In addition, since the *in vivo* pressure is cyclic in nature, the generated pressure should be cyclic too. This will be addressed in the methodology section (chapter IV). Studies have shown that pressure magnitude and pulse frequency are both important parameters in determining the effects of cyclic pressure, therefore both parameters will be considered in this study.

Shear stress experienced by the AV is complex, since the two surfaces (ventricularis and fibrosa) see completely different flow conditions. One is mainly laminar, and one is secondary turbulent flow.

This thesis will focus on the ventricularis side. Shear stress on the ventricularis has recently been estimated and its effects on leaflet cell synthetic activity was studied [169]. However, it was not clear in that study whether the cell viability was maintained; therefore, it has become questionable as to whether the responses truly resonate that of an intact valve. Therefore, in this study, we seek to maintain the tissue viability as much as possible. To achieve this purpose, a new tissue procurement method needs to be developed as well as methodologies for tissue viability assessment. The system will be the same as that used by Weston et al. [169], but the endpoints will be more comprehensive. In addition, the role of the endothelium in the valvular response to shear will also be studied. Since the endothelium is the direct sensor of shear stress, it must play an important role, through either mechanotransduction or by secretion of paracrine factors, in affecting the underlying interstitial cells. This is quite likely since literature has shown that treating SMCs with EC conditioned media could result in various types of biological responses [105].

To provide a background for these studies, a thorough literature review is presented in Chapter II, discussing anatomic features of the aortic valve, valve replacement options, and a review of previous studies relating mechanical forces to cellular function. This discussion leads into the specific aims of this thesis, which are presented in Chapter III. Chapter IV describes the methodologies that have been employed in these studies. These methodologies include the systems for pressure study, shear stress study and the biological assays used in both studies. Chapter V presents the results from the two studies. Chapter VI is a discussion on the results with an attempt to explain the mechanism on the molecular and cellular level, as well as the significance and limitations of the study. Following the discussion chapter, is a chapter of conclusions which summarize the major findings from this study and their implications. The thesis ends with a chapter on future directions which speculate on the areas that need to be further explored.

# CHAPTER II

# BACKGROUND

This chapter will present background information that will define the rationale for this thesis research. The first section deals with anatomy and function of the heart, the aortic valve anatomy and cellular structure. The second section focuses on the hemodynamics and mechanical stresses in the aortic valve, followed by a section of literature review on mechanical forces verses cellular function. The chapter concludes with the rationale for the thesis research.

## *2.1 The Heart and the Aortic Valve*

### 2.1.1 The Heart

The heart (Fig.1) is one of the most important organs in the entire human body. Its primary function is to pump oxygen-rich blood to the rest of the body, and pump the oxygen-depleted blood back to the lungs. A normal heart has four chambers: the right and left atria, and the right and left ventricles. The right heart collects oxygen-depleted blood from the venous circulation and pumps it into the pulmonary circulation, where blood is re-oxygenated in the lungs. Blood then returns to the left heart and is forced into the systemic circulation by left ventricle (LV) contraction. Blood flow through the heart is regulated by four one-way valves: the aortic valve, the mitral valve, the pulmonary valve and the tricuspid valve. One contraction and one dilation of the heart consist one cardiac cycle, which lasts about 860 ms for a normal heart rate of 70 beats per minute (bpm). The contraction is called systole and the dilation is called diastole, with a duration ratio of 1:2. At the onset of systole, LV pressure rises due to isovolumetric contraction and eventually exceeds the pressure in the aorta, causing the aortic valve to open and allowing blood to be ejected into the aorta. As systole ends, LV pressure decreases due to ventricular relaxation. The aortic pressure eventually becomes greater than the LV pressure, forcing the aortic valve to close (Fig.2). Recent studies by Yacoub et al [174] indicate proactive rather than merely passive involvement of the leaflet tissue in this opening and closing process. Typical resting conditions include a cardiac output of 5 L/min, a

cardiac frequency of 70 bpm, and an aortic pressure of 120 mmHg (systolic) / 80 mmHg (diastolic). During a person's lifetime, the aortic valve opens and closes about three billion times (70 bpm, with a life-expectancy of 70 years).

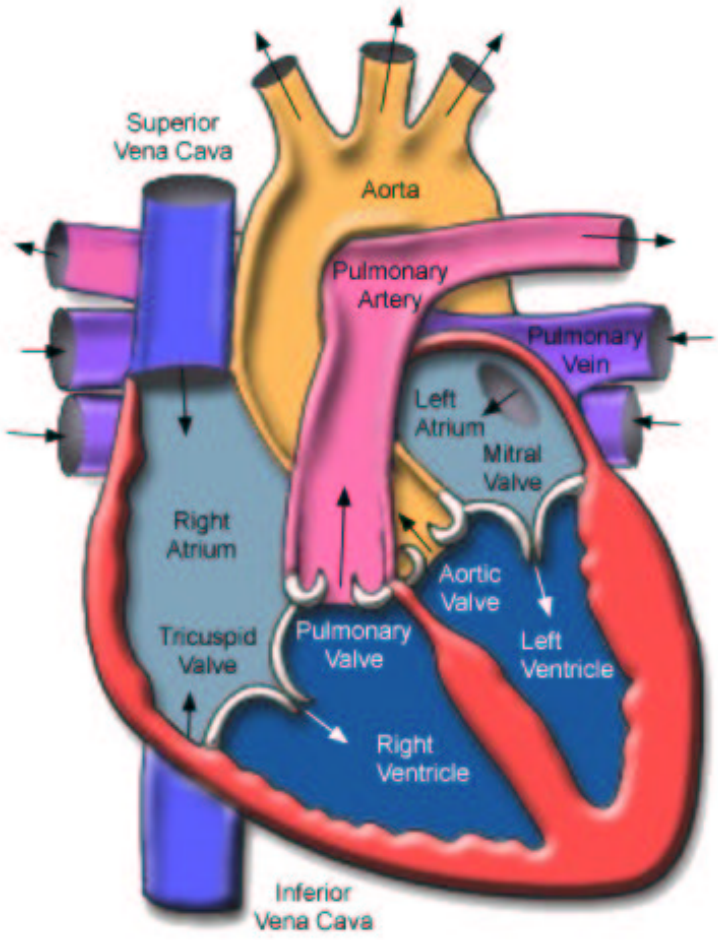


**Figure 1:** Heart anatomy, arrows indicate blood flow direction, Source: www.tmc.edu/ thi/ anatomy2.html.

### 2.1.2 The Aortic Valve

#### *2.1.2.1 Aortic Valve Anatomy*

The aortic valve (AV) is situated at the aortic root, regulating blood flow between the LV and the aorta. It consists of three leaflets, opening and closing synchronously during each cardiac cycle. The three leaflets are attached to each other at the commissures and named as the left coronary, the right coronary and the non-coronary leaflet, each according to its anatomical position. Behind each leaflet is a bulging cavity known as the sinus of Valsalva. The left and right coronary sinuses contain

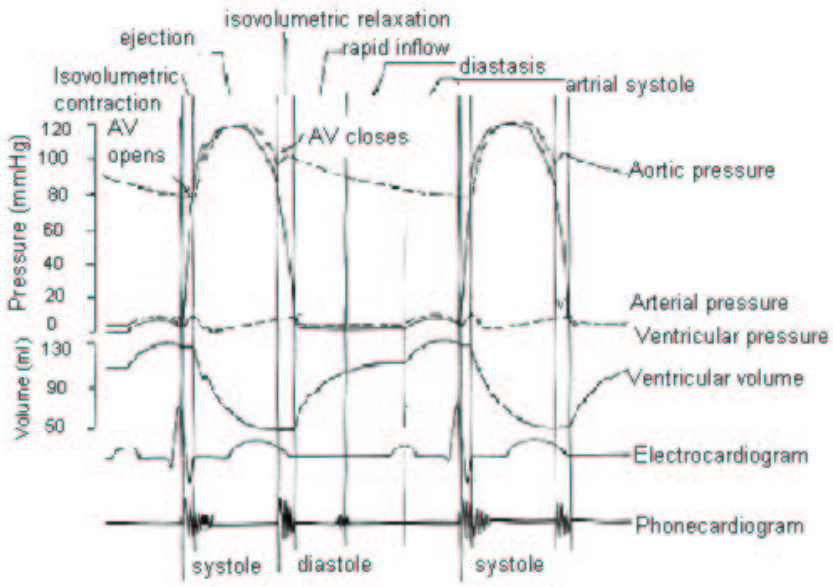


**Figure 2:** Events during a cardiac cycle, shown in the figure are electrocardiogram, phonecardiogram and pressure waveforms of the aortic valve, ventricle and the arterial system (from Guyton, 1991[57])

ostia that open into the left and right coronary arteries. The third sinus, the noncoronary sinus, does not feed a coronary artery. These structural components are very important for the proper function of the aortic valve [152]. During the opening phase, the commissures pull outward to aid leaflet opening. Vortices that develop in the sinuses during systole help close the leaflets. To prevent the leaflets from slamming shut with great impact, the sinuses absorb some of the shock of closing. This is known as stress sharing, as stresses are transmitted from the leaflet to the aortic wall. The elasticity of the aortic root also reduces impact forces.

The sinus of Valsalva is defined as the area between the aorta and the valve leaflet edge when the valve opens. A cross-section of the aorta at this point reveals that the wall of the aorta is thinner than the aortic wall distal to the sinus. In addition, this cross section also demonstrates a cloverleaf pattern to the aorta showing the ballooning of the sinuses of Valsalva. This space between the aortic surface of the valve cusp and the wall of the aorta behind the cusp is bounded caudally by the basal attachment of the aortic valve leaflet and cephalad by the sinotubular junction, which is the beginning of the aorta just downstream of the sinus. This space provides a reservoir of blood when the valve leaflets are open and also, as discussed later, functions to billow the valve leaflets to accelerate apposition during valve closing (Fig.4).

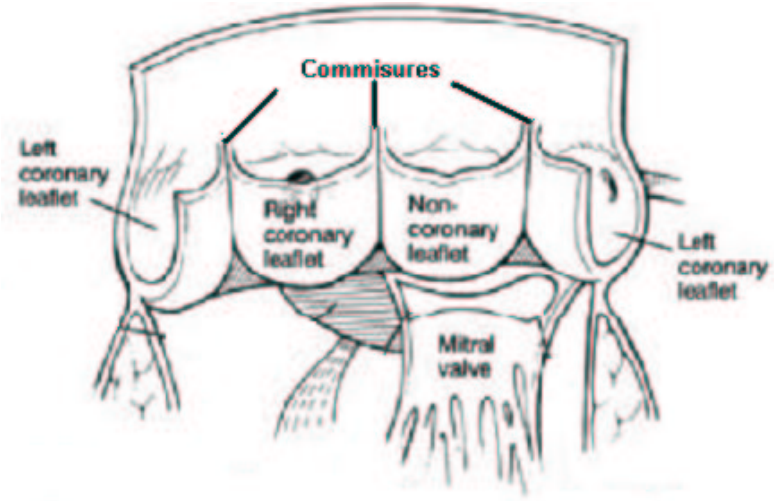


**Figure 3:** The aortic valve, opened at the midline of the left coronary leaflet; Source: http:// surgclerk.med.utoronto.ca/ Phase2/Cardiovascular/ 2AVD/AVD1.htm

The aortic valve annulus is part of the fibrous skeleton of the heart. It functions to support the valve and root of the aorta against the high pressures resulting from left ventricular systole. It consists of a ring of collagenous tissue that surrounds and supports the aortic orifice. The annulus is arranged as three arches. The distal parts of each arch blend with the fibro-elastic tissue of the aortic sinuses. The part of each arch that faces the lumen of the aorta blends with the lamina fibrosa of the valve leaflets. During aortic valve opening, the annulus descends and move forward; major decent occurs during the first half of systole whereas major forward motion occurs during the later half. When, or shortly after, the valve closes, the annulus starts to rise. The greater part of the ascent occurs during the first half of diastole whereas backward movement occurs during the second half [152].

The aortic valve is classically described as a semilunar valve. This description reflects the fact that leaflet attachments to the aorta are in one plane but are crescent-shaped. Each leaflet is approximately 308 $mm^2$ and weighs approximately 0.08 g with a volume of 1 ml. Although the normal aortic valve appears to have three equally sized leaflets, over 50 percent of people have one valve leaflet slightly larger than the others [2]. In addition, there is a trend for larger-sized hearts to be associated with larger valves.

Each of the leaflet contains thin sheets of connective tissue arranged in three or more layers of distinctly different density and composition. The endothelial surfaces of the leaflet are named as

the aortic surface and the ventricular surface, according to the anatomic position they face when the valve is closed. Both surfaces are covered with a monolayer of endothelial cells. On the aortic surface, the cells are aligned circumferentially with ridges at the leaflet surface [34, 152]. On the ventricular surface, which is directly exposed to systolic blood flow, the cells are also circumferentially oriented [34]. This surface is very smooth, perhaps to prevent flow disturbances [152]. Similar to vascular endothelium, the valvular endothelium likely serves as an important barrier against platelet or fibrin deposition [49] and probably has some similar biochemical function.

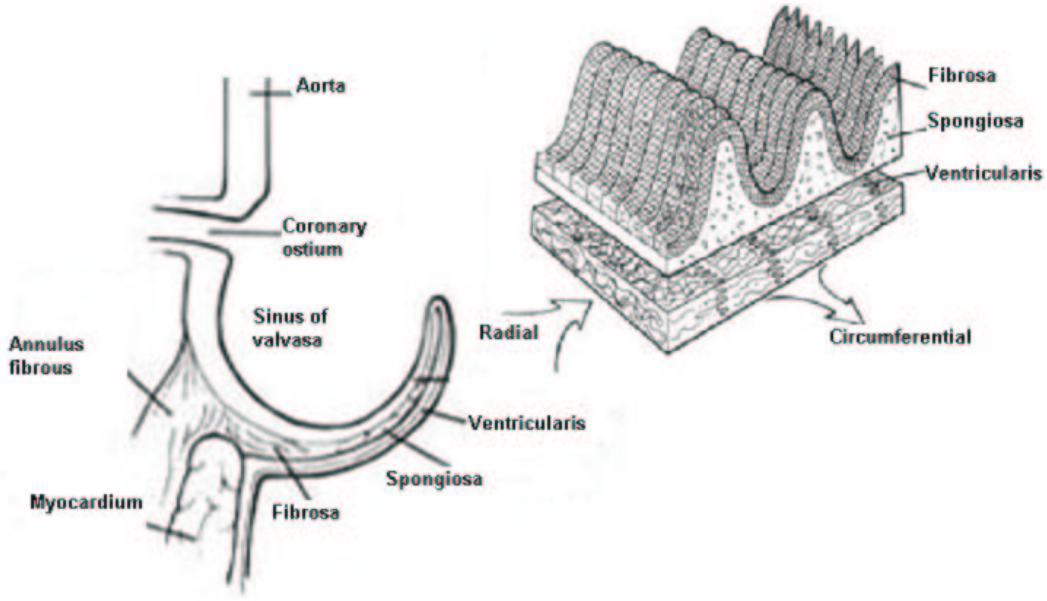


**Figure 4:** Aortic valve leaflet: side view showing the sinus, the sinotubular junction, the ostium and the leaflet; cross-sectional view showing the tri-layer structure of the leaflet; Source: http://www.ctsnet.org/edmunds/Chapter28section2.html

#### *2.1.2.2 Leaflet Structure*

Beneath the surfaces, the leaflet tissue is composed of three layers: the fibrosa, the spongiosa and the ventricularis. As can be seen in the figure (Fig.4), the arterial and ventricular sides of the aortic leaflet are associated with the corresponding aortic and ventricular wall. The endothelial layers of the leaflet form a continuum with the aortic endothelium or ventricular endocardium.

The fibrosa is the layer immediately beneath the aortic surface; it is very dense and is arranged as a series of parallel tendinous cords in a ridged sheet of tissue. It is also the strongest part of the leaflet and bears the majority of the stresses generated by diastolic pressure. Diastolic pressure

loading of the valve leads to tensile stresses on the leaflets, predominantly in the circumferential direction [152]. The fibrosa contains a dense layer of collagen fibers with a few elastic fibers scattered randomly among the collagenous fibrils. Collagen fibrils in the fibrosa are not intertwined or rippled within the sheets but instead lie parallel to one another, suggesting that the whole layer of tissue sustains continuing tension that straightens the fibrils. There are three major types of collagen in the aortic valve leaflets: collagen type I, type III, and type V collagen (all fibrillar collagen) with an approximate ratio of 85:10:5 [8]. Spaces between the collagen fibrils are filled with hydrated proteoglycans or protein polysaccharides, which appear to be attached to the collagen fibrils, helping to maintain the structure. At the same time, the extensive hydration of the proteoglycans would provide interfibrillar lubrication so that the fibrils could slip against each other, giving flexibility to the whole aggregation [152]. Proteoglycans are also believed to regulate polymerization of collagen fibers [60].

Just beneath the endothelial cells and their thick basal lamina on the ventricular side of the cusp lie strata of the ventricularis, which begins in the wall of the left ventricle and spreads into the leaflet. The superficial component of the ventricularis is an elastic layer two to several fibers thick, oriented principally in the radial direction. Internal to the elastic layer may be found a circumferentially oriented layer of collagenous fibers. In contrast to the ridged aortic surface, the ventricular surface is relatively smooth, suggesting the elastic tissue in the ventricularis might be involved in the maintenance of this feature. Since the ventricular surface is exposed to shear stress during the ejection phase of the cardiac cycle, a smooth surface is important for maintaining laminar blood flow on the ventricular side of the cusp during systole [152]. Although this force is directly experienced by the endothelial cells on the surface, it may be communicated to cells within the ventricularis, either directly through tensile forces or indirectly through signaling molecules released by the endothelium.

Between the fibrosa and the ventricularis is the spongiosa, a very loose, watery connective tissue of varying thickness, fiber composition and cellularity. This tissue forms the core of the leaflet near the base and is thicker near the attachments at the aortic wall and virtually absent near the free margin. The spongiosa layer of the AV leaflets normally contains low quantities of collagen and elastin, but large quantities of glycoaminoglycans (GAGs), such as hyaluronan and chondrotin/dermatan sulfate, likely in the form of the proteoglycans versican and decorin. There are four types of GAGs

in heart valves: hyaluronan, the chondroitin/dermatin sulfates, keratan sulfates and the heparan sulfate/heparan, with hyaluronan, and the chondroitin/dermatin sulfates representing 90% of total valvular GAGs. All GAGs, except the hyaluronan, are covalently linked to core proteins to form proteoglycans. Two major types of structurally associated proteoglycans are found in cardiovascular extracellular matrix (ECM): the large proteoglycans such as versican and the small proteoglycans such as biglycan and decorin. The large proteoglycans are trapped within the collagen meshwork of tissues as large macromolecular complexes formed through their non-covalent association with hyaluronan [56].

The semifluid nature of the spongiosa layer gives the leaflet considerable plasticity [152]. It is suggested that the principle function of this layer might be to help in reducing leaflet stresses by lubricating the relative motion of the other two layers as the leaflet bends [27] and by dampening forces in the fibrosa at valve closure.

#### *2.1.2.3 Cells in the Aortic Valve*

Valvular cells include endothelial cells (ECs) on the leaflet surfaces and interstitial cells (IC) within the tissue. Valvular ECs are analogous to arterial endothelial cells in the sense that both are in direct contact with blood flow. The first striking difference between valvular ECs and vascular EC is difference in their alignment patterns with respect to flow. Valvular ECs align perpendicular to blood flow, while vascular EC are well known to align parallel to flow. This difference is attributed to the stress pattern difference in the two types of tissues: circumferential in the leaflets and radial in the vessel. A recent study [18] showed that this feature was maintained in *in vitro* cultured cell monolayers. DNA microarray results from the same study also demonstrated different gene profiles for the two types of ECs. Not only are valvular ECs quite different from vascular ECs, the valvular EC itself is likely to be a heterogeneous population. First of all, ECs from the ventricular surface originated from the endocardium, while those on the aortic surface are an extension of the aortic endothelium. Secondly, the ventricular ECs are exposed to a pulsatile laminar flow of around 5 L/min, while the aortic ECs are exposed to a flow of much lower magnitude. Based on these observations, it can be expected that ECs from the two sides may have phenotypic differences. In fact, research in this area has just emerged and some preliminary results did indicate differential

gene expressions [32].

The cardiac valve interstitial cells are a heterogenous and dynamic population of specific cell types that have unique characteristics [151]. These cells are descended from endocardial cells that have undergone an epithelial-to-mesenchymal transformation and cells that migrated in from extra-cardiac site during embryonic development. To date, at least three phenotypes of IC have been identified in mature native valves [151]. One type, the myofibroblasts, is characterized by prominent stress fibers, associated with smooth muscle $\alpha$-actin expression and is thought to be involved in proliferation and migration. This contractile phenotype rapidly remodels the extracellular matrix. The second phenotype is characterized by synthetic and secretory organelles associated with the expression of prolyl-4-hydroxylase, an enzyme essential for stabilization of the collagen triple helix, indicating these cells are actively synthesizing collagen. The third phenotype is smooth muscle cells that are seen either singly or in thin bundles.

Among the three cell phenotypes, myofibroblasts are likely to account for a large percent of the IC population and play an important role in valve function. This unique cell type has characteristics of both fibroblasts and smooth muscle cells. They display a highly plastic and diverse phenotype, depending on tissue origin and whether the tissue is normal or pathological. Valvular myofibroblasts have been found to express SM $\alpha$-actin, synthesize collagen and other matrix proteins, and are able to contract when immobilized in collagen gel. The unique characteristics of myofibroblasts may be critical for the life-long durability of cardiac valves. In addition, they may also contribute to the capacity of valve tissue to contract in response to vasoactive agents such as endothelin-1 and thrombovane $A_2$ [23]. Functionally, myofibroblasts and smooth muscle cells may play an active role in the opening and closing of the leaflets by pulling on collagen fibers in the fibrosa and ventricularis [152].

The EC and IC are thought to interact with each other. ECs are directly exposed to blood flow and may serve as a mechano-transducer or secrete molecules for the ICs lying deep within the matrix. A recent study [11] also showed that there is interplay between these two types in immunogenicity.

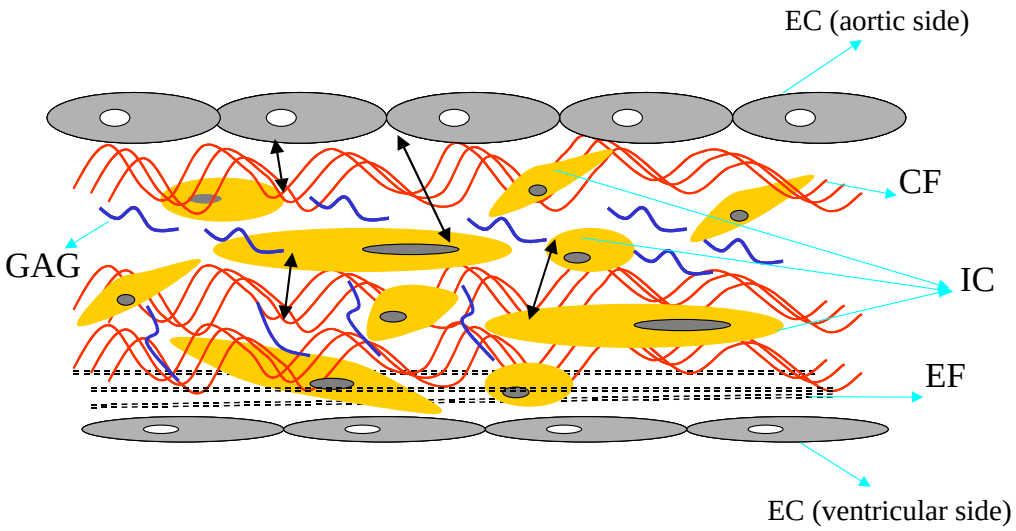


**Figure 5:** Schematic drawing of the leaflet structure, EC: endothelial cells, IC: interstitial cells, CF: collagen fibers, EF: elastic fibers, GAG: glycoaminoglycans, ⟷: cell-cell, cell-matrix interactions

#### *2.1.2.4 Cellular Activity in the Normal Aortic Valve*

The normally functioning AV is a dynamic structure which undergoes constant renewal in response to mechanical loading. A pioneering study by Schneider and Deck [122] showed that protein and GAG synthesis in the leaflet was greater than in static tissues from the intestine, dermis, and tail. DNA synthesis was observed throughout the leaflet, but was more pronounced in growing rats than mature rats. The same study also identified the sites of protein and GAG synthesis in rat aortic valve leaflets. They found that the attachment zone (highest bending stresses) showed the highest GAG synthesis, while the region between the attachment and the midpoint showed the greatest protein synthesis (diastolic pressure loading). The authors attributed the patterns of synthesis to the stress pattern in the leaflets. Such renewal is thought to be due to the presence of viable, metabolically active ICs in the native valve, this may explain the longevity of native valves compared to bioprosthetic heart valve replacements, most of which do not have viable cells.

### 2.1.3 Mechanical Forces on the Aortic Valve

Physiologically, the human AV is exposed to a harsh & diverse mechanical environment. The major forces include diastolic pressure, shear stress and bending stresses. The following section is a detailed description of theses forces and the stresses they generate in the AV leaflet.

#### *2.1.3.1 Diastolic Pressure*

During diastole, the average pressure loading onto the AV is around 100 mmHg for normal people. This pressure generates tensile stress on the leaflets. This stress is mainly borne by the collagen fibers in the fibrosa and may be transmitted to the cells that are aligned with the collagen fibers [118]. Schneider and Deck suggested that active protein synthesis in the leaflet maintains the strength required to withstand diastolic loading. Christie et. al. [27] showed that under very little or no transvalvular pressure, the leaflets looked pale and the collagen fibers were in a ”crimped” state; as pressure increased, valve leaflets became translucent and the collagen fibers were straighten out. Although the diastolic pressure is known, the resulting stress and/or strain within the leaflet can only be estimated. By using the radiopaque marker technique in combination with membrane stress analysis, Thubrikar et al [152] came up with a circumferential stress of 2.4 MPa during diastole. Numerical simulations of a 120 mmHg pressure load on bioprosthetic valves suggest that pressure is transmitted through tensile and compressive forces throughout the cusp [28]. In stented bioprosthetic xenografts, tensile stresses up to 0.5 MPa were observed near the free margin adjacent to the stent posts, which are located at the junctions between two leaflets. Compressive stresses up to 0.1 MPa were found near the base of the stent posts. For stentless human allografts, tensile stresses up to 0.5 MPa were also calculated, but they occurred in the belly area, while negligible tensile stress was observed near the free margin or the commissures. No compressive stresses were found in the human allograft. By using magnetic resonance imaging (MRI) defined geometry, Grande et al [55] determined a peak tensile stress of 0.5 MPa and a maximum strain of 15% in human aortic valve.

#### *2.1.3.2 Bending*

Bending stresses arise from the motion of the leaflets during the course of the cardiac cycle [152]. Individual cells may experience compression or tension during bending, depending upon their position within the leaflet. Bending creates internal shear as the ventricularis and fibrosa are deformed. The spongiosa, which lies between these layers, serves to lubricate their relative motion to prevent tissue damage. Two modes of bending occur in the leaflet. First, the belly of the leaflet undergoes reversal of curvature during valve opening and closing. Active protein synthesis in this region may

be a response to bending [122]. Secondly, the attachment zone acts as a hinge during leaflet motion. This area exhibits high GAG synthesis, which may be a response to bending stresses [122]. A study using radiopaque marker demonstrated circumferential bending strains of 2% in systole and 2.2% in diastole [153]. Similar studies by Deck et al. [35] estimated bending strains to be about 5.1%. However, the temporal and spatial resolution of this technique was limited. More detailed *in vitro* experiments have been performed using dip-cast polyurethane valves with a trileaflet structure similar to the human aortic valve [30]. The leaflets were marked with a grid and videotaped during hemodynamic testing under physiological pulsatile flow conditions. Bending strain and bending stress were determined from leaflet curvature by shell bending theory and the physical properties of polyurethane. The greatest bending was observed during the opening phase; with a maximum strain of 14.5% and the maximum stress of 1.22 MPa. During the closing phase, the maximum strain and stress were only 8.3% and 0.71 MPa, respectively. Bending was minimal at peak systole (6.9% strain, 0.58 MPa stress). Porcine aortic valves tested under similar conditions exhibited a higher degree of curvature [29], but the authors did not address bending stresses since the physical properties of the leaflet tissue were unknown.

#### *2.1.3.3 Shear Stress*

The aortic valve leaflets are exposed to shear stress during systole as blood is ejected through the valve. Shear stresses experienced by the two surfaces of the AV are different due to the different flow profiles. Flow on the ventricular side is pulsatile (only present during systole) and laminar, flow on the aortic side is also laminar but of a much lower magnitude. The ventricular surface is the focus of this thesis. The average shear stress on the ventricular surface of the aortic valve was estimated to be 12-40 dynes/cm$^2$ during systole, with peak values up to 80-100 dynes/cm$^2$ [168]. Shear stress generates tensile stresses on the endothelial cells which cover the leaflet surface. The ECs may transmit the mechanical signal to underlying interstitial cells and extracellular matrix through the release of signaling molecules or by direction force transmission through cell-cell and cell-ECM connections.

## *2.2 Heart Valve Disease & Surgical Interventions: State-of-the-art and Challenges*

Malfunctioning of the AV falls into two major categories: aortic stenosis and aortic regurgitation or incompetence. Aortic stenosis refers to obstruction of flow at the level of the aortic valve. Aortic stenosis can be caused by three major reasons: 1) Calcified aortic stenosis, 2) Rheumatic aortic stenosis and 3) Degenerative aortic stenosis. Aortic regurgitation is defined by incompetence of the aortic valve, in which a portion of the left ventricular forward stroke volume returns to the chamber during diastole. Causes for AV regurgitation include cusp prolapse or cicatricial shortening of cusps with rolled edges, dilation of sinus aorta, cystic medial necrosis, and coaptation failure of the cusps. Treatment for heart valve disease depends on the type and severity of the diagnosis. In some cases, only careful monitoring is needed; in others, medications can control the symptoms and slow or halt the progression of the disease. However, more serious cases require surgery to repair or replace defective valves. Currently, there are four major options for AV replacement: mechanical valves, bioprosthetic valves, allograft valves and autograft valves.

### 2.2.1 Mechanical Valves

Mechanical valves account for nearly half of the replacement valves. The first clinical use of a cardiac valvular prothesis took place in 1952, when Dr Charles Hufnagel implanted a caged ball valve for aortic insufficiency. Since then, 50 different mechanical designs have originated worldwide. These valves have progressed from the initial caged ball valves, to disk valves & tilting-disc valves, and to the modern bileaflet valves. Currently, the bileaflet valve constitutes the majority (about 80%) of implanted mechanical valves [176]. These valves are distinguished from other mechanical valves mainly because of their closest approximation to central flow as achieved in a natural heart valve. All MHV prostheses have a similar basic structure with three essential components: 1) the occluder (such as a ball, a disc or a hinged leaflet), 2) the housing and 3) the sewing ring. Most contemporary MHV prostheses have pyrolytic carbon as a major component, while some have metal components (e.g. titanium) also. The sewing cuff is made with synthetic fabrics (e.g. Dacron), with or without a filler (e.g. Teflon) between the layers of the fabric [17]. The major advantage of mechanical heart valves is their lifelong durability; therefore they are suitable for people who do not want additional

valve surgery in the future. The major disadvantage of mechanical valves is their blood clotting potential, which makes it necessary for the recipient to be on lifelong anti-coagulant therapy. The anti-coagulant used causes birth defects in the first trimester of fetal development, rendering mechanical valves unsuitable for women of child-bearing age. Current research on mechanical valves has been able to produce materials that do not cause clotting in the blood stream as well as a new design of an entire valve that will not induce coagulation.

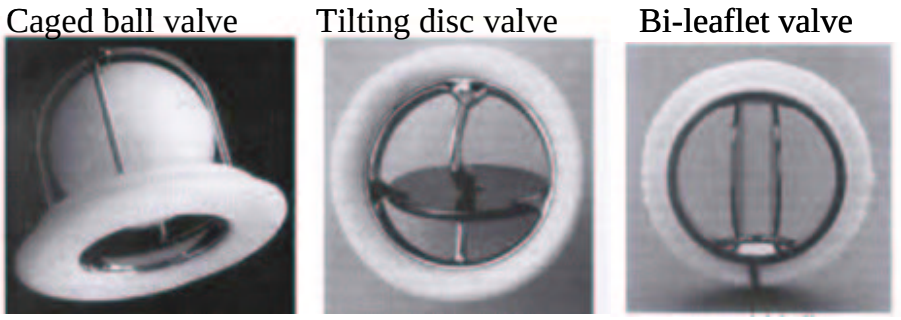


**Figure 6:** Major types of mechanical valves, source: http://www.sts.org/doc/3621

### 2.2.2 Bioprosthetic Valves

The next big category for AV replacements are the bioprosthetic valves (BHVs), which account for about 40% of replacement valves. As its name indicates, a bioprosthetic valve is made of biological material, which is most commonly a fixed porcine valve or bovine pericardium. In contrast to mechanical heart valves, BHVs have higher thrombo-resistance and their central flow pattern are more approximate to native aortic valves. Currently, there are three major types of BHVs commonly in clinical use: glutaraldehyde-pretreated stented porcine aortic valve, glutaraldehyde-pretreated stentless porcine aortic valve and glutaraldehyde-pretreated stented bovine pericardial valve. Stentless valves are more recently developed (first approved by FDA in 1997) and their principle advantage over stented BHVs is that they allow for the implantation of a larger BHV (than stented) in any given aortic root, which may enhance hemodynamics,ventricular remodeling and patient survival. [125] Since the biological materials used in BHVs are of animal origin (porcine or bovine), which, if untreated, would result in severe immunological problems. To attenuate this problem, these valves are pretreated with glutaraldehyde to cross-link the surface antigens. The side effects of this fixation are compromised tissue microstructure and mechanical properties [125]. The durability of bioprosthetic

valves is therefore limited as compared with mechanical valves, with an average longevity of 7-15 years. The most common cause of bioprosthesis failure is stiffening of the tissue due to the build up of calcium. Calcification can cause a restriction of blood flow through the valve (stenosis) or cause tears in the valve leaflets. Since younger patients have a greater calcium metabolism, bioprostheses tend to be better suited to senior citizens. Recent research on BHVs have been focused on the following areas: 1). Improvement of the fixation methods (e.g. zero fixation or dynamic fixation, using tissue fixatives other than glutaraldehyde ); 2). Development strategies to inhibit calcification such as removal of a calcifiable component of the biomaterial and decellularization; 3). The perfection of stentless valves [125].

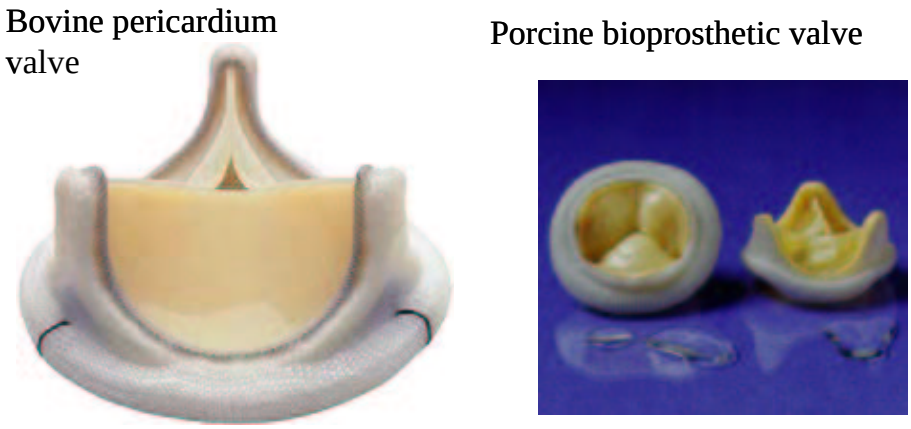


**Figure 7:** Major types of bioprosthetic valves, source: http://www.sts.org/doc/3621

### 2.2.3 Allograft Valves

Human aortic valve allografts (also called homografts) are obtained from cadavers, sterilized by incubating in antibiotics, followed by cryopreserved (without chemical cross-linking) by freezing with protection from crystalization by dimethyl sulfoxide, followed by storage at -196$^{o}$C in the vapor over liquid nitrogen. They are implanted directly into the aortic root without a stent. AV allografts have exceptionally good hemodynamic profiles and a low incidence of thromboembolic complications without chronic anti-coagulation. These valves are free of degeneration and or replacement for periods of up to 10-15 years. This superior performance was once attributed to the initial fibroblast viability at implantation [14, 136, 80]. However, this theory became controversial as following studies began to reveal progressive loss of normal structural complexity and cellularity

in allograft valves soon after implantation [87]. A new explanation for the clinical success of cryopreserved allografts hypothesizes that the preservation of cellular viability is not the primary feature, but that this indicates better preservation of the leaflet matrix, aiding durability [84].

The mode of failure of cryopreserved valves inserted on the left side of the heart is most frequently incompetence caused by leaflet rupture, distortion with retraction, or perforations. In contrast, right-sided valves in children who have right ventricle to pulmonary artery conduits usually stenose as a result of somatic growth of the recipient,with or without calcification of the leaflets or distal vascular wall. The most critical issue in the pathology of valve allografts relates to cell viability, ECM integrity and mechanisms of deterioration including the role of immune responses. Studies have shown that antibiotics treatment and ischemic intervals during the cryopresevation were important factors that cause damage to tissue viability, but short-term antibiotics exposure (less than 24 hrs) and ischemia less than 12 hrs were acceptable. Current research on cryopreserved valves is focused on improving preservation protocols so that damage to the native valve structure is minimized.

### 2.2.4 Autograft Valves

The term autografts originated from the Ross procedure, in which a patient's diseased AV is replaced by his/her own pulmonary valve (PV) , and the PV position was then replaced by an allograft pulmonic valve. Clinical results show that leaflets of the autograft valves appears to retain normal architecture and staining qualities of cells and ECM for at least 6 years. The long term survival and freedom from complications for patients with aortic valve disease are better with the Ross Procedure than any other type of valve replacement [125]. After 20 years, only 15% of patients require additional valve procedures. In cases where a human pulmonary artery homograft is used to replace the patients' pulmonary valve, freedom from failure has been 94% after 5 years, and 83% at 20 years. The tissues of the patients' pulmonary valve have not shown a tendency to calcify, degenerate, perforate, or develop leakage [125]. In children and young adults, or older particularly active patients, this procedure offers several advantages over traditional aortic valve replacement with manufactured prostheses. Longevity of the pulmonary autograft in the aortic position is superior to bioprostheses such as the bioprosthetic porcine valves. A drawback of this procedure is that

it is highly demanding on the surgeon's skillfulness and some patients' conditions may not allow a two-valve surgery. Despite their superior performances as compared with prosthetic valves, both allograft and autograft valves are limited in use due to their shortage of supply.

Although the current replacement valves seem to differ in their advantages and disadvantages, they do share one common weakness: the lack of growth potential. This problem is extremely important for the pediatric population, as children will require repeat surgeries as they grow. This calls for the need for a living valve, which shall not only have performance at least equal to the best valves available, but shall be free of all the problems mentioned so far, and has the ability of adapting to the environment and remodelling accordingly. The desirable characteristics of this new generation of valves are summarized in the following table [125]. Tissue engineering seems to be a promising approach to achieve this goal.

**Table 1:** Desirable characteristics of a tissue engineered heart valve, adapted from Schoen & Levy [125]

| |
|---|
| Endothelial blood-contacting surface |
| Cellular potential for ECM synthesis, remodeling and repair |
| Appropriate heterogenicity, anisotropy and amount of ECM |
| Stable geometry but potential growth with patient |
| Absence of deleterious immunological and inflammatory processes |
| Resistance to calcification |
| Resistance to tissue overgrowth |
| Stable mechanical properties |
| Large effective orifice area |
| Prompt and complete closure |
| Resistance to infection |
| Chemically inertness and lack of hemolysis |
| Easy and permanent insertion |

### 2.2.5 Tissue Engineered Heart Valves

Presently, there are two major approaches towards making a tissue engineered heart valve (TEHV): a TEHV based on biological scaffolds and TEHVs based on synthetic scaffolds [91]. Biological scaffolds that have been used for TEHVs include decellularized xenograft valves, autologous collagen and autologous fibrin gel. The concept of a decellularized valve originated from the need

of removing the immunogenic cellular components while in the meantime, retaining the essential ECM proteins that can serve as an intrinsic template for cell attachment. The maintenance of mechanical properties depends on the decellularization technique used and the degree of cross-linking. In general, non-fixed acellular valve leaflets have been shown to promote remodeling of the prothesis by inducing neovascularization and recellularization by the host; and to possess sufficient mechanical integrity to withstand physiological conditions after implantation, even in the aortic position. Although acellular matrices as a scaffold material might be promising for future clinical use, important disadvantages include the infectious risk when using animal-derived materials, as well as immunological complications. In fact, the first clinical application of this concept in children showed rapid failure of heart valves due to severe foreign-body reactions associated with a 75% mortality rate. To create a TEHV that is completely autologous, thus would be free of the complications as seen in the acellular grafts, the scaffold material must degrade while autologous tissue is developing. Two types of biodegradable biomaterials have been used for TEHV so far: collagen and fibrin. Collagen as a scaffold material has been made into various forms: foam, gel, sheet or a sponge [116, 150]. The disadvantage of collagen is that it is very difficult to obtain from the patient, therefore nowadays most collagen are of animal origin, and since the degradation of collagen is very slow, scaffold materials will still be present at the time of implantation, thus presenting risks of immune response or inflammation. Fibrin [175, 68] can be obtained from the patient blood; therefore no immune responses are expected. Additionally, the degradation of fibrin can be controlled. As a scaffold material, fibrin has disadvantages including low diffusion capacity, and poor overall mechanical properties. Synthetic materials that have been tested for TEHV scaffold include polyglycolic acid (PGA), polylactic acid (PLA) and PLGA (PGA-PLA copolymer) which all belong to the aliphatic polyester family and polyhydroxyalkanoates (PHAs)[5, 134, 129]. The major limitation of the aliphatic polyesters are their thickness, initial stiffness and non-pliability, all of which making the fabrication of a trileaflet valve a difficult process. PHAs are thermoplastic and therefore can be easily molded into any desired shape; however, they do have a drawback of being degrading very slowly. Cells that have been used for TEHV include dermal fibroblasts and vascular-derived cells. Vascular cells have been shown to be superior to dermal fibroblasts, and constructs seeded with venous cells were superior to those seeded with arterial cells with respect to

collagen formation and mechanical stability. Although autologous venous cells represent the most promising cell source for clinical use in the near future, other cells including genetically engineered allogenic vascular cells and stem cells are also being explored to alleviate the potential shortage of venous cells.

Despite of the tremendous progress that has been made on TE products during the last few decades, a functional, stable TEHV that is competitive with current replacement valves is still a long way off. Critical issues in TEHV research include searching for the optimal scaffold material, the optimal cell source as well as the optimal *in vitro* preconditioning conditions . Preconditioning is required since the newly formed cell-scaffold composites are generally too weak to withstand the *in vivo* mechanical loading conditions. This is especially true for the aortic position. Indeed, various studies have shown that mechanical preconditioning can accelerate tissue maturation, resulting in higher mechanical strength as well as tissue morphology that is closer to the native counterparts [96, 62]. Currently, there are a number of systems patented for heart valves : the Pearson system [103] which simulates the *in vivo* conditions for heart valves, the Goldstein system [54] that imitates the dynamic flow environment of the aorta, the Dumont system [42] which mimics the circulation system and the Hoerstrup pulse duplicator [62]. Although these systems all have their own advantages in TEHV preconditioning, the optimal conditions still remain undetermined. For this purpose, a more thorough understanding is needed of the relationship between the mechanical and structural characteristics of a native valve and the stimuli (biological and mechanical) that are required to mimic these characteristics *in vitro*. In light of this, the goal of this thesis will be to determine the relationship between mechanical stimuli and biological properties of native aortic valve (see chapter III, specific aims); and the following section will present a review on the relationship between mechanical forces and cellular function, with pressure and shear stress being the two main mechanical factors considered.

## *2.3 Mechanical Forces and Cellular Function*

Heart valve leaflets experience pressure, shear stress, and bending during the cardiac cycle. On a cellular level, these forces are experienced as shear stress, tension, and compression. A growing body of evidence has demonstrated that mechanical forces can modify cell behavior. Although little

research regarding heart valve leaflets is available, studies have been conducted for a variety of cell systems. Several recent studies are reviewed here, focusing on a few cell types - endothelial cells, fibroblasts, chondrocytes, smooth muscle cells, and osteoblasts. Results obtained from a variety of species are presented, so the possibility of different results from different species should be kept in mind.

### 2.3.1 Pressure

Hydrostatic pressurization has been a frequently used modality for compression of cells, tissue or explant cultures, although very few studies have looked at pressure and valvular tissue or cells. The effects of pressure on valve leaflets properties will be one of the primary goals in this thesis. Following is a review of recent studies on the effects of pressure on cellular function. The majority of these studies have been conducted on vascular endothelial cells, smooth muscle cells, chondrocytes and osteoblasts. The following review will focus primarily on vascular cells, which are more relevant to valvular cells, but literature on other cells will be included when data on vascular cells are not available.

One of the first-observed effects of hydrostatic pressure on cellular function is on cell proliferation. Tokunaga et al [156] reported that exposure of human umbilical vein EC (HUVEC) to constant pressure of 80 mmHg resulted in significant increases in cell growth as compared to atmospheric controls; however, pressure higher than 80 (160 mmHg) appeared to have an inhibitory effect on EC proliferation. Consequently, researchers have worked with various cell types and pressure regimes. Also with HUVEC, Schwartz et al found that exposure to lower pressures ranging from 1.5 to 15 cm $H_2O$ (equivalent to 11 mmHg) stimulated proliferation of these cells, along with an increase of alpha V integrin. A similar phenomenon was also found with bovine aortic ECs (BAEC) as shown by the studies of Acevedo [4] and Sumpio [142]. In contrast, smooth muscle cells exposed to high pressure (120 mmHg and above) showed enhanced DNA synthesis [61, 160].

Similar effects on cell proliferation have also been observed in studies with cyclic pressure. Shin studied the responses of HUVECs under cyclic pressures of 60/20, 100/60 and 140/100 mmHg at 1 Hz for 24 hrs. Under low serum/growth factor conditions, exposure to 60/20 mmHg led to an increase in total cell density, apoptosis and DNA synthesis. Under normal serum conditions,

exposure to 60/20 or 100/60 mmHg led to an increase in DNA synthesis, but not apoptotic index. Under low serum, 140/100 mmHg led to reduced cell death, under normal serum, 140/100 mmHg led to reduced DNA synthesis. Vouyouka et al [160] exposed BAEC to 110/160 mmHg (cyclic, 1 Hz) for up to 5 days and compared them with constant pressure of 135 mmHg. They found that cell proliferation was significantly decreased under cyclic pressure but the decrease was similar to that under constant pressure. A subsequent conditioned media study indicated that ECs exposed to cyclic pressure, but not constant pressure, secrete an autocrine factor with inhibitory properties on cell proliferation. The effects of cyclic pressure are dependent on both mean pressure level and pulse frequency. The frequency-dependency of cyclic pressure was shown in the study by Nagatomi et al [95], in which they found that for the same duration of cyclic pressure exposure, a higher frequency (1.0 Hz) caused significant changes in osteoblasts proliferation, while a lower frequency (0.25 Hz) did not.

Another effect of pressure on cellular function is extracellular matrix (ECM) production. Evidence of pressure on ECM synthesis was mostly found in chondrocytes and osteoblasts, but not very often on vascular cells, possibly due to the differences in emphasis when it comes to studying these cells. Both in vivo and in vitro studies have shown that pressure affects ECM matrix production. Increased pressure causes higher collagen and proteoglycan synthesis in intervertebral disc cells [64], and increased collagen remodelling in non-human primate myocardium [164]. A study by Mizuno et al [88] showed significant increases (1.3 fold) in GAG synthesis in bovine articular chondrocytes grown in collagen sponge after exposure to hydrostatic pressure of 2.8 MPa for 15 days. Ishihara et al studied the effects of hydrostatic pressure on matrix synthesis in the intervertbral disk. Their results showed that application of hydrostatic pressure in the range of 1-7.5 MPa for only 20 s was able to stimulate matrix synthesis in bovine caudal and human lumbar interverbral disks. Increasing pressure to 10 MPa led to inhibition on matrix synthesis.

Other effects of pressure on cellular function include changes in cell morphology and cytoskeleton, endothelial barrier function, as well as induction of matrix-metalloproteinase (MMPs). Cell alignment was generally not affected by pressure. Using confocal imaging, Salwen et al [119] studied bovine pulmonary artery ECs exposed to hydrostatic pressures of 1.5, 5 and 10 cm $H_2O$ for 7 days. Results showed cell bilayering after exposure to 1.5 and 5 and trilayering after exposure to

10 cm $H_2O$ for 7 days. F-actin filaments reorganized into centrally located, parallel, stress fibers in confluent cells, into peripheral bands in subconfluent, multilayered cells, and into multilayers in the plane perpendicular to the applied force. One of the earliest studies on the effects of pressure on MMPs expression and activity was conducted by Chesler et al [22]. Porcine carotid arteries were mounted onto an in vitro organ culture system and exposed to a steady laminar shear stress of 15 dyne/cm$^2$ with a transmural pressure of 100 or 200 mmHg for 24 and 48 hrs. Results showed enhanced MMP-2 and MMP-9 activity in response to pressure, but not to shear stress. A more recent study by Lehoux et al [77] examined a wide range of pressures including low (10 mmHg), intermediate (80 mmHg) and high (150 mmHg), on MMPs activity in mice carotid arteries maintained in organ culture for up to 3 days. At low pressure, only MMP-2 activity was enhanced ($168 \pm 13\%$, $p < 0.05$) as compared with 80 mmHg, whereas at high pressure (150 mmHg), both MMP-2 and MMP-9 activity was increased ($182 \pm 32\%$, $p < 0.05$, and $194 \pm 21\%$, $p < 0.01$, respectively). The involvement of MMPs in pressure-induced cellular responses has also been observed from *in vivo* studies. Camp et al [19] studied the matrix accumulation mechanism in spontaneously hypertensive rats. Their results indicated that increased MMP-2 and MMP-9 activity contributes to hypertensive remodelling. On the other hand, a clinical study by Zervoudaki et al [178] found that plasma concentrations of active MMP-2 and MMP-9 are depressed in patients with essential hypertension.

From these studies, it is apparent that pressure exerts its effects in a complex manner. Influencing factors include differences between constant and cyclic pressure, cyclic pressure frequency and magnitude, as well as cell types and species. Although the mechanism by which hydrostatic pressure affects cells are not fully understood, there is evidence showing that factors including alpha V integrin, basic FGF, and VEGF-C are involved in these processes, while TGF-$\beta$ and IL-1 have been excluded. Using DNA microarray, Shin et al [127] investigated the transcription of genes in HUVEC under cyclic pressure. Cyclic pressure selectively affected the transcription of 14 genes that included a set of mechanosensitive proteins involved in hemostasis (tissue plaminogen activator), cell adhesion (intergrin-alpha 2) and cell signaling (Rho B, cytosolic phospholipase A2), as well as a unique subset of cyclic pressure sensitive genes such as endothelial growth factor (VEGF-C) and TGF-$\beta$ 2. Another recent study [66] showed that nitric oxide (NO) might be

**Table 2:** Summary of the effects of pressure on cellular function

| Cellular function | Pressure |
|---|---|
| **Proliferation** | |
| HUVEC/BAEC | ↑ at low pressure (<100mmHg),↓ at high pressure |
| SMC | ↑ and ↑ ERKS at high pressure |
| Osteoblasts | ↓ with cyclic pressure at 1 Hz, but not 0.25 Hz |
| EC-denuded Rabbit artery | ↑ at 80 mmHg |
| Dermal fibroblasts | ↓ at both 60 and 120 mmHg |
| **ECM production** | |
| Intact rabbit artery | ↑ at 150 mmHg, but not at 80 mmHg |
| Chondrocytes | GAG synthesis ↑ |
| Dermal fibroblasts | ↑ fibronectin |
| Intervertebral Cells | Collagen & proteoglycans synthesis ↑ |
| Intervertebral disk | ↑ at 1-7.5 MPa, but ↓ at 10 MPa |
| **MMPs activity** | |
| Porcine carotid artery | MMP-2, MMP-9 activity ↑ at 200 mmHg |
| Mice carotid artery | MMP-2 ↑ at 10 mmHg, MMP-2, MMP-9 activity ↑ at 150 mmHg |
| SHR rat | ↑ MMP-2, MMP-9 activity, ↑ TIMP-4 activity |
| Hypertensive patients | MMP-2, MMP-9 ↓ during essential hypertension |

involved in the pressure-induced proliferation of SMCs. In this study, human aortic smooth muscle cells (HASMC) were exposed to 160 mmHg pressure for 3 hours, with or without the addition of an NO-releasing drug, Nipradilol (3,4-dihydro-8-(2-hydroxy-3-isopropylaminoproxy)-3-nitroxy-2H-1-benzopyran) ($10^{-6}$M). Three hours under high pressure resulted in an approximately 380% increase in cell proliferation compared to non-pressurized controls. Nipradilol addition resulted in approximately 40% reduction in cell proliferation compared to that shown by pressurized HASMC as a vehicle control. Three hours of 160-mmHg pressure resulted in a 25% increase in the amount of activated extracellular signal-regulated kinase (ERKs). Nipradilol presence led to approximately 26% reduction in activated ERKs.

### 2.3.2 Shear Stress

Due to its apparent significance to atherosclerosis, the effects of shear stress on vascular endothelial cells have been extensively studied. One of the earliest recognized effects of shear stress is the elongation and realignment of endothelial cells. Cultured endothelial cells exposed to steady laminar shear stress elongate in the direction of flow [37, 67]. Actin stress fibers in the cytoskeleton also

align with flow and increase in number with increasing shear stress [173]. Recent studies [97] show that morphological changes of EC under shear were driven by the assembly and reorientation of stress fibers. The authors imposed physiological levels of shear stress on cultured endothelium for up to 96 hours and then permeabilized the cells and exposed them briefly to fluorescently labeled monomeric actin at various time points to assess actin assembly. Alternatively, monomeric actin was microinjected into cells to allow continuous monitoring of actin distribution. Actin assembly occurred primarily at the ends of stress fibers, which simultaneously reoriented to the shear axis, frequently fused with neighboring stress fibers, and ultimately drove the poles of the cells in the upstream and/or downstream directions. Actin polymerization occurred where stress fibers inserted into focal adhesion complexes, but usually only at one end of the stress fiber. Neither the upstream nor downstream focal adhesion complex was preferred. Changes in actin organization were accompanied by translocation and remodeling of cell-substrate adhesion complexes and transient formation of punctate cell-cell adheren junctions.

Another effect of shear stress on ECs is on migration. Shiu et al [130] investigated the effect of shear stress on the migration speed of individual endothelial cells on fibronectin-coated surfaces. Under static conditions, cell migration speed had a bell-shaped relationship with fibronectin concentration. Shear stress significantly increased the migration speed at all fibronectin concentrations tested and shifted the bell-shaped curve upwards. Shear stress also induced the activation of Rho GTPase and increased the traction force exerted by endothelial cells on the underlying substrate, both at the leading edge and the rear. The inhibition of a Rho-associated kinase, p160ROCK, decreased the traction force and migration speed under both static and shear conditions and eliminated the shear-enhancement of migration speed.

Some effects of steady laminar shear stress on the synthetic activity of cultured endothelial cells are summarized in the following table. Shear stress affects the expression of proteins that control many opposing functions, such as vasodilation and vasoconstriction, thrombo-resistance and thrombogenesis, and normal cell morphology and atherosclerosis. Changes in the production of these proteins are regulated at the level of the gene, perhaps through a shear-stress responsive element [111].

**Table 3:** Effects of shear stress on cellular function

| **Cellular Function** | **Shear stress** |
|---|---|
| **Vasoactivity** | |
| Endothelin -1 | ↑ or ↓ |
| Nitric Oxide | ↑ |
| Nitric Oxide Synthesase | ↑ or not changed |
| inducible Nitric Oxide Synthesase | ↑ |
| Renin | ↑ |
| Histamine | ↑ |
| **Cytokines** | |
| Transforming growth factor $\beta$-1 | ↑ or unchanged |
| Platelet derived growth factor (PDGF) | ↑ or ↓ or unchanged |
| Basic fibroblast growth factor | ↑ or unchanged |
| Heparin-binding epidermal growth factor (HB-EGF) | ↑ |
| Erythropoietin | ↓ |
| **Proto-Oncogenes / Transcription factors** | |
| c-jun | ↑ |
| c-fos | ↑ |
| Nuclear factor | ↑ |
| **Chemoattractants / Adhesion molecules** | |
| Intracellular adhesion molecule-1 (ICAM-1) | ↑ |
| Vascular cell adhesion molecule-1 (VCAM-1) | ↓ |
| Endothelial leukocyte adhesion molecule-1 (ELAM-1) | ↓ |
| Monocyte chemotactic protein-1 (MCP-1) | ↓ |
| **Antioxidants** | |
| Mn-superoxide dismutase (SOD) | ↑ or unchanged |
| Cu/Zn-SOD | ↑ |

Transduction of shear stress into gene regulation is now an active area of research and was recently reviewed by Papadaki and Eskin [101]. The cell membrane contains many integral receptors, adhesion molecules, and ion channels which may be directly activated or deactivated by shear stress. These integral receptors and proteins can also trigger secondary events within the cell itself. In addition to such secondary messaging, more direct signal transduction may occur. Studies reviewed by Patrick et al. [102] have shown that actin filaments are required for signal transduction. These filaments are anchored in the cell membrane and are linked to the nuclear membrane. Thus, the tension on these filaments may signal directly the nucleus to elicit a specific cellular response.

In addition to these effects on endothelial cells, shear stress also affects fibroblasts, and smooth muscle cells. Vanhee [158] exposed 3T3 fibroblasts, an immortalized cell line, to a shear stress of 20

dyne/cm$^2$ using a parallel plate flow chamber. The cells did not align with the direction of flow, in contrast to endothelial cells. Fibroblast proliferation, determined from $^3$H-thymidine incorporation, was decreased under shear stress compared to static conditions. Apenberg et al [6] demonstrated that shear stress induces apoptosis in vascular SMC via an autocrine Fas/FasL pathway. Wang et al [162] studied the effects of shear stress on P2 receptors using human umbilical veins with intact endothelium. Results show that in SMCs, high shear stress (25 dyne/cm$^2$) decreased P2X1 receptors, whereas P2Y2 and P2Y6 receptors were upregulated. Decreased expression of the contractile P2X1 receptor could lead to reduced vascular tonus and increased blood flow. Because P2Y2 and P2Y6 receptors stimulate growth and migration of SMCs, increased expression of these receptors could promote vascular remodeling induced by shear stress. The pattern of upregulation of mitogenic P2Y receptors and downregulation of contractile P2X1 receptors is similar to changes seen in the phenotypic shift from contractile to synthetic SMCs.

Shear stress has also been shown to be able to regulate MMPs. Magid et al [82] demonstrated that oscillatory but not unidirectional shear significantly increases MMP-9 mRNA as well as secretion of the MMP-9 protein ($p < 0.05$) in cultured ECs. In contrast, cell-associated protein levels of Tissue Inhibitor of MMP 1 (TIMP-1), an inhibitor of MMP-9, are insensitive to the shear regimen. The activity of the full MMP-9 promoter is 3-fold higher ($p < 0.05$) in unidirectional shear compared with static conditions, and the activity is further increased approximately 10-fold by oscillatory shear ($p < 0.01$) over unidirectional flow. These effects are realized via a shear-sensitive c-myc binding site at -152 in the MMP-9 promoter.

Not only are cells are responsive to shear stress, they are also able to distinguish among and respond differently to different types of shear stress. As the Magid study showed above, unidirectional steady shear and oscillatory shear seem to have differential effects on cultured ECs. In addition, oscillatory shear and pulsatile shear have also been shown to have different effects on cellular function. Hwang et al [65] studied the effects of pulsatile (mean shear($\tau$(ave)): 25 dyne/cm$^2$) vs. oscillatory shear stress(mean shear($\tau$(ave)): 0 dyne/cm$^2$) on NADPH oxidase subunit expression. Under oscillatory shear, gp91phox mRNA expression was upregulated by 2.9$\pm$0.3-fold, and its homologue, Nox4, by 3.9$\pm$0.9-fold ($p<0.05$, n=4), with a corresponding increase in O2-* production rate. In contrast, pulsatile flow downregulated both gp91phox and Nox4 mRNA expression

(by 1.8±0.2-fold and 3.0±0.12-fold, respectively), with an accompanying reduction in O2-* production.

Compared with vascular cells, studies on the effects of shear stress on valvular cells are very few. Using a modified parallel plate system, Weston et al [169] studied the effects of steady laminar shear stress (1,6, and 22 dyne/cm$^2$) on the biosynthetic activity of porcine aortic valve leaflets. Results show that protein, GAG, and DNA synthesis increased during static incubation but remained at basal levels after exposure to flow. The alpha-smooth muscle (alpha-SM) actin distribution observed in fresh leaflets was proportionately decreased after exposure to antibiotics and not recovered by either static incubation or exposure to flow. A more recent study by Butcher et al [18] compared porcine aortic EC and porcine aortic valvular ECs under 20 dynes/cm$^2$ steady laminar shear stress or static incubation for 48 hours. The aortic valve ECs were observed to align perpendicular to flow, in contrast to the aortic ECs aligned parallel to flow. Valvular EC alignment was dependent on Rho-kinase signaling, whereas vascular EC alignment was dependent on both Rho-kinase and phosphatidylinositol 3-kinase signal pathways. The effects of shear stress will be one of the focuses of this thesis (see specific aims, chapter III).

### 2.3.3 Stretch

The effects of stretch have been considered with several cell types. Smooth muscle cells, which reside in the medial layer of blood vessels, are exposed to cyclic stretch through pulsatile changes in blood pressure. Therefore, the effects of stretch on cultured SMCs has been extensively studied and recently reviewed by Williams [170]. When exposed to a physiological strain, SMCs retain their native contractile phenotype, with abundant contractile proteins and little synthetic activity. In a static system, the absence of tensile forces gives rise to a synthetic phenotype of SMCs. These cultures are proliferative, with increased biosynthetic capability and reduced contractile proteins. Conversely, in a culture with supraphysiologic tensile forces, an intermediate phenotype exists, with abundant contractile proteins and high synthetic activity. Cells are in a proliferative mode, which would lead to hypertrophy *in vivo*. Although heart valves contain few smooth muscle cells, these results are significant because the myofibroblasts in the leaflet possess certain smooth muscle characteristics that may be modulated in a similar manner. Endothelial cells lining the vessel lumen

are also exposed to cyclic strains *in vivo* and have thus been examined in culture. Cyclic uniaxial stretching of an endothelial cell monolayer causes the cells to align perpendicular to the applied stretch [67]. Cyclic stretching also affects protein secretion, but not in the same manner as shear stress [85, 24]. However, the transduction of this force to the nuclear level appears to involve the same secondary messenger pathways and regulated genes [24]. Similar studies have also been performed on cultured fibroblasts, the cell type found in the adventitia of blood vessels. Buck [16] cultured fibroblasts onto a silicone substratum, which was uniaxially stretched and released at 4 cycles/min (0.07 Hz). The cells aligned perpendicular to the axis of stretching. Similar alignment was observed by Rivas-Gotz et al. [113] after 10% stretching at 10 cycles/min (0.17 Hz). They also reported that proliferation was decreased by cyclic stretching. A different alignment pattern was observed for sustained, not cyclic, stretching of neonatal cardiac fibroblasts [157]. In their model, cells aligned parallel to the direction of stretch. They also reported increased content of noncollagenous proteins, myosin heavy chain, and DNA. Collagen synthesis by cyclically stretched cardiac fibroblasts was examined by Carver et al. [21]. Collagen type III mRNA expression and synthesis increased, but collagen type I expression was unaffected. Chondrocytes have also been studied. Cyclic stretch causes increased GAG synthesis compared to static controls [75, 38].

Mechanical stretch was also found to affect MMPs in cultured cells. The study by Wang et al [162] investigated HUVECs under cyclic stretch (20% of maximum elongation, at 60 cycles/min) for up to 24 hours. Results show that cyclical stretch significantly increased protein synthesis and mRNA expression for MMP-14 and -2 from 2 to 24 h. MMP-2 activity (zymography) was induced by cyclical stretch and was attenuated by TNF-alpha monoclonal antibody and SP600125. Asanuma et al [7] studied the effect of physiological strain levels (5%) of stationary or cyclical (1 Hz) uniaxial strain on the MMPs expression and activity in cultured human vascular SMCs. Stationary strain significantly increased MMP-2 mRNA levels at all time points, whereas cyclic strain decreased it after 48 h. Both secreted and cell-associated pro-MMP-2 levels were increased by stationary stretch at all times ($p < 0.01$), whereas cyclic strain decreased secreted levels after 48 h ($p < 0.02$). MMP-9 mRNA levels and pro-MMP-9 protein were increased after 48 h of stationary stretch ($p < 0.01$) compared with both no strain and cyclic stretch.

Sotoudeh et al. [137] suggested that the alignment of certain cell types upon cyclic uniaxial

stretching is due to deformations in the substrata. In uniaxial stretching devices, one end of the material is anchored, while the other end is pulled at a certain frequency. Although displacement is uniaxial, the stretching results in a biaxial strain distribution within the material. Compressive strains are induced perpendicular to the direction of stretching, corresponding to the alignment patterns observed for endothelial cells and fibroblasts. Sotoudeh et al. developed a device that imposes an equibiaxial strain, exposing all cells on the material to the same stress field. Their preliminary results showed no morphological changes in endothelial cells after stretching with a 20% area change at 1 Hz. Synthetic responses to equibiaxial strain have not yet been reported.

Studies on the effects of stretch on valvular cells have just started, but have already produced exciting results. Ku et al [72] studied the effects of cyclic stretch (0-20%) on valvular ICs for up to 5 days. Their results showed upregulation of collagen synthesis by valve ICs after exposure to stretch; and a 14% strain showed the highest increase in both intracellular and secreted collagen production.

### 2.3.4 EC-SMC Interaction and Hemodynamic Forces

The interactions between endothelial cells and smooth muscle cells have been a well-established fact and there are abundant evidences in literature. Under static co-culture conditions, ECs have been shown to stimulate SMC proliferation, modulate SMC morphology and organizational growth pattern [104], depress SMC contractile potential [161], inhibit SMC migration and collagen production [105] mainly through the release of growth factors. On the other hand, co-cultured SMCs can induce EC gene expression of intercellular adhesion molecule-1 (ICAM-1), vascular adhesion molecule-1 (VCAM-1), and E-selectin, while attenuating EC gene expression of endothelial nitric oxide synthase (eNOS) [39]. Recent studies indicate that hemodynamic forces can alter these interactions. Chiu et al [25, 26] demonstrated that coculture with SMCs under static condition induced EC gene expressions of ICAM-1, VCAM-1, E-selectin, as well as growth-related oncogene-alpha and monocyte chemotactic protein-1, and shear stress was found to abolish these SMC-induced gene expressions. These EC responses under static and shear conditions were not observed in the absence of close communication between ECs and SMCs, and they were also not observed when ECs were cocultured with fibroblasts instead of SMCs. Using a novel parallel-plate flow device in

which only the EC side of the co-culture to shear stress, Nackman [94] studied the regulatory effects of ECs on SMCs under 24 hours' exposure to shear. It's known that under static culture, ECs can stimulate the proliferation of SMCs. Their results show that in the presence of shear stress, SMC proliferation decreased significantly from 362 $\pm$ 65 cpm/microgram DNA (control, mean $\pm$ SEM) to 68 $\pm$ 43 cpm/microgram (1 dyne/cm$^2$) and 99 $\pm$ 18 cpm/microgram (10 dynes/cm$^2$)($p < 0.05$). EC proliferation after flow decreased as compared with no-flow controls 71 $\pm$ 15 cpm/micrograms DNA (control, mean $\pm$ SEM) to 29 $\pm$ 5 cpm/microgram (1 dyne/cm$^2$) and 21 $\pm$ 4 cpm/microgram (10 dynes/cm$^2$)($p < 0.05$). In addition to shear stress, hydrostatic pressure has also been shown to be able to alternate the EC-SMC interaction. A study by Vouyouka et al [161] compared rat aortic SMC proliferation and contractility (indexed by dihydropyridine (DHP)-receptor level) in independent and EC coculture under ambient and high pressure (130 mmHg). Results showed that ECs suppressed SMC proliferation on day 1 of coculture in both atmospheric and high pressure (20% inhibition vs independent culture, $p \leq 0.05$). By day 3, cocultured SMCs under atmospheric pressure displayed no EC-mediated inhibition, and at day 5, atmospheric cocultured SMCs revealed statistically significant enhanced proliferation as compared with SMCs in independent cultures. However, cocultured SMCs exposed to 130 mmHg pressure displayed sustained sensitivity to EC growth inhibition at both days 3 and 5 of the experiment. Coculture decreased SMC DHP-receptor levels under atmospheric pressure. However, this effect was abolished in cocultures exposed to high pressure. This interaction issue will be addressed in the second aim of this study (see specific aims, chapter III) by examining valvular responses to applied shear stress with or without the presence of endothelium.

## *2.4 Rationale for Thesis Research*

As mentioned earlier in this chapter, the aortic valve is exposed to a harsh and diverse mechanical environment and there are constant interactions between the AV and the surrounding hemodynamics. On one hand, alterations in the AV material properties or structure will lead to changes in the surrounding hemodynamics; on the other hand, changes in hemodynamics have been shown to cause tissue remodeling in the AV. However, the cellular and molecular mechanisms behind these relationships still remain largely unknown. A fundamental understanding of these mechanisms is

necessary for the elucidation of aortic valve biology and pathophysiology, as well as critical for the development of a TEHV. Therefore, the current thesis will aim at determining the effects of two independent mechanical factors: pressure and shear stress, on the biological properties of porcine aortic valve leaflets. The two factors are to be studied separately instead of being combined so as to pinpoint the effects of each individual factor without interference from the other. Native valve tissue is chosen since it retains both the cells and the native ECM, providing a better representation of native valves than cell culture models and an excellent three-dimensional model for TEHVs.

# CHAPTER III

# HYPOTHESIS AND SPECIFIC AIMS

Cardiac valves are highly sophisticated dynamic structures that undergo constant tissue renewal and interact closely with their hemodynamic environment. On one hand, altered hemodynamics are known to induce biological changes which ultimately result in changed material and mechanical properties of the valve. On the other hand, the alterations in valve material and mechanical properties will lead to abnormal hemodynamic function. By far, the cellular and molecular events associated with these interactions remain largely unknown; so is the role of each individual mechanical factor in these processes. Elucidating the relationship between mechanical loading conditions and aortic valve biology will not only provide insights into valve pathology but also guidance for the development of a tissue engineered heart valve.

This thesis is intended to determine the mechano-biological relationships in heart valves by using an *in vitro* tissue culture model. **The overall hypothesis is that mechanical factors, such as pressure and shear stress, when applied independently *in vitro*, are able to induce changes in aortic valve biology.** Native porcine AV leaflets are chosen to be the objects of study due to their anatomical similarities to human AVs as well as their abundant supply. The effects of pressure and shear stress are to be studied separately. Valve biology is to be assessed by collagen synthesis, sGAG synthesis, tissue morphology, cell phenotype and activities of matrix metalloproteinase (MMPs) and cathepsins (cysteine-dependent lysosomal proteases).

## *3.1 Specific Aim I: Determine the Influence of Pressure on the Biological Properties of Porcine AV Leaflets*

### 3.1.1 The Influence of Constant Static Pressure

Under normal conditions, the AV leaflets undergo an average pressure load of 100 mm Hg during diastole. This value can go up to around 200 mmHg in patients with severe hypertension. Consequently, constant static pressures of 100 mmHg (physiological), 140 mmHg (hypertensive), and

170 mmHg (severe hypertensive) will be studied to cover both the physiological and pathophysiological range. This will enable us to determine the effects of pressure magnitude alone on the biological properties of the valve. For this purpose, an *in vitro* pressure system will be developed to generate the desired pressure levels. The system will be validated to ensure that pressure is the sole significant affecting factor, and the viability of the tissue is maintained. Native porcine AV leaflets will be exposed to each pressure level for a period of 48 hours, with control leaflets cultured under atmospheric pressure. Since the pressure loading is mainly borne by the collagen-rich extracellular matrix, the endpoints of this study will include collagen synthesis, sGAG synthesis, DNA synthesis/cell proliferation, changes in cell phenotype ($\alpha$-SM actin), tissue morphology and changes in MMPs/Catepsins activity. Methodologies will include radiolabeling (matrix synthesis), immunohistochemstry (cell phenotype, MMPs/cathepsins), western blotting ($\alpha$-SM actin, MMPs/cathepsins), gelatin zymography (MMPs/cathepsins) and general histology (tissue morphology).

### 3.1.2 The Influence of of Cyclic Pressure

The actual pressure load on the AV is dynamic and changes during different points of the cardiac cycle. Under normal conditions, the pressure is 80/120 mmHg with a pulse rate of 1.167 Hz (based on a normal heart rate of 70 beats per minute (bpm)). Therefore, a cyclic pressure system will be a better representation of the *in vivo* pressure loading conditions and provide more insights into the *in vivo* pressure effects. Various studies in the literature have shown the effects of cyclic pressure on cellular function are dependent on both the frequency and magnitude of the applied pressure. Therefore, the influence of both parameters will be investigated in this study. First of all, a system will be developed to generate cyclic pressure of various magnitudes and frequencies. The system will then be validated for both mechanical performance and biological performance. Native porcine AV leaflets will be exposed to each pressure condition for 48 hours, with leaflets cultured under atmospheric pressure as controls.

(1) Pressure magnitude effect: Cyclic pressure at normal heart rate (70 bpm/1.167 Hz), with pressure magnitudes of 80-120 mmHg, 120-160 mmHg, and 150-190 mmHg;

(2) Frequency effect: Cyclic pressure with frequencies of low (30 bpm/0.5 Hz), normal (70 bpm/1.167 Hz), and high (120 bpm/2 Hz) with pressure magnitude of 80-120 mmHg;

(3) Extreme pressure conditions (High pressure magnitude, high frequency): Cyclic pressure with magnitude of 150-190 mmHg, and frequency of 2 Hz.

The biological endpoints will include collagen synthesis, sGAG synthesis, DNA synthesis/cell proliferation, cell phenotypical changes ($\alpha$-SM actin), tissue morphology and changes in MMP/Cathepsin activity. Methodologies will include radiolabeling (matrix synthesis), immunohistochemstry (cell phenotype, MMPs/cathepsins), western blotting ($\alpha$-SM actin, MMPs/cathepsins), gelatin zymography (MMPs/cathepsins) and general histology (tissue morphology).

## *3.2 Specific Aim II: Determine the Influence of Shear Stress on the Biological Properties of Porcine AV Leaflets*

### 3.2.1 The Influence of Shear Stress on Leaflets with Intact Endothelium

Under normal flow conditions (cardiac output of 5 L/min), average shear stress upon the AV ventricular surface is estimated to be within the range of 12-40 dyne/cm$^2$ (mean 26.4 $\pm$ 7 dyne/cm$^2$) during systole, with a peak value of 80-100 dyne/cm$^2$. This shear stress is sensed by the endothelial cells on the ventricular surface and transmitted to the interstitial cells entrapped in the extracellular matrix. The focus of this sub-aim is on the effects of shear on leaflets with an intact endothelium. For this purpose, native porcine AV leaflets are to be carefully handled so as to preserve the endothelium, the presence of which is verified by scanning electron microscopy (SEM). Steady laminar shear stresses of 1, 9, 25, 40 and 80 dyne/cm$^2$ will be examined using an in-house designed modified parallel plate chamber. Native porcine AV leaflets, with the ventricularis surface facing flow, will be mounted onto the plate and oriented in such a way that flow direction is from the base to the free edge. The flow exposure will last for 48 hours and the biological endpoints will include endothelial cell retention and alignment, collagen synthesis, sGAG content, cell phenotypical changes, tissue morphology and changes in MMP/Cathepsin activity. Methodologies will include SEM (endothelial retention and alignment), colorimetric biochemical assays (matrix synthesis and content), immunohistochemstry (cell phenotype, MMPs/cathepsins), western blotting ($\alpha$-SM actin, MMPs/cathepsins), gelatin zymography (MMPs/cathepsins) and general histology (tissue morphology).

### 3.2.2 Effects of Shear Stress on Leaflets without Endothelium

It is well established that vascular ECs co-cultured with SMCs can affect the properties of SMCs through the release of paracrine factors and vice versa. The first sub-aim of specific aim II focused on the effects of shear stress on an intact leaflet, which is like a co-culture model of ECs and ICs within their native extracellular matrix. It will be interesting to know how the ICs respond to shear without the presence of ECs. Hence, the focus of this section will be on the effects of shear stress on leaflets with the endothelium removed. Thus, the observed biological responses will be derived solely from the ICs. This study will provide some insights onto the interaction between valvular ECs and ICs and also serve as a model for endothelial injury. Native porcine AV leaflets are denuded by gently rubbing the ventricular surface. The efficacy of this denudation is examined by using SEM and routine Hematoxylin and Eosin staining. Afterwards, the tissue will be exposed to steady laminar shear of 1, 9, 25, 40 and 80 dyne/cm$^2$ for 48 hours, with leaflets under static incubation as controls. Tissue mounting and orientation is the same as in the first sub-aim. The endpoints of this study will include collagen synthesis, sGAG content, cell phenotype changes, tissue morphology and changes in MMP/cathepsin activity. Methodologies will include colorimetric biochemical assays (matrix synthesis), immunohistochemstry (cell phenotype, MMPs/cathepsins), western blotting ($\alpha$-SM actin, MMPs/cathepsins), gelatin zymography (MMPs/cathepsins) and general histology (tissue morphology).

## *3.3 Summary of Specific Aims*

The hypothesis of this research is that exposure to applied pressure or steady shear stress *in vitro* will induce changes in aortic valve biology. To test this hypothesis two specific aims regarding the relationship between pressure or shear stress and valve biology will be examined: (1) To examine the effects of pressure, including both constant and cyclic pressure, on valve biology; (2) To examine the effects of shear stress on valve biology and the role of endothelium in this process. Specific aim I addresses the effects of pressure (both physiological and pathophysiological), including the design of a pressure system and the biological responses of porcine AV leaflets under various pressure conditions. Specific aim II focuses on the effects of steady laminar shear stress ranging from close to zero to peak values, with or without the presence of the endothelium. Responses observed in

these studies with native leaflets may help predict the responses of cells in tissue engineered leaflets grown under similar conditions.

# CHAPTER IV

# METHODS

## *4.1 Tissue Procurement*

Fresh (warm ischemia less than 30 minutes) porcine aortic valves were obtained from a local slaughterhouse (Holifield Farm, Covington, GA) and transported back to the laboratory in ice-cold sterile Dulbecco's Phosphate Buffered Saline (DPBS, Sigma, D5652, St Louis, MO). Upon arrival at the laboratory, the leaflets were dissected from the aortic root and washed in sterile DPBS 3 times. Each leaflet was then trimmed to leave only a rectangular portion in the central belly area. This rectangular piece (8 x 10 mm) was further cut into two symmetric pieces at the mid-line. One piece was exposed to pressure or steady shear stress, the other piece was cultured at atmospheric condition to serve as control. Both pieces of tissue were incubated in Dulbecco's Modified Eagle Media (DMEM, Sigma D5648) at 37$^{o}$C overnight prior to experiment set-up. This procedure is illustrated by the following diagram (Fig.8).

## *4.2 Pressure Study Methods*

### 4.2.1 System Development and Validation

#### *4.2.1.1 Design Criteria*

Under physiological conditions, the aortic valve is exposed to an averaged pressure of about 100 mmHg. This value can rise to 200 mmHg in patients suffering from severe hypertension. This pressure load of the AV is cyclic in nature with a frequency of 1.167 Hz (equivalent to a heart rate of 70 beats per minute). It produces a dual-effect on the valve leaflets: normal stresses caused by the hydrostatic part of the pressure, and cyclic stretch which is caused by the dynamic nature of the pressure load. The goal of this project was to investigate the isolated effects of hydrostatic pressure on valve biology.

The first criterion of the system is that it shall be able to generate a wide pressure range which covers the 100-200 mmHg range at various frequencies. Secondly, this system needs to be compact;

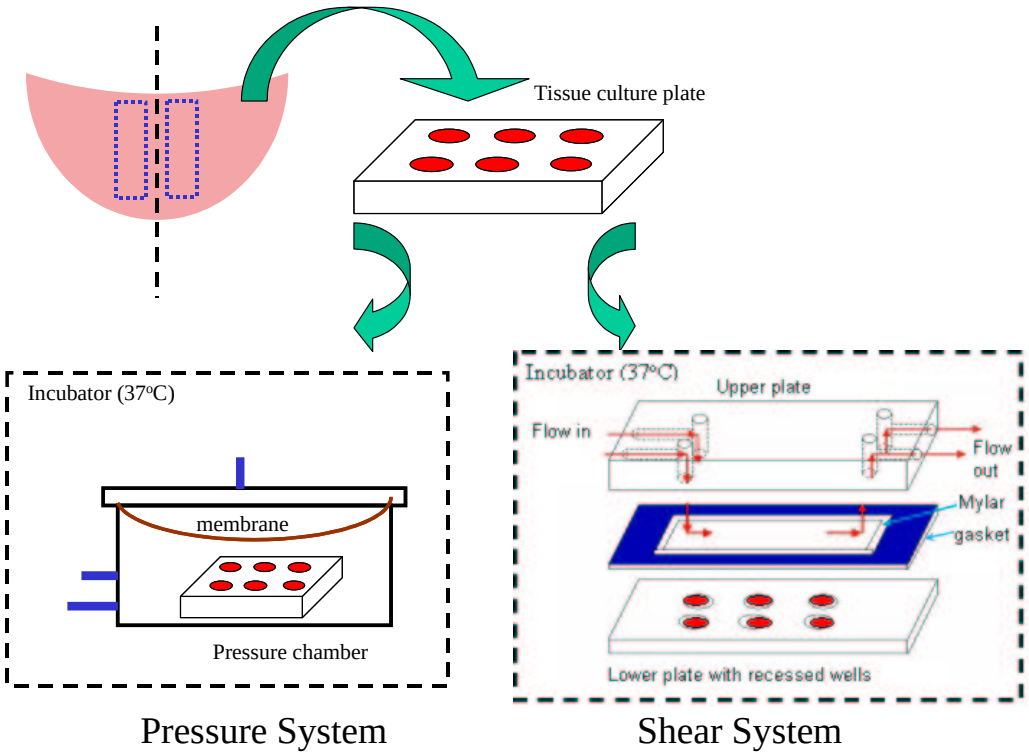


**Figure 8:** Tissue procurement procedure: Porcine aortic valve leaflets were dissected from the aortic root and two symmetric pieces around the middle line were cut out and placed in a tissue culture plate overnight. Afterwards, one piece was placed in the pressure system (or shear stress system), the other piece was incubated at atmospheric pressure to serve as control

ideally it shall fit in an incubator to allow for control of temperature and a 5% $CO_2$ humidified atmosphere. The height of a 10 cubic feet incubator (Fisher Scientific, 11-687-810) is 89 cm; therefore this system should be no higher than 89cm. Thirdly, sterilization of the components in the system should be straightforward. Finally, it should be cost-effective.

#### *4.2.1.2 Development*

Currently, there are two major modalities for studying the effects of hydrostatic pressure *in vitro*: the liquid column method and the gas compression method [15]. The liquid column method generates pressure by creating a column of culture media over the cultured cells or tissue. This method is not suitable for the current study due to the height of the column required to produce the desired pressure range (1.36 m for 100 mmHg, and 2.72 m for 200 mmHg). The gas compression method was chosen due to the wide pressure range it generates and also the easiness for implementation. The only drawback of this system is the potential secondary effects caused increased partial pressures in

$CO_2$ and $O_2$. However, according to Tanck et al [148], these changes are confined to a superficial layer (50$\mu$m thick) of the culture media under cyclic pressure conditions, therefore it will not affect the tissue which lies about 1.5 cm below. To ensure that these effects are indeed negligible, pH of the medium and the oxidization status of proteins will be checked after the experiment.

The final system (Fig.9) consists of a polycarbonate chamber (J.M Machining, Lawrenceville, GA), a 1/16 " thick silicone membrane (McMaster Carr, 9010K122), a pulse generator system, a 5% $CO_2$ air tank, a compressed air tank, and the pressure monitoring system. Components that need to be sterile (pressure chamber and the silicone membrane) can be sterilized in the autoclave. The silicone membrane separated the chamber into two compartments: the lower compartment which was connected to the $CO_2$ tank and the upper compartment connected to the compressed air supply. The pressure in the lower compartment was assumed to be equal to that in the upper compartment once the membrane had reached an equilibrium position. Compressed air flow was regulated by a solenoid valve attached to a pulse generator system. Cyclic air flow generates periodic expanding and relaxing of the silicone membrane, thus generating a cyclic ambient pressure in the lower compartment of the chamber. Porcine aortic valve leaflets were immersed in a media-containing tissue culture plate placed in the lower part of the pressure chamber. Therefore, the tissues were exposed to a cyclic ambient pressure. Various pressure magnitudes (140, 170 mmHg) and amplitudes (20, 40, 60 mmHg) can be obtained easily by adjusting the compressed air flow and the $CO_2$ rich air flow. Pulse frequency can also be adjusted by changing the control parameters in the pulse generator (e.g., 0.5 Hz, 1.167 Hz and 2 Hz).

The pulse generator system was composed of a computer, the pulse generator box and a solenoid valve. The solenoid valve was connected to the compressed air tank on one end, and to the pressure chamber on the other end. A trigger (a program controlling the pulse frequency and the loading/unloading ratio) from the computer was imposed on the generator, which controlled the opening and closing of the solenoid valve, thereby generating a controlled cyclic compressed air flow into the upper compartment of the pressure chamber. For studies with normal frequency (1.167Hz), the total cycle time in the trigger was set to be 857 ms (based on a heart rate of 70 bpm), with a loading/unloading ratio of 2:1 (simulating the physiological diastolic:systolic ratio). The total cycle times for 0.5 Hz and 2 Hz studies were 2 s and 500 ms respectively; and the loading/unloading

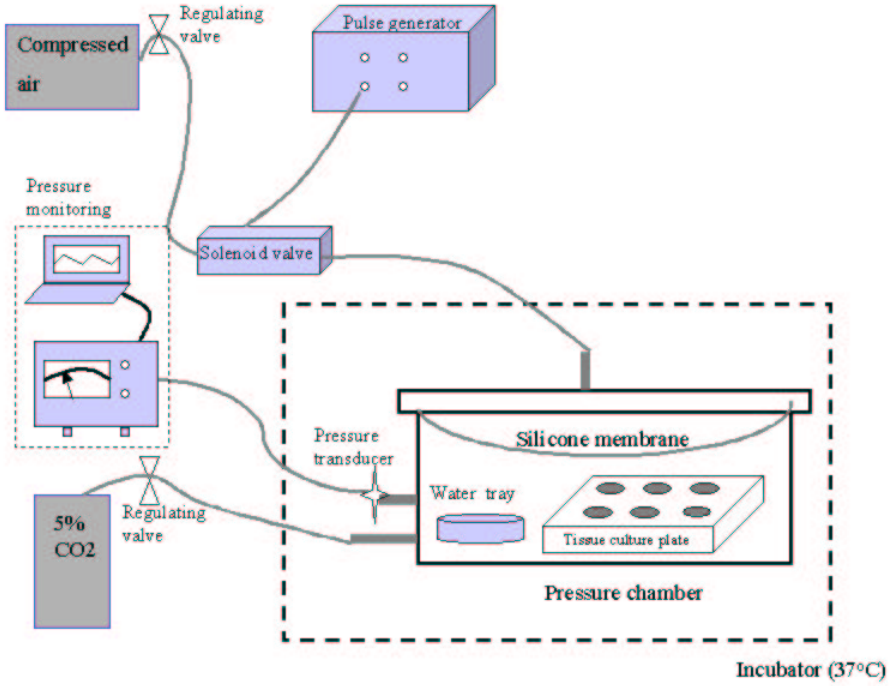


**Figure 9:** Schematic drawing of the cyclic pressure system: Valve leaflet tissue was placed in the media-containing tissue culture plate, which is placed in a pressure chamber. The pressure chamber is divided to two compartments by a silicone membrane: the lower part is filled with 5% $CO_2$ and the higher part is filled with compressed air. Compressed air flow is adjusted by a solenoid valve connected to a pulse generator system. Cyclic air flow results in periodic expanding and relaxing of the silicone membrane, thus generating a cyclic pressure in the lower part of the chamber. Humidity in the lower part was maintained by placing a small water tray, pressure is monitored by a pressure transducer attached to the lower part of the chamber

ratios were both at 2:1.

To generate constant static pressure, the same system was used with the omission of the compressed air system. Thus the final system only contains the pressure chamber, the silicone membrane, the 5% $CO_2$/air tank and the pressure monitoring system. Pressure magnitude is changed simply by adjusting the $CO_2$/air flow into the chamber.

The pressure monitoring system consisted of a signal amplifier module (Validyne Engineering, CD-12, Northridge, CA) and a multimeter (John Fluke MFG Co., Fluke 27) or a laptop computer.

Pressure inside the chamber was measured by inserting a disposable sterile needle (Beckton Dickinson & Co, B-D 18G1$\frac{1}{2}$) into the lower compartment. This needle was connected to a disposable pressure transducer (Argon Division of Maxiim Medical, 041-500-503), which was connected to the signal amplifier module. The signals were then transmitted to a multimeter for digital reading. Pressure was calculated from the voltage readings using a calibration curve, which was obtained by using a *U*-shaped manometer prior to the experiment set up. Alternatively, dynamic cyclic pressure signals from the signal amplifier module were transmitted to the labtop computer through an interface box. Pressure waveforms were directly recorded using Labview 5.1 (National Instruments, Austin, TX) software on the laptop, with the calibration curve being incorporated in the program.

#### *4.2.1.3 Validation*

As mentioned earlier, the compressed air system may cause secondary effects by increasing dissolved $CO_2$ and $O_2$ in the medium, which may cause some harmful effects to the cultured tissue. According to calculations by Tanck et al [148], these effects should be negligible for the pressure ranges examined in this study. In order to confirm this, the system was experimentally validated. Parameters chosen for system validation were tissue viability, medium pH and protein oxidization in the tissue.

Fresh valve leaflets incubated in DMEM were placed in the system and run for 96 hrs. Tissue viability was assessed by Ethidium-homodimer and Hoechst staining, in which dead cells stained pink/red (Ethidium-homodimer), while live cells appeared blue (Hoechst). Media pH was measured and compared with atmospheric controls. Protein oxidization was measured by using Oxyblot, a western blot procedure for oxidized proteins.

### 4.2.2 Biosynthetic Activity Measurement: Radiolabeling

Radiolabeling is a versatile technique for quantifying synthetic activity. By incubating tissues in media containing a radiolabeled precursor molecule, such as an amino acid, the incorporation of that precursor into a macromolecule such as a protein, in a given period of time can be quantified. The more active the cellular processes, the more precursors will be incorporated; resulting in radioactivity in the tissue at the end of the experiment. Therefore, the radioactivity of the tissue can be used as a measure of its biosynthetic activity. In these experiments, three radioactive precursors

$^{3}$H-proline,$^{3}$H-Thymidine and $^{35}$S sodium sulfate were used to determine the net synthesis of collagen, DNA and sGAG respectively. The term "net synthesis" could also be viewed as accumulation and describes the difference between total synthesis and degradation. Degradation rates were not measured. Details of the assay protocols and statistical analysis are presented below.

Single Radiolabeling

Collagen synthesis was measured by single radiolabeling. The precursor for collagen synthesis was L- [5-$^{3}$H] proline (ICN Biomedicals, 20060E, Costa Mesa, CA). Prior to the experiment, aliquots of the radioactive precursor were added to the media, to give a final concentration of 10 $\mu$Ci·mL$^{-1}$. Upon completion, the samples were removed from the system, dehydrated, weighed and digested in Proteinase K at 55$^{o}$C overnight or longer until the tissue was completely digested. The digestion solution was vortexed and a 100 $\mu$l aliquot was taken out from each sample, and added into a scintillation vial containing 2 ml liquid scintillation cocktail (CytoScint ES, ICN Biomedicals) for each sample. The vials were then loaded onto a scintillation counter (Beckman, LS5000-TD) and under went scintillation counting. The scintillation counter provided the raw data in counts per minute (CPM). Collagen synthesis was expressed as $^{3}$H content found in the tissue digestion solution normalized by tissue dry weight (cpm/mg).

Dual Radiolabeling

DNA and GAG synthesis were assayed by using a dual radiolabeling protocol [63]. $^{3}$H-Thymidine (ICN Biomedicals, 24041) and $^{35}$S sodium sulfate (ICN Biomedicals, 64041) were used as precursors for DNA synthesis and GAG synthesis, respectively. As with the single radiolabeling technique, aliquots (0.5 mCi in 0.0005 ml $H_2O$) of $^{35}$S sodium sulfate were added to media (10 $\mu$Ci·mL$^{-1}$); then 0.5 ml $^{35}$S labelled media was transferred to a cryovial; then $^{3}$H-Thymidine (0.5 mCi in 0.25 ml $H_2O$) was added to the $^{35}$S labelled media (10 $\mu$Ci·mL$^{-1}$), and then 0.5 ml dual radiolabeled media was transferred to another cryovial for later calibration. Dual radiolabeled medium was used for each pressure condition. Sample processing and data analysis were identical to the single radiolabeling labelling method, except that the scintillation counting from the dual radiolabelled media was converted to single labeled counting first.

## *4.3 Shear Stress Study Methods*

### 4.3.1 The Modified Parallel Plate System

The modified parallel plate system was previously described by Weston [168]. In brief, the whole system (Fig.10)consists of the modified parallel plate, a flow dampener (Cole-Parmer), a reservoir, and a peristaltic pump (7553-80, Cole-Parmer, Vernon Hills, IL). Flow was driven by the pump and circulated through the loop sequentially via the reservoir, the parallel plate, a flow meter(Omega,FL-203A, Stamford,CT), the flow dampener and back to the reservoir. A major difference between this system and the traditional parallel plate system was that the lower plate was machined with 6 wells, recessed 0.050 in. (1270 $\mu$m) from the surface. The spacing between the wells ensured flow development before each one in case any disturbances occurred. The depth of each well accommodated a silicone rubber disc (either 508 or 794 mm thick) and a leaflet up to 793 mm thick. To hold the leaflet in place, a polycarbonate cover was attached to the well. This cover exposed a circular portion (7.9 mm diameter) of the leaflet to shear stress. The silicone rubber disc was cut to 7.9 mm diameter to push the leaflet into the opening. Since the thickness of individual leaflets varies, color-coded Mylar shim stock (Precision, Downers Grove, IL) could be placed underneath the rubber disc to offset thinner leaflets. As a result, each leaflet was mounted flush with the surface. The flow channel was formed from Mylar (Dupont Teiji Films, MYLAR® A/500 gauge,VA), and the Mylar was surrounded with a rubber gasket material to prevent leakage from the chamber. The single flow channel was 7.6 cm wide by 6.4 cm long. The height, along with the flow rate through the chamber, could be varied to produce different shear stress conditions.

Shear stress on the leaflet in the parallel plate system is calculated by using the formula:

$$\tau = \frac{6Q\mu}{H^2 w}$$

where, Q is flow rate, $\mu$ - medium viscosity, H - channel height, w- channel width

Therefore, a desired shear stress can be obtained by varying the channel height and the flow rate. However, the criteria for laminar flow must be satisfied: (1) Re $<$ 2000, (2) the entrance length LE, which is calculated as LE = 0.05 H Re, must be small compared to the total length to ensure flow development, and (3) the width of the channel should be much greater than its height; Jouret [69]

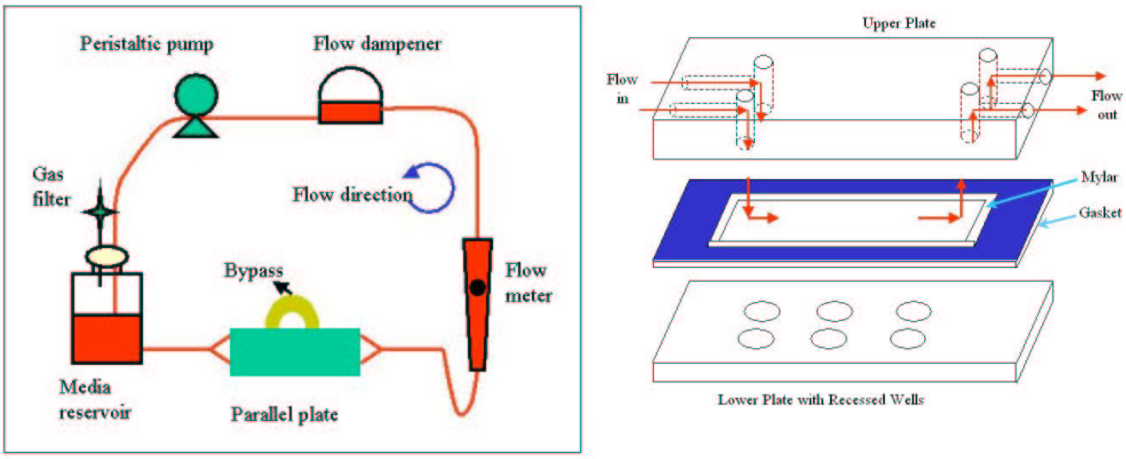


**Figure 10:** Modified parallel plate system: left- flow loop, right- the modified parallel plate; flow is driven by a peristaltic pump and measured by a flow meter; valve leaflets mounted in the parallel plate were exposed to steady laminar shear stress; arrow indicates flow direction.

observed laminar flow with a ratio B/H as low as 46, although many studies have employed larger ratios.

Shear levels of 1, 9, 25, 40 and 80 dyne/cm$^2$ were studied with each experiment lasting 48 hours. Relevant parameters for each shear condition are listed in the table below.

**Table 4:** Parameters (Re, Q, L, w) under different shear conditions

| Shear stress (dyne/cm$^2$) | 1 | 9 | 25 | 40 | 80 |
|---|---|---|---|---|---|
| Flow rate (Q: mL/min) | 12 | 100 | 275 | 196 | 392 |
| Channel Height (H: $\mu$m) | 381 | 381 | 381 | 254 | 254 |
| Channel Width (w: cm) | 7.6 | 7.6 | 7.6 | 7.6 | 7.6 |
| Channel Length (L: cm) | 6.4 | 6.4 | 6.4 | 6.4 | 6.4 |
| Re | 20 | 166.67 | 458.33 | 326.67 | 650 |
| Entrance length (LE: cm) | 0.0381 | 0.3175 | 0.873 | 0.414 | 0.8255 |

### 4.3.2 Endothelium Removal

In the denudation study, porcine AV leaflets were collected as in the other experiments. After dissecting them from the aortic root, the leaflets were rinsed with sterile DPBS 3 times. The endothelium on the ventricular surface was removed by gently rubbing the surface with a sterile cotton bud. The efficacy of the removal was examined by SEM and Hematoxylin and Eosin staining (see below for detailed protocols). Shown next is a SEM comparison of an intact leaflet vs. a denuded

leaflet.

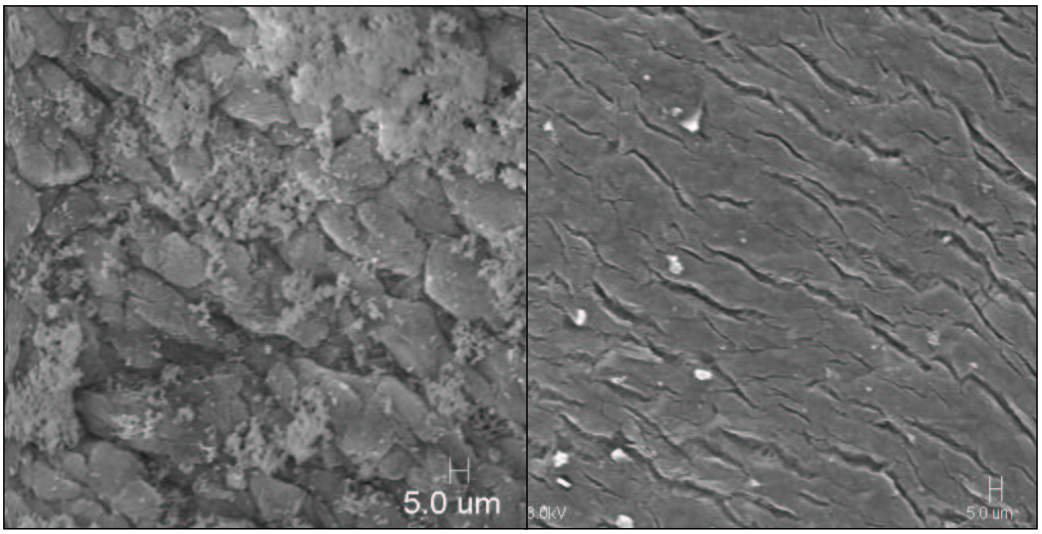


**Figure 11:** Valve leaflets before (left) and after (right) endothelial removal, SEM images of the ventricular surface,left: 500X, right: 390X; note the absence of cells on valve surface after EC removal

### 4.3.3 Biochemical Assays for Valve Synthetic Activity

The running volume of the shear stress loop went as high as 400 ml in order to obtain a shear stress of 80 dyne/cm$^2$. This made it unfeasible to use the radiolabeling method for valvular synthetic activity measurement for two reasons. Firstly, the total amount of radioactive precursor needed would be vast (4 mCi) as compared to the pressure experiments (250 $\mu$Ci); secondly, the radioactive media would be circulating throughout the whole loop, therefore, every component of the loop would be contaminated after the experiment, which creates a big burden for cleaning up as well as safety concerns. Thus, alternative methods for extracellular matrix (including collagen, elastin and GAG) analysis were investigated.

#### *4.3.3.1 Collagen Assay*

The Sircol Collagen assay kit (Biocolor, S1000) in which collagen is stained with Sirius Red was used to measure collagen synthesis. Sirius red is an anionic dye with sulphonic acid side chain groups which react with the side chain groups of the basic amino acids (lysine, arginine) present in collagen. The specific affinity of the dye for collagen is due to the elongated dye molecules becoming aligned parallel with the long, rigid structure of native collagen that have intact triple

helix organization. Samples from the experiments were dehydrated, weighed, and then incubated in pepsin (Sigma P6887) in 0.5 M acetic acid buffer (enzyme:tissue dry weight = 1:3) overnight at room temperature with vigorous stirring. This digestion method was the method of choice for recovering the recently synthesized collagen pool from the tissue. Pepsin cleaves off part of the C-terminal non-helical region of the alpha-chains that make the triple helix of tropocollagen. After tissue digestion, a 100 $\mu$L aliquot from each sample was taken and placed into labelled 1.5 ml microcentrifuge tubes; meanwhile collagen standards were prepared with each tube containing 0, 5, 10, 25 and 50$\mu$g collagen, respectively. The volume of each collagen standard tube was adjusted to 100 $\mu$l by adding the appropriate amount of 0.5 M acetic acid. Afterwards, 1 ml of Sircol Dye reagent (Sirius Red in picric acid) was added to each tube, the tubes were then capped and placed on a mechanical shaker for 30 minutes. During this time, the Sircol dye bound to soluble collagen and the dye regent was designed so that the collagen-dye complex would precipitate out of solution. After mixing, the centrifuge tubes were transferred to a micro-centrifuge and spun for 10 minutes at 12000 x g. The tubes were drained to remove the unbound dye solution. This was done by simply inverting the tube onto a paper towel and allowing it to drain. Remaining droplets were removed by gently tapping the inverted tube on the tissue paper. The bound dye was released into solution by adding 1 ml of the alkali reagent (containing 0.5 M sodium hydroxide) to each tube. The tubes were then capped and placed on a vortex mixer to release the bound dye; the samples were ready for measurement within 10 minutes. The measurement was performed on a microplate reader (Spectra Max Gemini Microplate, Spectrophotometer, Sunnyvale CA) using a blue-green filter. A 96-well clear round/flat bottom plate containing the samples (two duplicates for each, 200 $\mu$l per well) was placed in the plate reader drawer and the absorbance was read at a wavelength of 540 nm. The readings were saved as a text file and copied to an Excel spreadsheet. A standard curve was obtained by plotting the collagen standard absorbance readings against their known collagen concentrations. Collagen concentration in the samples was derived by using the absorbance readings and the standard curve.

#### *4.3.3.2 Sulfated Glycoaminoglycan (sGAG) Assay*

The Blyscan sGAG assay kit (Biocolor, B1000) in which sulfated proteoglycans and glycoaminoglycans are stained with the cationic dye 1,9-dimethylmethylene blue, was used to measure sGAG synthesis. Under the conditions given in the assay, this dye will bind to the polysaccharide component of proteoglycans and/or the protein-free GAGs. Samples from the experiments were dehydrated, weighed, and then processed to extract the sGAGs. The extraction was done by using freshly prepared Pronase (Sigma, P6911), dissolved in 0.1 M tris-acetate, 10 mM calcium acetate, pH 7.8 with a tissue dry weight: enzyme ratio of about 1:30. The digestion took 24 to 48 hours at 37$^o$C with stirring. After tissue digestion, a 25 $\mu$l aliquot from each sample was taken and placed into labeled 1.5 ml centrifuge tubes; meanwhile GAG standards were prepared with each tube containing 0, 1, 2, 3, 4 and 5$\mu$g GAG respectively. The volume of the GAG standards and valve sample tubes was adjusted to 100 $\mu$L by adding the appropriate amount of deionized water. 1 ml of Blyscan dye regent (1,9-dimethylmethylene blue in an inorganic buffer) was added into each tube. The tubes were then capped and placed on a mechanical shaker for 30 minutes. During this time, the Blyscan dye bound to sulfated GAGs and the dye regent was designed so that the GAG-dye complex would precipitate out of solution. After mixing, the centrifuge tubes were transferred to a micro-centrifuge and spun for 10 minutes at 10000 x g. The tube was inverted over a paper towel and allowed to drain. Remaining droplets were removed by gently tapping the inverted tube on the tissue paper. The bound dye was released into solution by adding 1 ml of the dissociation reagent (containing a chaotropic salt in an aqueous propan-1-ol solution) to each tube. The tubes were then capped and placed on a vortex mixer to release the bound dye; the samples were ready for measurement within 10 minutes. The measurement was performed on a microplate reader (Spectra Max Gemini Microplate, Spectrophotometer, Sunnyvale, CA) using a red filter. A 96-well clear round/flat bottom plate containing the samples (two duplicates for each, 200 $\mu$l per well) was placed in the plate reader drawer and the absorbance was read at a wavelength of 656 nm. The readings were exported to a text file, and copied to an Excel spreadsheet. A standard curve was obtained by plotting the sGAG standard absorbance means against their known GAG concentrations. sGAG content in the samples was derived by using the absorbance readings and the standard curve.

### 4.3.4 Scanning Electron Microscopy (SEM)

Scanning Electron Microscopy (SEM) provides high-resolution imaging of fine surface morphology and was used in this study to check the endothelium integrity and alignment on the AV leaflet surface. SEM produces a largely magnified image by using electrons instead of light to form an image. A beam of electrons is produced at the top of the microscope by an electron gun. The electron beam follows a vertical path through the microscope, which is held within a vacuum. The beam travels through electromagnetic fields and lenses, which focus the beam down toward the sample. Once the beam hits the sample surface, electrons and X-rays are ejected from the sample. Imaging is typically obtained using secondary electrons for the best resolution of fine surface topographical features. The orientation of surface features influences the number of electrons that reach the secondary electron detector, which creates variations in image contrast that represent the sample's surface topography.

As the SEM utilizes vacuum conditions and uses electrons to form an image, special preparations must be done to the sample. All water must be removed from the samples because the water would vaporize in the vacuum. All metals are conductive and require no preparation before being used. All non-metals need to be made conductive by covering the sample with a thin layer of conductive material. This is done by using a device called a "sputter coater" (see detailed protocol below).

#### *4.3.4.1 Sample Preparation*

After exposure to shear, static incubation or denudation, the leaflet tissues were immediately rinsed with 0.2M sodium cacodylate buffer (pH 7.2, Electron Microscopy Science: 11652), and then fixed in 2.5% glutaraldehyde (Electron Microscopy Science: 16019) in cacodylate buffer (pH 7.2) for 1-2 hours. Afterwards, the tissue was rinsed with 0.2 M cacodylate buffer 3 times, each for 10 minutes; followed by serial dehydration steps in 25% alcohol, 50%, 70%, 90% twice, and 100 % twice, each for 0.5 to 1 hour. The subsequent sample drying was achieved by using hexamethydisilazane (HMDS, Electron Microscopy Science: 16700) (ratios in ethanol : HMDS, starting from 100% ethanol going to 100% HMDS): 100% Ethanol$\Rightarrow$ 2:1 $\Rightarrow$ 1:1 $\Rightarrow$ 1:2 $\Rightarrow$ 100% HMDS, each step last for about 30 minutes. After this, the samples were rinsed with 100% HMDS three times, the HMDS

(the level should just cover the sample) for the last time and leave the tube containing the sample open in a fume hood and allow the HMDS to evaporate, this might take overnight. After overnight drying (tissue became white), the samples were adhered to an aluminium stub (SPI: 01506-BA) using conductive, double sided carbon adhesive tape (SPI: 05081-AB) and then sputter coated with gold (about 100 Angstroms thick). The sputter coater used an electric field and argon gas. The sample was placed in a small vacuum chamber. Argon gas and an electric field caused an electron to be removed from the argon, making the atoms positively charged. The argon ions then became attracted to a negatively charged gold foil. The argon ions knocked gold atoms from the surface of the gold foil. These gold atoms fell and settled onto the surface of the sample producing a thin gold coating. After sputter coating, the samples were kept desiccated until ready to be analyzed under a scanning electron microscope (Hitachi S-800).

Detailed operation of the SEM can be found in the appendices. Briefly, the gold-coated samples were loaded onto the sample base, which was then moved into the sample exchange chamber (SEC). The SEC was then closed and evacuated. Once both the SEC and the sample chamber (SC) reached high vacuum, the manual door (MV) was open so that the rod could be inserted into the SC, and the sample base was loaded onto the stage. The rod was then pulled back and the MV was closed afterwards. The SC air valve was open when both the SEC and SC lights were flashing green, indicating high vacuum. The accelerating voltage was set to be 15 kV, and the emission current should be 10 $\mu$A. The SEM needed to be flashed if the initial emission current was not 10 $\mu$A. The starting magnification was 40 X to locate the sample, and fine details of the sample were viewed under 7K - 10K X. Images were captured by using the Iridium/iXRF software and saved as .imx files and exported as .jpg or .tif afterwards.

## *4.4 Common Methods for both Specific Aims*

### 4.4.1 Tissue Viability

One key issue that is to be addressed in this study is the viability of the AV leaflets, both before and after the mechanical treatment. MTT assay is a method for a quick check of tissue viability. MTT is a pale yellow colored tetrazolium salt soluble in an aqueous solution until it is reduced to a purple-blue precipitate. This reaction takes place in functional mitochondria within viable cells

and this ability is lost in dead or metabolically incompetent cells [110, 179]. The method used in this study is a modification of the MTT assay on porcine carotid arteries [58]. It consists of three major steps : (1) Incubation in MTT (Sigma, M 2128, 1 mg·mL$^{-1}$ in DPBS) at 37$^o$C for 30 min; (2) Photograph the leaflet using a Kodak digital camera; (3) Images are transferred to a computer and analyzed by Sigma Scan (measuring the staining intensities).

Ethidium Homodimer - Hoechst staining is a quantitative method to assess tissue viability. Ethidium Homodimer is a high affinity fluorescent nucleic acid stain. It binds to both DNA and RNA in a sequence-independent manner and with a $>$30-fold fluorescence enhancement. The DNA binding of each Ethidium Homodimer covers four base pairs and is believed to occur by intercalation. Because the dye is highly positively charged, it can not cross cell membranes to stain living cells. Therefore it is used as a dye for dead cells with disrupted membranes. Hoechst 33258 is a fluorescent dye that can permeate cell membrane and intercalate with the A-T regions of DNA. Since it is membrane -permeable, Hoechst stains the nuceli of all cells, both live and dead. A combination of these two dyes was used in this study so that the amount of cell death could be estimated. During the last 24 hours of the experiment, Ethidium Homodimer (0.5 mM, Biotium) was added to culture media supplemented with 10% calf serum. The samples were fixed in 10% neutral formalin, processed, embedded in paraffin and cut into 5 $\mu$m sections. The sections were then deparaffinized and incubated in 1 mg·mL$^{-1}$ Hoechst 33258 (Fluka, 14530) at 37$^o$C for 1 hour, cover-slipped and viewed under fluorescent microscope (Zeiss LSM 510). Dead cells appeared red (Ethidium) under the microscope, and live cells appeared blue (Hoechst). By comparing the number of dead cells with total number of cells, we can determine the viability of the tissue.

### 4.4.2 Histology: Tissue Preparation

There are four steps in tissue preparation. The first step is tissue fixation, which stabilizes and preserves the tissue. A variety of chemicals can be used for fixing histological specimens. Routine fixation often uses a solution of formaldehyde (formalin) which reacts with proteins and other organic molecules to stabilize cell structures. This solution is buffered and osmotically balanced to minimize shrinkage, swelling, and other collateral damage. Ideally, fixation should be accomplished extremely quickly to minimize post-mortem changes in cell structure. Since the fixation

rate is limited by diffusion, ideal tissue preservation requires that fixatives be delivered as closely as possible to each cell. Rapid delivery of a fixative can be accomplished either by perfusion or by immersion. An alternative to chemical fixation is freezing, followed by direct sectioning of the frozen specimen. The morphology and microanatomy of frozen sections is poor when compared to well-fixed paraffin embedded specimens, but they do have certain advantages. Frozen sections do not require hours of fixation and embedding; therefore, they can provide immediate diagnostic information to a surgeon in the operating room. Frozen sections can also permit analysis of small diffusable molecules or of enzyme activity whose presence would be lost during chemical fixation and paraffin processing. Both chemical fixation and freezing were used in this study. Post fixation, tissue specimens are routinely embedded in a solid material which will support very thin sectioning. To embed a tissue sample, tissue water is replaced first by solvents (such as alcohol and xylene) and then infiltrated with a liquid such as melted wax (paraffin) or a resin solution which can be subsequently solidified by cooling or polymerization, respectively. Sectioning is the production of very thin slices from a tissue sample. The equipment used for sectioning is called a microtome. The following is a summary of the tissue preparation procedure used in this study.

After each experiment, the leaflets pieces were fixed in 10% neutral formaldehyde (VWR, 3323-1) at room temperature overnight and then transferred to 70% alcohol and stored at $4^oC$ before tissue processing. The fixed leaflets were then put into plastic cassettes and placed in a tissue processor (Shandon Pathcentre Tissue Processor, Shandon Pittsburgh, PA) and for routine overnight tissue processing. Tissue processing was necessary to remove extractable water and replace it with a medium that provides support upon thin sectioning. There are three steps in tissue processing. First, tissues were dehydrated by successive incubation in graded alcohol from low to high concentrations. Second, the tissue was cleared using xylene. Finally, the tissue was infiltrated with liquid paraffin , resulting in a paraffinized strip of tissue. After tissue processing, the cassettes with tissues inside were transferred to an embedding machine (Shandon Histocentre 2, Tissue Embedding System). The samples were placed onto a mold filled with liquid paraffin which was cooled until solidified. The paraffin embedded tissue blocks were mounted onto a microtome (Rotary Microtome HM 355S, Microm International GmbH) to be cut into 5 $\mu$m thick sections. The sections were placed onto positively charged microscope slides, which were then placed in a $37^oC$ oven overnight to ensure

optimal adhesion. The slides were stored at room temperature prior to staining.

In cases where the antigenicity may be lost due to chemical fixation or paraffin processing, frozen sections were used. Immediately following the experiment or tissue harvest (for fresh controls), leaflet tissues were immersed in optimal cutting temperature (OCT) medium within a plastic mold and snap frozen in liquid nitrogen. The frozen samples were kept at -80$^o$C until sectioned. Sectioning of the frozen samples was performed using a cryostat (Microm Cryostat, Cryostat HM 560 MV); slices of 7 $\mu$m thick were cut and kept frozen until stained.

### 4.4.3 General Histological Staining

Cells are essentially transparent, with little or no intrinsic pigment. Even red blood cells, packed with hemoglobin, appear nearly colorless when unstained, unless packed into thick masses. Stains are used to confer contrast, to make tissue components visibly conspicuous. Certain special stains, which bind selectively to particular components, may also be used to identify those structures. The essential function of staining is simply to make structures visible.

This section will include a description of the procedures used to perform general histology (Hematoxylin and Eosin staining, Movat's pentachrome staining), as well as immunohistochemistry for various proteins ($\alpha$-Smooth muscle actin, MMPs, Cathepsins etc.).

#### *4.4.3.1 Routine Hematoxylin and Eosin Staining*

Hematoxylin and Eosin (H and E) staining is a commonly used staining method for tissue structure visualization. Hematoxylin is a basic dye that stains acid structures purple or blue. Structures like Chromatin (i.e., cell nuclei) and ribosomes that are stained by basic stains are described as basophilic. Eosin is an acidic dye that stains basic structures red. Structures such as collagen fibers, red blood cells, muscle filaments and mitochondria that are stained by acid stains are described as acidophilic. H and E staining was done automatically on a staining machine (Leica Autostainer,# 74710254). Paraffin sections were first run through a series of xylene substitutes (3 stations, 5 minutes each) and alcohols (100% x 2, 95% and 75%, each for 2 minutes), then washed in water for 2 minutes prior to immersing into hematoxylin for 30 seconds. Afterwards, the slides went through water (2 minutes), acid alcohol (1 second), and water (1 minute), Scott's solution (30 seconds) and were then washed in water for 2 minutes. Following this, the slides were immersed in acid alcohol

for 1 minute before being stained with Eosin for 30 seconds. Subsequently, the slides were run through a series of alcohols (95%: 30 seconds, 100%: 1 minute, 100%: 2 minutes x 2) and xylene substitute (twice, each for 2 minutes) and finished in xylene. A resinous mounting agent was applied and the slides were coverslipped and allowed to dry overnight before viewing.

#### *4.4.3.2 Movat' pentachrome staining*

Movat's staining is a procedure that allows for the demonstration of a variety of tissue elements in a single section [93]. For the unique structure like that of the AV, it provides a very good evaluation method to see how badly the native structure has been altered under pathologically conditions (e.g., floppy valves) or how close a TE-valve resembles the native valve in terms of structure. Our procedure was based on Garvey's modification of Movat's staining [53], and was optimized to get the best possible results. The procedure consists of the following major steps (after deparaffinization). The slides were firstly incubated in alcian blue at 60$^{o}$C for 10 minutes, this was to stain the ground substance as well as glycoaminoglycans (GAG)). Afterwards, they were washed in tap water and then immersed in a modified Verhoeff solution at room temperature for 6-7 min. The Verhoeff solution was a mixture of three stock solutions: A (Hematoxylin in absolute alcohol), B (Ferric Chloride in distilled water) and C (potassium iodide and iodine in distilled water) with a volume ratio of 3:2:1. It is is a special stain for the elastic fibers and cell nuceli. The next step was quick a rinse in aqueous ferric chloride for 5-10 seconds to get rid of excessive Verhoeff stain. Then the slides were immersed in plasma stain allowing for visualization of fibrin, cytoplasm and muscle tissue. This was followed by a 15 minutes' immersion in polyacid to remove the excessive plasma stain. Subsequently, the slides were dehydrated in a graded alcohol and then stained in saffron (Saffron du Gatinais in absolute ethanol, Baker 3801) for 15 minutes to 1 hour. Saffron binds to collagen and gives it a yellow color. Since saffron is soluble in water, the dehydration must be complete to prevent saffron loss. After saffron staining, the slides were dehydrated in a series of alcohol and cleared in xylene, and finally mounted with a resinous media and coverslipped for microscopic viewing. The expected staining results were: nuclei- blue black, elastic fibers- black, cytoplasm and fibrin-red, collagen-yellow and ground substances blue.

### 4.4.4 Immunohistochemistry (IHC)

Immunohistochemistry (IHC) is the localization of proteins in tissue sections by the use of labeled antibodies as specific reagents through antigen-antibody interactions. Protein localization may be visualized by a number of detection systems, such as fluorescent dyes, enzymes, radioactive elements, or colloidal gold. There are various IHC techniques; direct (one step), indirect, PAP (peroxidase-anti-peroxidase) and the ABC (Avidin-Biotin-Complex) method. The ABC method was used for all IHC's performed. The ABC method is the most sensitive and widely used technique for IHC staining. Avidin, a large glycoprotein, can be labeled with enzymes or fluorephores and has a very high affinity for biotin. Biotin, a low molecular weight vitamin, can be conjugated to a variety of biological molecules such as antibodies. The technique involves three layers. The first layer is unlabeled primary antibody. The second layer is biotinylated secondary antibody. The third layer is a complex of avidin-biotin conjugated peroxidase. The peroxidase is then developed by diaminobenzidine (DAB) or other substrate to produce different colored end products. All incubations in primary antibody, secondary antibody, ABC or DAB are carried out in a humid chamber at room temperature to avoid slide drying. Recipes of all the solutions are attached in the appendix.

#### *4.4.4.1 $\alpha$-Smooth muscle Actin IHC*

$\alpha$-Smooth muscle actin IHC was used to detect $\alpha$-Smooth muscle actin positive cells. More than 50% interstitial cells in the aortic valve are positive of $\alpha$-Smooth muscle actin [151], and this percentage changes under diseased conditions when the myofibroblasts become activated [107, 109]. Therefore, $\alpha$-Smooth muscle actin was chosen as a marker to measure cell phenotypical changes. The staining protocol is summarized as following. Slides were placed in a staining rack and deparaffinized in xylene, and rehydrated by successive incubations in graded alcohols (100%, 95% and 70% ethanol), and finally immersed in water. Sections were subjected to 0.3% hydrogen peroxide (Sigma, H1009) for 15 minutes to halt exogenous peroxidase activity. Blocking serums were applied for 30 minutes to prevent nonspecific antibody reactions.

The primary anti-actin antibody 1A4 (DAKO, Carpenteria, CA) was then applied at a dilution of 1:30 (antibody volume to solution volume) for 60 minutes. Then, the secondary antibody, biotinylated horse anti-mouse immunoglobulin G (Vector Laboratories, Burlingame, CA) was applied at a

dilution of 1:400 for 30 minutes. The secondary antibody binds the primary antibody because of the mouse specificity. A tertiary component was then applied for 30 minutes to form an avidin-biotin complex (Vectastain Elite ABC Kit, Vector).

This complex was subsequently incubated for 10 minutes with 3',3'-diaminobenzidine (DAB) to form a brown stain (DAB Substrate Kit, Vector). The distribution of DAB staining identified the distribution of a-Smooth muscle Actin immunoactive cells; cell nuclei are counterstained using Gill's hematoxylene. After counterstaining, slides were dehydrated through ascending grades of alcohols and cleared in xylene. A resinous mounting agent was applied and the slides were coverslipped and allowed to dry overnight before viewing.

#### *4.4.4.2 BrdU (5-bromo-2-deoxy uridine) IHC*

Cell proliferation under the extreme pressure condition was studied using BrdU (Sigma) immunostaining. Prior to each experiment, BrdU was added to the media with a final concentration of 5 mg/mL. BrdU , an analog to thymidine can be incorporated into the DNA of dividing cells. BrdU immunohistochemistry was used to detect the amount of BrdU present in the tissue. After deparaffinization, the slides were pretreated with Proteinase K (1mg/mL,10 minutes) and HCL (4N, 10 minutes) to expose and uncoil the DNA, thus exposing the BrdU antigen. Afterwards, slides were incubated with anti-BrdU (DAKO, M744, 1:20) for 1 hour at room temperature. Slides were then washed in PBS twice, each for 5 minutes and then exposed to a biotinylated secondary antibody (anti-mouse IgG, Vector, BA 2001, 1:400) for 30 minutes followed by 1 hour incubation in ABC-Vector Red complex from the alkaline phosphatase standard kit (Vector Laboratories, AK-5000). Lastly, an alkaline phosphatase substrate solution (Vector Laboratories, SK-5100) was applied to the sections and incubated in the dark for 20-30 minutes until color developed. Cell nuclei were counterstained with hematoxylin and appeared as blue in the final staining image. Native porcine carotid artery with a proliferating rate of 10% were used as positive controls; negative controls were the same valve leaflet tissue section with the omission of the primary antibody. The percentage of proliferating cells (BrdU positive) was calculated and averaged over all the samples under the same experimental condition.

#### *4.4.4.3 Matrix Metalloproteinases IHC*

Matrix Metalloproteinases (MMPs) are a family of about 20 zinc- dependent endopeptides that play an important role in physiological tissue renewal as well as disease processes such as arthritis and cancer [51]. MMPs are produced by a variety of cells including fibroblasts, smooth muscle cells, cardiac myocytes, and valvular interstitial cells [41]. The current study is focused on two MMPs: MMP-2 and -9, also called the gelatinases, since both have been reported to be present in porcine tissue. The presence and distribution of MMP-2 and -9 was detected by immunohistochemistry. MMP-2 and MMP-9 were detected using a similar IHC protocol. Paraffin-embedded leaflet cross sections (5$\mu$m thick) were first deparaffinized, washed in PBS for 5 minutes and then immersed in 1% $H_2O_2$ for 30 minutes to block the endogenous peroxidase. Afterward, the slides were washed in PBS twice, 5 minutes each before incubation in primary antibody (ani-MMP-2,EMD Bioscience, IM33L, dilution of 1:20 (50 $\mu$l primary antibody stock plus 850 $\mu$l PBS plus 100 $\mu$l horse serum (Vector Laboratories, S2000) for 1 hour, followed by 2 washes in PBS and then 30 minutes incubation in the secondary antibody (anti-mouse IgG, dilution of 1:400 (2.5 $\mu$l secondary antibody stock plus 20 $\mu$l normal horse serum plus (1000-22.5)$\mu$l PBS)). After the secondary antibody incubation, the slides were washed twice in PBS and incubated in Avidin-Biotin-Conjugate (ABC)-peroxidase complex (Vector Laboratories, PK-6100) for 1 hour and then washed in PBS for 5 minutes twice. Subsequently, the slides were incubated in DAB (Vector Laboratories, SK-4100) until color develops; the exact time varies with the amount of antigens in the tissue, but total development time was less than 10 minutes. Slides were then washed in water for 5 minutes and then counterstained with hematoxylin. A resinous mounting agent was applied and the slides were coverslipped and allowed to dry overnight before viewing.

#### *4.4.4.4 Cathepsin IHC*

Cathepsins are cysteine-dependent lysosomal proteases that belong to the family of papain-like peptidases and they are involved in unspecific bulk proteolysis in the lysosomes. These enzymes have been shown to have elastolytic activity and collagenolytic activity as well. So far, it is known that seven cathepsins are expressed ubiquitously in mammalian tissues; B, C, F, H, L, O and Z [141]. Other members of the family exhibit cell-type-specific expression; e.g. cathepsin S is expressed in

peripheral antigen-presenting cells, but cathepsin K is mainly found in osteoblasts. A previous study showed that Cathepsin S and K activity was present in myxomatous heart valves [107]. In the current study, cathepsins B, L, and S will be studied by using IHC, these enzymes were chosen since they were shown to be present in the porcine valve by Western blotting. Following is a summary of the Cathepsin L IHC protocol. Tissue, snap frozen in liquid nitrogen, was cut into 7 $\mu$m thick sections. Frozen sections were thawed at room temperature and then immersed in acetone for 5 minutes. The slides were then washed in PBS twice, 5 minutes each, followed by immersing in 0.3% $H_2O_2$ for 15 minutes to block the endogenous peroxidase. After this step, the slides were incubated in 2% BSA/PBS for 15 minutes to suppress non-specific binding. The blocking step was followed immediately by primary antibody incubation (anti-cathepsin L, dilution of 1:20, Santa Crutz, S6501) for 1 hour followed by 2 washes in PBS, each for 5 minutes. Next was the secondary antibody incubation (anti-goat IgG, 1:400) for 30 minutes, followed by 2 washes in PBS and then incubation in ABC-peroxidase for 1 hour. Subsequently, the slides were incubated in DAB (Vector Laboratories, SK-4100, Burlingame,CA) until color developed, the exact time varies with the amount of antigen in the tissue, but total development time was less than 10 minutes. Slides were then washed in water for 5 minutes and counterstained with hematoxylin. A resinous mounting agent is applied and the slides are coverslipped and allowed to dry overnight before viewing. The other two Cathepsins, B and S , are detected in a similar fashion with primary antibodies anti-cathepsin B (EMD sciences, PC41) and anti-cathepsin S (Santa Crutz, SC-6503) and secondary antibodies anti-mouse IgG and anti-goat IgG respectively.

#### *4.4.4.5 Microcopy & Image analysis*

Slides from different staining procedures (H & E, immnuohistochemistry, and Movat's staining) were viewed using a Nikon E600 microscope. Images were taken by using a CCD camera (Qimaging) and analyzed by using ImagePro (ImagePro plus, MediaCybernetics). At least three images were captured for each slide, with magnifications ranging from 4X, 10X, 20X and 40X. Most of the images presented in the results chapter were 20X or 40X when necessary. Images from different samples were compared both qualitatively and quantitatively for cell number, tissue structure integrity (H & E); $\alpha$-SMC active cells (immunohistochemistry), and ECM organization (Movat's

staining). For each mechanical treatment, at least five samples were included to ensure statistical validity.

### 4.4.5 Western Blotting

The use of immunohistochemistry allows determination of the distribution pattern of the protein of interest (actin, MMPs, TIMPs, Cathepsins), but does not allow quantitative analysis. As a complementary study, Western blotting is performed to allow quantitative measurement of the proteins of interest. Western blotting is an immunoblotting technique that relies on the specificity of binding between the protein of interest and an antibody raised against that particular protein. In Western blotting, proteins are first separated by size, in a thin gel sandwiched between two glass plates. This technique is called SDS-PAGE (Sodium Dodecyl Sulfate Poly-Acrylamide Gel Electrophoresis). The proteins in the gel are then transferred to a PVDF, nitrocellulose, nylon or other support membrane. This membrane can then be probed with solutions of antibodies. Antibodies that specifically bind to the protein of interest can then be visualized by a variety of techniques, including chemoluminescence or radioactivity. All the Western blots in this study are visualized by chemoluminescence.

Following is a brief summary of the whole procedure from protein extraction to visualization of the blot. The tissue extraction protocol was taken from the literature [77]. Leaflet samples after exposure to pressure / shear were snap frozen in liquid nitrogen and then homogenized in ice-cold lysis buffer (in mmol/L:Tris-HCl 20 (pH 7.5), EGTA 5, NaCl 150, glycerol-phosphate 20, NaF 10, sodium oethovanadate 1, 1% Triton X-100, 0.1% Tween 20 and protease inhibitors)to extract proteins from the tissue. The tissue lysates then underwent a protein assay to determine the amount of total protein in each sample.

#### *4.4.5.1 SDS-PAGE*

Based on the protein content in each sample, tissue lysate, lysis buffer and reducing 5X were mixed together at certain ratios such that the final protein concentration were all set to 1 $\mu$g/$\mu$L. Samples were kept on ice prior to being loaded onto the gel. The gel is composed of two sections: the stacking gel at the top and the separating gel at the bottom. The separating gel contains:(for 2 gels) water 6.48 ml, separating buffer 3.2 ml, protogel 5.34 ml, 1.5% APS 0.8 ml, 10% SDS 160 $\mu$L

and TEMED 15 $\mu$L. The stacking gel contains: water 1.9 ml, stacking buffer 1 ml, protogel 1 ml, 1.5% APS 1 ml, 10% SDS 50 $\mu$l and TEMED 4 $\mu$l. The separating gels were first poured onto the 1.5 mm plates, after 10-15 minutes, when it becomes solidified, pour the stacking gel onto its top, insert the green little combs into the stacking gel. Wait for another 10-15 minutes for the stacking gels to solidify. Then the combs are removed, and the gels are ready for sample loading. Take the protein samples (tissue lysate plus lysis buffer plus reducing 5 X) prepared before and load 40 $\mu$L into each well. Once the samples were loaded, be sure to include the protein standard and a positive control and started the electrophoresis. The starting voltage was 80 volts, it was changed to 120 volts after the samples had passed through the stacking gel. After about 45 minutes, the gels were ready to be transferred to the membrane. The proteins in the gel were then placed onto a nitrocellulose membrane, with the protein-rich side facing the membrane. Membranes were first immersed in methanol and then placed onto the gel cassettes with a filter paper and a filter pad lying underneath. The gel was transferred onto the membrane, another filter paper and filter pad was placed on top of the gel before closing the cassette. The cassette should be closed very tightly to squeeze out air bubbles. The gel cassettes are then placed into the transfer unit (with a stir bar inside) with the black side facing the black side of the electrode unit. The transfer unit was then placed in a plastic container filled with ice and placed on top of a stir plate. Set the voltage to 30 V for overnight transfer. This was the actual blotting process and was necessary in order to expose the proteins to antibody. The membrane was sticky and bound proteins non-specifically.

After the proteins were transferred onto the membrane, the membrane was first immersed in blocker buffer for 1 hour to prevent non-specific protein interactions between the membrane and the antibody protein before washed in PBS/Twin buffer for 10 minutes twice. Subsequently, the membrane is immersed in primary antibody (MMP-2, -9, TIMP-2: 1:1000, mouse; Cathepsin L: 1:500, goat; Cathepsin B: 1:1000,Cathepsin S: 1:500, rabbit) for 2 hours. Following the primary antibody incubation, the membrane is washed three times, each for 5 minutes in blocker buffer, followed by 1 hour incubation in secondary antibody (1:2000). Afterwards, it was washed three times in blocker buffer (5 minutes each), twice (5 minutes each) in PERK buffer. Finally, the membrane was stained with 6 mL chemoluminescent CDP Star solution (12 $\mu$L plus 240 $\mu$L assay buffer added with water) for 5 minutes on the belly dancer (maximal speed). The membranes were

then placed onto plastic wrap which was folded in edges and flipped over to drive out air bubbles.

Afterwards, the wrapped membranes were placed into the autoradiocassette and closed. The autoradiocassette was taken to the dark room with red light on. A Kodak XAR film (Eastman Kodak) was placed onto the wrapped membranes in the autoradiocassette and exposed for desired amount of time (1 minutes, 10 minutes or 30 minutes) before being placed into the autoradiography apparatus to develop. The developed film will have dark bands corresponding to the protein of interest. Since the first antibody only recognizes the protein of interest, and the second antibody only recognizes the first antibody, if there is stain present on the membrane then the protein of interest must also be present on the membrane. Thus, the protein bands on the membrane that were stained contained the protein that was to be detected, the other locations on the membrane did not. Size approximations were done by comparing the stained bands to that of a pre-stained protein size marker.

### 4.4.6 Gelatin Zymography

Zymography is a technique that analyzes enzymatic activity of proteases, which cannot be achieved by either IHC or Western blotting, which detect both the active form and the latent form of the enzyme but allows no determination of the actual activity of this enzyme. The zymography technique involves the electrophoresis of secreted protease enzymes through discontinuous polyacrylamide gels containing enzyme substrate (either gelatin or B-casein). After electrophoresis, removal of SDS from the gel by washing in 2.5% Triton X-100 solution allows enzymes to renature and degrade the protein substrate. Staining of the gel with commassie blue allows the bands of proteolytic activity to be detected as clear bands of lysis against a blue background. In this study, gelatin zymography was used to analyze the enzymatic activity of MMPs and Cathepsins. Following is brief summary of the procedure. 12.5% polyacrylamide gels are mixed with 0.2% gelatin. The gels were poured onto 0.75 mm plates and Loading volume was 15-20 $\mu$L per well. The gels are running at at 80V at 4$^o$C till the bromophenol blue marker dye reaches the very bottom of the gel. The zymogels are then rinsed with renaturing buffer (2 X 15 min for MMPs, 3 X 10 min for Cathepsins) at room temperature. Afterwards, they are washed with assay buffer for at least 30 min at room temperature, then incubated overnight in assay buffer at 37$^o$C. After the overnight incubation, the gels are

washed with water for 10 min, and then stained with a solution of 0.25% Coomassie blue R250, 40% methanol and 10% acetic acid for 2 hr at room temperature and destained with 40% methanol, 10% acetic acid until the bands of lysis became clear.

### 4.4.7 Image Processing

Images from the western blot and zymograms were obtained by scanning (hp-scanjet 3970) the films or gels into a computer. The images were then loaded into Scion Image software (Scion Corporation, release $\beta$ 4.0.2). Loaded images were enlarged 16 X, and six 40 square pixel rectangle areas were measured above (background) and within the band on the western blots or gelatin zymograms (crude values). The measurements were then copied to Microsoft Excel and background values were subtracted from crude measurements to obtain net optical density. These densities corresponded to protein expression level (western blot) or gelatinolytic activity level (zymogram) and were quantified by densitommertric analysis. The data from the pressure/shear samples and controls samples were then analyzed using Wilconxon signed rank test to check for statistical difference.

## *4.5 Data Analysis*

All the quantitative data, i.e. scintillation counting (synthetic activities in the pressure study), cell number counts (BrdU positive cells), microplate reader readings (collagen and sGAG in the shear study), and the densitomeritric measurements from the Western blots and zymograms, were analyzed using the Minitab software (Minitab 12, Minitab) for statistical analysis. Since the sample sizes in this study were relatively small (as low as 6), and the data distribution was not always normal (Fig.12), the commonly used paired t-test, one sample t-test and F-test are not applicable, because they all assume a normal distribution. Alternatively, a set of non-parametric tests which place no restriction on the distribution or sample size were used for statistical analysis. Instead of specific parameters of a population (such as the means or variance), the nonparametric tests compare the relative locations of the probability distributions of the sampled populations. Many nonparametric methods use the relative ranks of the sample observations rather than their actual numerical values. In this study, the one-sample Wilcoxon signed rank test, which is analogous to the one-sample t-test for normally distributed data, was used to detect the difference between controls and the pressure

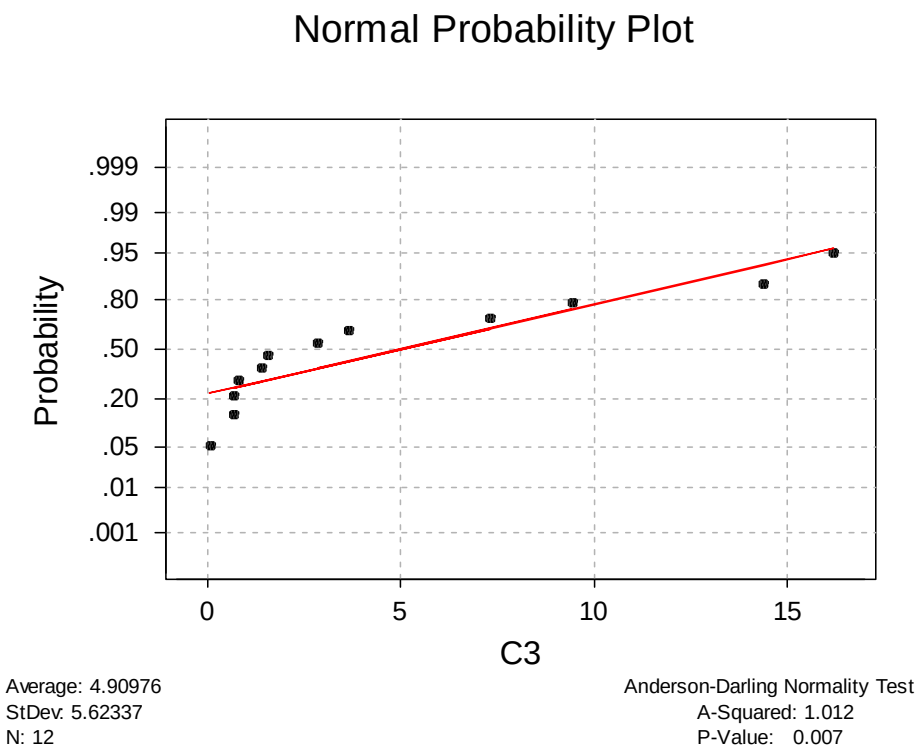


**Figure 12:** A sample data set which is not normally distributed (normality is not valid for p $< 0.05$): data shown are ratios of collagen synthesis from the 25 dyne/cm$^2$ shear stress experiment

or shear stress. The only assumption for the one-sample Wilcoxon test and confidence interval is that the data are a random sample from a continuous, symmetric population. When the population is normally distributed, this test is slightly less powerful (the confidence interval is wider, on the average) than the t-test. It may be considerably more powerful (the confidence interval is narrower, on the average) for other populations. Following is the mathematical theory behind the Wilcoxon signed rank test.

Hypotheses:

$$H_0 : median = m_0 \text{ versus } H1 : median \neq m_0$$

where $H_0$ is the null hypothesis, $H1$ is the alternative hypothesis, and $m_0$ is the hypothesized median of the given sample population.

Under this assumption, and suppose the sample population has n samples which are depicted as $X_1, X_2, X_3, \ldots, X_n$. The absolute values of differences (”D”), $D_1 = X_1 - m_0$, $D_2 = X_2 - m_0$,..., $D_n = X_n - m_0$ that is, the values $|D_1|, |D_2|, \ldots, |D_n|$ are ranked.

Define $T^+ = \sum_1^n s_i r(|D_i|)$ and $T^- = \sum_1^n (1 - s_i) r(|D_i|)$ where

$$s_i = 1(D_i > 0)$$

and $r(|D_i|)$ is the rank of $(|D_i|)$. Under $H_0$, the $s_i$'s are iid (**I**ndependent and **I**dentically **D**istributed) Bernoulli(1/2) random variables. Thus, when $H_0$ is true:

$$E(T^+) = \sum_1^n \frac{r(|D_i|)}{2} = \frac{n(n+1)}{4}$$

and

$$Var(T^+) = \sum_1^n \frac{[r(|D_i|)]^2}{4} = \frac{n(n+1)(2n+1)}{24}$$

where $E(T^+)$ and $Var(T^+)$ are the expectation and variance of $T^+$ respectively. The Wilcoxon statistic $\frac{T^+ - ET^+}{\sqrt{Var(T^+)}}$ is approximately normal when sample size n is large. Therefore, the p-value can be calculated by using $P(\frac{T^+ - ET+}{\sqrt{Var(T^+)}} \leq t) = \Phi(t)$.

The original data consist of n (number of leaflets) paired readings (pressure vs. control or shear vs. control) from the scintillation counter (cpm/mg), ImagePro (cell number), or the microplate reader ($\mu$g/mg). In order to minimize the influence from the biological variability between different leaflets, a ratio of pressure versus control or steady shear stress versus control was taken. These ratios were then pooled together and input into the Minitab software for analysis. This column of data is our sample (e.g. collagen synthesis by the leaflets) population $X_1, X_2, X_3, \ldots, X_n$ and the hypothesis is (the hypothesized median $m_0$ is set as 1.0):

$H_0$ : No significant difference between the two treatments (e.g. pressure vs. control), i.e. median = 1.0

vs.

$H_1$ : There is significant difference between the two treatments, i.e. median $\neq$ 1.0

Reject the null hypothesis $H_0$ when p is less then 0.05, that is, accept the alternative hypothesis that there is significant difference between the two treatments when p $<$ 0.05. Showing below is an example output from the one sample Wilcoxon signed rank test with a sample size of 11 ($n = 11$) and each sample ($X$) being the ratio of sGAG content between shear and control :

**Wilcoxon Signed Rank Test**

Test of median = 1.000 versus median not = 1.000

| | N | N for test | Wilcoxon Statistic | P | Estimated Median |
|---|---|---|---|---|---|
| C1 | 11 | 11 | 60.0 | 0.018 | 1.159 |

**Wilcoxon Signed Rank Confidence Interval**

| | N | Median | Estimated Confidence | Achieved Confidence | Interval |
|---|---|---|---|---|---|
| C1 | 11 | 1.159 | 95.5 | ( 1.030, | 1.690) |

**Figure 13:** An example of the one sample Wilcoxon signed rank test in Minitab, data has 11 entries,each entry is a ratio of GAG content relative to control, median is 1.159 and the p value is 0.018, indicating the median is significantly different from the hypothesized median 1.0; the confidence interval showed that 95.5% of the data falls in the range of 1.03 to 1.69; i.e. most of the ratios are greater than 1.0

# CHAPTER V

# RESULTS

This chapter will present data from the two studies: pressure effects and shear stress effects. It will start with results from the pressure study, followed by the results from the shear study, and concludes with a summary of all the results.

## *5.1 Influence of Pressure on the Biological Properties of AV Leaflets*

### 5.1.1 System Validation

One disadvantage of generating hydrostatic pressure by gas compression is the potential secondary effect caused by physical changes in the media rather than by pressure itself. As the hydrostatic pressure in the organ culture experiments was applied through gas phase, the volume (gas phase) in the culture system decreased during compression, leading to increases in partial pressures of $CO_2$ and $O_2$, which resulted in their increased absorptions in the culture medium. These physical changes, once reaching a certain magnitude, can induce biological responses in the cultured cell or tissue. This issue has been addressed both theoretically by Tanck et al [148] and experimentally by Vouyouka et al [160] and Watase et al [163] in literature. According to Tanck et al's calculations, changes in dissolved oxygen and carbon dioxide are negligible for the pressure levels at or below 30 kPa (above atmosphere). The highest pressure studied in the current project was about 25 kPa (190 mmHg), below 30 kPa, therefore, the secondary effects should be minimal according to the theoretical calculations. Vouyouka et al measured the pH of the media at atmospheric and elevated pressure conditions (135 mmHg and 120-160 mmHg, 1.167 Hz) after 1, 3 and 5 days of pressurization. They found no significant decreases in pH due to increased dissolved $CO_2$, confirming the theoretic calculations by Tanck. In the same study, the authors also measured the LDH activity of BAECs cultured under various pressure conditions and found no significant difference in LDH activity between atmospheric control, static pressure (135 mmHg) and cyclic pressure (120-160 mmHg, 1.167 Hz), suggesting minimal cell death or injury caused by pressure. To exclude to

effects of increased partial $O_2$, Watase et al [163] performed an experiment with higher partial $O_2$ but same total pressure, and found no difference in bovine aortic SMC growth or morphology as shown in the elevated pressure study.

In the current study, the secondary effects were evaluated by measuring three parameters of the system: medium pH, leaflet cell viability and protein oxidation status (oxidative stress).

Increases in $CO_2$ partial pressure in the gas phase may result in deviations in medium pH from the normal value (7.4) and might cause damage to leaflet cell viability and other metabolic functions. Media samples were collected after the pressure experiment and the pH of each sample was measured. Table.5 lists pH differences between pressure samples and their atmospheric controls from the cyclic pressure experiment with a mean pressure of 170 mmHg at a frequency of 1.167 Hz. The highest pressure level (170 mmHg) was chosen due to the fact that under this condition, the increases of $CO_2$ partial pressure would be highest and changes in medium pH, if any, should be highest too. Therefore, if no significant changes are seen under this condition, we can assume the changes under other pressure conditions are also negligible. The medium pH in the pressure samples were comparable to those under atmospheric conditions, with a maximal deviance of only 0.04 (Wilcoxon signed rank test, n = 8, $p > 0.05$).

**Table 5:** Comparison of medium pH under pressure (mean of 170 mmHg at 1.167 Hz) and atmospheric conditions

| sample | 1 | 2 | 3 | 4 | 5 | 6 | 7 | 8 |
|---|---|---|---|---|---|---|---|---|
| pH deviation from control | 0.01 | -0.03 | -0.02 | 0.03 | -0.04 | 0.01 | -0.02 | 0.03 |

Leaflet cell viability was chosen as a validation parameter for the simple fact that in order to respond to any mechanical forces, the cells have to be alive. Valve leaflets were incubated in DMEM under cyclic pressure (mean pressure: 170 mmHg, 2 Hz) for 96 hr and stained with Ethidium Homodimer and Hoechst 33258. Results showed that cell viability was very high after 4 days' incubation in the system (Fig.14), with only minimal cell death (red staining, indicated by arrows, less than 1%) present. This demonstrated that there was no detrimental effects on leaflet cell viability caused by the experimental system.

The highest increase in oxygen partial pressure in this study was about 22% (170 mmHg/760

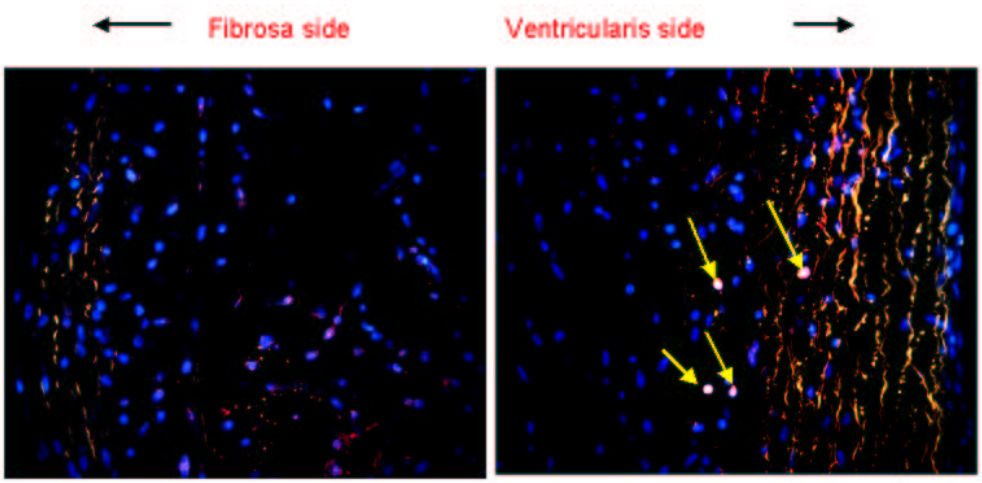


**Figure 14:** Leaflet tissue viability after 96 hrs in the pressure system, shown is a cross section of an AV leaflet under 40X fluorescent microscope, left: the fibrosa side of the leaflet, right: the ventricularis side of the leaflet; Ethidium-homodimer Hoechst staining, dead cells stain red/pink (indicated by arrows), live cells are blue

mmHg). Increased oxygen partial pressure leads to increased dissolved oxygen ($DO_2$) in the medium, which may affect cell metabolism without causing any gross damage to cell viability. This effect was assessed by looking at the protein oxidization status using oxyblot. Results showed the amount of oxidized proteins in the leaflet was similar between elevated pressure and atmospheric controls, indicating that the detrimental effects caused by the increased oxygen partial pressure was negligible (Fig.15).

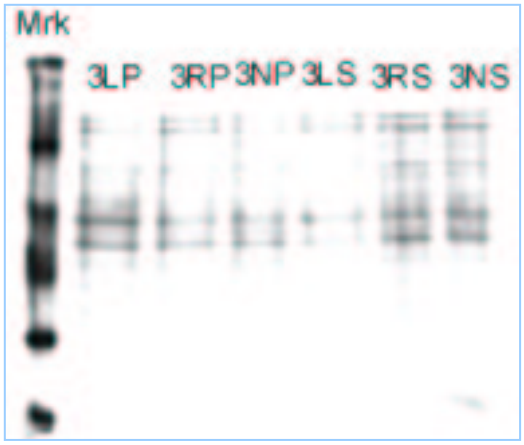


**Figure 15:** Protein oxidation under pressure and control: LP, NP, RP- samples under pressure, LS, NS, RS- samples under atmospheric control, Western blotting results

The pH measurements, cell viability and protein oxidation results all confirmed that the pressure

range in this study did not generate appreciable damages to the leaflet tissue. Thus the biological responses that were to be observed later on in this study were indeed caused by the application of high pressure and not by the secondary effects.

Using the pressure system, two types of pressure regimes were studied: constant static pressure (0 Hz) and cyclic hydrostatic pressure (with various magnitudes and frequencies). Below is a table (Table.6) summarizing all the experiments that were performed and the endpoints that were studied.

**Table 6:** Pressure Study: Summary of Experiments

| | Constant (0 Hz) | Cyclic |
|---|---|---|
| Pressure Conditions | 100 mmHg<br>140 mmHg<br>170 mmHg | **Magnitudes Effect**<br>80-120 mmHg, 1.167 Hz<br>120-160 mmHg, 1.167 Hz<br>150-190 mmHg, 1.167 Hz<br>**Frequency Effect**<br>0.5 Hz, 80-120 mmHg<br>1.167 Hz, 80-120 mmHg<br>2 Hz, 80-120 mmHg<br>**Combined**<br>2Hz, 150-190 mmHg |
| Biological Endpoints | Collagen synthesis<br>sGAG synthesis<br>DNA synthesis<br>$\alpha$-SMC actin expression<br>Tissue morphology<br>MMP-2,-9 expression | Collagen synthesis<br>sGAG synthesis<br>DNA synthesis/cell proliferation<br>$\alpha$-SMC actin expression<br>Tissue morphology<br>MMP-2, -9 expression & activity<br>Cathepsin B, L, S expression & activity |

### 5.1.2 Influence of Constant Pressure

Constant static pressure was achieved by using the cyclic pressure system without the compressed air tank and the pulse generator system. Simply, the pressure chamber was filled with 5% $CO_2$/air and the pressure magnitude was adjusted by adjusting the $CO_2$/air flow into the chamber. All experiments lasted for 48 hrs with conditions and biological endpoints listed in the Table 6.

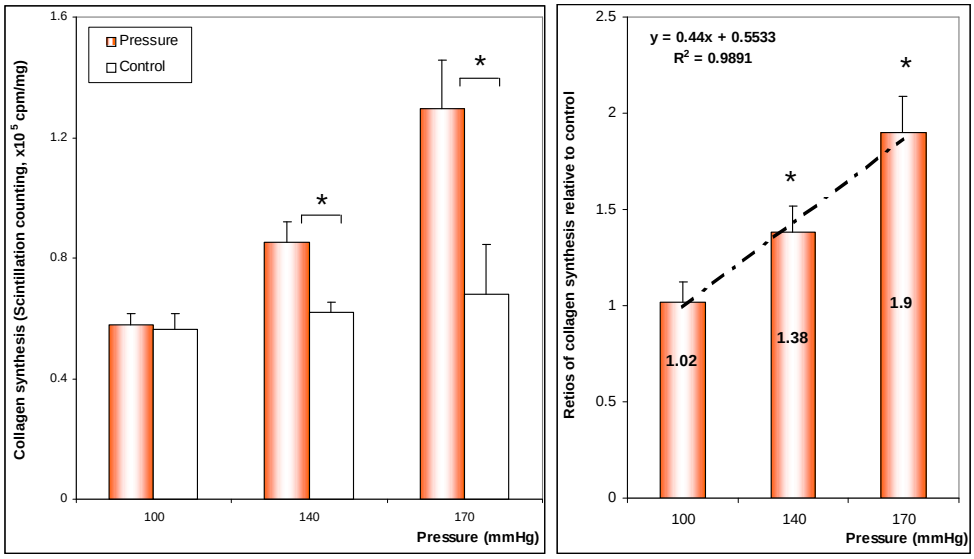


**Figure 16:** Collagen synthesis under constant static pressure: left - collagen synthesis expressed in scintillation counting (cpm/mg), right - Ratio of collagen synthesis relative to control; $*$ indicates statistical significance, $p < 0.05$

#### *5.1.2.1 Collagen synthesis*

Collagen synthesis was measured by $^3$H-proline radiolabeling and expressed as scintillation counting per minute (cpm) normalized by sample dry weight (mg). Results showed that collagen synthesis increased under contant static pressure (Fig.16). These increases were found to depend on the pressure level: at physiological pressure (100 mmHg), there was a slight but statistically insignificant increase as compared to control; at hypertensive pressure (140 mmHg), the increase was about 38$\pm$7% (Wilcoxon Signed Rank Test, $p < 0.05$); and at severe hypertensive pressure (170 mmHg), the increase went up to 90$\pm$10%. Ratios of collagen synthesis relative to control were plotted against pressure levels, the regression line showed a linear relationship between collagen synthesis and pressure magnitude within the investigated pressure range ($r^2 = 0.959$).

#### *5.1.2.2 sGAG synthesis*

The valve leaflet is very rich in glycoaminoglycans (GAG) and proteoglycans. These molecules are either dispersed between collagen fibers in the ventricularis or concentrated in the spongiosa, which consists mainly of GAGs and water. The role of GAG in valve function is believed to provide lubrication between the fibrosa and the ventricularis during valve opening and closing. There are studies

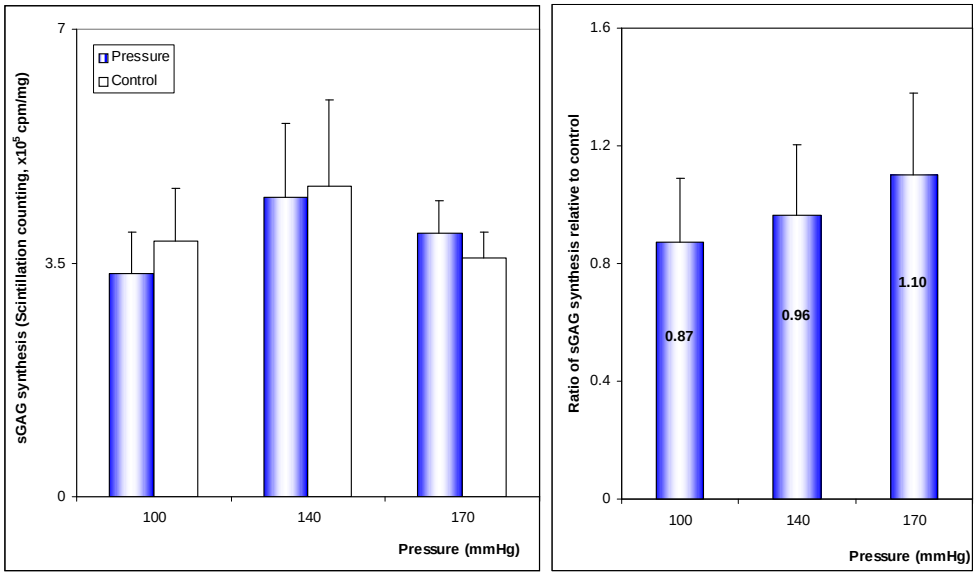


**Figure 17:** sGAG synthesis under constant static pressure: left - sGAG synthesis expressed in scintillation counting (cpm/mg), right - Ratio of sGAG synthesis relative to control

showing that sGAG synthesis was most active in the basal region, concurrent with the maximal bending stresses [123]. sGAG synthesis was measured by using $^{35}$-sulfate radiolabeling and expressed as scintillation counting per minute (cpm) normalized by sample dry weight (mg). Results showed that sGAG synthesis in the AV leaflets was not significantly affected by elevated constant pressure (ratios to controls are not significantly different from 1.0, Fig.17). The differences between samples exposed to elevated pressure and those cultured under atmospheric conditions were not statistically significant (Wilkoxon signed rank test, $p > 0.05$) for all pressure levels.

#### *5.1.2.3 DNA synthesis*

DNA synthesis, an indicator of cell proliferating activity, was measured using $^{3}$H-Thymidine radiolabeling. Fig.18 shows DNA synthesis expressed as scintillation counting per minute (cpm) normalized by sample dry weight (mg) and as ratios of synthesis under pressure and control. Valvular DNA synthesis under constant static pressure was comparable to DNA synthesis at atmospheric pressure at all pressure levels except 100 mmHg (Wilkoxon signed rank test, $p > 0.05$). At 100 mmHg, the constant pressure group had about 26% less newly synthesized DNA than atmospheric controls (Wilkoxon signed rank test, $p < 0.05$).

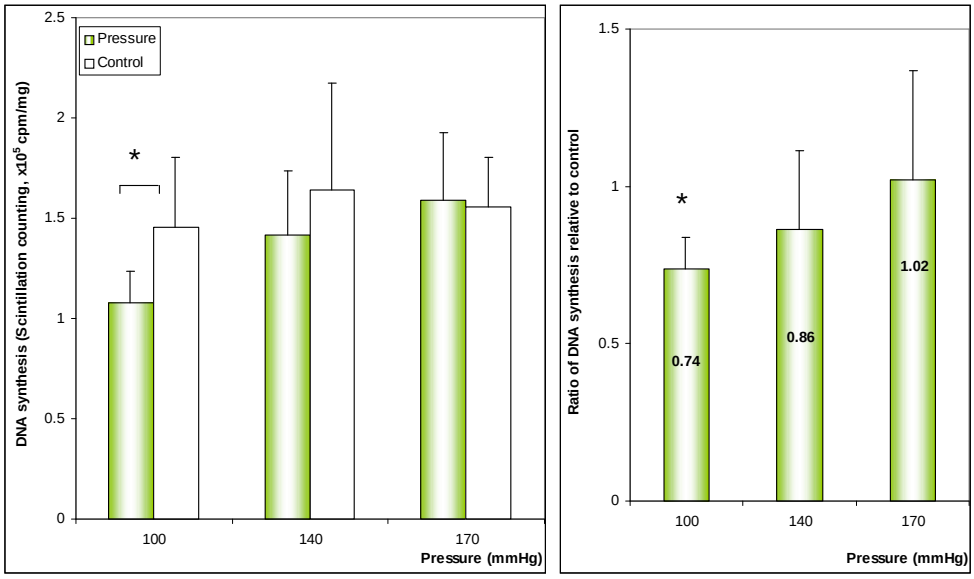


**Figure 18:** DNA synthesis under constant static pressure: left - DNA synthesis expressed in scintillation counting (cpm/mg), right - Ratio of DNA synthesis relative to control

#### *5.1.2.4 $\alpha$-SM actin immunohistochemistry (IHC)*

Among the three major cell phenotypes in valvular ICs, myofibroblasts and SMCs are distinct from the fibroblasts in their expression of $\alpha$-SM actin. $\alpha$-SM actin in the valve leaflet is associated with its contractile properties, which are very important for valve normal function. Using $\alpha$-SM actin IHC, the distribution of these contractile cells, as well as the phenotype shift that might occur due to the changes in the culture environment can be detected. In each experiment, six or more leaflets were collected. Each leaflet was cut into three pieces, one served as fresh control (fixed immediately after dissection from the aortic root), one exposed to constant pressure and one exposed to atmospheric pressure. The latter two were both incubated for 48 hrs. Shown below are three representative images of $\alpha$-SM actin immunostaining in the AV leaflets from the three treatments(Fig.19).

As shown in Fig.19, $\alpha$-SM actin in the fresh native AV can be found in all three layers: the fibrosa, the spongiosa and the ventricularis. After 48 hrs' *ex vivo* organ culture, the amount of $\alpha$-SM actin declined significantly and the remaining $\alpha$-SM actin was mainly concentrated in the ventricularis. There was no significant difference between constant pressure and atmospheric control in $\alpha$-SM actin distribution or quantity (Wilcoxon signd rank test, p $>$0.05), indicating that constant static pressure did not affect cell phenotypic shift in the AV leaflet.

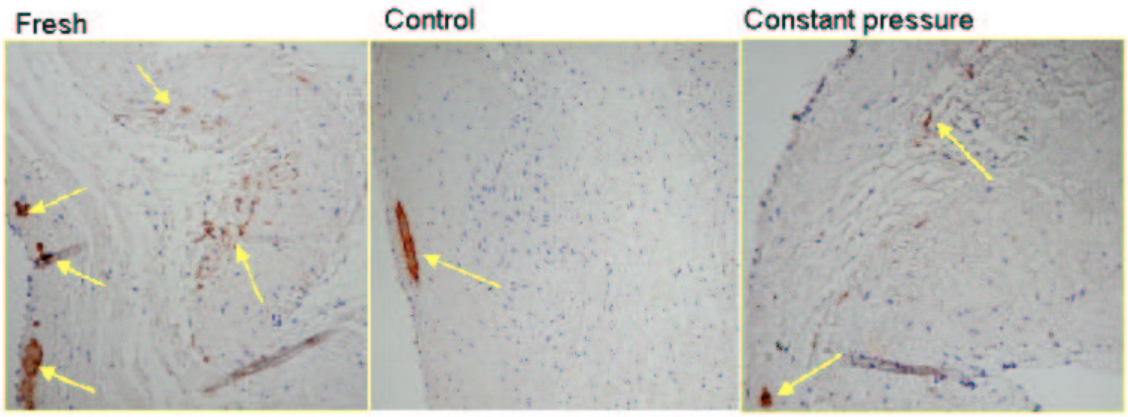


**Figure 19:** $\alpha$-SM actin IHC, actin stained brown (indicated by arrows), cell nuclei counter-stained blue, from left to right: fresh AV leaflets, leaflets cultured under atmospheric pressure for 48 hr, leaflets cultured under hypertensive pressure (170 mmHg) for 48 hr

#### *5.1.2.5 Tissue morphology: routine Hematoxylin and Eosin staining (H & E)*

Tissue morphology was assessed by routine H & E staining. Each leaflet was divided into three pieces and subjected to three treatments: fresh, constant pressure and control. Staining results revealed normal leaflet structure after exposure to constant pressure for 48 hrs, regardless of the pressure level (Fig.20). The characteristic trilaminar leaflet structures were well preserved and the cell density retained. These histological findings demonstrated that the experimental system was capable of maintaining the normal histological structure (i.e. ventricularis, spongiosa and the fibrosa) with the retention of the cellular components and preservation of the extracellular matrix.

### 5.1.3 Influence of Cyclic Pressure

#### *5.1.3.1 Magnitude Effect*

The effects of pressure magnitude were studied by fixing the pulse frequency at 1.167 Hz and setting the pressure range to be physiological: 80-120 mmHg, hypertensive: 120-160 mmHg and severe hypertensive: 150-190 mmHg. For each experiment, leaflets cultured under atmospheric pressure were used as controls.

**Collagen synthesis**

Collagen synthesis under cyclic pressure increased in a similar fashion as under constant static

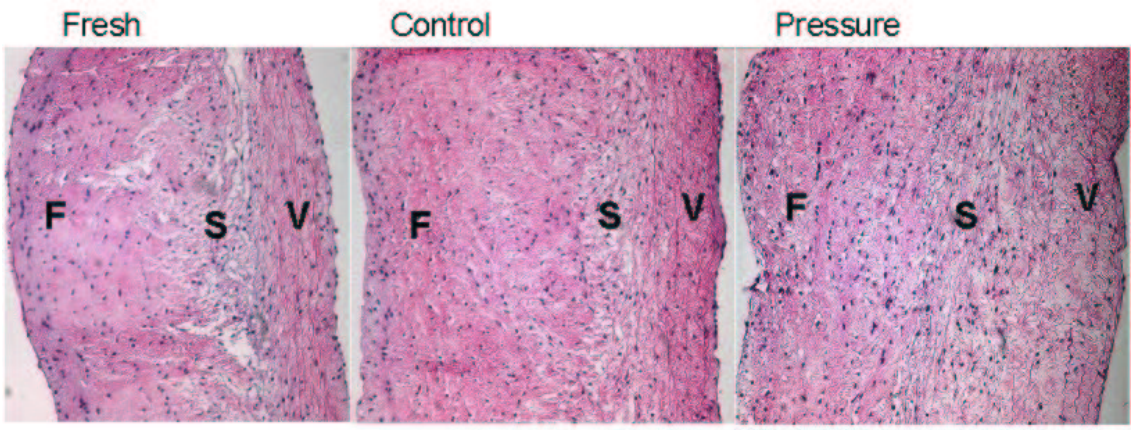


**Figure 20:** Tissue morphology after exposure to constant static pressure, routine H and E staining, cell nuclei stained purple or blue, cytoplasm stained pink, F-fibrosa, S-spongiosa, V-ventricularis

pressure (Fig.21). At 80-120 mmHg (mean of 100 mmHg), there was a slight increase under pressure, but the difference was statistically insignificant. As pressure rose to 120-160 mmHg (mean of 140 mmHg), this increase became greater and statistically significant (45%,Wilkoxon signed rank test, $p < 0.05$). This trend continued as the pressure went up to 150-190 mmHg (mean of 170 mmHg), at which the net increase was 118% (Wilkoxon signed rank test, $p < 0.05$). Ratios of collagen synthesis relative to control were plotted against pressure magnitude. The regression line showed a linear relationship between increases in collagen synthesis and pressure magnitudes ($r^2 = 0.926$).

**sGAG synthesis**

sGAG synthesis under cyclic pressure demonstrated different behavior from that under constant static pressure. Under cyclic pressure, sGAG synthesis was no longer unresponsive to pressure, instead, it was enhanced in a similar fashion as was collagen synthesis (Fig.22). There was a slight, but statistically insignificant increase (13%,Wilkoxon signed rank test, $p > 0.05$) at 80-120 mmHg. As pressure rose to 120-160 mmHg (mean of 140 mmHg), this increase became greater and statistically significant (65%,Wilkoxon signed rank test, $p < 0.05$). This trend continued as the pressure went up to 150-190 mmHg (mean of 170 mmHg), at which the net increase was 130% (Wilkoxon signed rank test, $p < 0.05$). Ratios of sGAG synthesis relative to control were plotted against pressure magnitude, the regression line showed a linear ($r^2 = 0.996$) relationship between increases in

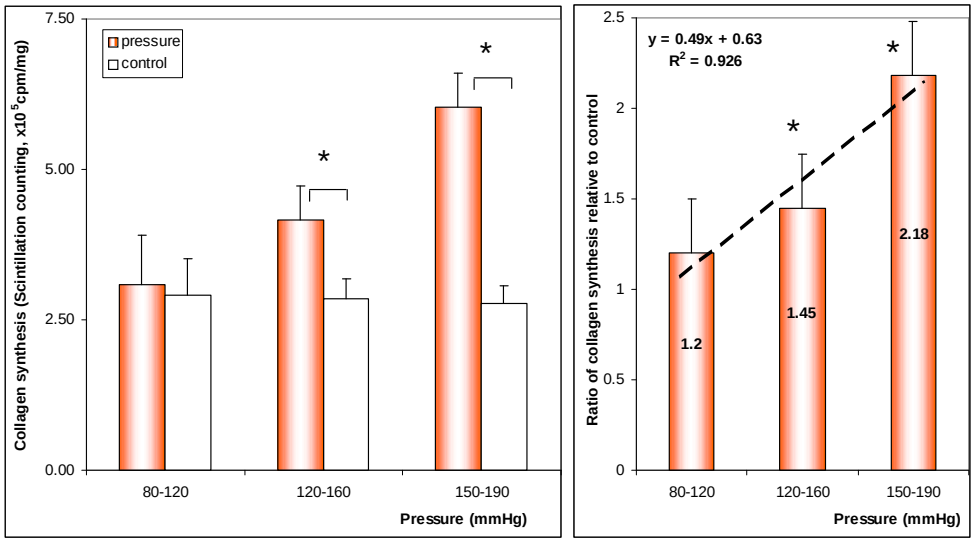


**Figure 21:** The influence of pressure magnitude on collagen synthesis: left - collagen synthesis in scintillation counting (cpm/mg), right -Ratio of collagen synthesis relative to control; $*$ indicates statistical significance, $p < 0.05$

sGAG synthesis and pressure magnitudes.

**DNA synthesis**

In contrast to collagen and sGAG synthesis, valvular DNA synthesis was not as significantly affected by cyclic pressure magnitude (Fig.23). Average DNA synthesis in the pressure groups was all higher than their atmospheric controls, but due to the large variations in the data, none of the differences were statistically significant (Wilkoxon signed rank test, $p > 0.05$).

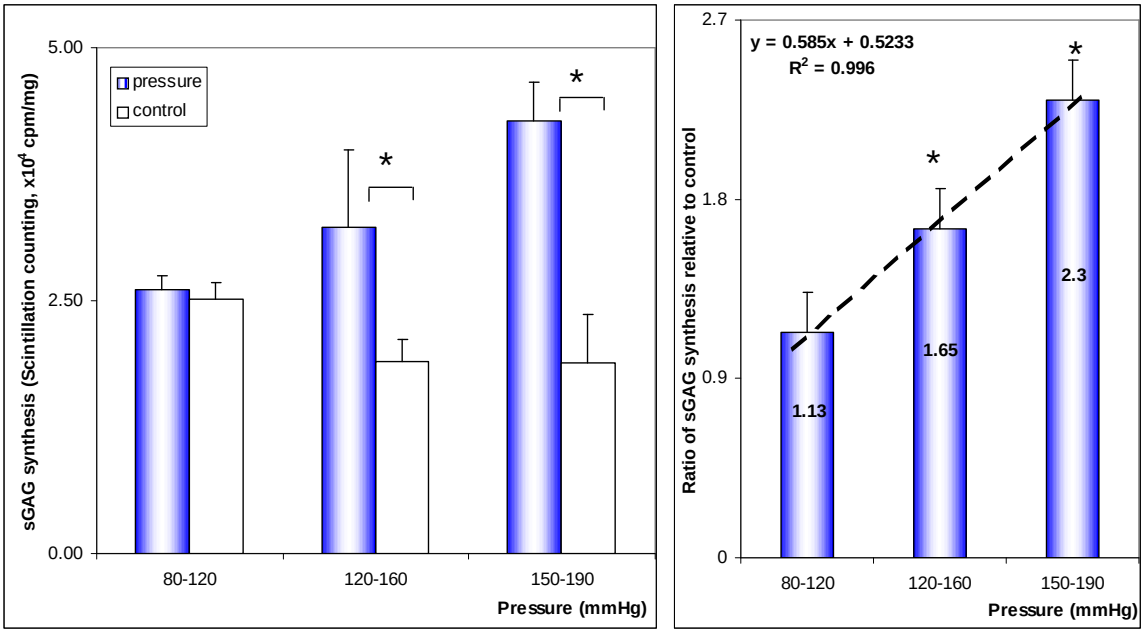


**Figure 22:** The influence of pressure magnitude on sGAG synthesis: left - sGAG synthesis in scintillation counting (cpm/mg), right -Ratio of sGAG synthesis relative to control; $*$ indicates statistical significance, $p < 0.05$

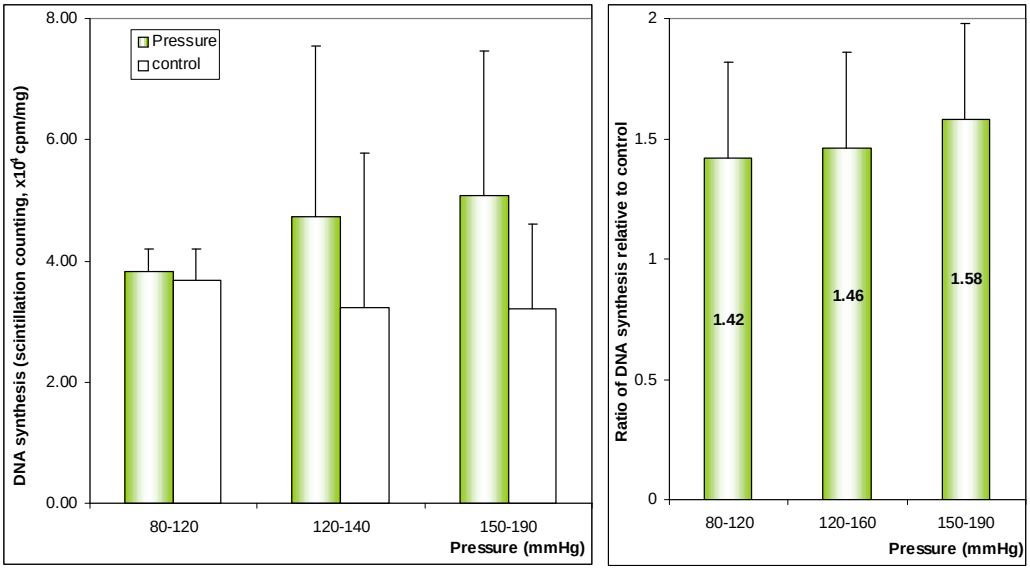


**Figure 23:** The influence of pressure magnitude on DNA synthesis: left - DNA synthesis in scintillation counting (cpm/mg), right -Ratio of DNA synthesis relative to control

### *5.1.3.2 Frequency Effect*

The effects of pulse frequency were studied by fixing the pressure magnitude at a physiological level (80-120 mmHg) and setting the pulse frequencies at 0.5, 1.167 and 2 Hz. Similar to the study on magnitude effects, leaflets cultured at atmospheric pressure were used as controls.

**Collagen synthesis**

The effects of pulse frequency on collagen synthesis in AV leaflets are shown in Fig.24. Collagen synthesis under pressure (80-120 mmHg) was higher than the control by about 26% at low frequency (0.5 Hz). This difference was statistically significant (Wilkoxon signed rank test, $p < 0.05$, n = 12). There was no significant difference between pressure and control at 1.167 Hz (Wilkoxon signed rank test, $p < 0.05$, n = 8), which was consistent with results from the magnitude effects study. Similar results were also observed with the 2 Hz experiment, where collagen synthesis was found to be comparable to atmospheric control.

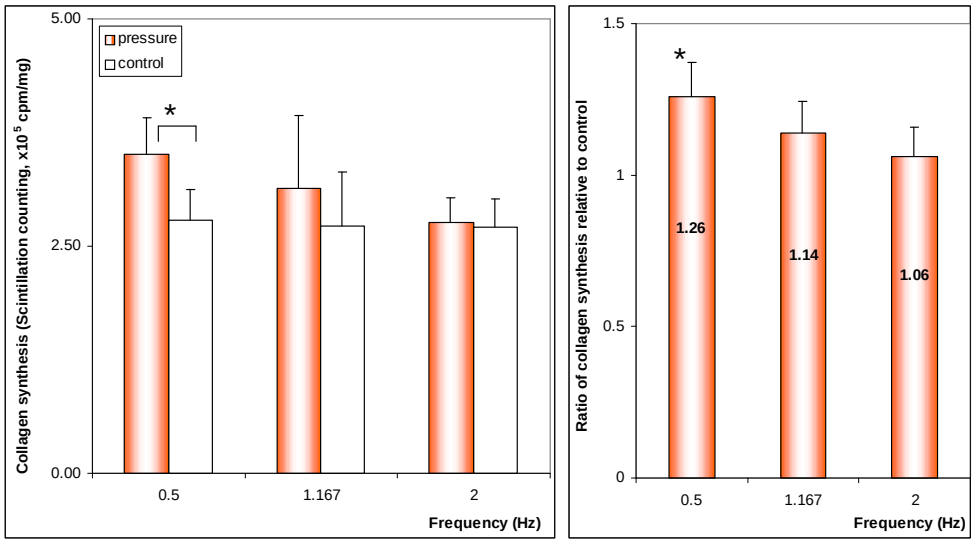


**Figure 24:** The influence of pulse frequency on collagen synthesis: left - collagen synthesis in scintillation counting (cpm/mg), right -Ratio of collagen synthesis relative to control; $*$ indicates statistical significance, $p < 0.05$

**sGAG synthesis**

sGAG synthesis follow the same trend as like collagen with respect to pulse frequency (Fig.25). There was a slight increase (14%) in sGAG synthesis at 0.5 Hz (Wilkoxon signed rank test, $p <$

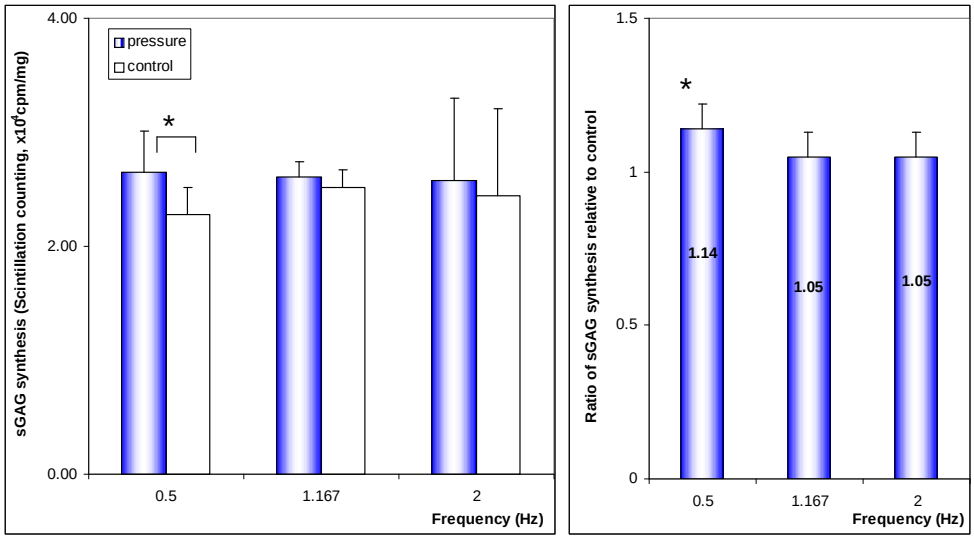


**Figure 25:** The influence of pulse frequency on sGAG synthesis: left - sGAG synthesis in scintillation counting (cpm/mg), right -Ratio of sGAG synthesis relative to control; $*$ indicates statistical significance, $p < 0.05$

0.05, n = 20); but no differences from the atmospheric controls for the other two frequencies (1.167 and 2 Hz).

**DNA synthesis**

Results so far have shown that DNA synthesis was not significantly affected by either constant static pressure or cyclic pressure at normal frequency (1.167 Hz), indicating that other factors other than pressure magnitude might be more influential on leaflet cell DNA synthesis. Results from the frequency effects study (Fig.26) showed that pulse frequency was a more influential factor on valvular DNA synthesis. At the low frequency (0.5 Hz), there was no significant difference in DNA synthesis between pressure (80-120 mmHg) and control. As expected, the difference was negligible also at 1.167 Hz as shown earlier in the magnitude effects study (see Fig.23). However, at the high frequency (2 Hz, corresponding a heart rate of 120 bpm), DNA synthesis in the AV leaflets was significantly increased by 72% (Wilkoxon signed rank test, $p < 0.05$) as compared with atmospheric controls.

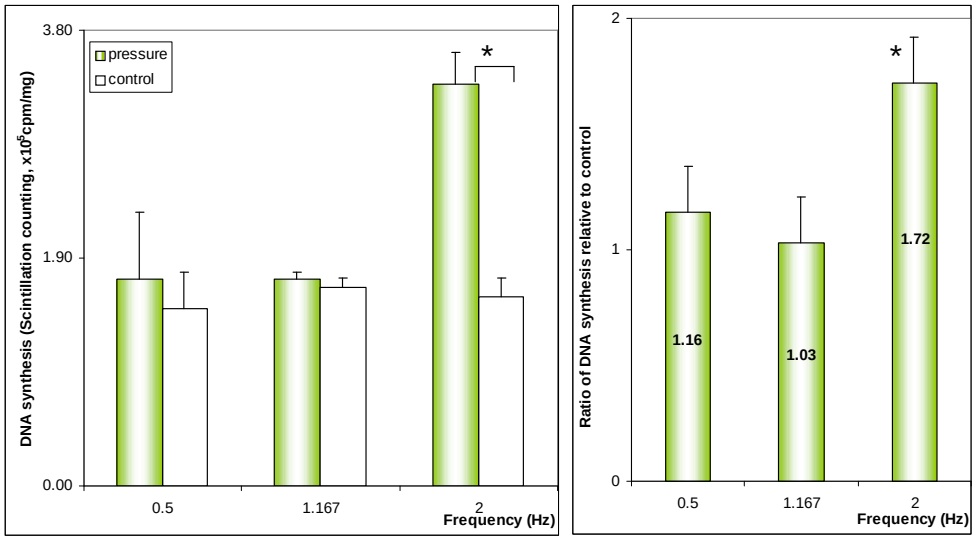


**Figure 26:** The influence of pulse frequency on DNA synthesis: left - DNA synthesis in scintillation counting (cpm/mg), right -Ratio of DNA synthesis relative to control

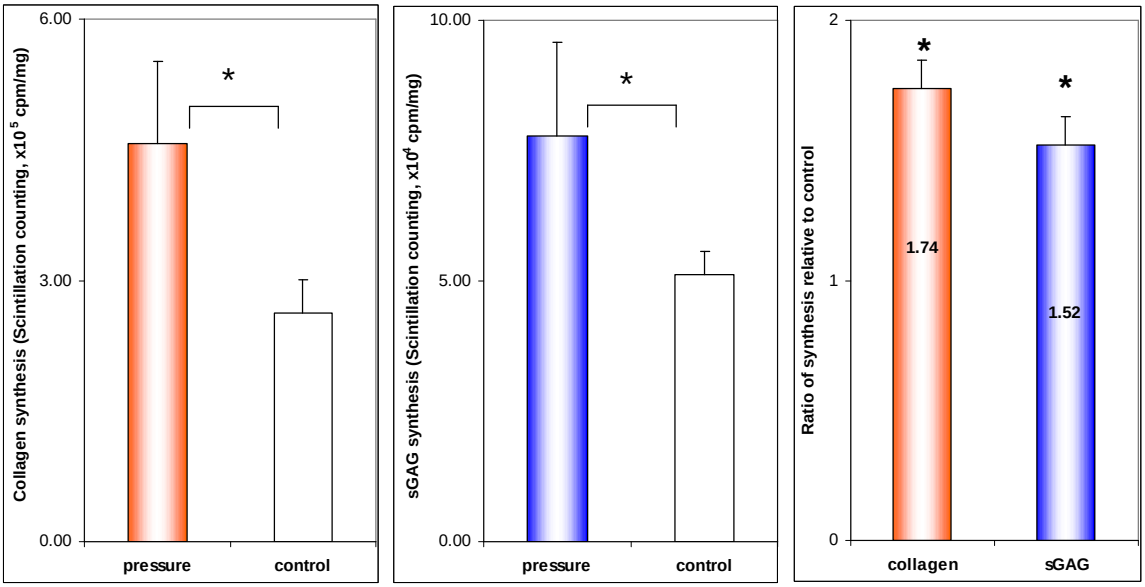


**Figure 27:** Collagen and sGAG synthesis under extreme pressure conditions : left - Collagen synthesis in scintillation counting (cpm/mg), middle - sGAG synthesis in scintillation counting (cpm/mg), right - Ratio of synthesis relative to control; $*$ indicates statistical significance, $p < 0.05$)

### 5.1.4 Extreme Pressure Conditions: high magnitude (150-190mmHg), high frequency (2 Hz)

The above results showed that pressure magnitude and pulse frequency were two important parameters that determines the effects of cyclic pressure. These two parameters of cyclic pressure appeared to have differential effects when studied in isolation. The aim of this section was to study the combined effects of these two parameters by looking at cyclic pressure conditions combining the highest frequency (2 Hz) with highest magnitude (150-190 mmHg). Collagen synthesis and sGAG synthesis were measured by dual radiolabeling, cell proliferation was measured by BrdU staining.

#### *5.1.4.1 Collagen and sGAG synthesis*

Radiolabeling results (Fig.27) showed that both collagen and sGAG synthesis were significantly increased under extreme pressure conditions. Compared with atmospheric controls, collagen synthesis increased by 74% and sGAG synthesis increased by 52% (Wilkoxon signed rank test, $p < 0.05$). These net increases were lower than those under high pressure magnitude (150-190 mmHg) and normal frequency (1.167 Hz): 74% versus 118% in the case of collagen synthesis and 130% versus 52% for sGAG synthesis.

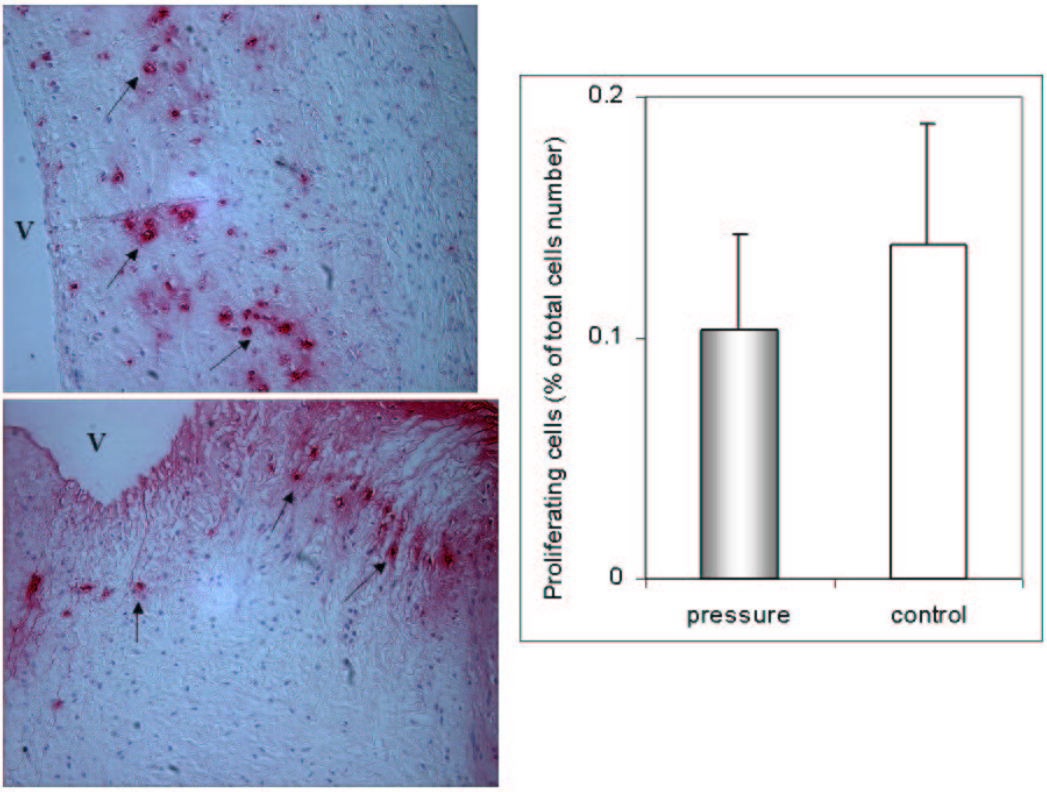


**Figure 28:** Cell proliferation under extreme pressure conditions : left - BrdU immunostaining, proliferating cells stain red, upper panel: control, lower panel: cyclic pressure, V-indicating the ventricularis side of the leaflet right - Comparison of proliferating percentage between pressure and control

#### *5.1.4.2 Cell proliferation*

Cell proliferation was detected by BrdU immunostaining. Proliferating cells had BrdU in their nuclei and were stained as pink, non-proliferating cells were devoid of BrdU and counter-stained as blue. The number of proliferating cells in each sample was counted and divided by the total cell number to get a proliferating percentage. Proliferating percentages from 6 samples were averaged and compared between pressure and control. As shown in the figure (Fig.28), proliferating cells were present in both pressure and control samples. However, the percentage was very low (less than 1%, total cell count per slide: 30,000) in both cases and there was no significant difference between the two conditions (Wilkoxon signed rank test, $p > 0.05$).

#### *5.1.4.3 $\alpha$ - SM actin IHC*

Similar to the constant pressure study, $\alpha$ - SM actin IHC was used to measure cell phenotypic changes in the leaflets. For each experiment, at least six leaflets were collected. Each leaflet was cut into three pieces, one served as fresh control, one exposed to cyclic pressure and one cultured under atmospheric pressure. The latter two were both incubated for 48 hr. Shown in Fig.29 are typical staining images of $\alpha$ - SM actin under the three different treatments. $\alpha$-SM actin in the fresh native AV was much more abundant and present in all three layers: the fibrosa, the spongiosa and the ventricularis. After 48 hrs' of *ex vivo* organ culture, the amount of $\alpha$-SM actin declined significantly and the remaining $\alpha$-SM actin was mainly concentrated in the ventricularis. There was no significant difference between cyclic pressure and atmospheric control in $\alpha$-SM actin distribution or quantity, indicating the presence of cyclic pressure did not affect cell phenotypic shift.

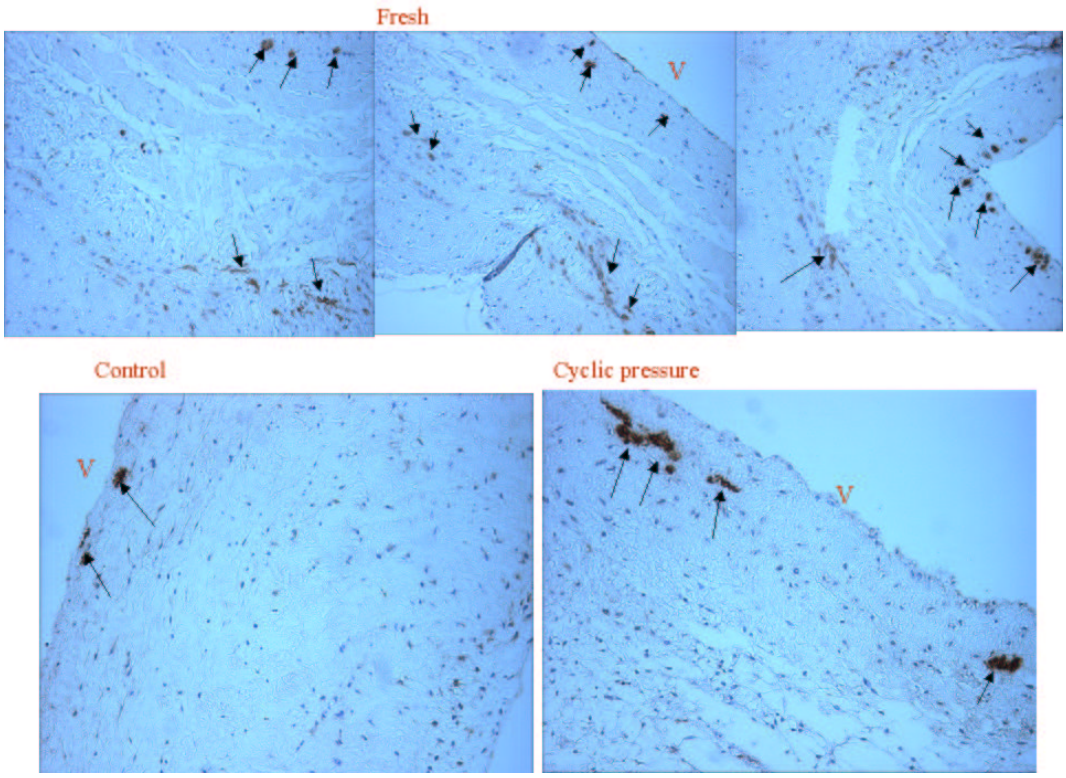


**Figure 29:** $\alpha$ - SM actin IHC, actin stained brown (indicated by arrows), cell nuclei counterstained blue, V-indicating the ventricularis side, top panel: different areas of a fresh leaflet section, bottom panel: left-control, right-cyclic pressure (mean: 170 mmHg, 1.167 Hz)

### *5.1.4.4 Tissue morphology*

Tissue morphology was assessed by routine H and E staining. Again, three pieces of each leaflet were taken and subjected to three treatments: fresh, pressure and control. Staining results (Fig.30) revealed normal leaflet structure after exposure to cyclic pressure for 48 hr, regardless of the pressure magnitude or frequency. The characteristic leaflet trilaminar structures were well preserved and the cell density retained. These histological findings demonstrated that the experimental system was capable of maintaining the normal histological structure (i.e. ventricularis, spongiosa and the fibrosa) with the retention of the cellular components and preservation of the extracellular matrix.

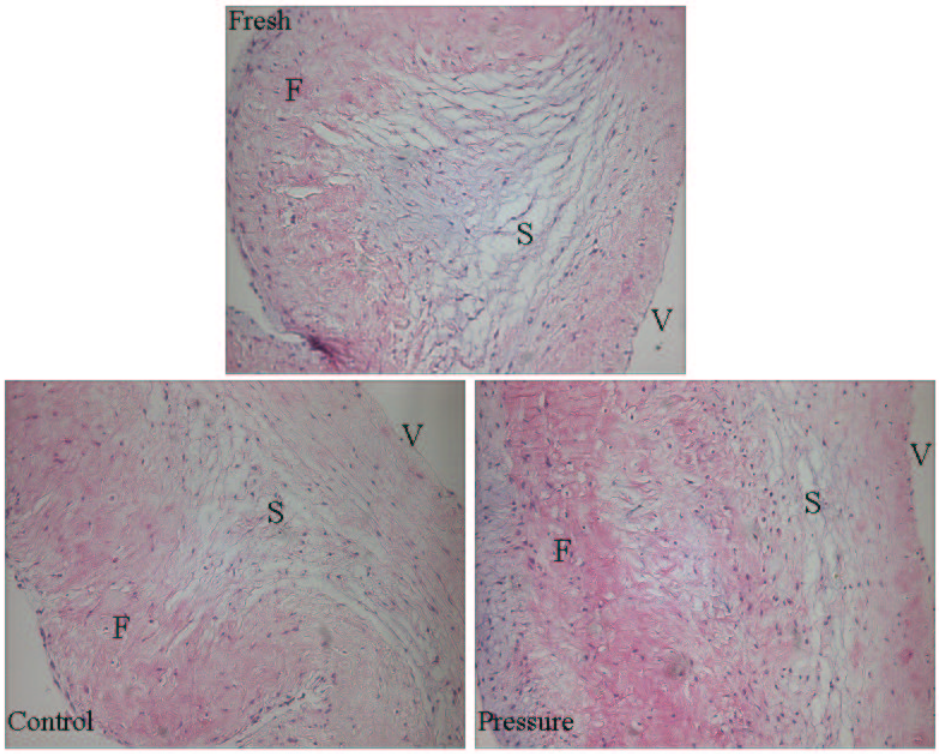


**Figure 30:** Routine H & E staining, cell nuclei appeared dark blue or purple, cytoplasm was pink, F-fibrosa, S- spongiosa and V- ventricularis, top: fresh AV leaflet, bottom left: control, bottom right: cyclic pressure (mean: 170 mmHg, 1.167 Hz)

### *5.1.4.5 MMPs and Cathepsins*

**MMP-2 and MMP-9 IHC**

MMP-2 and -9 IHC staining results (Fig.31, Fig.32) showed that fresh valves had minimal MMP-9 positive staining. Valves exposed to pressure and static incubation displayed higher levels

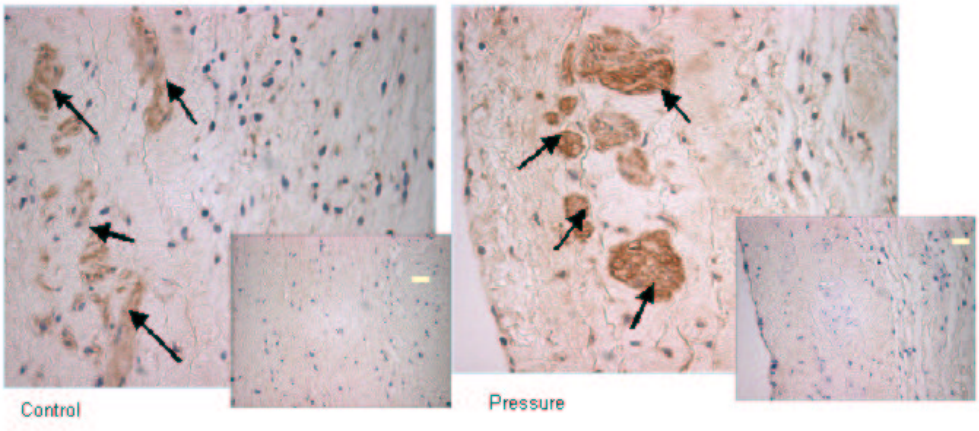


**Figure 31:** MMP-2 IHC, MMP-2 stained brown (indicated by arrows), cell nuclei counter-stained blue, insert - negative control with the omission of primary antibody

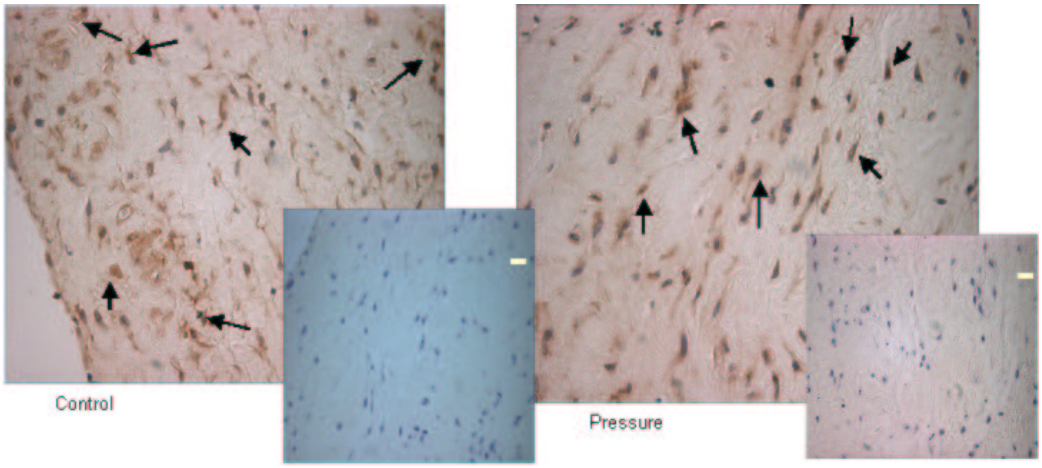


**Figure 32:** MMP-9 IHC, MMP-9 stained brown (indicated by arrows), cell nuclei counter-stained blue, insert - negative control with the omission of primary antibody

of MMP-9 than fresh valves. The majority of MMP-9 was detected in the spongiosa and fibrosa, and was retained around the cell nuclei. MMP-2 was more prominent than MMP-9 in fresh valves, and increased in both the controls and pressure samples. Both MMPs were located mainly in the spongiosa and fibrosa, indicating that valve interstitial cells are the major sources of these MMPs.

**MMP-2 and MMP-9 Western blotting and Zymography**

Western blotting (Fig.33)showed no difference in the amount of MMP-2 and -9 between cyclic pressure and atmospheric controls; but MMP-2 was more prominent than MMP-9. MMP-2 and -9 zymograms (Fig.34)also showed similar MMP activities between the cyclic hypertensive pressure conditions and atmospheric controls.

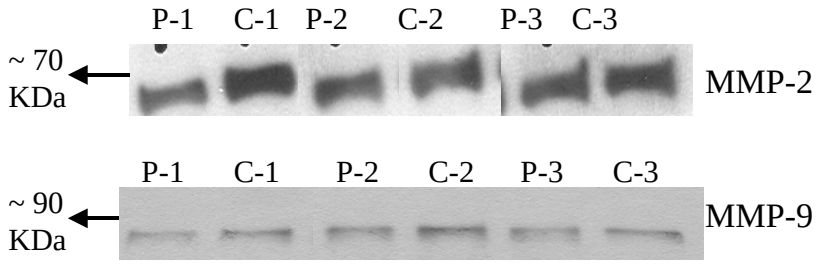


**Figure 33:** MMP-2, MMP-9 Western blotting, top - MMP-2, bottom - MMP-9; P-1,C-1 indicate two sections from one leaflet and exposed to hypertensive pressure (170 mmHg) and atmospheric pressure, respectively. The nomenclature also applies to P-2, C-2 and P-3, C-3. Note that there were no significant differences in either MMP-2 or MMP-9 between the P's and C's.

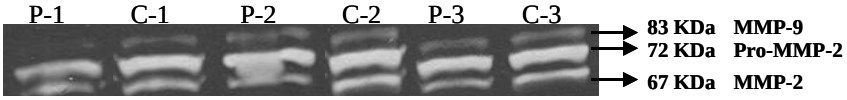


**Figure 34:** MMP-2, MMP-9 zymogram, active MMP-2: 67 kDa, active MMP-9: 83 kDa; P-1,C-1 indicate two sections from one leaflet and exposed to hypertensive pressure (170 mmHg) and atmospheric pressure, respectively. The nomenclature also applies to P-2, C-2 and P-3, C-3. Note that there were no significant differences in the activities of MMP-2 and -9 between the P's and C's.

**Cathepsins**

**Cathepsin Immunohistochemistry**

Immunohistochemistry staining for cathepsin B showed that the enzyme was located mainly along the endothelial surfaces, with some staining in the interstitial area as well. The staining pattern showed a very diffusive (not concentrated in certain areas), mainly extracellular localization of the protein ( Fig.35).

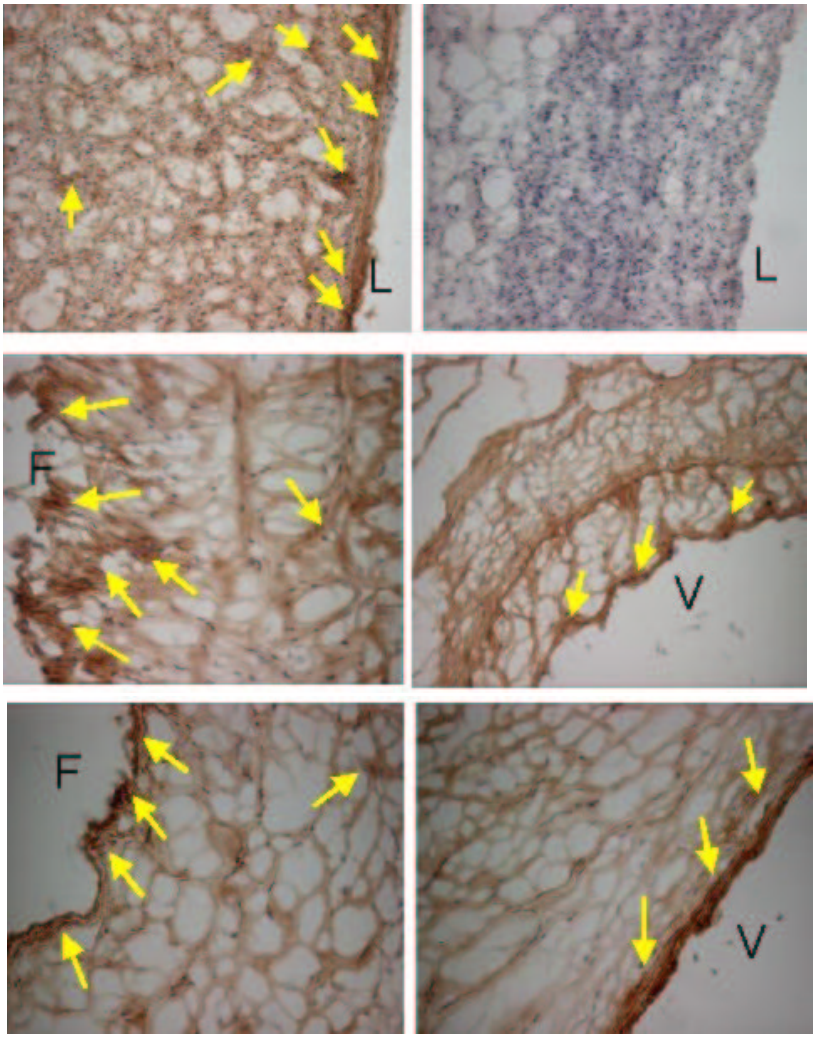


**Figure 35:** Cathepsin B IHC, cathepsin B stains brown, indicated by arrows; top panel: Left: positive control (porcine pulmonary artery), right: negative control, L indicates the lumen side; middle panel: Porcine AV leaflets under static incubation for 48 hrs, F- fibrosa side, V-ventricularis side; bottom panel: Porcine AV leaflets under hypertensive pressure (170 mmHg, 1.167 Hz) for 48 hrs

Immunohistochemistry staining for cathepsin L showed that the enzyme was located mainly in the interstitial space, with very little staining on the endothelial layer (except for the pulmonary artery positive controls). In contrast to cathepsin B, cathepsin L was mainly concentrated around cell nuclei, indicating that the enzyme was largely intracellular (Fig.36).

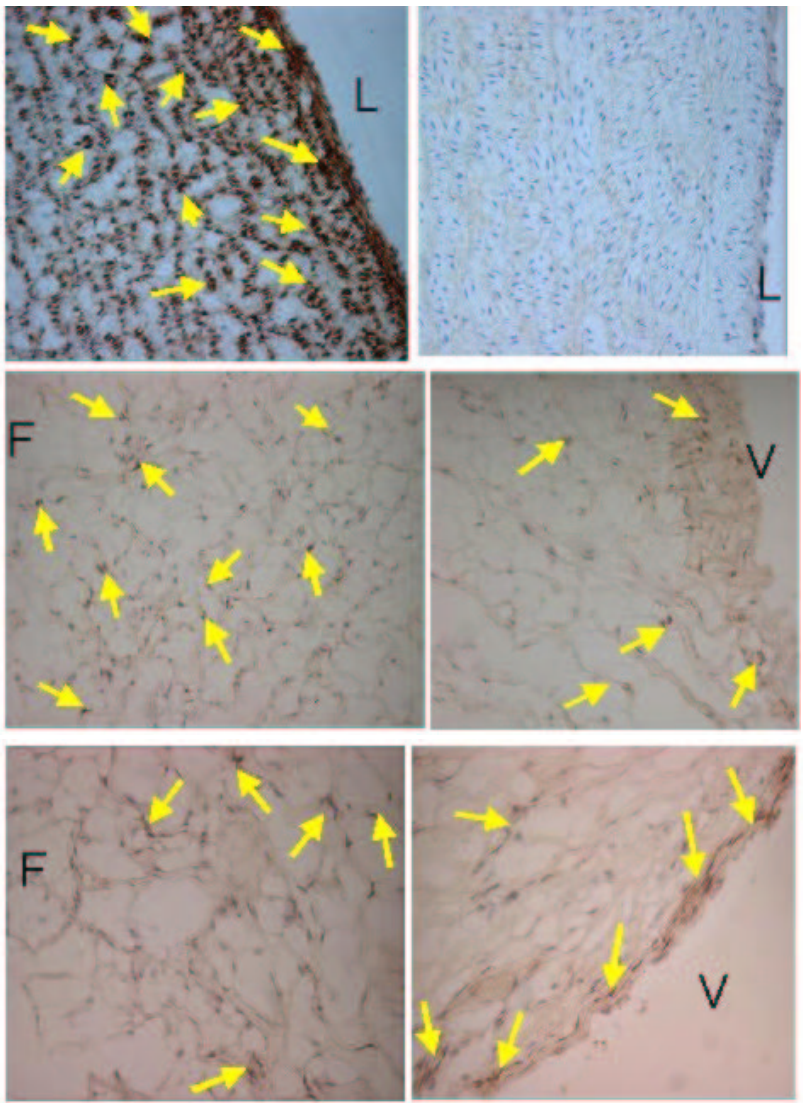


**Figure 36:** Cathepsin L IHC, cathepsin L stains brown, indicated by arrows, cell nuclei counter-stained blue; top panel: Left: positive control (porcine pulmonary artery), right: negative control, L indicates the lumen side; middle panel: Porcine AV under static incubation for 48 hrs; bottom panel: Porcine AV under static incubation for 48 hrs, F- fibrosa side, V-ventricularis side

Cathepsin S staining showed a similar pattern to that of cathepsin L. Majority of the enzyme was located around cell nuclei, diffusive staining was also present, but the amount was very small (Fig.37).

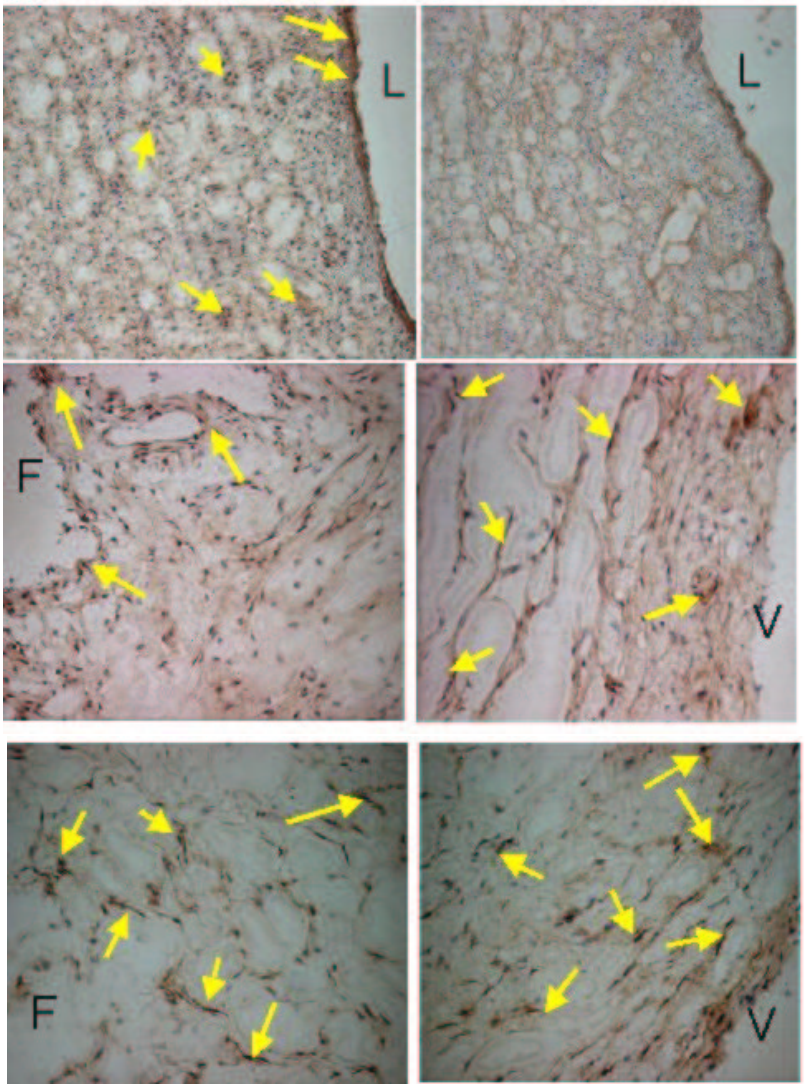


**Figure 37:** Cathepsin S IHC, cathepsin S stains brown, indicated by arrows; top panel: Left: positive control (porcine pulmonary artery), right: negative control, L indicates the lumen side; middle panel: Porcine AV under static incubation for 48 hrs; bottom panel: Porcine AV under hypertensive pressure (170 mmHg, 1.167 Hz) for 48 hrs, F- fibrosa side, V-ventricularis side

**Cathepsins Western Blotting & Gelatin Zymography**

Shown below are the western blotting and zymography results of cathepsin B, L and S (Fig.38). In contrast to MMPs, cathepsin profile varied significantly between the different treatments. Gelatin zymography (Fig.38) results showed that cathepsin L activity in samples exposed to hypertensive pressure was significantly lower (37% less) than that in the control samples. Cathepsin S levels under hypertensive pressure decreased compared to atmospheric controls as shown by western blot. Cathepsin B was present in all the samples, but there were no significant differences in either expression or activity between the different treatments. Cathepsin K was not detectable in any of the samples, including both the controls and those exposed to hypertensive pressure.

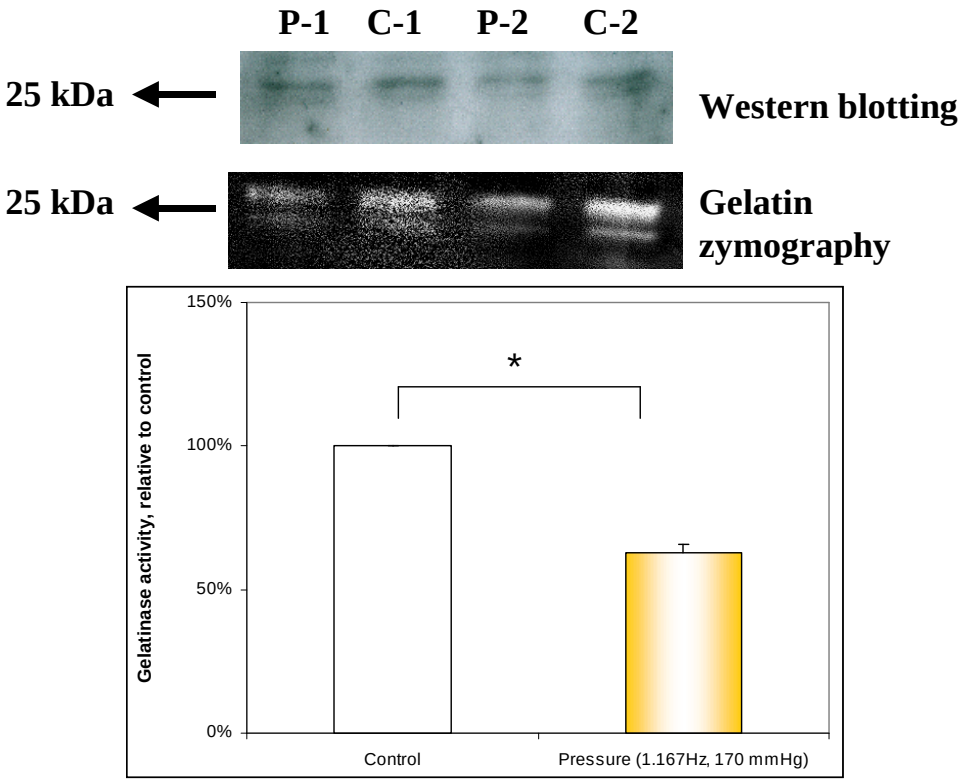


**Figure 38:** Cathepsin L activity in AV leaflets, comparison between pressure and control, top - cathepsin L zymogram, bottom - quantified cathepsin L activity; P-hypertensive pressure (170 mmHg), C- atmospheric controls, $* \; p < 0.05$

## *5.2 Influence of Shear Stress on the Biological Properties of AV Leaflets*

The shear stress study consists of two subsets of experiments: shear stress on intact leaflets and shear stress on denuded leaflets. Table.7 summarizes all the experimental conditions, as well as the biological endpoints studied in the shear stress study.

**Table 7:** Shear Stress Study: Summary of Experiments

| | Intact Leaflets | Denuded Leaflets |
|---|---|---|
| Shear | 1,9,25,40 & 80 dyne/cm$^2$ | 1,9,25,40 & 80 dyne/cm$^2$ |
| Biological Endpoints | Endothelial retention & alignment<br>Collagen synthesis<br>sGAG content<br>$\alpha$-SMC actin expression<br>Tissue morphology<br>MMP-2, -9 expression & activity<br>Cathepsin B, L, S expression & activity | Collagen synthesis<br>sGAG content<br>$\alpha$-SMC actin expression<br>Tissue morphology<br>MMP-2, -9 expression & activity<br>Cathepsin B, L, S expression & activity |

### 5.2.1 Influence of Shear Stress on Intact Leaflets

In this part of study, the leaflets were carefully handled in such as way that any contact with the endothelium on the ventricular surface was kept to a minimum. Valve leaflets handled in this way were then viewed under SEM to check for the completeness of endothelium (see Fig.41). The influence of shear stress was studied by using the modified parallel plate system, with the ventricularis surface of the leaflet facing flow. Steady laminar shear stresses of 1, 9, 25, 40 and 80 dyne/cm$^2$ were applied to the AV leaflets for 48 hrs, with leaflets under static incubation as controls. At the end of each experiment, the leaflets were examined by SEM for endothelial retention and alignment; by measuring collagen synthesis and sGAG content for valvular synthetic activity; by histology techniques for tissue morphology and cell phenotypical changes and by western blot and zymograms for MMPs and cathepsins.

#### *5.2.1.1 Leaflet Cell Viability*

Before collecting any data on valvular responses to shear, representative sections of the samples that had been exposed to shear were taken and stained with EthD Homodimer and Hoechst 33258 for

cell viability assessment. Staining results showed that more than 99% of the cells were alive (blue) after exposure to shear, which is comparable to the cell viability under static incubation (Fig.39).

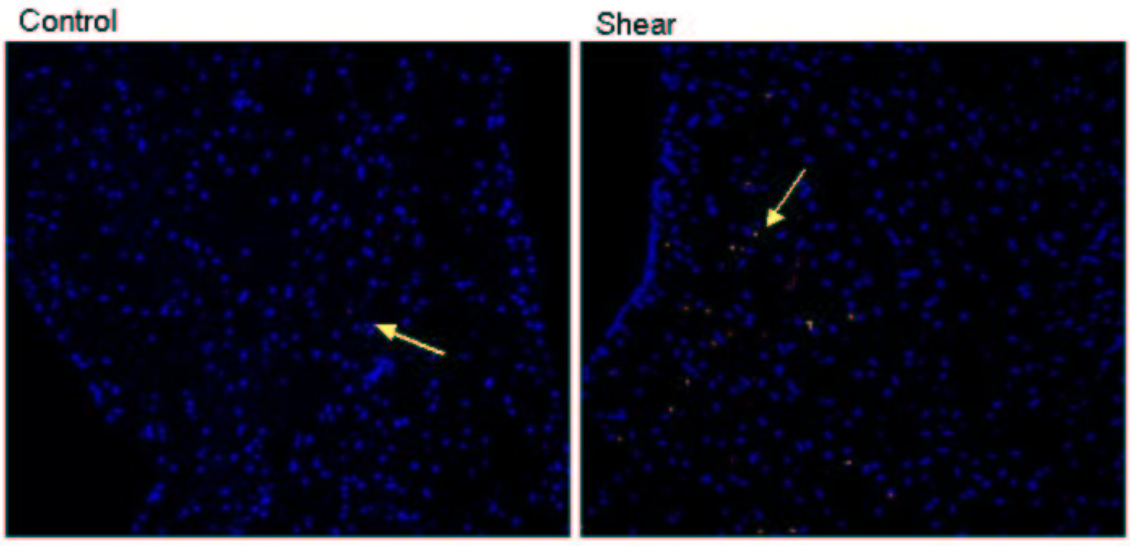


**Figure 39:** Leaflet cell viability after exposure to shear, Ethidium-homodimer Hoechst staining, dead cells stain red/pink and indicated by arrowa, live cells are blue

#### *5.2.1.2 Endothelial cell retention and alignment*

One of the most frequently noticed effects of steady laminar shear stress is on cell alignment. For example, vascular endothelial cells under static culture generally have a random alignment; once exposed to steady laminar shear, they will quickly assume an alignment that is parallel with the shear direction. *In vivo* studies have shown that valvular endothelial cells align perpendicularly to flow [34]. This unique phenomenon was attributed to fact that the dominant stress in the AV leaflets was in the circumferential direction. Therefore, it is of interest to know if this alignment will persist in an *in vitro* flow system, in which shear stress was the only mechanical factor and the dominant stress was in the radial direction. Another concern of exposure to shear stress as high as 80 dyne/cm$^2$ was the retention of endothelial cells, since the physiological shear stress experienced by the AV has an average of 22-40 dyne/cm$^2$ [168]. Both cell retention and alignment were examined using SEM. Shown in Fig.40 are some typical SEM images of a valve leaflet exposed to physiological shear (mean of 25-40 dyne/cm$^2$) for 48 hrs. As shown in these images, the AV leaflets were still covered with an intact EC layer after exposure to shear, and these cells were aligned perpendicular to flow

direction, similar to *in vivo* observations.

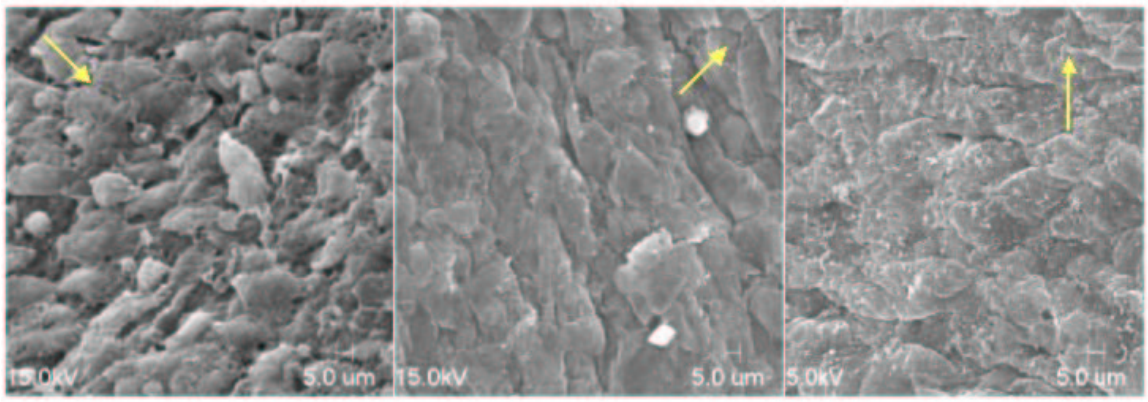


**Figure 40:** SEM images of the AV leaflet ventricular surface after exposure to physiological shear (25-40 yne/cm$^2$) for 48 hrs, arrow indicates flow direction. Three images are from three different leaflets

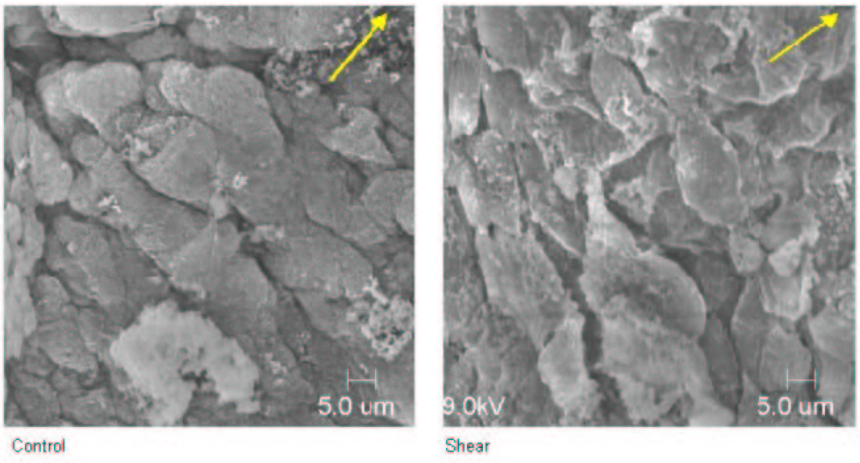


**Figure 41:** SEM image of the AV leaflet ventricular surface after exposure to 80 dyne/cm$^2$ shear for 48 hr, left - control, right - shear, arrow indicates flow direction (shear) and *in vivo* flow direction (control)

Shown in Fig.41 are the SEM images of leaflet exposed to peak shear stress level of 80 dyne/cm$^2$ or under static incubation (control) for 48 hrs. It is clear from these images that endothelial cells were still present after 48 hrs of continuous exposure to 80 dyne/cm$^2$ and cell alignment was still perpendicular to flow. In the case of static incubation, where there was no applied mechanical stress on the leaflets, endothelial alignment was also similar to the *in vivo* observations.

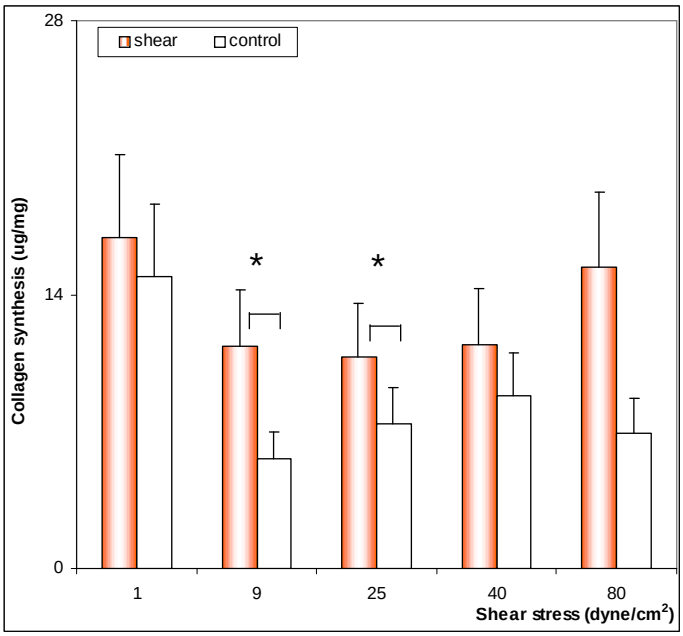


**Figure 42:** Collagen synthesis by intact AV leaflets under shear, collagen synthesis in AV leaflets under shear vs. static control, expressed in $\mu$g/mg, $*$ indicate statistical significance, p $<$0.05

#### *5.2.1.3 Collagen synthesis*

Collagen synthesis in the AV leaflets exposed to shear was measured by using the Sircol collagen assay. The amount of newly synthesized collagen ($\mu$g) as obtained from the microplate reader, was normalized by sample dry weight (mg) and compared with the static controls. The results are shown in both actual amount of collagen (Fig.42) and in ratios of shear to static controls (Fig.43). The latter was used to eliminate the influence of biological variability among different valves. As shown in the results collagen synthesis was significantly enhanced at 9 dyne/cm$^2$ with a net increase of 99% ($p < 0.01$) and at 25 dyne/cm$^2$ with a net increase of 63% ($p < 0.02$) (Fig.43). The differences between shear and static control at 1, 40 and 80 dyne/cm$^2$ were statistically insignificant (Wilkoxon signed rank test, $p > 0.1$). Therefore, 9-25 dyne/cm$^2$ appeared to be the shear range that induces collagen synthesis in the AV leaflets. There was no clear patten between shear level and collagen synthesis.

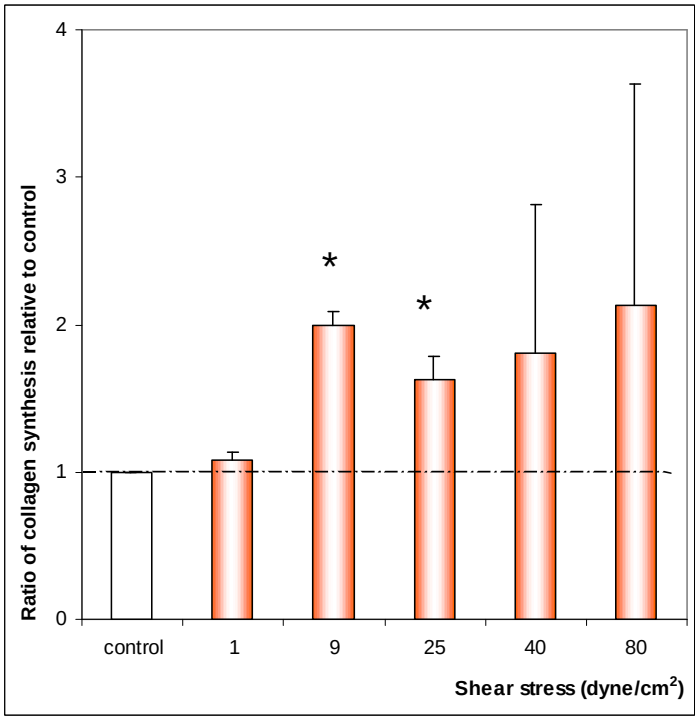


**Figure 43:** Collagen synthesis by intact AV leaflets under shear, collagen synthesis expressed as ratios between shear and control, $*$ indicate statistical significance, p $<$0.05

#### *5.2.1.4 sGAG content*

sGAG content was measured by using the Blyscan sGAG assay. The amount of sGAG ($\mu$g) as obtained from the microplate reader, was normalized by sample dry weight (mg) and compared with the static controls. Similar to the collagen synthesis data, sGAG content was shown in both actual amount of sGAG (Fig.44) and in ratios of shear to control (Fig.45). Results showed that samples exposed to shear at 25 and 40 dyne/cm$^2$ had less sGAG than the static controls . The differences were 15% (Wilkoxon signed rank test, p $<$ 0.02) for 25 dyne/cm$^2$ and 22% (p $<$ 0.04) for 40 dyne/cm$^2$, respectively (Fig.45). All the other shear levels (1, 9 and 80 dyne/cm$^2$) did not cause any statistically significant changes in sGAG content (Wilkoxon signed rank test, p $>$ 0.1).

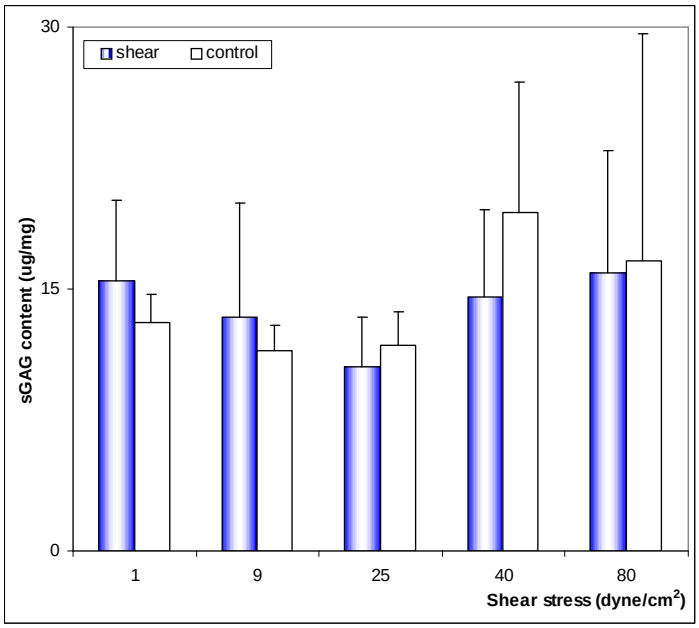


**Figure 44:** sGAG content in intact AV leaflets after exposure to shear, sGAG content in AV leaflets under shear vs. static control, expressed in $\mu$g/mg.

#### *5.2.1.5 $\alpha$ SM actin IHC*

Similar to the pressure study, $\alpha$-SM actin IHC was used to measure valvular cell phenotypic changes after exposure to shear stress. For each experiment, at least six leaflets were collected. Each leaflet was cut into three pieces, one served as fresh control, one exposed to shear stress and one under static incubation. The latter two both lasted for 48 hrs. Shown in Fig.46 are representative staining images of $\alpha$ - SM actin under the three different treatments. As shown in the figure, $\alpha$-SM actin in the fresh native AV was more abundant and present in all three layers: the fibrosa, the spongiosa and the ventricularis. After 48 hrs' *ex vivo* organ culture, the amount of $\alpha$-SM actin declined significantly and the remaining $\alpha$-SM actin was mainly concentrated in the ventricularis. There was no significant difference between shear stress and atmospheric control in $\alpha$-SM actin distribution or quantity, indicating that shear stress did not affect cell phenotypic shift.

#### *5.2.1.6 Tissue morphology*

Tissue morphology was assessed by routine H & E staining. In each experiment, three pieces of each leaflet were taken and subjected to three treatments: fresh, shear stress and static incubation.

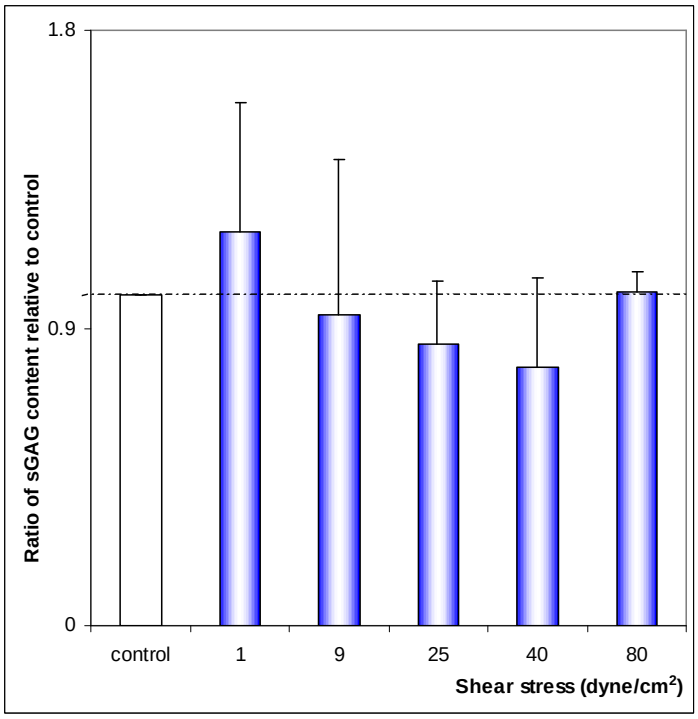


**Figure 45:** sGAG content in intact AV leaflets after exposure to shear, ratio of sGAG content relative to control at various shear levels

Staining results (Fig.47) revealed normal leaflet structure after exposure to shear stress for 48 hr, regardless of the shear magnitude. The characteristic leaflet trilaminar structures were well preserved and the cell density was retained. These histological findings demonstrated that the experimental system was capable of maintaining the normal histological structure (i.e. ventricularis, spongiosa and the fibrosa) with the retention of the cellular components and preservation of the extracellular matrix.

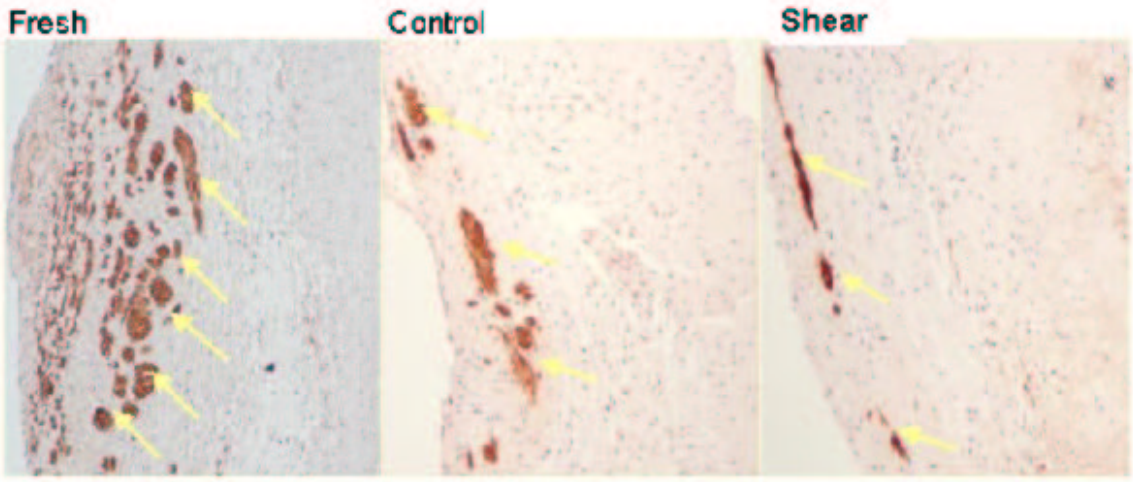


**Figure 46:** $\alpha$ - SM actin IHC of intact AV exposed to shear, actin stained brown and indicated by arrows, cell nuclei counter-stained stained blue

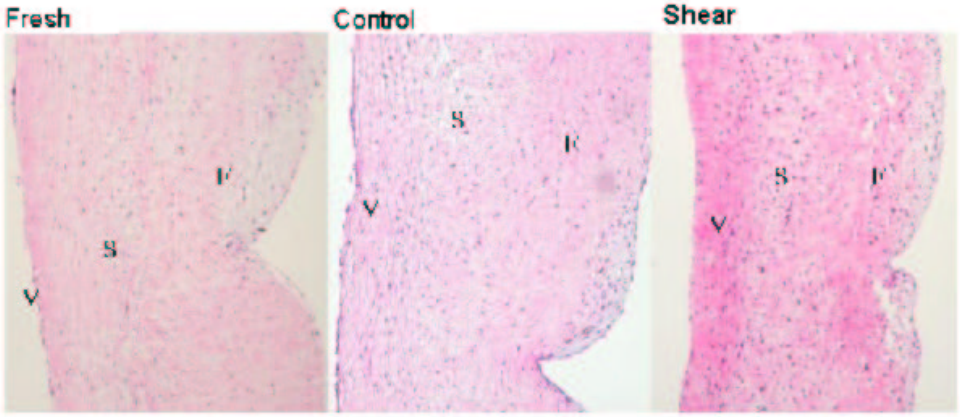


**Figure 47:** Routine H and E staining of intact AV exposed to shear, cell nuclei stained purple or dark blue, cytoplasm stained pink; F-fibrosa, S-spongiosa, V-ventricularis

### *5.2.1.7 MMPs and Cathepsins*

**MMP-2 and MMP-9 IHC**

MMPs expression and distribution were detected by using IHC (peroxidase ABC) on formalin fixed, paraffin-embedded sections. Results showed that both MMP-2 and MMP-9 were present in all the samples, although MMP-2 was present in higher quantity than MMP-9 (Fig.48,Fig.49). The proteinases were mainly located around the interstitial cells, but some sections also demonstrated MMP-9 around the endothelial cells (Fig.49).

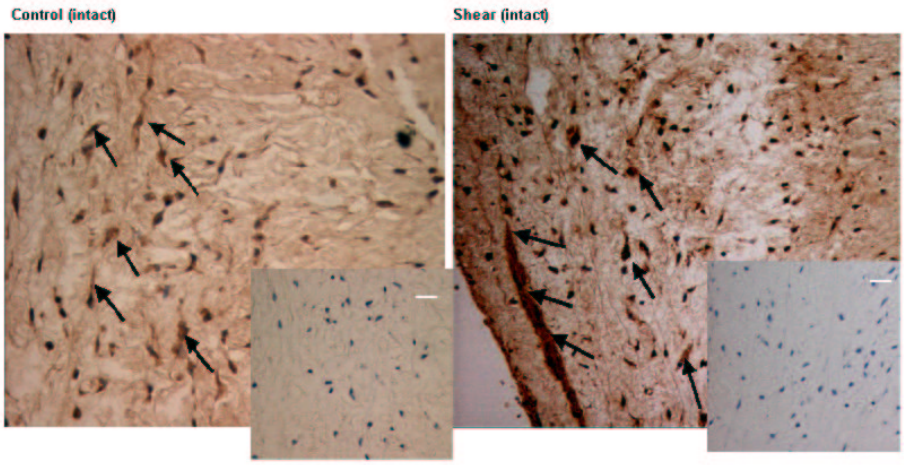


**Figure 48:** MMP-2 IHC, MMP-2 stained brown (indicated by arrows), cell nuclei counter-stained blue, insert - negative control with the omission of primary antibody

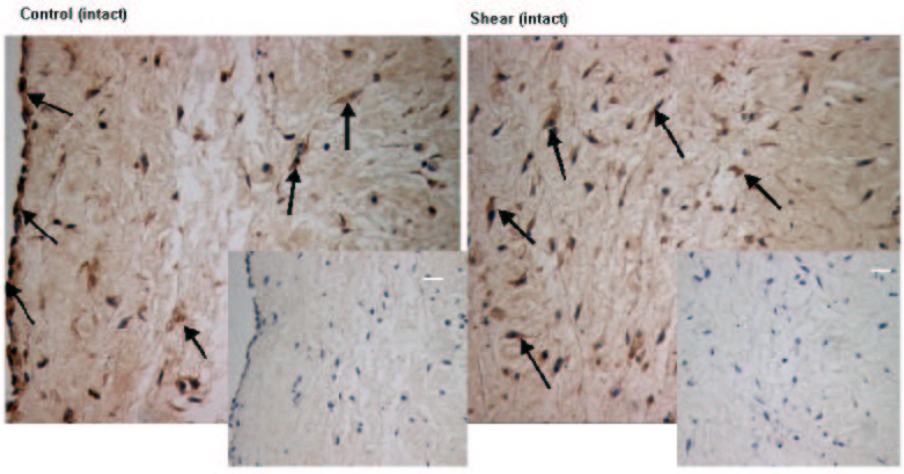


**Figure 49:** MMP-9 IHC, MMP-9 stained brown (indicated by arrows), cell nuclei counter-stained blue, insert - negative control with the omission of primary antibody

**MMPs/Cathepsin Western Blotting & Zymogram**

Although both MMP-2 and -9 protein expression and activities were detected in all the samples, they were not significantly affected by steady laminar shear. Cathepsin L activity was lower in the shear samples as compared with the static controls. Cathepsin B was present in all samples, but the fresh valve appeared to have more cathepsin B than both shear and static incubation, and there was no significant difference between the latter two (Fig.50). TIMP-2 and cathepsin K were not detected in any of the samples.

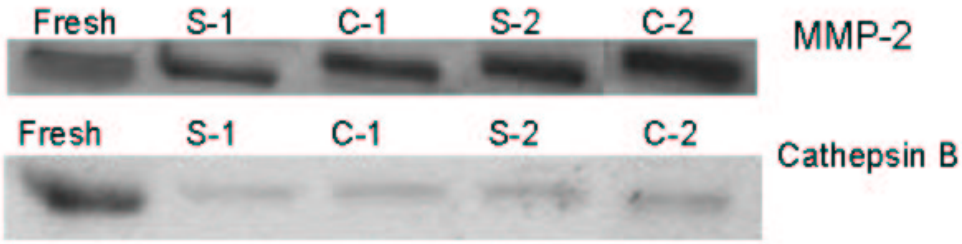


**Figure 50:** MMP-2, Cathepsin B western blotting of intact AV leaflets exposed to shear stress, up: MMP-2 western blot, down: cathepsin B western blot; S-shear stress, C-control, note there were no significant differences in either MMP-2 or cathepsin B between shear stress and controls

### 5.2.2 Influence of Shear Stress on Denuded AV Leaflets

To study the role of endothelium in AV leaflets' responses to shear, the endothelium on the ventricular surface was removed and the denuded leaflets were exposed to the same shear stress levels as the intact leaflets. In the intact leaflets, the observed responses represented a co-culture model of the endothelial cells and the interstitial cells; while in the denuded leaflets, the responses should be solely from the interstitial cells. The difference in results from these two type of experiments should then shed light on the role of endothelium in valvular responses to shear. Biological endpoints in the denudation study were the same as in the intact leaflet study.

Endothelial cell removal was achieved by gently rubbing the ventricular surface using a sterile cotton bud. The removal efficiency was verified using routing H & E staining and SEM. Shown below (Fig.51) is the H & E and SEM images of a denuded leaflets. The figure indicates the removal was very efficient, leaving almost no endothelial cells on the surface.

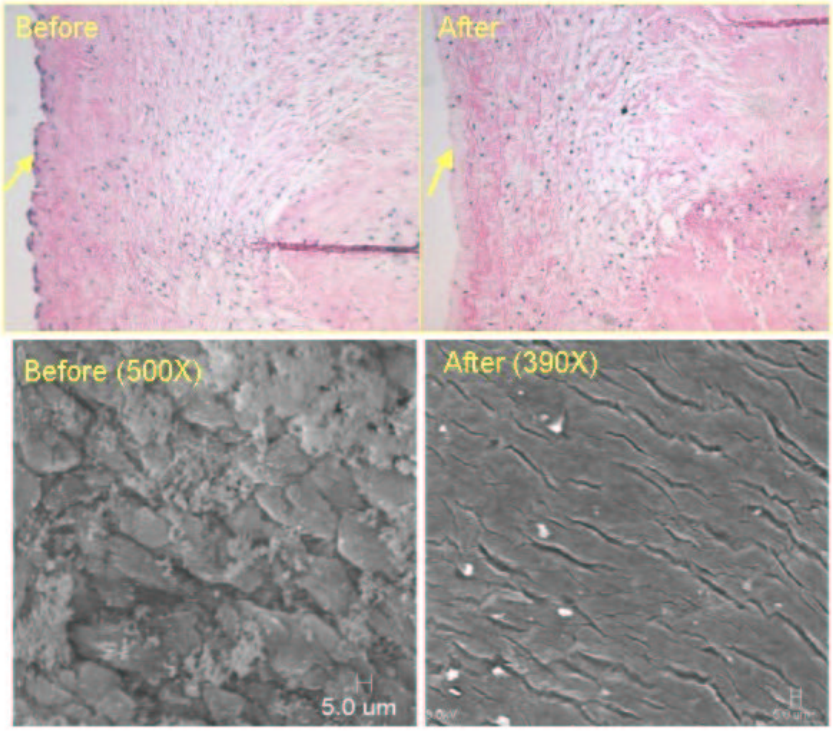


**Figure 51:** Endothelial removal, top - routine H & E staining, note the absence of cells on the ventricular surface (indicated by arrows) after denudation, bottom - SEM of an leaflet surface before and after denudation

#### 5.2.2.1 *Collagen synthesis*

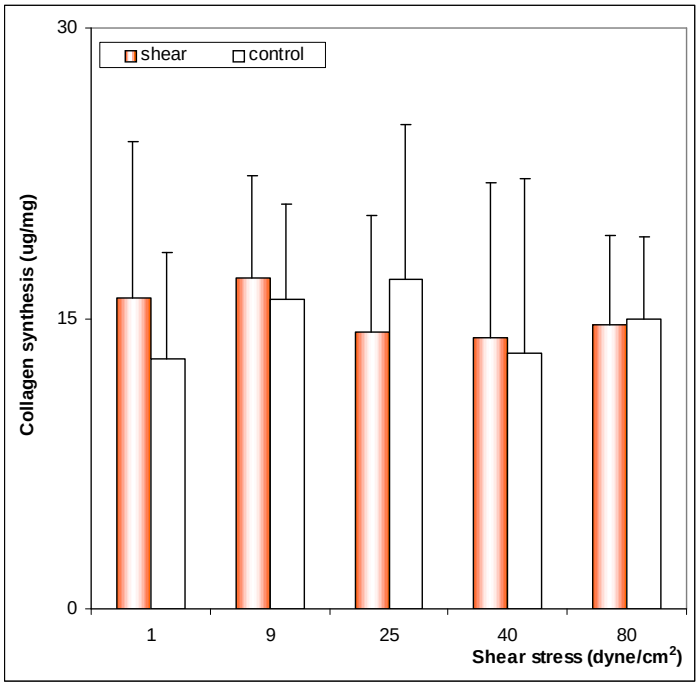


**Figure 52:** Collagen synthesis in denuded leaflets under shear, collagen synthesis under shear vs. control, expressed in $\mu$g/mg.

Collagen synthesis in the denuded leaflets exposed to shear is shown in Figs.52 and 53. Fig.52 showed the actual amount of newly synthesized collagen in $\mu$g, Fig.53 shows the ratios of newly synthesized collagen between steady shear stress and static control. In contrast to the results from the intact leaflets study, there was no significant difference in collagen synthesis between samples exposed to shear and under static incubation at any shear level. This suggests that endothelial cells were important for the shear-induced collagen synthesis.

#### 5.2.2.2 *sGAG content*

sGAG content results in the AV leaflets are shown in Figs.54, and 55. Fig.54 shows the actual sGAG content in $\mu$g, Fig.55 shows the ratios of sGAG content between shear stress and static controls. At a shear stress of 1 dyne/cm$^2$, there was no significant difference in leaflet sGAG content between steady shear stress and static control. At 9 dyne/cm$^2$, the leaflets exposed to shear had about 16% more sGAG than the static controls (Wilcoxon signed rank test, $p < 0.05$); and for a shear of 25

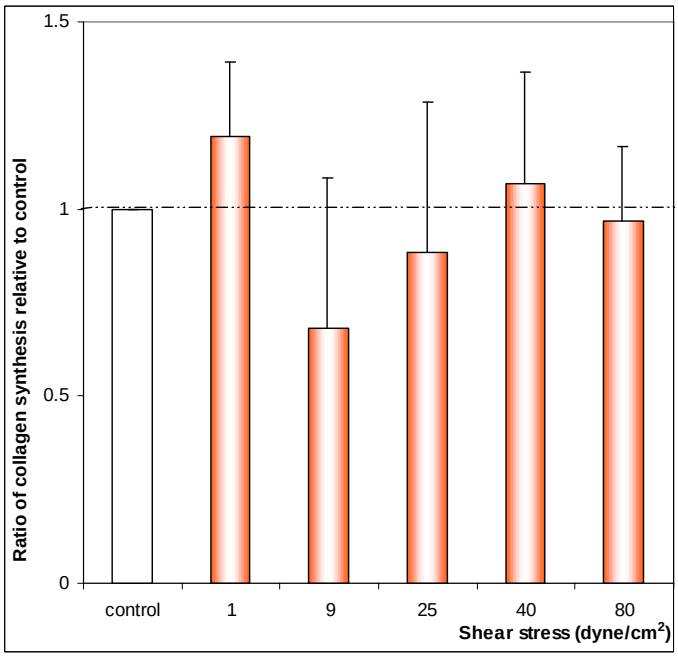


**Figure 53:** Collagen synthesis in denuded leaflets under shear, ratios of collagen synthesis in denuded leaflets relative to control

dyne/cm$^2$, the increase was about 42% (Wilcoxon signed rank test, $p < 0.05$). At 40 dyne/cm$^2$, the leaflets exposed to shear had 30% more sGAG but the statistical significance was at $p < 0.1$. No significant difference between shear and control was observed at 80 dyne/cm$^2$ ($p > 0.1$).

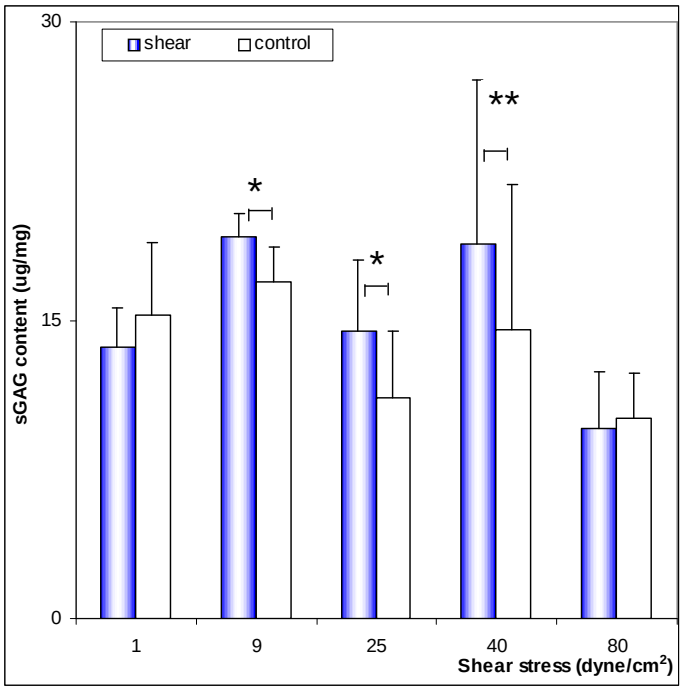


**Figure 54:** sGAG content in denuded leaflets under shear, sGAG content under shear vs. control, , expressed in $\mu$g/mg. $*$ indicates $p < 0.05$,$**$ indicates $p < 0.1$

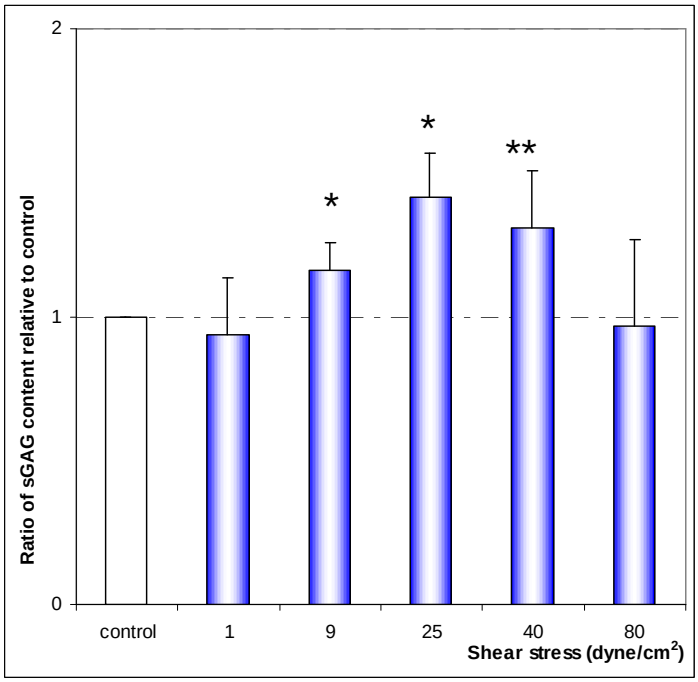


**Figure 55:** sGAG content in denuded leaflets under shear, ratios of sGAG content relative to control, $*$ indicates $p < 0.05$,$**$ indicates $p < 0.1$

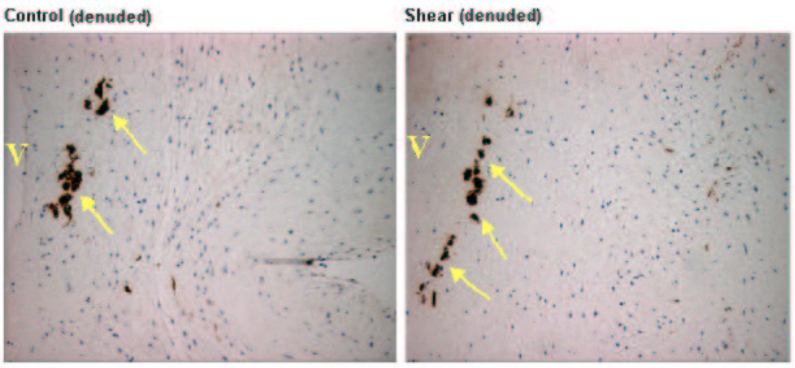


**Figure 56:** $\alpha$ - SM actin IHC of denuded AV exposed to shear, actin stained brown and indicated by arrows, cell nuclei counter-stained stained blue; V-ventricular surface

#### *5.2.2.3 $\alpha$ - SM actin IHC*

Similar to the pressure study, $\alpha$ - SM actin IHC was used to measure valvular cell phenotypic changes exposure to shear stress. For each experiment, at least six leaflets were collected. Each leaflet was cut into three pieces, one served as fresh control, one exposed to steady shear and one under static incubation. The latter two both lasted for 48 hr. Shown in Fig.56 are typical staining images of $\alpha$ - SM actin under the three different treatments. As shown in the figure, $\alpha$-SM actin in the fresh native AV was more abundant and present in all three layers: the fibrosa, the spongiosa and the ventricularis. After 48 hrs' *ex vivo* organ culture, the amount of $\alpha$-SM actin declined significantly and the remaining $\alpha$-SM actin was mainly concentrated in the ventricularis. There was no significant difference between shear stress and atmospheric control in $\alpha$-SM actin distribution or quantity, indicating that shear stress did not affect cell phenotypic shift.

#### *5.2.2.4 Tissue morphology*

Tissue morphology was assessed by routine H and E staining. In each experiment, each of the denuded leaflets were divided into three pieces and subjected to three treatments: fresh, shear stress and static incubation. Staining results (Fig.57) revealed normal leaflet structure after exposure to shear stress for 48 hrs, regardless of the shear level. The characteristic leaflet trilaminar structures were well preserved and the cell density retained. These histological findings demonstrated that the experimental system was capable of maintaining the normal histological structure (i.e. ventricularis, spongiosa and the fibrosa) with the retention of the cellular components and preservation of the

extracellular matrix.

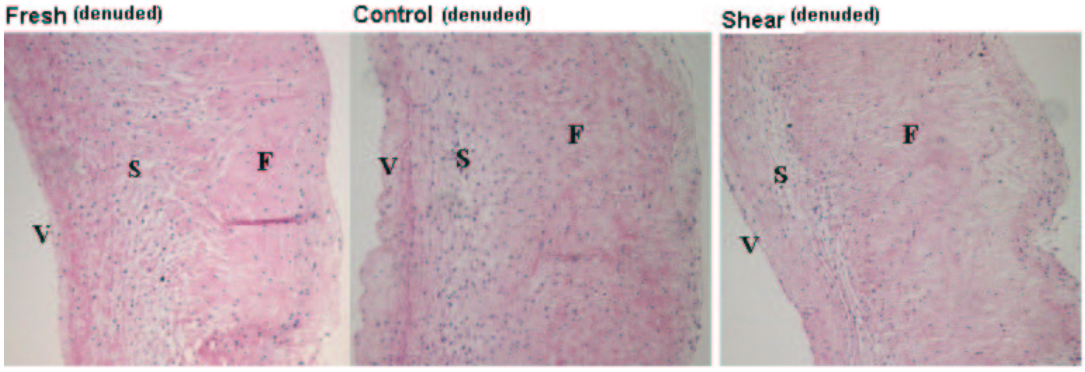


**Figure 57:** Routine H and E staining of denuded AV leaflets exposed to shear, cell nuclei stained purple or dark blue, cytoplasm stained pink

#### *5.2.2.5 MMPs IHC*

MMPs expression and distribution was detected by using IHC (peroxidase ABC) on formalin fixed, paraffin-embedded sections. Results showed that both MMP-2 and MMP-9 were present in all samples, although MMP-2 was present in higher quantity than MMP-9 (Fig.58,Fig.59). Since these were denuded leaflets without an endothelium, the proteinases were only detected around the interstitial cells.

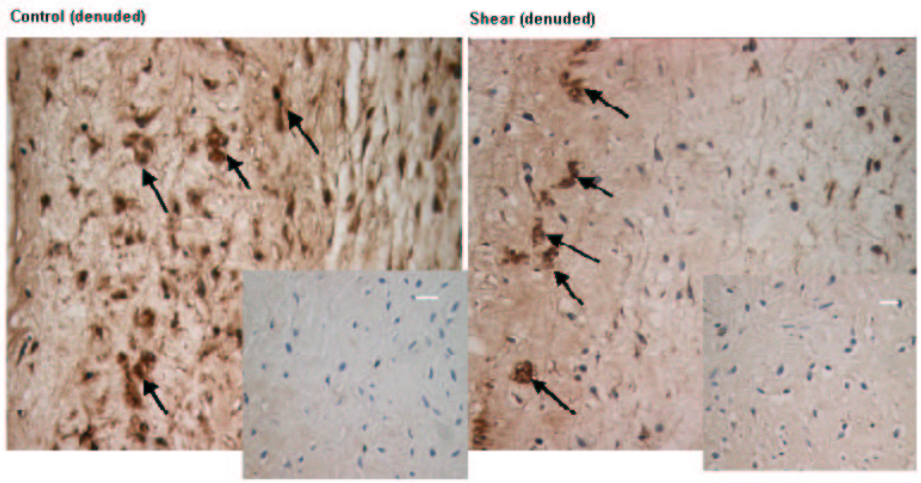


**Figure 58:** MMP-2 IHC on denuded leaflets: control vs. shear, MMP-2 stained brown (indicated by arrows), cell nuclei counter-stained blue, insert - negative control with the omission of primary antibody

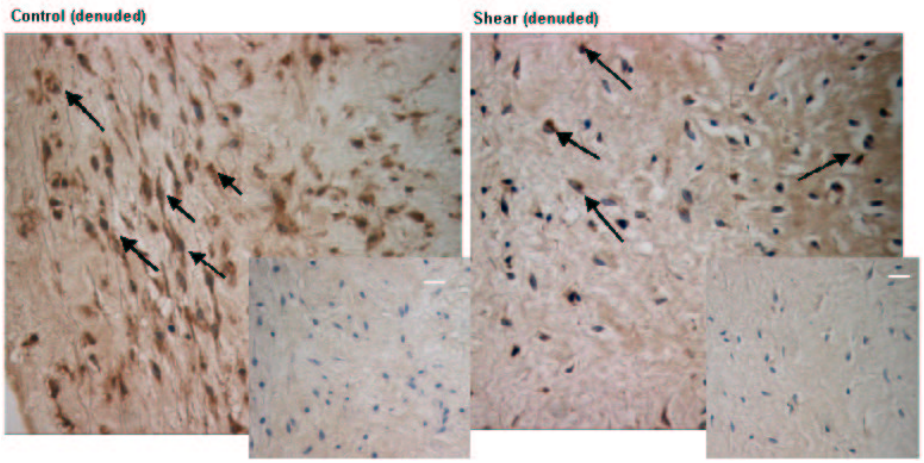


**Figure 59:** MMP-9 IHC on denuded leaflets: control vs. shear, MMP-9 stained brown (indicated by arrows), cell nuclei counter-stained blue, insert - negative control with the omission of primary antibody

#### *5.2.2.6 MMPs/Cathepsin Western Blotting & Zymogram*

In the denuded leaflets, cathepsin L activity was almost non-detectable, regardless of the mechanical treatment. Shown in Fig.60 are the western blotting results on MMP-2 and cathepsin B. Similar to the study with intact leaflets, MMP-2 was more prominent than other enzymes, but there was no difference between shear and static incubation. Cathepsin B was present in all samples, but the fresh valves appeared to have more cathepsin B than both shear and static incubation. There was no significant difference between the latter two. TIMP-2 and cathepsin K were not detected in any of the samples.

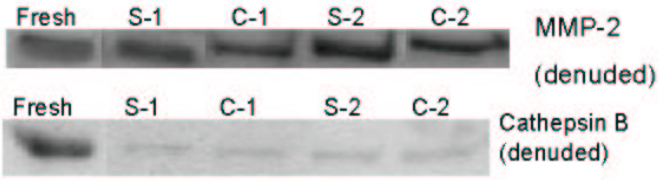


**Figure 60:** Western blotting of denuded AV exposed to shear stress, up: MMP-2 western blot, down: cathepsin B western blot; S-shear stress, C-control, note there were no significant differences in either MMP-2 or cathepsin B between shear stress and controls

## *5.3 Summary of Results*

To summarize, results from this study showed that AV leaflets were able to respond to applied hydrostatic pressure and steady laminar shear stress within 48 hr. As expected, the two mechanical factors were shown to have different effects on valve biological properties. Hydrostatic pressure (constant or cyclic) induced extracellular matrix synthesis in a pressure-magnitude dependent manner. In addition, the synthesis of collagen and sGAG was correlated under cyclic pressure. Cyclic pressure at high frequency(2 Hz) and normal magnitude (80-120 mmHg) was beneficial for cell proliferation. Steady laminar shear stress within the physiological range (9-40 dyne/cm$^2$) stimulated collagen synthesis in intact leaflets. The same shear stress levels induced sGAG synthesis in denuded leaflets.

The observed increases in collagen synthesis under both pressure and shear stress were accompanied with a reduction in cathepsin L and S activity and expression, indicating a possible common biochemical pathway of matrix remodeling under the two different mechanical conditions. Matrix metalloproteinses (MMP-2, MMP-9) were present in all samples but were not affected by any of the mechanical treatments. Cathepsin B expression was higher in the fresh valves than the samples under 48 hr *in vitro* culture (pressure, shear or control). However, there was no significant difference in cathepsin B expression between the various mechanical treatments.

# CHAPTER VI

# DISCUSSION

## *6.1 Uniqueness of Study*

The close correlations between mechanical stresses and heart valve biology have long been evidenced by clinical observations and animal studies [165, 122, 171]. According to these studies, the structural components of the aortic valve normally undergo constant renewal in response to mechanical loading [165] and the sites of protein and GAG synthesis in the leaflets are correlated with the functional stresses [123]. Similarly, alterations in mechanical loading alter biosynthetic behavior of valve cells. For instance, collagen synthesis in mitral valve leaflets was enhanced as a result of altered stress distribution due to left ventricular infarctions [106]. Recently, this issue has been addressed by *in vitro* cell culture studies [18, 72]. These studies demonstrated that shear stress altered the gene expression of porcine valvular endothelial cells [18] and mechanical stretch upregulated collagen synthesis in porcine valvular interstitial cell [72].

As mentioned above, *in vivo* (clinical or animal studies) and *in vitro* cell culture studies represent two most common models for biomedical research and have provided valuable insights into heart valve biology and pathology. However, they both have some limitations. *In vivo* models provide the most representative information, but they are generally costly and involve a complex interplay between biochemical and mechanical factors, making it impossible to isolate the effects of each individual affecting factor. *In vitro* cell culture studies are simple, inexpensive and have a well defined biochemical and mechanical environment; but the native extracellular matrix of the cells is often lost, therefore the cells are seeing a microenvironment which differs from their native environment. As a result, observations from cell culture studies may deviate from *in vivo* findings. For example, *in vitro* cell culture studies showed that 50-90% of valvular interstitial cells were $\alpha$-Smooth Muscle actin positive, in contrast to the 2.5% as demonstrated by immunostaining of native valve leaflets [109, 151, 43]. Clearly, there is need for bridging between the two types of models.

With that in consideration, the current study took an intermediate approach by using an *ex vivo*

tissue culture model. In a tissue culture system, cells are maintained in their native extracellular matrix [22], thus providing a better representation of their *in vivo* biological reactions than cell cultures. Studying the effects of mechanical forces on valvular cells staying in the whole leaflet tissue is particularly relevant in light of the findings that extracellular matrix composition is a key determinant of cellular responses to mechanical stimuli [112, 172]. Compared with *in vivo* studies, tissue culture systems have the advantage of being inexpensive and having a well-characterized biochemical and mechanical environment. Therefore, it can be used to study the effects of mechanical factors separately without the interference of hormonal factors or vice versa.

## *6.2 Extracellular Matrix Homeostasis vs. Mechanical Stresses*

Homeostasis is defined as a state of equilibrium that exits between different but interdependent elements or groups of elements in a living organism. This concept is often invoked when considering salt and water balance and factors which serve to maintain constant the volume and composition of extracellular fluid. Recently, it has been recognized that tissue can act independently of hormones to maintain their own function through de novo generation of a variety of substances that have autocrine and paracrine properties on constitutive cell populations [166]. Therefore, connective tissue homeostasis is described as the self-regulation of extracellular matrix (ECM) structure and cellular composition, a self-determination of cell mobility, differentiation, replication, apoptosis and the growth and regression of its structural protein scaffolding. Various tissue culture studies have shown that connective tissue homeostasis can be regulated by externally applied biochemical and mechanical signals [58, 22].

### 6.2.1 Heart Valve ECM Matrix Synthesis & Mechanical Stresses

ECM of the aortic valve leaflets is mainly composed of collagen, elastin and glycoaminoglycans (GAG). The collagen network is the major bearer of tensile stresses caused by diastolic pressure or shear stress. Elastin fibers give the leaflet pliability so as to minimize the obstruction to blood flow and GAGs disperse within the matrix to provide lubrication during leaflet movement. All three components are critical for normal valve function and the abnormities in any of them could lead to compromised valve function. However, since elastin is known to have a relatively longer turn-over

time and not expected to have any significant changes during the experiment period (48 hrs), it was not included in the ECM synthesis study. Collagen synthesis and sGAG synthesis were measured by using radiolbeling in the pressure study; and by colormetic biochemical assays in the shear stress study due to the limits on radioactive material usage and safety concerns.

This study demonstrated that exposure to hypertensive pressure (140 mmHg and above) led to enhanced collagen and sGAG synthesis by the aortic valve leaflets. This finding was consistent with both *in vivo* and *in vitro* observations. Clinically, hypertension has been associated with fibrosis, which involves the excessive deposition of collagen. In cases where no fibrosis was present, collagen turnover was stimulated under hypertension. For instance, Botney et. al [13] demonstrated active collagen synthesis in small muscular arteries from patients with pulmonary hypertension. In a study on hypertensive rats, Willems et al [171] detected increases in type I and type II collagen mRNAs by *in situ* hybridization in hypertensive animals. sGAG synthesis has also been shown to be upregulated in hypertensive animals as well as in cells isolated from hypertensive animals [79, 121]. The current study used $^{3}$-H proline and $^{35}$-S to label newly synthesized collagen and sGAG respectively. Proline is a major amino acid residue in collagen molecules and can be incorporated in the ECM by valvular interstitial cells during their collagen metabolism. The same principle also applies to sGAG labeling with $^{35}$-S. The culture medium was supplemented with sufficient amount of $^{3}$-H proline (10 $\mu$Ci/ml) and $^{35}$-S $Na_2SO_4$. Therefore, the faster the metabolic activity of the cells, the more $^{3}$-H and $^{35}$-S will be found in the tissue at the end of the experiment. Thus, the amount of $^{3}$-H/$^{35}$-S activity in the tissue reflects the metabolic activity of the cells. Meanwhile, the radiolabels could also be returned back to the media via the release of newly synthesized collagen to the media.

Many *in vitro* studies on the effects of pressure have demonstrated altered ECM synthesis by elevated pressure. Most of these studies were performed with chondrocytes, osteoblasts or other cells of orthopedic origin. The results are mixed depending on the pressure level. In general, ”low pressure” showed stimulatory effects on matrix synthesis, and ”high pressure” demonstrated inhibitory effects on ECM synthesis of the cells [64, 98, 115]. But the threshold for ”high pressure” may differ for each cell type. For instance, osteoblasts responded to 13 kPa (97.82 mmHg) (”low”) pressure with enhanced activity, and a pressure of 200 kPa (1500.5 mmHg) (”high”) led to inhibition on its activity [115]; whereas for bovine articular chondrocytes, pressure of 2.8 MPa will be still

considered ”low pressure” and able to stimulate ECM synthesis, only pressure at 10 MPa or above showed inhibitory effects [88]. In the current study, pressure magnitude ranges from 13.32 kPa (100 mmHg) to 22.37 kPa (170 mmHg), both are well below any of the high pressure thresholds. Therefore the tissue were exposed to ”low pressure” ranges and the observation of enhanced ECM synthesis was consistent with the findings in literature.

Apart from the magnitude, pulse frequency was also found to be an important factor in determining the effects of pressure on valve biology. Collagen synthesis was increased at 0.5 Hz by 26% but remained at baseline level (atmospheric controls) at 1.167 and 2 Hz. Since both the duration of experiment and the loading/unloading ratio were the same for all frequencies, being 48 hr and 2:1, respectively; the total loading time was identical among the three different frequency conditions. The only differences therefore, are the total number of cycles and loading rate. The number of cycles was greatest at 2 Hz (345600 cycles), lowest at 0.5 Hz (86400 cycles) and intermediate at 1.167 Hz (201657 cycles). It appeared that smaller number of cycles are slightly more beneficial for collagen synthesis. However, this hypothesis was not confirmed by a preliminary study comparing valvular collagen synthesis at 48 and 96 hrs, under cyclic pressure of 150-190 mmHg at a frequency of 2 Hz (Fig.61, Fig.62). This experiment showed collagen synthesis at 96 hr (691200 cycles) was significantly higher than that at 48 hr (345600 cycles), contradictory to the results from the frequency study. Therefore, it is most likely that the observed differences are due to the differences in loading rates [147]. At lower frequency, the time it takes to reach maximal pressure was longer than at higher frequencies; therefore the loading rate was lower.

Another important finding from the current study was that constant static pressure and cyclic pressure showed differential effects on valvular ECM synthesis. Both types of pressure resulted in the enhancement of collagen synthesis, and the increases were of a similar magnitude (Table.8). sGAG synthesis on the other hand, was drastically different between constant and cyclic pressure. Constant pressure did not seem to cause any significant changes in sGAG synthesis, but cyclic pressure led to significant increases in sGAG synthesis. The differential effects between constant and cyclic pressure have been reported by other research groups [160, 74]. The study by Vouyouka et al [160] indicated there were two different working mechanisms for cyclic pressure and constant pressure (even though they may show similar effects on the cell): cyclic pressure causes the release

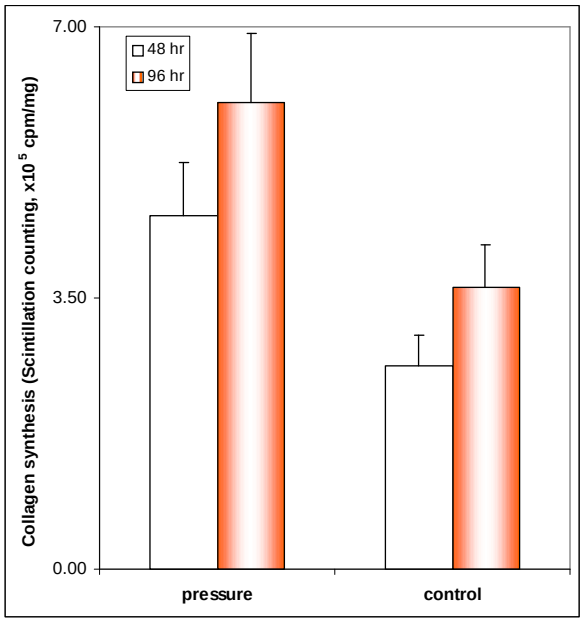


**Figure 61:** Comparison of collagen synthesis after 48 and 96 hrs under pressure, pressure condition: high magnitude (150-190 mmHg), high frequency (2 Hz)

of a paracrine factor from the cells which was not seen with constant pressure. The same reason probably accounts for the observed differences in valvular matrix synthesis under the two types of pressure conditions. From a biomechanical perspective, this observation may be related to the mechanical functions of collagen and sGAG in the leaflet tissue. As mentioned earlier, the major function of collagen fibers is to bear the tensile stress generated by pressure, the magnitude of this stress will not change much as long as the mean pressure remains the same. Therefore, we saw a similar pattern of collagen synthesis under constant and cyclic pressure. GAG molecules form a hydrogel, which encloses the collagen fibers; and their functions are to withstand compressive stresses and also serve as a lubricant for the relative movement between the fibers. Under cyclic pressure, the collagen fibers experienced stress in a cyclic fashion, and some relative motion may occur between the fibers; causing an increased turnover of GAGs. Under constant pressure, this kind of relative motion is not likely to happen since the fibers experienced constant stress throughout experiment. Therefore no significant changes in GAG synthesis were observed.

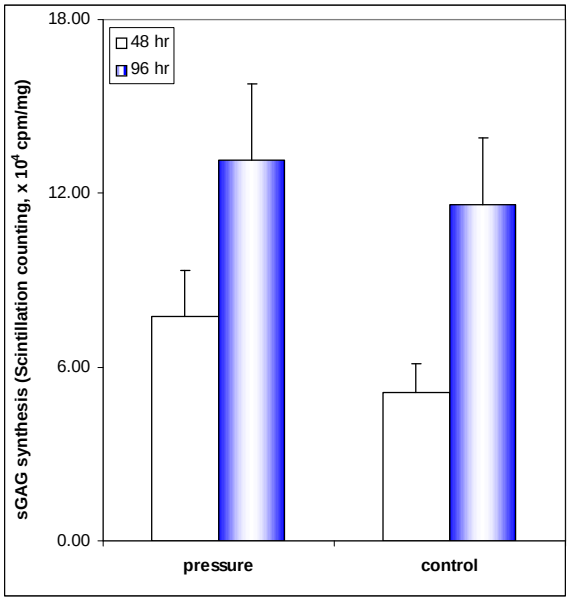


**Figure 62:** Comparison of sGAG synthesis after 48 and 96 hrs under pressure, pressure condition: high magnitude (150-190 mmHg), high frequency (2 Hz)

**Table 8:** ECM synthesis (ratios relative to control) under pressure: Constant vs Cyclic pressure, None-no significant difference from control

| | | 100 mmHg | 140 mmHg | 170 mmHg |
|---|---|---|---|---|
| Collagen | Constant | None | 138% | 190% |
| | Cyclic (1.167 Hz) | None | 145% | 218% |
| sGAG | Constant | None | None | None |
| | Cyclic (1.167 Hz) | None | 165% | 230% |

### 6.2.2 Cell Turn-over

Cell proliferation was measured by using $^{3}$H-thymidine in this study. $^{3}$H-thymidine was added to the culture media as a building block for the formation of DNA molecules. This method measures the overall cell proliferating activities in the leaflet tissue; including contributions from both the ECs and the ICs. Our results indicated that cell proliferation under pressure was not significantly different from that at atmospheric pressure except that at 100 mmHg, the proliferation was inhibited by pressure, resulting in a 24% less DNA synthesis than controls. This may be due to several reasons. Firstly, since the whole leaflet tissue was used in this study, the observed effects were a combined effects from the ECs and the ICs as well as their interactions. It has been shown in the literature that pressures greater than 80 mmHg caused inhibitory effects on EC proliferation

[156, 4, 142, 160]; while SMCs exposed to hypertensive pressure (120 mmHg and above) were shown to have a higher proliferation rate than controls [61, 160]. These findings may be helpful in explaining our results. At 100 mmHg, EC proliferation was inhibited while IC proliferation was not significantly affected, therefore resulting in a decrease in the overall DNA synthesis. At 140 mmHg and 170 mmHg (both are above 120 mmHg), ECs were inhibited and at the same time, ICs were stimulated; the decreases in ECs and the increases in ICs may cancel each other, resulting in no significant changes in total DNA synthesis in the leaflet tissue. This theory remains to be verified since valvular ECs and ICs may behave differently under pressure as compared with vascular ECs and SMCs. The second explanation has to do with the fact that valves used in this study were from adult pigs and the cell proliferating activity is generally very low. In addition, there was no serum present in the culture media and therefore cell proliferation might be depressed, and any differences caused by pressure could pass non-observed due to the relatively low activity.

Although hypertensive pressure did not seem to affect cell proliferation much, high pulse frequency, on the other hand, showed significant increases in DNA synthesis. The effects of frequency have been less extensively studied as the effects of pressure magnitude. A recent study by Nagatomi et al [95] demonstrated that for the same duration of cyclic pressure exposure, a higher frequency (1.0 Hz) caused significant increases in osteoblasts proliferation, while a lower frequency (0.25 Hz) did not. The frequencies in the current study were 2, 1.167 and 0.5 Hz, and we observed increased proliferation at 2 Hz. These two studies are consistent in that both showed that pulse frequency was an important regulator of cell proliferation, and higher frequencies had stimulatory effects on proliferation; although the threshold frequency might be quite different for each cell type (valvular cells: 2 Hz, osteoblasts: 1 Hz).

Hypertensive pressure has also been shown to affect cell apoptosis. Although this was not included in this study, it is an important marker that is worth studying in the future. The pressure effects on apotosis were dependent on both pressure level and serum conditions in the culture medium. Shin et al [127] found that under low serum/growth factor conditions, exposure to 60/20 mmHg cyclic pressure led to an increase in total cell density, apoptosis and DNA synthesis of cultured HUVEC. Under normal serum conditions, exposure to 60/20 or 100/60 mmHg resulted in an increase in DNA synthesis, but there were no significant changes in apoptotic index. A study

of generic hypertension showed that SMCs from spontaneously hypertensive rats had significantly higher DNA synthesis ($5.2\pm0.9$ vs. $2.4\pm0.7$ cpm X $10^3$) than the normotensive rats. In addition, SMCs from hypertensive rats also showed higher apoptosis rates upon serum deprivation than SMCs from normal rats [36].

## *6.3 Endothelial Cell Alignment vs. Shear Stress*

Vascular endothelial cells are very sensitive to flow. It is well known that under static conditions, ECs have cobblestone morphology and appear as randomly distributed. Once exposed to steady flow, these cells quickly adopt an elongated morphology and align parallel to flow direction within a few hours [78, 138]. This alignment will return to random once the shear is removed or changed to oscillatory shear. EC alignment pattern has been shown to be achieved through the reorganization of cytoskeletal filaments and focal adhesion complex. Like in blood vessels, the surfaces of valve leaflets are also lined with ECs, which are critical to maintaining a non-thrombogenic surface, transport of nutrients and transduction of mechanical and biochemical signals. The first striking difference between valvular and vascular ECs was an *in vivo* observation in 1986, in which the valvular ECs were found to align perpendicular to flow direction [34]. This was recently verified in a study by Butcher et al [18] using an *in vitro* culture of porcine valvular ECs. This study also showed different focal adhesion patterns between vascular and valvular ECs. The same study also verified that vascular endothelial alignment is calpain-, Rho-kinase- and PI3K-dependent, whereas valvular EC alignment is calpain-, Rho-kinase-dependent but PI3K-independent.

The current study showed that after 48 hrs exposure to steady shear stress (regardless of the shear stress level), ECs on the ventricular surface of the leaflets remained perpendicular to flow (SEM images, Fig.41). This is not surprising since the flow applied onto the tissue was oriented from basal to the free edge of the leaflet (radial direction, perpendicular to original EC alignment), exactly the same as *in vivo* flow direction. Therefore, according to the results by Butcher et al [18], the ECs should remain in the circumferential direction, which is perpendicular to flow. To further determine the relationship between valvular EC alignment and shear stress direction, a preliminary study was performed with flow being oriented in the circumferential direction of the leaflet ($90^o$ degrees from the *in vivo* flow direction and parallel to the original EC alignment) at a shear stress

level of 40 dyne/cm$^2$ for 48 hrs. EC alignment was visualized by staining the f-actin stress fibers and cell nuclei in the ECs. F-actin is a part of the cytoskeleton of ECs and has been shown to assume a concurrent alignment with the endothelial cells [18]. The tissue was first treated in 0.1% triton X-100 for 20 min to permeablize the tissue so as to allow penetration of the fluorefores (DAPI, Phalloidin) into the cells. After washing with PBS for three times (5 min each), the tissues were incubated in DAPI/Phalloidin (DAPI, 0.5 U/ml) stains cell nuclei, phalloidin (20 U/ml) stains f-actin) for 20 min at 37$^o$C. The stained tissues were then washed in PBS and mounted onto glass slides and viewed under confocal microscope. Fresh aortic valve leaflets were used for comparison. Shown in Fig.63 are two representative images of the staining from a fresh valve leaflet and a leaflet exposed to steady shear stress for 48 hrs. The fresh valve leaflet shows a nice alignment pattern perpendicular to the *in vivo* flow direction (i.e. circumferential), just as shown in the SEM images (Fig.41). After exposure to shear stress, the cells became less packed, and began to shift the orientation from the circumferential direction toward the radial direction, that is, the *in vivo* flow direction (perpendicular to the *in vitro* flow direction). This finding verified that valvular ECs retained in their native extracellular matrix, just like ECs cultured in monolayer, have the tendency to align perpendicular to flow direction. The complete change of alignment from the circumferential to radial direction takes more than 48 hrs, longer than monolayer cell cultures, probably due to the constraints from the ECM.

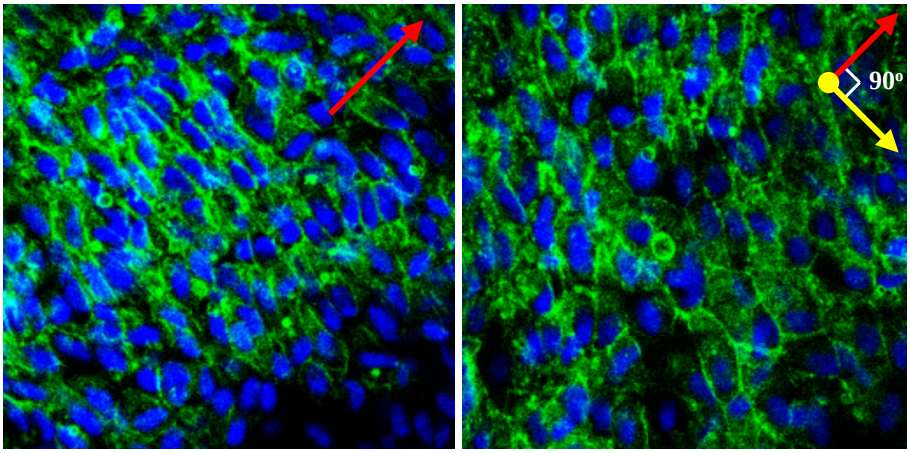


**Figure 63:** Confocal images of the endothelial cells on the ventricular surface of an AV leaflet,cell nuclei stained as blue, f-actin stained as green, left: fresh valve leaflet, right: leaflet under shear stress of 48 hrs; red arrow indicates *in vivo* flow direction, note that in fresh valves, endothelial cells align perpendicular to *in vivo* flow direction; yellow arrow indicates *in vitro* flow direction

## *6.4 Mechanical Stimuli and Protease Activities*

### 6.4.1 Pressure and Protease activities

As shown in the results chapter, valvular MMP-2 and MMP-9 expression and activity did not change with elevated pressure. This is apparently inconsistent with previous findings in literature [77, 22]. Lehoux et al found that MMP-9 activity increased by 94% in blood vessels kept at a high intraluminal pressure of 150 mmHg. In another study, both MMP-2 and MMP-9 were found to be activated in porcine arteries cultured at 100 mmHg and 200 mmHg, respectively, relative to controls at zero pressure [22]. This inconsistency might be due to the difference in tissue type (valves vs. blood vessels) or difference in the pressure mode. Both studies cited were experimented with intraluminal pressure, which generated dual effects on the tissue: normal stress and cyclic stretch. It is likely that hydrostatic pressure and cyclic stretch influence MMP-2 and MMP-9 differently: cyclic stretch activates MMPs but hydrostatic pressure did not affect MMP-2 or MMP-9. The lack of changes in MMP-2 and -9, however, does not exclude the possibility of alterations in other members of the MMPs family or tissue inhibitors of MMPs (TIMP). Other MMPs that have been discovered in heart valve tissues include MMP-1, MMP-13 and MT-MMP (membrane type - MMP). Two types of TIMPs: TIMP-1 and TIMP-2, are especially important. A preliminary western blotting experiment did not detect any TIMP-2 in our valve samples.

We observed significant decreases in the expression and activities of cathepsin L and S in AV leaflets exposed to hypertensive pressure as compared to atmospheric control. Previous studies on pressure effects on cathepsins showed mixed results depending on the cell types as well as the species. A study by Suzuki et al [146] showed decline of cathepsin B activity in association with arterial hypertension in myocardial cells, while the activities of cathepsin H and L were unchanged. Paczek and colleagues [99] found significant decrease in cathepsin B-content in the kidney of Goldblatt rats exposed to systemic hypertension in comparison with normotensive control animals. On the other hand, Sasahara et al [120] demonstrated significantly higher cathepsin B and D activities in aortic ECs from hypertensive rats than ECs from normotensive rats and a study by Rozek et al reported [117] increases in cathepsin D activity in cardiac muscle cells after 8 weeks of hypertension. It is obvious from these results that cathepsins expression and activity profiles under hypertension are quite diverse and may be subjected to the influences of the specific animal model as well as

the cell types. Regardless of the differences in the various models, it appears that cathepsins B and D are often involved in hypertension related processes. Both cathepsin B expression and activity were measured in this study, but the results showed no significant differences between hypertensive pressure and control. Cathepsin D was not included in our study, although it has been found to be present in human valve leaflets. The differences in results between the current study and literature might be due to three reasons: 1). The experiment was relatively short (48 hr as opposed to 8 to 20 weeks), therefore the long-term changes were not observed; 2). Cathepsin profiles in the valve leaflets are different from any of the above mentioned cell types; 3). The absence of cyclic stretch in the current study might account for the difference. Based on these results we presume that the observed increases in collagen and sGAG synthesis under hypertensive pressure might be a result of a synergistic interaction between hemodynamic factors and biochemical factors which include the lysosomal proteinase. The measured synthetic activity (radioactivity) is a result of the balance between newly synthesis and proteolysis. Under hypertensive conditions, proteolysis was lower due to the inhibition of cathepsins L and S. Consequently, the synthesis-proteolysis balance shifted toward synthesis, resulting in a higher radioactivity in the leaflets.

### 6.4.2 Shear stress and protease activities

Similar to the pressure studies, MMP-2 and MMP-9 were not significantly different from baseline levels after exposure to steady shear stress. Previous studies on shear stress regulation of MMPs showed mixed results. Generally, low shear (1 dyne/cm$^2$ or lower) lead to activation of MMPs [143, 144, 10] and high shear (6 dyne/cm$^2$ or higher) result in downregulation of MMPs [144, 100]. As regards to MMP-2 and MMP-9, the study by Bassiouny [10] showed that low flow ($21\pm1$ mL/min), low shear led to upregulation of MMP-2 activity and mRNA in rabbit arteries. The authors attributed the observed results to release from shear-activated SMCs or platelets or indirectly via cytokine-mediated pathways. On the other hand, the study by Palumbo [100] demonstrated that exposure to shear stress (12 dyne/cm$^2$) for 15 hr downregulated MMP-2 activity in bovine aortic SMCs. Both studies showed comparable MMP-9 activity and expression between the flow/shear group and the static incubation controls. The shear stress in our system was about 25 dyne/cm$^2$, which falls into the high shear category, but we did not observe any significant differences in MMP-2 between shear

and control. This might be due to the difference between vascular cells and valvular cells.

In contrast to MMP-2 and -9, cathepsins profiles was found to change significantly with shear stress. In the group where collagen synthesis was enhanced (25 dyne/cm$^2$, intact leaflets), cathepsin L expression and activity were lower than the static incubation control. Cathepsin S activity was slightly higher under shear than control; cathepsin B activity was significantly lower under shear stress than controls. The shear-induced inhibition of cathepsins activity was also observed with the denuded leaflets, indicating that valve interstitial cells are shear sensitive. The concurrence between cathepsins inhibition and collagen synthesis stimulation indicated that these proteases might be involved in the shear stress-induced collagen synthesis. Whether these cathepsins are really involved in these process or not can be verified by further studies with their inhibitors. There is a scarcity of literature on the effects of shear stress on cathepsin activity. One study by Fukuda et al [50] indicated that exposure to fluid shear stress caused release of cathepsin B, leading to the cleavage of CD18 on neutrophilis. In our study, cathepsin B activity was downregulated by steady shear stress, suggesting that the shear-cathepsin B relationship was cell type specific.

## *6.5 Mechanotransduction Under Pressure and Shear stress*

### 6.5.1 Mechanotransduction Under Pressure

The mechanism by which cultured cells or tissues sense changes in pressure remains to be resolved. Several possible force transducer systems have to be explored. For example, pressure might induce morphological changes in valvular ECs and ICs through compression. Hydrostatic pressure results in dilatational stress in the cells and tissue. This dilatational stress may cause reorganization of cytoskeleton [119] and opening or closing of ion channels [44, 81], resulting in intracellular responses. Studies on obligate barophiles, animals and bacteria that live in high hydrostatic pressure environments, has provided insights on how changes in pressure could, in the absence of motion, result in biologic responses. Bartlett and co-workers [9] showed that increases in pressure on a deep-sea bacterium caused an approximately 70-fold increase in the OmpH, a membrane-localized, porin-type protein involved in transport of small nutrients into the cell. Action potential propagation and synaptic transmission have also been reported to be strongly inhibited by pressure, as do the activities of membrane $Na^+$-$K^+$-ATPase and adenosine receptors [135]. A recent study suggested

that lipid rafts and caveolae serve as mechanotransduction sites within the plasma membrane [47]. Whether other membrane systems, such as adenlate cyclase or phosphoinositide, which have been implicated in signal transductions processes involving cyclic strain or shear stress, are also affected by pressure remains to be tested.

Although the mechanisms by which hydrostatic pressure affects cells are not fully understood, there is evidence showing that factors including alpha V integrin, basic FGF, and VEGF-C are involved in pressure-induced cellular processes, while TGF-$\beta$ and IL-1 have been excluded [126, 128]. A recent study on HUVECs showed that cyclic pressure selectively affected the transcription of 14 genes that included a set of mechanosensitive proteins involved in hemostasis (tissue plaminogen activator), cell adhesion (integrin-alpha 2) and cell signaling (Rho B, cytosolic phospholipase A2), as well as a unique subset of cyclic pressure sensitive genes such as endothelial growth factor (VEGF-C) and TGF-$\beta$ 2 [127]. Two other studies reported the involvement of extracellular signal-regulated kinase (ERKs) and c-JUN N-terminal kinase (JNK)in pressure-induced cellular responses [66, 92]. Both types of kinase were activated by hypertentisive pressure (160 mmHg) and could be suppressed by angiotensin converting enzymes (ACE) inhibitors. In addition, the phosphorylated c-Src was increased by pure pressure stress. A more recent study showed that sustained hydrostatic pressure induced protein tyrosine phosphorylation, activation of extracellular signal-regulated kinase (ERK)1/2, and enhanced expression of c-fos [47]. Another recent study [66] showed that nitric oxide (NO) might be involved in the pressure-induced proliferation of SMCs.

We have observed significant increases in valvular synthetic activity in response to elevated hydrostatic pressure. Since the valve leaflets is a composite structure including ECs, ICs and the extracellular matrix, the observed increases in valvular synthetic activity is very likely a synergetic action of all three components. The ECs sense the pressure directly and respond by releasing cytokines or growth factors that might affect the metabolism of underlying ICs, which are the major labor force for matrix production. The ECM can serve as a connection between the ECs and ICs or transmit the stress to ICs. The ICs react with enhanced matrix production either directly to the dilatational stress or to the paracrine factors released by the ECs. This process may involve many biochemical factors. The observed increases in ECM synthesis could be due to either increases in synthesis or a shift of the synthesis-degradation balance, in which lysosomal cathepsins L and S

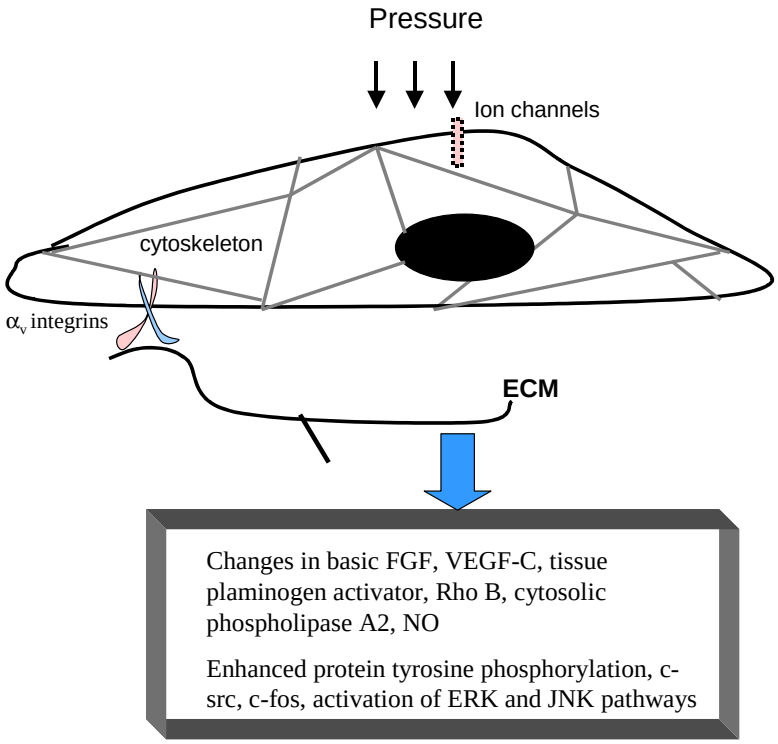


**Figure 64:** Mechanotransduction of pressure stress ([66, 92, 127, 126, 44]), pressure may affect the cells through cytoskeleton reorganization, opening/closing ion channels (e.g. $K^+$ channels) or acts directly on membrane proteins. Consequently these will lead to changes in signaling molecules, pressure-sensitive proteins, protein phosphorylation and activation of signaling pathways such as ERK and JNK.

might be involved. The mechanism issue can be further elucidated by studying changes in gene expression as well as enzymatic activities in the valvular cells.

Based on the results from this study and the findings in literature, the following biochemical pathway of pressure-induced valvular biological changes is proposed (Fig.65). Pressure exerts normal stress on leaflet tissue, which contains both ECs and ICs. In response, the ECs and ICs may undergo some cytoskeletal reorganization [119] or open/close their mechanosensitive ion-channels [44, 81]. Consequently, this may lead to a series of intracellular events which include the inhibition of cathepsins S and L, as observed in this study. The inhibition of lyosamal proteases leads to a slower degradation of collagen or other matrix proteins, eventually resulting in higher matrix synthesis. Pressure may also cause stimulation of cathespin D [120, 117], which is normally expressed by heart valve interstitial cells (VIC) [71] and known to have the ability to stimulate Angiotesin II production [145] by VICs. Angiotensin II, in the presence of TGF-$\beta$, or endothelin, has been

shown to enhance collagen synthesis in heart valves [70]. As a result, the amount of collagen is also increased. Cathepsin D was not included in the current study due to the lack of experience with this protease as well as the time limitation of this project. Both cathepsin D and angiotensin II should be included in future studies and this type of studies will provide important insights into underlying mechanisms of mechanotransduction in heart valves.

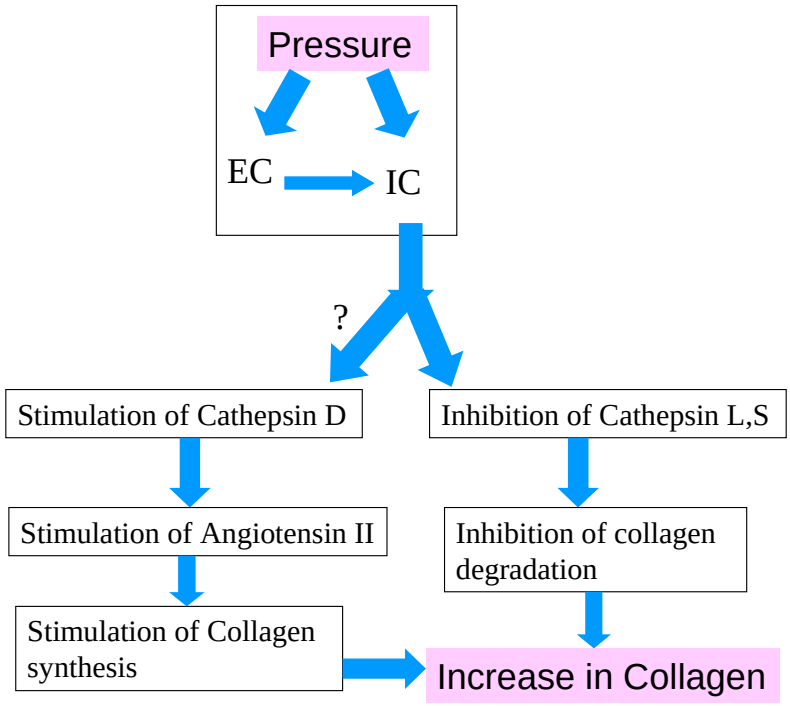


**Figure 65:** Proposed biochemical pathways depicting pressure and valvular synthetic activity; ? - indicates speculative only, not proved; collagen was mainly synthesized by the ICs, which can be affected by pressure either directly or through the ECs

### 6.5.2 Mechanotransduction Under Steady Shear Stress

Transduction of shear stress into gene regulation is now an active area of research and was recently reviewed by Shyy & Chien [131] and Helmke & Davies [59]. Fluid flow may act directly on transmembrane proteins or the lipid bilayer itself. In addition, the plasma membrane contains structures that are capable of both transmitting force to the cytoskeleton and transducing forces into biochemical signals. For example, caveolae putatively play a role in modulating membrane tension [114], and these membrane invaginations are rich in signaling molecules, including some that interact with actin stress fibers [48]. In addition to caveolae, apical plaques composed of $\alpha_5\beta_1$ integrin, vinculin,

talin and paxillin are structurally linked to the cytoskeleton. Integrin-mediated mechanotransduction includes multiple kinases (eg, FAK, c-Src, and Fyn), adaptor molecules (eg, CAS and Shc), guanine nucleotide exchange factors (GEFs) (eg, C3G and son of sevenless [Sos]), and small GTPases (eg, Rap1 and Ras) in activating MAPKs (eg, ERK). Under static conditions, the mechanosensitive integrins are in an inactive conformation, and various signaling molecules are not phosphorylated or assembled as a signaling complex. Shear stress activates the integrins by switching them to an active conformation, with increases in their affinity and avidity for cognate ECM proteins. Through specific interaction of the $\alpha$ and $\beta$ subunits of the activated integrins, the FAK/c-Src and the Cav-1/Fyn pathways are activated to elicit cascades of phosphorylation on various downstream effectors and their assembly through SH2 and SH3 interactions. The two pathways converge at the level of Raf-MEK-ERK in ECs in response to shear stress. Additionally, the force signal can also be transmitted to the nucleus and cell-cell junctions in the membrane via tension of the cytoskeleton, resulting in intracellular events. Support for transmission through intracellular junctions mainly comes from the molecular interactions between these junctions and the cytoskeleton. For instance, adherens junctions, composed of VE-cadherin, $\alpha$- and $\beta$-catenin, and plakoglobin are found to adapt their structure concurrently with the cytoskeleton.

In our experimental system, steady shear stress was applied directly onto the ventricular surface; the aortic surface did not see any flow. The ventricular surface was covered with a layer of endothelial cells, which are in direct contact with flow. The transduction of the shear force was likely through the endothelial layer and then transmitted to the underlying interstitial cells either through cell-cell junction, cell-ECM junctions or by the release of paracrine factors from the ECs. In the case of the denuded leaflets, where there were no ECs on the ventricular surface, force transmission was likely achieved through the ECM-cell junctions. The ECM experienced tensile stress upon exposure to shear stress, and this stress was transmitted to the ICs by connections between the cells and the matrix [168]. The ICs in turn respond with increased matrix production as well as decreased cathepsins expression.

Most of the above cited studies were performed on monolayer cell cultures, while the current

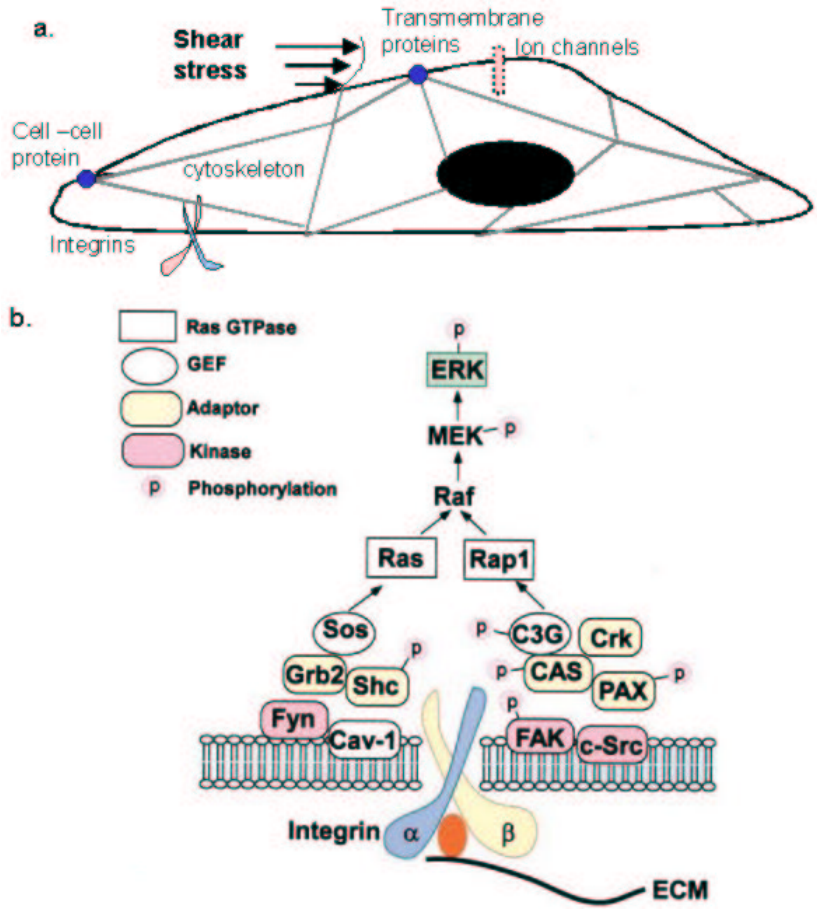


**Figure 66:** Mechanotransduction of shear stress: a. Force transmission via transmembrane proteins, or cytoskeleton; b. Integrin-mediated mechanotransduction includes multiple kinases, adaptor molecules, guanine nucleotide exchange factors (GEFs), and small GTPases in activating MAPKs, adapted from Shyy & Chien [131].

study is dealing with a much more complex system: leaflet tissue comprising various cell phenotypes as well as native extracellular matrix proteins. The mechanotransduction and force transmission will be much more complicated due to the interactions between different cell types and the involvement of matrix proteins. The other issue needs to be addressed is that only a few studies are related to heart valve cells. Therefore, one must be cautious while trying to extrapolate the findings to valvular cells, since many studies have shown that the biological effects of mechanical stimuli are often dependent on the specific cell type [156, 160]. The real mechanotransduction mechanism in valvular cells still needs to be studied specifically using cell culture or tissue culture.

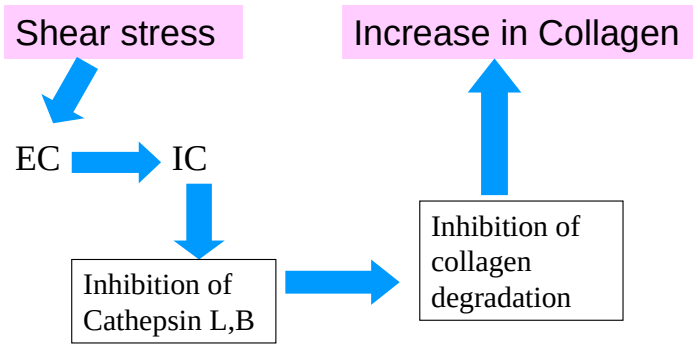


**Figure 67:** Proposed biochemical pathways depicting shear stress and valvular synthetic activity; collagen was mainly synthesized by the ICs, which can be affected by shear via the interaction with the ECs

## *6.6 Interaction between Valvular ECs and ICs*

Normal AV leaflets are covered with ECs on both the inflow surface and the outflow surface and populated by ICs within the extracellular matrix. ECs of a normal valve are polygonal, aligned with the internal collagen framework of the valve, which is generally arranged circumferentially with the free edge of the leaflet. Since healthy valves lack a microvasculture [46, 167], the ECs are most likely responsible for regulating interactions between blood and interstitial cells, which include metabolic and inflammatory processes. Additionally, valvular ECs may also affect the ICs through the release of paracrine factors such as nitric oxide and vasodilatory prostanoids [73, 133]; likely with the aid of nerve terminals found in their proximity [83]. The communications between ECs and ICs are likely achieved through cytokines, matrix components, and growth factor expressions as well as by direct mechanical connections (tensegrity) [31, 33]. Although quite obvious and very important, the interaction between valvular ECs and ICs has been only studied very in a very limited manner. A *in vitro* study by Batten et al [11] showed that there is interplay between these two types in immunogenicity.

The current study has addressed this issue of EC-IC interaction by studying the matrix synthesis of two types of leaflets: leaflets with intact endothelium (”intact leaflets”) and leaflets denuded of endothelium (”denuded leaflets”), under steady laminar shear stress at physiological levels. The intact leaflet serves as an EC-IC co-culture model, embedded within their native extracellular matrix; the denuded leaflets are a model with ICs only. The difference between these models therefore, provide insights into the interactions between the ECs and the ICs in the valve leaflets. We have

observed in this study that the presence or absence of ECs resulted in very different valvular responses to shear stress. GAG content was enhanced by shear in the denuded leaflets, but not in the intact leaflets. Therefore, the presence of ECs may play an inhibitory role on GAG production by the ICs; a similar phenomenon was observed by Stevens et al in 1998 with a co-culture of bovine ECs and SMCs [139]. It is not clear whether the biochemical pathways involved are similar in the two studies. Collagen synthesis was enhanced by shear stress in the intact leaflets, but not in the denuded leaflets. This is apparently inconsistent with the well-established fact that endothelial cells have inhibitory effects of collagen synthesis in co-cultured SMCs [105, 159, 161]. This inconsistency might be caused by the presence of mechanical stimuli vs. mere static culture [159, 161]; or differences between native valvular ECM and artificial ECM used in cell culture such as collagen, laminin and fibronectin [104], and differences between valvular cells and vascular cells, including both ECs and ICs [18].

## *6.7 Clinical Relevance and Significance of Study*

### 6.7.1 Clinical Relevance

#### *6.7.1.1 Relevance to Hypertension*

Hypertension is a frequent and serious disease affecting to various degrees all parts of the cardiovascular system. Functional adaptation of small arteries and arterioles to acute and chronic increases in hemodynamic forces are likely to precede the irreversible structural alterations (remodeling) observed in hypertension. Elucidation of the nature of cellular mechanisms activated by the presence of increased pressure and shear stress could advance our knowledge regarding the pathogenesis of hypertension.

The pressure study simulated pressure conditions ranging from physiological to severe hypertensive. According to American Heart Association's statistics [3], one of every five Americans have high blood pressure (systolic pressure at 140 mmHg and higher, diastolic pressure of 90 mmHg or higher). Hypertensive patients have higher risks for developing heart attack, stroke and congestive heart failure. Prior to these end events, many times there is tissue fibrosis, and hypertrophy following the onset of hypertension.

Hypertension has been shown to be a risk factor for degenerative aortic valve stenosis (20%

increase in risk), a condition in which the valve leaflets become thickened with disarray of collagen fibers, deposition of cellular waste and calcium [140]. This might be related to our findings that matrix synthesis activity has been upregulated under hypertensive pressure. Another issue is related to the observation that leaflet thickening is much more prevalent in the non-coronary position of the AV than either the left or the right- coronary leaflets. This was proposed to be related with the pressure loading conditions on each of the leaflets [177]. Young et al [177] simulated the pressure loading of the three leaflets and found pressure loading of the left- and right-coronary leaflets was 5.8% to 17% less than that of the non-coronary leaflet, due to the presence of coronary perfusion at these two positions. Therefore, they attributed the prevalence of leaflet thickening in the non-coronary leaflet to the higher pressure loading during diastole. Unfortunately, they did not perform a structural analysis of the three leaflets. Therefore, it is not clear whether the thickening is caused by excessive deposition of extracellular matrix or due to something else.

#### *6.7.1.2 Relevance to Endothelial Injury*

The shear stress study simulated physiological shear stress levels, therefore the observed responses can be used for understanding normal valve biology under physiological conditions. This study showed that shear stress levels within the physiological range resulted in higher collagen synthesis than static controls. The current experiment design did not allow us to determine whether this difference between shear and control is due to the stimulation of collagen synthesis under shear or the inhibition of collagen synthesis under static incubation. Inclusion of a fresh control would help to distinguish whether shear maintained the native level of collagen synthetic activity or it has abnormally stimulated it. If the first case holds true, then we could infer that fluid shear stress is essential to maintain the normal activity of the leaflet tissues.

The denudation study was aimed at determining the role of endothelium in valvular responses to shear stress, but the results can also be used for understanding valvular endothelial injury and the subsequent events of tissue remodeling. Clinically, damage/loss of the endothelium could occur due to bacterial infection (endocarditis), abnormal mechanical stresses (aortic stenosis), auto-immune

reactions (rheumatic valve disease) or catheterization during cardiac surgery. Damage to the endothelium may lead to thrombus formation, formation of verrucae and increased inflammatory infiltrate, subendothelial proliferation and migration, altered expression of cytokines and growth factors leading to the formation of myxomatous valves. In an *in vitro* tissue culture system where blood is replaced by cell culture medium and no inflammatory responses are present, consequences of endothelial denudation are restricted to subendothelial proliferation and migration, altered expression of cytokines and growth factors and their consequences. We did not study subendothelial proliferation and migration, but we observed increased sGAG content upon exposure to shear stress in the denuded leaflets. This has some resemblance to a myxomatous valve, which is characterized with an enlarged spongiosa and abnormal accumulation of proteoglycans. This similarity suggests that endothelial injury and flow combined might be the responsible factors for the accumulation of proteoglycans in myxomatous valves.

### 6.7.2 Significance of Study

The significance of these results is two-fold. Firstly, it helps to improve the understanding the acute responses of the AV to hypertensive pressure/endothelial injury. Recent clinical retrospective studies indicate that the hypertension as a risk factor for valvular disease such as aortic valve stenosis (AVS). However, it is not yet clear how hypertensive pressure was involved in AVS pathophysiology, especially during the early stages of the disease. Results from this study showed that hypertensive pressure could induce changes in valve matrix synthesis within 48 hrs, indicating that valvular matrix remodeling may contribute to the development of AVS in hypertensive patients. The denudation study showed increased sGAG synthesis under shear stress, which resembles the characteristics of a myxomatous valve, supporting the hypothesis that EC injury might contribute to the development of myxomatous valve disease. Finally, the involvement of cathepsins in these processes suggest a drug therapy targeting cathepsin enhancement might slow down the remodelling process induced by abnormal mechanical stimuli.

Secondly, the results can be applied to the development of a production scheme for tissue engineered heart valves. Recent reports suggest that mechanical conditions during perfusion are important in guiding the development of tissue engineered constructs [96, 62]. In the present experiments,

native porcine aortic valve leaflets were used as a model for tissue engineered leaflets to see if a simple hydrostatic pressure or steady shear stress would produce leaflets with synthetic activities and cell phenotypes approximating the native valves. Results from the present study suggest that hypertensive pressure may expedite the cellular components of TE constructs to develop their own matrix and cyclic pressure with high pulse frequency would help the cells to proliferate in order to get a sufficient seeding density. This can be very useful since the current most extensively studied bioreactor for TEHV, i.e., the pulse duplicator system developed by Hoerstrup et al [62], was not able to produce sufficient amount of collagen during *in vitro* conditioning [108]. The pressure conditions were relatively low: 30 and 55 mmHg; and this could be the reason for the observed slow collagen deposition process. Our results from the denudation study suggest that upon implantation, an *in vitro* endothelialized construct will have a different matrix synthesis pattern as compared with a construct seeded with only interstitial cells. Neither hydrostatic pressure or steady shear stress was sufficient to maintain the native SM-actin phenotype. Therefore, future experiments should examine the addition of bending forces to this pressure system, in the hopes of defining a bioreactor configuration capable of producing cellular synthetic activity and phenotypes comparable to native valves.

## *6.8 Limitations of Current Study*

Although the current study has addressed a very important problem, that is, the relationship between of mechanical stresses and heart valve biology; it still have a lot areas which need improvement but are beyond the scope of this project. There are three major areas need to be further explored and improved upon.

### 6.8.1 Limitations of the Pressure System

The current pressure system is limited in that it does not mimic the exact pressure loading experienced by the aortic valve. Physiologically, the aortic valve is exposed to a pulsatile pressure of 80/120 mmHg (diastolic/systolic). This pressure causes the leaflets to stretch in a rhythmic-pulsatile fashion (cyclic stretch) as well as compressing the elements of the valve leaflet. The pressure generated by the current system exerted compression onto the leaflets, but did not cause significant

stretching of the tissue. Because of this difference, the biological responses observed in this study may not match exactly the remodelling processes occurring under hypertension. However, results from the current study demonstrated that hydrostatic pressure by itself was able to induce changes in valve biological properties, implying that the transvalvular pressure exerts its influence on valve biology at least partially through compression of the tissue. The effects of cyclic stretch can be studied separately by using a different system.

Another limitation of the current pressure study is that it did not take into consideration differences of the pressure loading on the two sides of the leaflets. Cells close to the aortic surface are under diastolic pressure (80 mmHg for normal people) during two thirds of the cardiac cycle; whereas the cells close to the ventricular side experience systolic pressure (120 mmHg, normal people) for one third of a cardiac cycle. Because of these inherent differences in mechanical loading, cells on in the aortic valve leaflets are likely to possess heterogenous phenotypes or gene profiles; hence their responses to mechanical stimuli such as pressure, might be also different. This problem will be very challenging by tissue culture method due to limitations on isolation and measurement techniques. The promising approach will be cell culture studies using isolated EC and ICs from the two sides of the valve leaflets, will rely on the successful isolation of pure cell populations [132].

### 6.8.2 Limitations of the Shear Stress Study

The first limitation of the shear stress study was that the shear stress in our experimental system was steady, while *in vivo*, the cells on the ventricular surface see a pulsatile shear during systole. This can be easily overcome be adding two check valves to the current system (Fig.68) and using a piston pump instead of the peristaltic pump to generate the desired waveforms. The check valves only allow flow in one direction.

The second limitation has to do with the differential phenotypic properties of endothelium on the two surfaces of the leaflets. As shown in the schematic drawing (Fig.69), there are three distinct flow regions in the AV apparatus: the aortic wall of the sinus of Valsalva characterized with low, disturbed flow; the side of the leaflets facing the aorta with low shear, laminar flow and the side facing the ventricle with high shear, laminar flow [86]. Clinical observations have revealed distinct patterns of valve lesions in these three regions and associated them with the mechanical environment. A recent

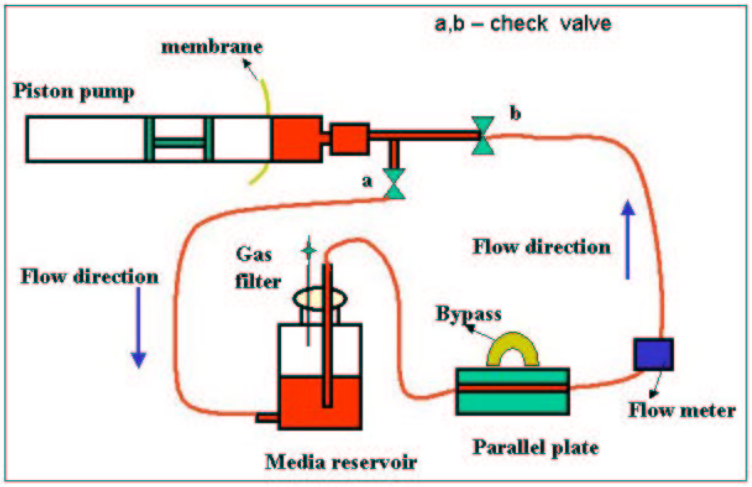


**Figure 68:** Schematic drawing of a pulsatile shear system, including a piston pump, a media reservoir, two check valves a and b, and the parallel plate device. The working principle is as following: When the piston moves forward, valve a opens and valve b closes, therefore fluid is pumped directly from the pump head into the reservoir, and there is no flow through the parallel plate, resembling the diastole phase; when the piston moves backward, valve a closes and valve b opens, fluid is sucked out from the reservoir, pass through the parallel plate and enter into the pump head; resembling the systolic phase. Flow is measured by an electronic -magnetic flow meter downstream the parallel plate. Frequency and amplitude of the pulsatile shear can be varied by altering the waveform on the pump.

study by Simmons et al [132] compared ECs from the aortic side versus ECs from the ventricular side of the aortic leaflet. Their results revealed differential transcriptional profiles across multiple pathways, including prominent representation of proliferative, apoptotic and calcification pathways [132]. The current study is focused on the ventricular surface and the ECs on the aortic side were not taken into consideration. Therefore, the observed results might not match exactly the outcomes under physiological flow conditions, as a number of studies have shown that different types of shear often result in remarkably different responses in cultured cells. However, it does provide insights into the valvular cell responses to shear stress in a three-dimensional context, which would certainly facilitate the development of a tissue engineered valve.

### 6.8.3 Oxidative Stresses in Tissue Culture

Oxidants such as hydrogen peroxide ($H_2O_2$) are implicated in mediating a wide array of human diseases including atherosclerosis, cancer, and neurodegenerative diseases. Oxidants contribute to disease processes by causing damage to biomolecules and altering cellular metabolism. Key

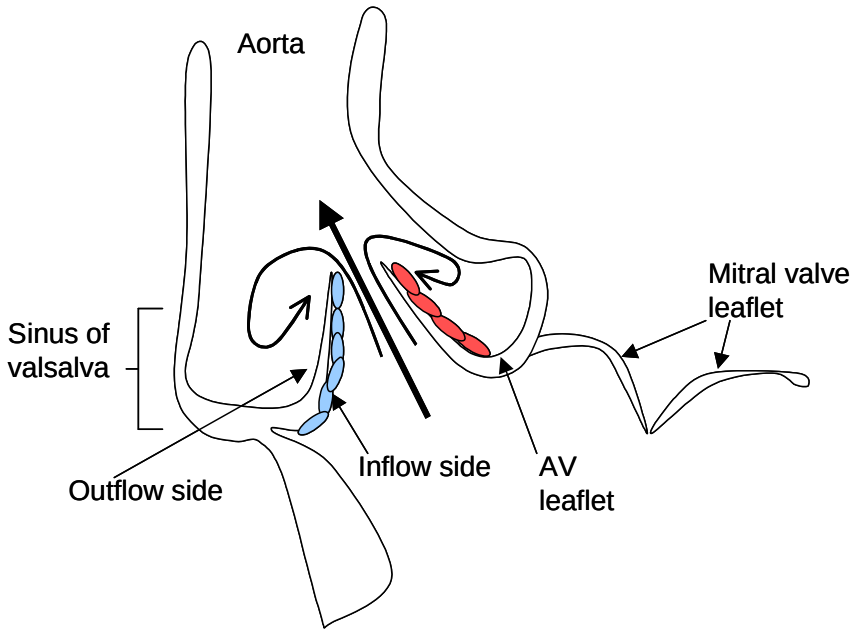


**Figure 69:** Diagram of anatomy and flow patterns of the aortic valve. Vortexes form in the sinuses of the Valsalva during systole. Flow separates beyond the tip of the leaflets and rejoins at the aortic wall, where the shear layer may become disturbed. Endothelial cells on the inflow and outflow sides are depicted in blue and red respectively. (adapted from an article by Mehrabian et al [86])

among the targets for oxidative damage are structural proteins and enzymes. Oxidized proteins may present cytotoxity to the cells or affect their normal function. For instance, incubating HUVEC with oxidised LDL-cholesterol will lead to increased release of von Willebrand factor (vWF) from endothelial cells [12]. Oxyblot (Oxyblot detection kit, Serologicals, GA) was used to detect the amount of oxidized proteins in leaflet tissues cultured under hypertensive pressure and atmospheric pressure, due to the concern that the increase in dissolved oxygen caused by elevated pressure might have significant effects on the tissue and thereby masking the effects of pure pressure. Our results did not show significant differences between the hypertensive pressure and atmospheric control groups in protein oxidation. But both did show evidence of oxidized proteins, which were not seen in the fresh native valves. This indicates the removal of the valves from the animal, the transport or the handling, may cause some oxidization to the tissues. Our time-serial experiments showed that the oxidation happened as early as 6 hrs after incubation. Future studies are needed to determine which proteins become affected by oxidative stress, to what degree they are modified and the functional consequences of the modifications.

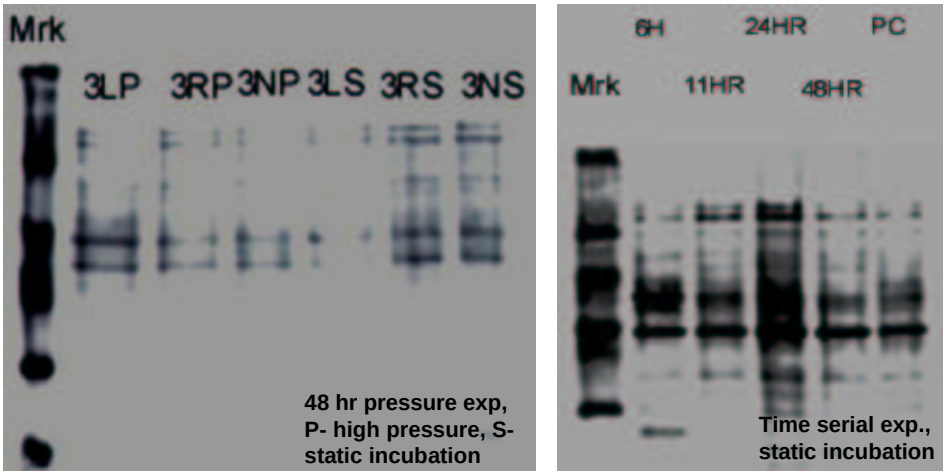


**Figure 70:** Oxyblot of valve leaflets under static incubation and hypertensive pressure; note that there are four bands shown up on most of the samples; this was not seen in the fresh valves (data not available)

### 6.8.4 Limitation of the measurement techniques

Matrix synthesis and cell proliferation in the pressure study were measured by radiolabeling, which is based on the radioactivity of the tissue at the completion of the experiment. Tissue samples were vacuum dried and digested in proteinase K. 200 $\mu$l of the resulting solution were then placed in a liquid scintillation counter for radioactivity measurement. The liquid scintillation counter gives an average error rate of around 8% for $^{3}$H- counting and around 5% for $^{35}$S-counting (calculated based on the differences between scintillation counting results from duplicates of the same sample). Therefore, any difference that to be considered significant shall be greater than the measurement error. All the significant differences we have observed in this study were above the error range (14% to 130% of increases). The other issue that should be considered is the half-life of the radioactive precursor. This won't be a problem for $^{3}$H, which has a half life of 12 years; but for $^{35}$S-, it may become a problem, since the half life is only 80 days. Therefore, the $^{35}$S-$Na_2SO_4$ shall be purchased within a month before the experiment and should be well documented and calibrated upon each use.

The shear stress study used colormetric assays for matrix synthesis measurement. These assays involve a series of tissue digestion, formation of a substrate-dye complex (precipitate), dissolving of this complex with a dissociation reagent and reading of absorbance in a spectrometer using a 96 well plate. Collagen was read at 540 nm and sGAG at 656 nm. Measurement errors may occur due to

poor pipetting techniques, loss of the substrate-dye complex during the removal of the excessive dye reagent, quality variations of the dye reagent and dissociation reagent from lot to lot, poor standard curves (not linear), and reading accuracy of the spectrometer. Most of the errors can be overcome by good laboratory practice and the error of the spectrometer can be minimized by taking multiple duplicates and calculating the average. The reading error from the spectrometer averages around 5% (calculated based the absorbance values from duplicates of the same sample).

## *6.9 The Issue of Biological Variability*

As any studies that involve using animal tissue, the issue of biological variability among the different valves has been a confounding factor in interpreting the results. The variability comprises two types of variations: inter-animal and intra-animal variations. Valves from different animals may show a wide range of biological activity due to the age, size and health condition of the animal. Heart valves in this study came from slaughterhouse pigs, which are generally 2.5-3 years old and weigh about 350-450 lbs. Each valve was visually inspected upon removal from the heart, valves with abnormal looking such as thickened leaflets or a yellowish color, were discarded. However, this is far from sufficient to exclude the biological variability issue. The other source of variability arises from the differences between the three leaflets: the non-coronary, the right and left coronary leaflets.

Following is the collagen synthesis data (48 hr static incubation) compiled from 22 aortic valves, i.e. 22 animals. These valves were collected on different days, the collagen synthesis of each leaflet was measured and pooled for statistical analysis. Below are the matrix plot of the data (Fig.71) and the results from the ANOVA analysis (Fig.72). Position means the three anatomical positions, with 1 indicating the left coronary position, 2- right coronary and 3- non-coronary.

As shown in the graph and the ANOVA results, valve ID is a more significant factor in determining collagen synthesis in the tissue than its anatomical position ($p=0$ vs. $p = 0.596$). That is, variability among the valves are much more significant than variability among the three leaflets within each valve. Similar results were also found with sGAG content (refer to appendices, section 4). Therefore, for ECM synthesis, the variations in results comes mainly from the biological variabilities between different valves. This variation caused big standard deviations in the data.

Since the major biological variability came from the valve-to-valve variabilities, one should

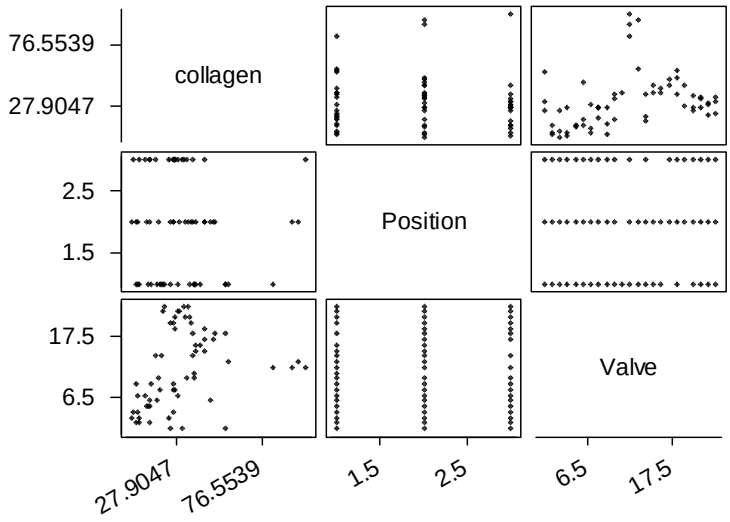


**Figure 71:** Matrix plot with variables of collagen synthesis, leaflet position and different valves. Of particular interests are the plots with collagen synthesis in the y-axis and leaflet position and valve ID in the x-axis respectively; note that the collagen synthesis varied from valve to valve, but the variations among the three different leaflets positions were relatively insignificant.

try his/her best to ensure that the valves are of roughly the same size, same age and same health conditions. Also, because of this, it would be more appropriate to use each valve as a sample, instead of each leaflet, so as to have a better statistical representation. Since the variations among the three leaflets in one valve were relatively small, they can serve as controls to each other, this way all three leaflets can be utilized. For instance, design of the pressure experiments could be improved by including multiple pressure systems at different pressure conditions, e.g. 100, 140, 170 mmHg, at the same time, and assign each leaflet randomly to one pressure condition. By doing this, we can get a direct comparison among the different pressure conditions and avoid the valve-to-valve variability as well as experiment-to-experiment variations such as the transportation time from the abattoir to the laboratory (i.e. the cold ischemic time).

**General Linear Model**

| Factor | Type | Levels | Values |
|---|---|---|---|
| Position | fixed | 3 | 1 2 3 |
| Valve | fixed | 21 | 1 2 3 4 5 6 7 8 9 10 12 13 14 15 16 17 18 19 20 21 22 |

**Analysis of Variance for collagen, using Adjusted SS for Tests**

| Source | DF | Seq SS | Adj SS | Adj MS | F | P |
|---|---|---|---|---|---|---|
| Position | 2 | 197.59 | 101.97 | 50.98 | 0.53 | 0.592 |
| Valve | 20 | 19540.59 | 19540.59 | 977.03 | 10.20 | 0.000 |
| Error | 36 | 3447.77 | 3447.77 | 95.77 | | |
| Total | 58 | 23185.96 | | | | |

**Figure 72:** ANOVA of collagen synthesis with respect to leaflet position and valves,note the p values

# CHAPTER VII

# CONCLUSIONS

This study has shown that porcine aortic valve leaflets cultured *in vitro* can respond to applied mechanical stimuli, namely, pressure or steady shear stress. Valvular responses to these two mechanical forces were different and appeared to both involve lysosomal cathepsins.

The effects of pressure are dependent on the pressure regime (i.e. constant vs. cyclic), pressure magnitude and pulse frequency as in the case of cyclic pressure. Constant pressure caused proportional increases in valvular collagen synthesis, but did not affect sGAG synthesis. Cyclic pressure at hypertensive level with normal frequency (1.167 Hz) caused increases in collagen and sGAG synthesis proportional to the mean pressure level. Cyclic pressure at high frequency (2 Hz) with physiological mean pressure level (80-120 mmHg) led to significant increases in DNA synthesis, but low frequency (0.5 Hz) resulted in slight increases in collagen and sGAG synthesis. Results from cyclic pressure experiment combining high magnitude and high frequency indicated a competing effects between pressure magnitude and pulse frequency, with pressure magnitude being the dominating factor. Neither constant or cyclic pressure showed no appreciable alterations on $\alpha$ -SM actin quantity or distribution during the experiment period as compared with atmospheric control. The valve tissue morphology was preserved under hypertensive pressure.

Endothelial cells on the porcine AV leaflets surface still remained circumferentially aligned even after exposure to steady laminar shear stress for 2 days. Changes in valvular synthetic activity under steady laminar stress were closely related to the presence of a viable endothelium on the ventricular surface. Leaflets with an intact endothelium responded to steady shear (9-40 dyne/cm$^2$) with increased collagen synthesis and slight decreases in sGAG content; while leaflets without an endothelium demonstrated increased sGAG content and baseline collagen synthesis under identical shear conditions. Similar to the pressure study, exposure to shear stress did not affect $\alpha$ -SM actin quantity or distribution as compared with static control. Tissue morphology was well preserved after exposure to shear stress.

Molecular biology studies showed that the observed increases in collagen synthesis under pressure or steady shear stress were concurrent with decreases in cathepsin activity and expression. Particularly, cathepsin S and L expression and activity were declined, cathepsin B was present but not affected by either mechanical force. This converse relationship between collagen synthesis and cathepsin activity indicated that cathepsins might be involved in valvular extracellular matrix remodeling. Immunohistochemistry results showed cathepsin production by both endothelial cells and interstitial cells.

In conclusion, pressure (both static and cyclic) or steady shear stress, each as an individual mechanical factor can induce changes in aortic valve biosynthetic activity. The effects of pressure depend strongly on pressure magnitude and pulse frequency; the influences from magnitude and frequency seem to be competitive. The effects of steady shear stress depend on the presence or absence of endothelial cells on the flow-contacting surface. Cathepsins expression and activity was inhibited by both pressure and steady shear stress, concurrent with the increases in collagen synthesis, suggesting a potential role of cathepsins in regulating valvular collagen synthesis.

# CHAPTER VIII

# RECOMMENDATIONS FOR FUTURE RESEARCH

The present study has examined the effects of hydrostatic pressure and steady laminar shear stress on the biological properties of porcine aortic valve leaflets. Based on the results, future studies can fall into the following categories: 1) Mechanism Study; 2). Kinetics study; 3) Effects of other mechanical factors; 4) Effects of mechanical stresses on valve calcification.

## *8.1 Molecular and Cellular Mechanisms of Mechanical Forces-induced Biological Changes in Heart Valves*

This study has observed significant increases in extracellular matrix synthesis within 48 hrs' exposure to pressure or shear stress. The process through which mechanical signals induce changes in biological properties is called mechanochemical transduction. Mechanical forces cause direct conformational changes in the extracellular matrix, which in turn may alter integrin structure and lead to activation of several secondary messenger pathways within the cell. Activation of these pathways leads to altered regulation of genes that synthesize and catabolize extracellular matrix proteins as well as to alterations in cell division. Another pathway through which mechanical signals are transduced involves deformation of gap junctions containing calcium-sensitive stretch receptors. Once activated, these channels trigger secondary messenger activation through pathways similar to those involved in integrin-dependent activation and allow cell-to-cell communications between cells with similar and different phenotypes. The third process pathway is through the activation of ion channels in the cell membrane. Additionally, mechanical forces can also activate growth factor and hormone receptors even in the absence of ligand binding.

Although the mechanism of hydrostatic pressure-induced biological changes are not fully understood, there is evidence showing the involvement of alpha V integrin [126], basic FGF, VEGF-C [128] as well as activated ERKs [47] in pressure-induced changes in vascular cells. Therefore, future studies should focus on the gene expression of molecules such as alpha V integrin, basic FGF,

VEGF-C and ERKs in order to elucidate the underlying mechanisms. This goal can be achieved by using tissue culture, as in the present study, or by using cultures of isolated valvular endothelial cells and valvular interstitial cells. Molecular biology techniques such as western/northern blotting, RT-PCR and DNA microarray will play a critical role in such studies. Angiotensin II and the renin-angiotensin system have been shown to be very important for valvular tissue homeostasis [145]. Therefore it should also be included in future studies for the purpose of elucidating the mechanism. In addition to the above mentioned molecular markers, the gene expression of cathepsins and MMPs shall also be included in the mechanism study, since we have seen decreased cathepsin expression and activity accompanied with increased collagen synthesis.

## *8.2 Biochemical Kinetics of the Mechanical Forces-induced Biological Changes in Heart Valves*

It is well established that cellular responses to mechanical stimuli are often time-dependent. For instance, a study by Tokungana et al [155] showed that the proliferation of EC cultured under hypertensive pressure (80 mmHg and higher) increased rapidly from day zero till day 3, then decreased gradually to baseline level by day 12. Another example is the study by Vouyouka et al [160], in which they found SMC proliferation was inhibited by cyclic hypertensive pressure, but the effect only became significant by day 5.

All the experiments in the present study had only one time point, i.e. 48 hrs. The observed results were therefore the accumulative results for the whole experimental period. Based on these data only it is not possible to tell how the process started, its evolution and the long-term results. These questions can be better understood by investigating various time points in addition to the 48 hr period. Both short term (less than 48 hr) and long term (beyond 48 hrs) kinetics are needed. Short times points studies, such as 6, 12, 24 and 36 hr will help to identify the initial events in response to the mechanical signals. It is likely that the changes in protein synthesis might not be appreciable at some of the shorter time points. Therefore, the preceding gene expression should be the focus in the short term studies. The other aspect of the kinetics study is the long-term effects. Compared to disease progression process (months to years) in patients, 48 hrs is relatively too short and may represent only transient responses. Long-term studies could provide a better representation

of clinical observations and also demonstrate the trend of the remodeling process. Indeed, some long-term (96 hrs) preliminary experiments on the cyclic pressure effects indicated that collagen and sGAG synthesis continued to increase from 48 to 96 hr, but the rates of increase were lower when compared to the first 48 hr and the differences between pressure and control became less significant at 96 hr. It is clear from these results that the long-term results will very likely be different from the 48 hr data. Unfortunately, the scope of this project does not allows for a comprehensive study of the time-dependency issue, it shall be addressed in future studies.

## *8.3 Effects of Other Mechanical Factors on Heart Valve Biology*

In addition to hydrostatic pressure and shear stresses, the AV leaflets experience other types of mechanical forces. These forces include cyclic stretch caused by the diastolic pressure, and bending stresses due to the opening and closing behavior of the valve leaflet. From relaxing stage in systole to fully stretched under diastole, the AV leaflets undergo a strain of about 20% during each cardiac cycle. Cyclic stretch might be the factor responsible for the $\alpha$-SM actin expression in the valve, since it is the only valvular behavior that is associated with the contractility of the leaflet as opposed to shear stress or hydrostatic pressure. Cyclic stretch has been shown to affect the synthetic activity, proliferation, apoptosis, MMPs activity and many other properties of various cell types including vascular ECs, SMCs and cardiac fibroblasts. A recent study [72] showed that cyclic stretch enhanced collagen synthesis in cultured valvular interstitial cells. Apart from that, there is very little information on the effects of stretch on valvular tissue or cells. The effects of cyclic stretch on the properties of valve leaflets can be studied by using an apparatus developed at Professor Michael Sacks'a lab at University of Pittsburgh. Strips of aortic valve leaflets are mounted onto the apparatus by suturing, the apparatus is filled with culture medium, and a motor generates dynamic biaxial stretch on the tissue. Biological endpoints shall include valvular synthetic activity, cell proliferation, cell phenotype, tissue morphology and changes in protease activities.

Bending stress in the AV leaflets is most prominent at the leaflet base region and the attachment sites. Areas of high bending stresses have been found to be correlated to sites of valve calcification. The areas of highest bending stresses have also be associated with active tissue renewal. Bending stresses *in vivo* are generated by the opening and closing behavior of the valve. This can be

duplicated *in vitro* by developing an organ culture flow loop, in which the whole valve apparatus (including the leaflets, the sinuses, the aortic root and the annulus) is preserved and mounted onto a valve holder. The flow loop is filled with culture media to provide nutrients to the tissue. A disadvantage of this method is that it generates not only bending stresses, but also flow and pressure. Therefore, it is hard to separate the effects of bending stresses from pressure and shear stress. Alternatively, a non-flow bioreactor can be developed by using magnets or other means to generate bending of the leaflet tissue [45]. In this way, the effects of bending stresses can be determined without the interference from other mechanical factors.

## *8.4 In Vitro Study on Mechanical Forces vs. Valve Calcification*

Calcification is the most common pathological finding in operatively excised heart valves. It typically begins deep within the substances of the cusps (intrinsic mineralization) [124]. Calcification can also occur in adherent thrombi or infective vegetations. Theories have been proposed to explain dystrophic calcification and its association with tissue necrosis in the valve, including matrix vesicles [149, 40]. Osteopontin, a bone matrix protein, has been detected in calcified human aortic and mitral valves [89, 20]. Additionally, a population of valve interstitial cells have been identified with osteoblast-like characteristics that spontaneously form calcific nodules in culture [89]. Another study with 324 excised calcified valves revealed close correlation between calcification and coronary artery diseases, peripheral arterial disease, hypercholesteralmia and hypertension [90]. The same study also revealed bone formation and bone morphogenic protein-2 and -4 (BMP-2/4) adjacent to the places of ossification.

The development of valve calcification has also been linked to mechanical stresses in the leaflet tissue, since calcium deposits in the leaflets often occur in areas with high stresses [154]. However, the molecular and cellular mechanisms are not fully understood due to the complex biochemical and biomechanical interplay involved in *in vivo*. *In vitro* systems such as the pressure system in the current study can provide an important tool for studying valve calcification under hypertensive pressure, especially at the early stages of the disease. In addition to mechanical stress, EC injury was also found to be involved in valve calcification process [76] and this can be studied using the denudation model. Calcium deposits can be detected by using Alizarin Red S (calcium appear red)

and von Kossas silver stains (calcium appear black) on frozen sections staining, and other markers such as osteopontin and BMP-2/4 should also be included in the study, since they have been shown to be involved in valve calcification.

# APPENDIX A

# MECHANICAL DRAWINGS OF THE PRESSURE SYSTEM

## *A.1 Pressure Chamber: Lid*

Drawing of the lid of the pressure chamber, made of polycarbonate material, features shown here include the holes (8, diameter : 3/16 inch, distributed evenly around the circumference) for tightening screws and the inlet for compressed air (diameter : 3/8 inch, located at center of the lid).

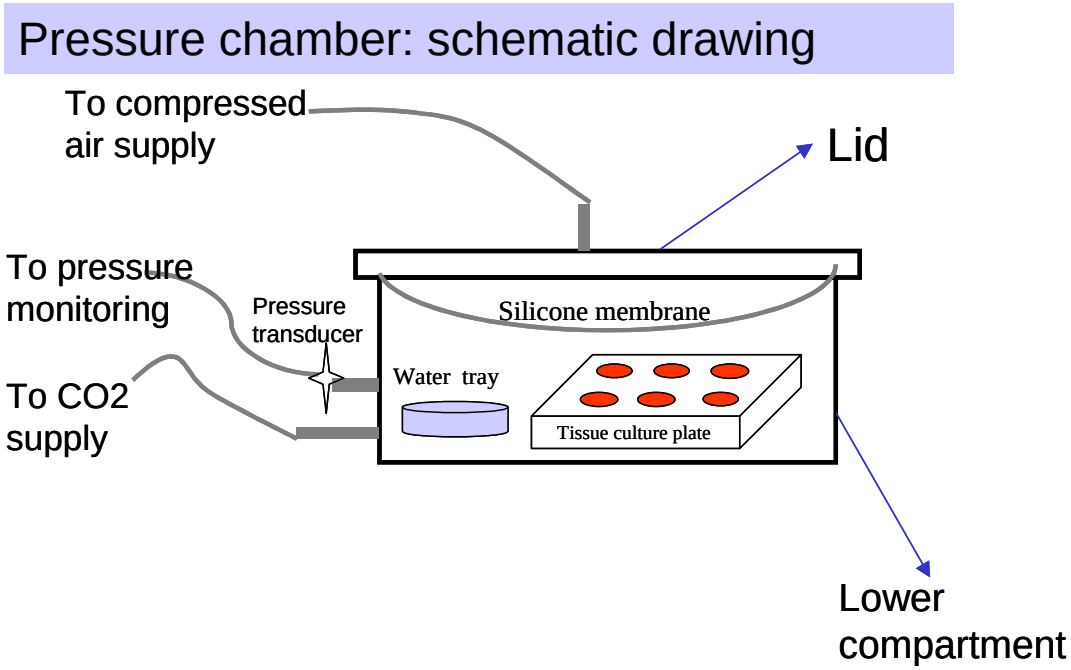


**Figure 73:** Schematic drawing of the pressure chamber: including the lid, the lower compartment and the silicone membrane

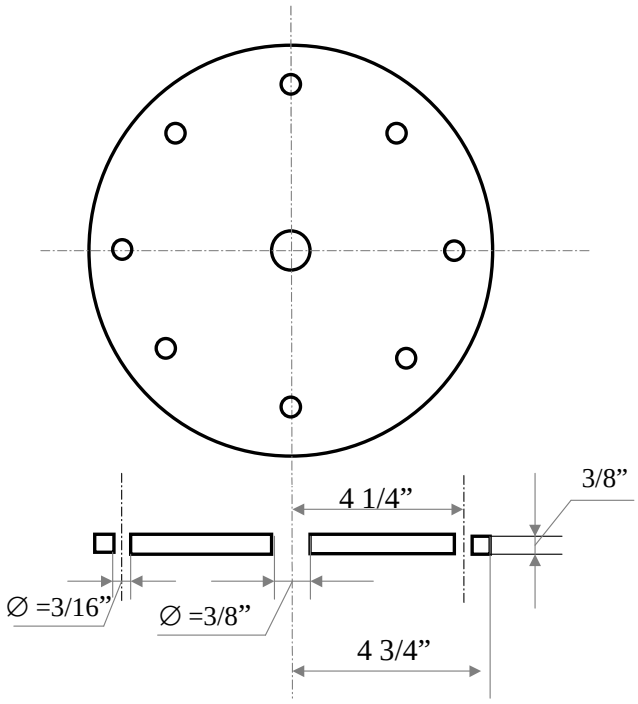


**Figure 74:** Lid of the pressure chamber, top: top view, bottom: side view, dimension not to scale

## *A.2 Pressure Chamber: Lower compartment (I)*

Drawing of the lower compartment of the pressure chamber (inner diameter (r): 3 1/8 inch, outer diameter (R): 4 3/4 inch), made of polycarbonate material, features shown here include the holes for tightening screws (8, diameter : 3/16 inch, distributed evenly around the circumference, 4 1/4 inches away from the center) and the groove (1/8 inch in width, located 3 3/8 inches away from the center) for a silicon O-ring.

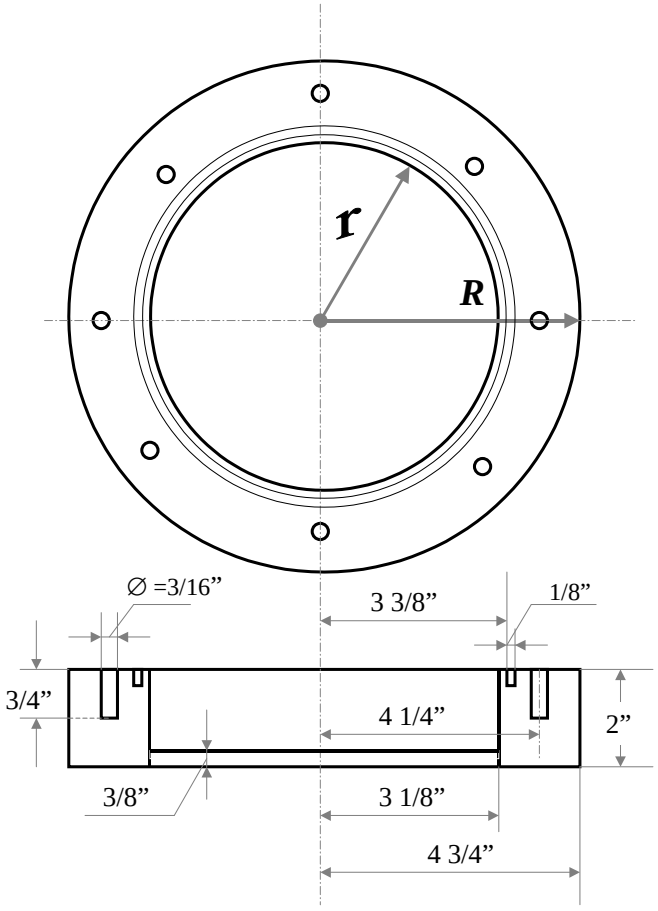


**Figure 75:** Lower compartment of the pressure chamber showing the screw holes and the groove, top: top view, bottom: side view, dimensions not to scale

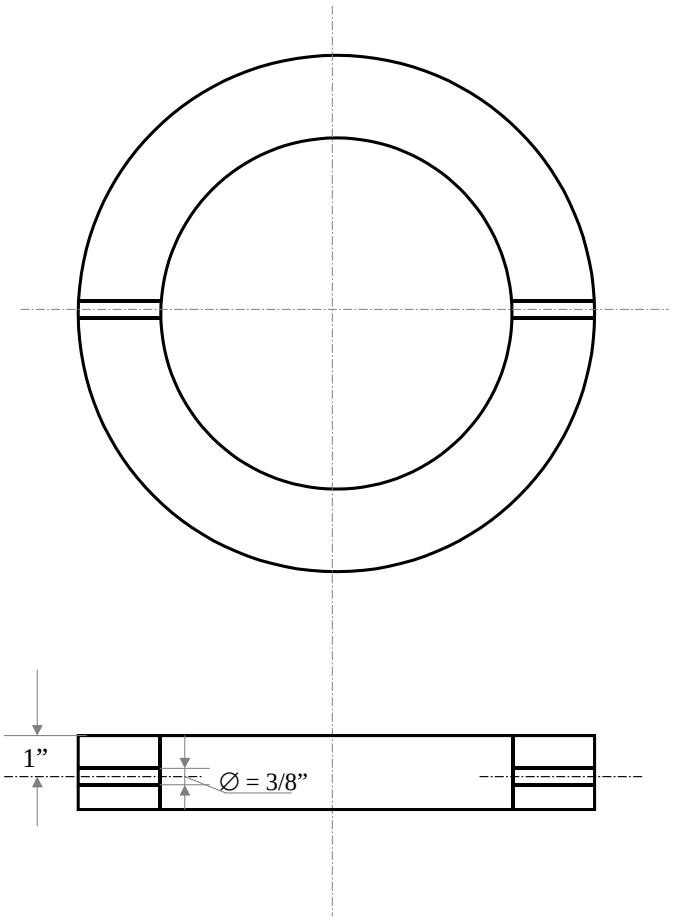


**Figure 76:** Lower compartment of the pressure chamber showing the gas inlet (left) and pressure transducer position (right), top: top view, bottom: side view, dimensions not to scale

## *A.3 Pressure Chamber: Lower compartment (II)*

Drawing of the lower compartment of the pressure chamber, made of polycarbonate material, showing here features including the inlet for $CO_2$/air and connections for pressure transducer (both have diameter of 3/8 inch and located 1 inch from top of the lower compartment.

## *A.4 Pressure waveforms*

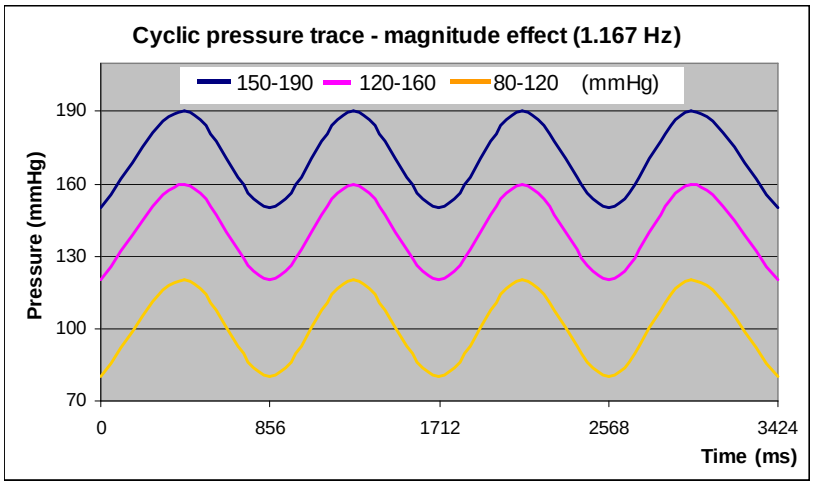


**Figure 77:** Pressure traces of cyclic pressure experiments: magnitude effects, where the frequency was set as 1.167 Hz; waveform remained stable throughout the experiment (48 hrs), shown only the first 4 cycles

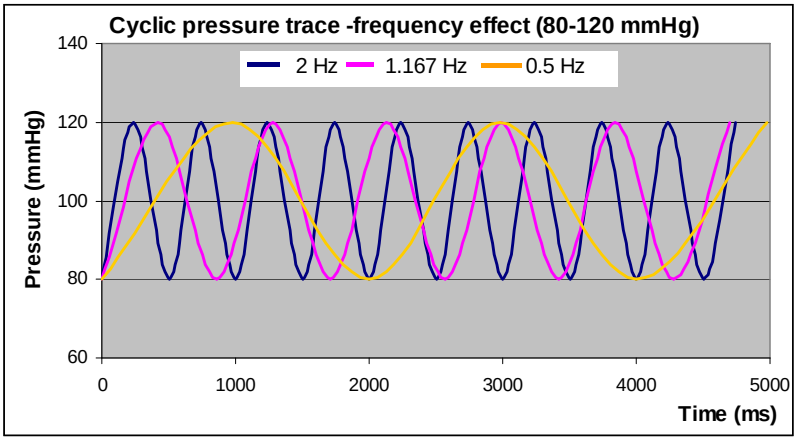


**Figure 78:** Pressure traces of cyclic pressure experiments: frequency effects, where the pressure magnitude was set at 80-120 mmHg; waveform remained stable throughout the experiment (48 hrs), shown only the first 5000 ms

# APPENDIX B

# FLOW CHAMBER: FLOW VISUALIZATION

The detailed design and calculations can be found in Matt Weston's thesis [168]. The laminar flow profiles was obtained by injecting a black ink into the chamber and capturing the path of the dye. Since the upper plate was opaque and not suitable for imaging, the dye was injected into the flow chamber from the back of the lower plate. Due to the symmetric design of the plate, only half the plate was used for the visualization. Three injection sites were chosen to represent flow at the center of the indented wells, at the edge of the wells and flow outside the wells (within the flow channel). Showing on the next page is the set-up of the flow visualization, followed by a snapshot and a video showing the laminar flow profile in the chamber.

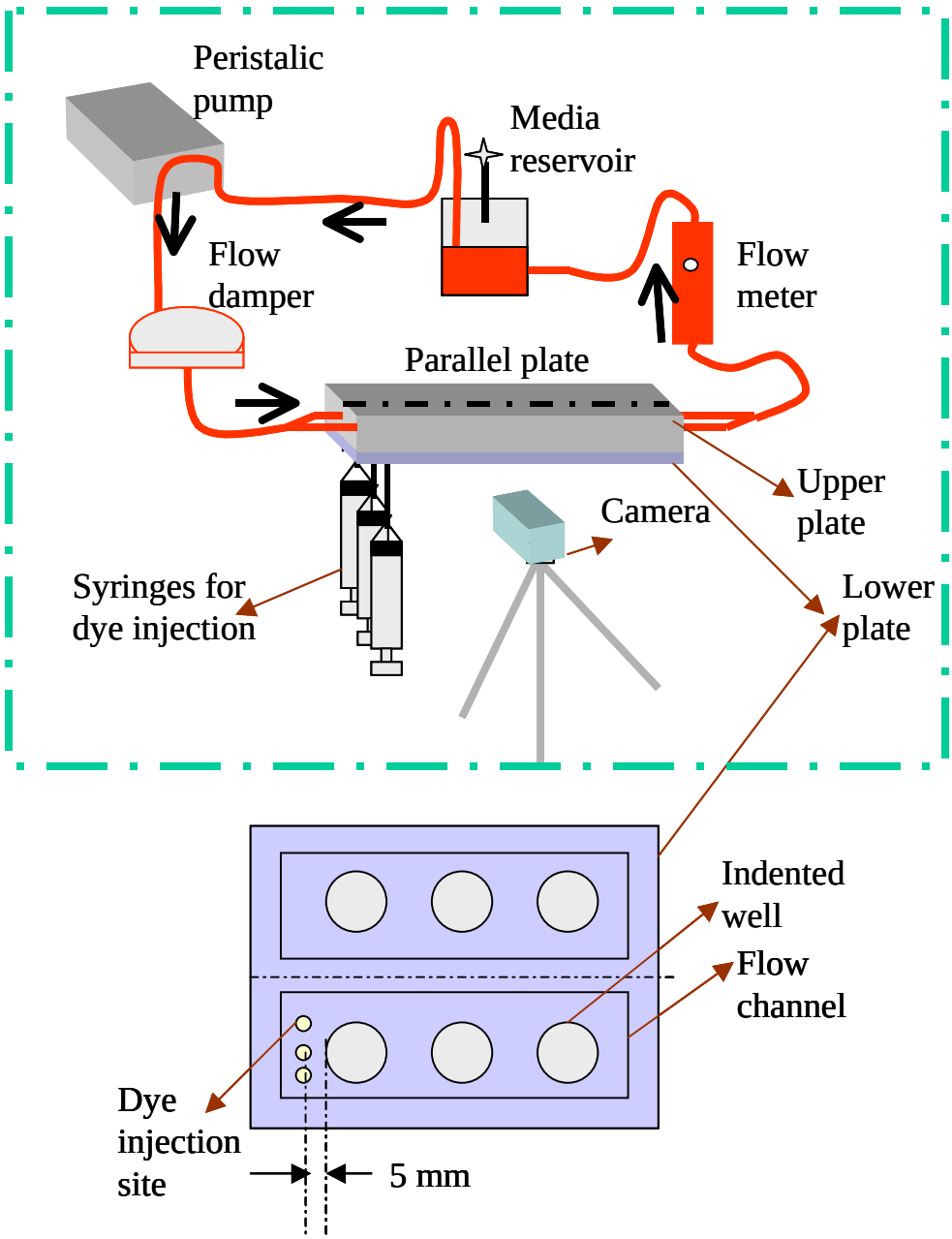


**Figure 79:** Flow visualization set up; major components of the flow system are the parallel plate, a flow meter, media reservoir, a flow damper and a peristalic pump that drives flow (Arrows indicate flow direction). The parallel plate system consists of two plates, the upper plate and the lower plate. The upper plate is made of 0.75" thick polycarbonate and appear opaque; therefore it is not suitable for imaging. The lower plate is thinner and transparent, therefore flow path is captured from underneath ( Dye was injected into the chamber from the back of the low plate and digital video camera shooting from below). Since the lower plate has a symmetric design, only half the plate was used for flow visualization. The dye (black ink) was injected at three sites, which are 5 mm away from the first indented well (containing leaflet tissue). The three sites were chosen to capture the flow at the center of the wells, at the edge of the wells and outside of the wells. Note: Dimensions not to scale.

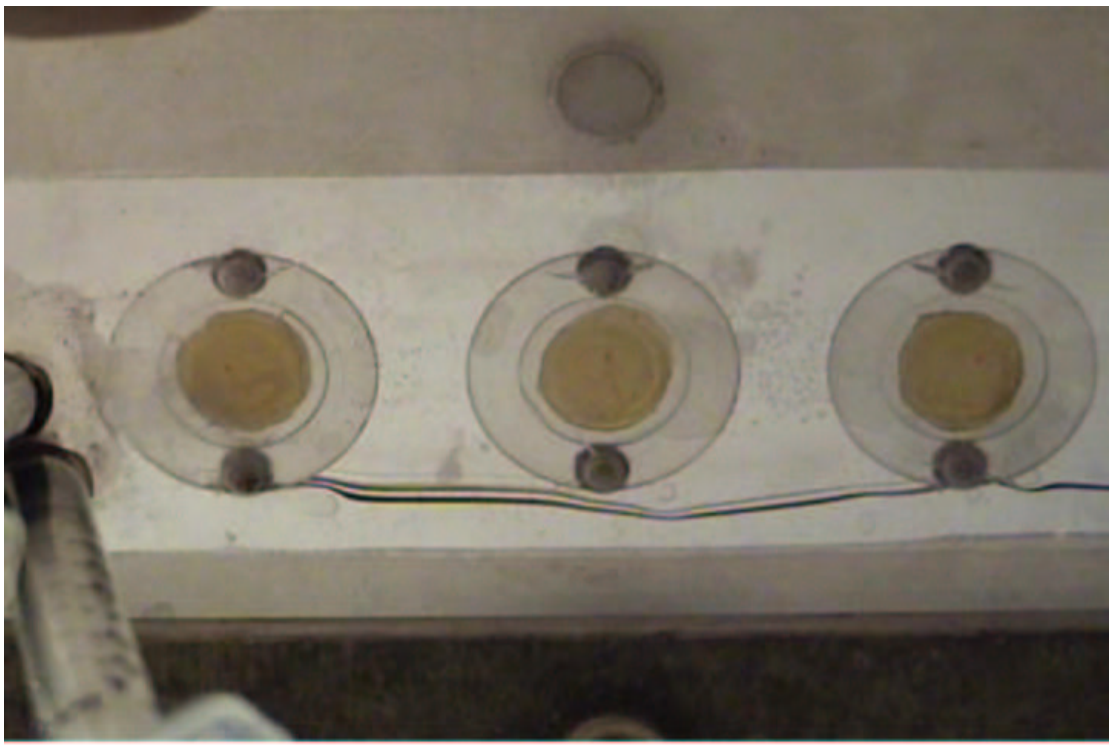

**Figure 80:** A snapshot of the flow path at the edge of the wells, only half of the plate (three wells) is shown, black line shows the path of the dye, nearly-straight line indicates laminar flow. Line not perfectly straight due to some air bubbles along the path.

# APPENDIX C

# PROTOCOLS

## *C.1 Deparaffinization*

### C.1.1 Procedure

1.xylene substitutes, 3 stations, 5 min each;

2. 100% alcohol, twice, 2 min each;

3. 95% alcohol, twice, 2 min each;

4. 75%, 2 min;

5. washed in water for 2 minutes.

#### *C.1.1.1 Regents and Solutions*

**Alcohol**: EMD#65347/85

**Xylene substitute**:EMD#XX0060-4

## *C.2 Routine Hematoxylin and Eosin staining for paraffin sections*

### C.2.1 Procedure

1. Deparaffinized slides are stained in Hematoxylin for 30 seconds;
2. Rinse in DI water;
3. Dip in acid alcohol;
4. Rinse in DI water;
5. Place in Scott's solution for 30 seconds;
6. Rinse in DI water;
7. Wash in 95% alcohol for 1 min;
8. Stain in alcoholic Eosin for 30 seconds;
9. Dehydrate through ascending grades of alcohol and clear to xylene. Mount in a permanent mounting media.

### C.2.2 Regents and Solutions

**Hematoxylin**:Dilute Gill's hematoxylin no.2 (Polysciences #04570) one to one with dH2O before use.

**Acid alcohol**:2ml HCl (Fisher #A144s) in 198 ml of 70% ethanol.

**Eosin**: EM Science #588X

**Scott's solution**: $NaHCO_3$: 2g, $MgSO_4.7H_2O$ : 20g, $dH_2O$ : 1000ml. Mix until dissolved.

**Xylene**:EMD#XX0060-4

## *C.3 Hoematoxylin counterstaining*

### C.3.1 Procedure

1. Hematoxylin for 10 seconds.
2. Rinse in tap water until clear.
3. Dip once in 1% acid alcohol.
4. Rinse in water.
5. Scott's solution for 20 seconds.
6. Rinse in water.
7. Dehydrate through graded alcohols then xylene.
8. Coverslip.

#### *C.3.1.1 Regents and solutions*

**Hematoxylin**: Dilute Gill's hematoxylin no.2 (Polysciences #04570) one to one with dH2O before use.

**1% Acid Alcohol**: 2ml HCl (Fisher #A144s) in 198 ml of 70% ethanol.

**Scott's Solution**

$NaHCO_3$: 2g, $MgSO_4.7H_2O$ : 20g, $dH_2O$ : 1000ml. Mix until dissolved.

## *C.4 Movat's pentachrome staining*

### C.4.1 Procedure

1. Fixed paraffin embedded tissue sections are deparaffinized (see deparaffinization protocol) and washed in 1X PBS for 5 min;

2. Rinse sections with 3% acetic acid;

3. Incubate sections in alcian blue at 60$^{o}$C for 10 min;

4. Rinse with DI water;

5. Incubate sections in Verhoff solution for 6-7 min;

6. Wash slides with warm tap water for 5 min, optionally dip slides in 2% ferric chloride till it's slightly dark;

7. Incubate sections in plasma stain for 10-15 min;

8. Rinse with DI water;

9. Incubate in polyacid for 10-15 min;

10. Rinse with 1% acetic acid; 11. Dehydrate with absolute ethanol twice;

12. Incubate sections in saffron for 10-15 min;

13. Dehydrate with absolute ethanol once;

14. Keep anhydrous and place in xylene;

15. Clearing and coverslip.

### C.4.2 Regents and solutions

**Alcian blue**: alcian blue (Sigma#101K1465), 100 ml DI water, 3.0 ml glacial acetic acid (Sigma#4K3441);

**Verhoeff**: Stock A (3), Stock B (2) and Stock C (1) mix; Stock A: 3.0g hemaroxylin (Fisher#H345-25) in 100 ml absolute ethanol; Stock B: 2.3g Ferric chloride hexhydrate (ICN Biomedicals#153500) in 100 ml DI water; Stock C: 4.0g potassium iodide (Sigma#20k0240), 2.0 iodine (ICN# 151346) in 100 ml DI water;

**Plasma Stain**: 80 ml 0.1% aqueous biebrich scarlet (ICN#154855), 20 ml 0.1% aqueous acid fuchsin (ICN#152600), 1 ml glacial acetic acid;

**Saffron**: 6.0g Saffron du Gatinais (VWR#3801/12) in 100 ml absolute ethanol, place at 56$^{o}$C for 2 weeks before use; **Polyacid**: 2.0g polyacid (EM#PX1055-4) in 100 ml DI water.

## *C.5 $\alpha$-SM actin immunohistochemistry*

### C.5.1 Procedure

1. Fixed paraffin embedded tissue sections are deparaffinized (see deparaffinization protocol) and washed in 1X PBS for 5 min;

2. Tissue sections are placed in 0.3% $H_2O_2$ for 10 min and washed in 1X DPBS twice for 5 min each;

3. Apply blocking serum, incubate sections in a humid chamber for 30 min, rt;

4. Blot off blocking serum and wash in 1X DPBS twice for 5 min, each;

5. Apply primary antibody, incubate sections in a humid chamber for 1h, rt;

6. Blot off primary antibody and wash in 1X DPBS twice for 5 min, each;

7. Apply secondary antibody, incubate sections in a humid chamber for 30min, rt;

8. Blot off secondary antibody and wash in 1X DPBS twice for 5 min, each;

9. Apply ABC, incubate sections in a humid chamber for 30min, rt;

10. Blot off ABC and wash in 1X DPBS twice for 5 min, each;

11. Apply DAB for 10 min;

12. Counterstaining (see counterstaining protocol) and coverslip.

### C.5.2 Regents and Solutions

**0.3% $H_2O_2$**: 30%$H_2O_2$ (Sigma#H1009) diluted in 1X DPBS;

**Blocking serum** (for 500$\mu$l): 10$\mu$l Normal swine serum (Vector#s-4000), 25$\mu$l Normal horse serum (Vector#s-2000),100$\mu$l avidin complex (Vector#SP-2001 SP-2001),365$\mu$l 1X DPBS;

**Primary antibody** (for 500$\mu$l): 10$\mu$l Normal swine serum (Vector#s-4000), 25$\mu$l Normal horse serum (Vector#s-2000),100$\mu$l biotin complex (Vector#SP-2001),365$\mu$l 1X DPBS, 16.67$\mu$l anti-$\alpha$-SM actin (DAKO#M0851);

**Secondary antibody** (for 500$\mu$l): 10$\mu$l Normal swine serum (Vector#s-4000), 25$\mu$l Normal horse serum (Vector#s-2000),465$\mu$l 1X DPBS;

**ABC**: Vextastain Elite ABC Kit (Vector# PK-6100), 4.9 ml 1X DPBS, 2 drops from bottle A, mix after addition, 2 drops from bottle A, mix. Make 30 min before application;

**DAB**: DAB substrate kit (Vector # SK-4100).

## *C.6 BrdU immunohistochemistry*

Please note: All antibodies and related reagents are temperature sensitive. Please keep at 4 $^{o}$C or on ice at all times. This will maintain the longevity of the reagents and limit antibody or reagent related problems with experiments.

### C.6.1 Procedure

1. Fixed paraffin embedded tissue sections are deparaffinized and washed in 1X PBS for 5 min;

2. Tissue sections are treated with 1g/ml proteinase K for 10 min. at room temp for antigen retrieval;

3. Wash slides in 1X PBS twice for 5 min. each, rt.

4. Immerse slides in 4N HCl for 10 min., rt.

5. Immerse slides in 1X TBE, pH 8.4 for 5 min., rt.

6. Immerse in 1X PBS. Check pH of buffer after 2 minutes. Apply primary antibody once pH is 7.0-7.5.

7. Blot off PBS and apply 150$\mu$l of primary antibody. Incubate sections in a humid chamber for 1h, rt.

8. Blot of excess antibody and wash slides in 1X PBS twice for 5 min. each, rt.

9. Apply 150$\mu$l of secondary antibody and incubate 30 min., rt in a humid chamber.

10. Blot off excess antibody and wash slides in 1X PBS twice for 5 min. each, rt.

11. Apply 150$\mu$l of prepared ABC mixture to each slide. Incubate in a humid chamber 1h, rt.

12. Blot off excess solution and wash slides in 1X PBS twice for 5 min. each, followed by one wash in 100mM tris pH 8.2 for 5 min.

13. Mix and apply substrate 2-3 drops per section. Incubate slides in the dark for 20-30 min., checking color reaction periodically. Stop reaction by blotting off substrate and rinsing in tap water twice for 5 min. each.

14. Hematoxylin counterstaining (see counterstaining protocol) and coverslip.

### C.6.2 Reagents and Solutions

**Anti-BrdU**: DAKO #M0744 Clone Bu20a

**Proteinase K**: Dissolve proteinase K (Sigma # P-4914) in dH2O for a stock concentration of 20mg/ml. Aliquot and store at -20$^{o}$C.

**10X PBS** (Boehringer Mannheim #1666789)

**1%BSA/PBS** - 1g fraction V BSA (Sigma #A2153) in 100ml 1X PBS. Mix until fully dissolved. Aliquot into 5ml volumes and store at -20$^{o}$C.

**Secondary antibody** : Prepare working dilution of the secondary antibody (Vector #BA2001: biotinylated horse anti-mouse IgG) in 1% BSA/PBS and add 2% normal horse serum. Prepare the secondary antibody at a 1/400 dilution.

**Alkaline Phosphatase Standard ABC Kit**: Prepare the working dilution of ABC-Vector Red complex from the alkaline phosphatase standard kit (Vector #AK-5000) after application of secondary antibody. Mix 5ml of 1X PBS, one drop of reagent A, and one drop of reagent B and allow to sit at rt, 30 min prior to use.

**Alkaline Phosphatase Substrate Kit I**: Make up alkaline phosphatase substrate solution (Vector #SK-5100) immediately before use. Add 5ml of 100mM tris pH 8.2, one drop levamisole (Vector #SP-5000), two drops each of reagent one, two, and three to a foil wrapped bottle.

## *C.7 MMP-2, -9 immunohistochemistry*

### C.7.1 Procedure

1. Fixed paraffin embedded tissue is deparaffinized, and rehydrated in descending grades of alcohol;

2. Sections are washed in 1X PBS 5 min;

3. Block endogenous peroxidase using 0.3% H2O2 in methanol (or PBS) for 30 min at rt;

4. Rehydrate in 1X PBS twice for 5 min. each, rt.

5. Prepare the working dilution of primary antibody in PBS/10% horse serum (50ml 1st Ab + 850ml PBS + 100ml horse serum). Incubate sections in a humid chamber for 1h, rt.

6. Blot off excess antibody and wash slides in 1X PBS twice for 5 min. each, rt.

7. Prepare working dilution of the biotinylated secondary antibody in 1X PBS, and add 2% of normal serum from the source animal of the secondary antibody. Apply and incubate 30 min., rt. in a humid chamber.

8. Blot off excess antibody and wash slides in 1X PBS twice for 5 min. each, rt.

9. Apply prepared ABC mixture to each slide. Incubate in a humid chamber 1h, rt.

10. Blot off excess solution and wash slides in 1X PBS twice for 5 min. each for 5 min.

11. Incubate tissue sections with the substrate (DAB) room temperature until suitable staining develops.

12. Wash the sections for 5 min in water.

11. Lightly counterstain sections with hematoxylin.

### C.7.2 Reagents and solutions

**PBS**: Sigma # D-5652

**MMP-9 monocolonal**: EMD science # IM37L

**MMP-2 monoclonal** : EMD science # IM 33L

**100 mM Tris**: pH8.2 Tris, Sigma # T-6066

**ABC kit**: Vector laboratories, PK 6100

**Peroxidase Substrate kit**: Vector laboratories, SK-4100

## *C.8 Sircol Collagen assay*

### C.8.1 Procedure

1. Digest tissue in pepsin-acetic acid (0.5 M) for overnight at rt, stir vigorously during this period, pepsin: tissue (wet weight) ratio of 1:10;

2. Prepare regent blanks (100$\mu$l 0.5 M acetic acid), collagen standard (aliquots containing 5,10, 25, 50 $\mu$g) and test samples (10-100$\mu$l); adjust the contents of all tubes to 100$\mu$l with 0.5 M acetic acid;

3. Add 1 ml Sircol Dye reagent and cap all tubes, mix;

4. Place tubes on a mechanical shaker for 30 min;

5. Transfer tubes to a micro centrifuge and spin at $>$ 10,000 xg for 10 min;

6. Invert the tubes to drain the unbound dye;

7. Add 1 ml alkali reagent and mix;

8. Transfer 200 $\mu$l aliquots of samples from tubes to a 96-well multi-well plate;

9. Place the plate in a microplate reader, set using a blue-green filter, read the absorbance at 540 nm.

### C.8.2 Regents and solutions

**Pepsin**(Sigma#P-6887): dissolve in 0.5 M acetic acid;

**Collagen standard**: Biocolor # S1010, sterile bovine acid-soluble type I collagen;

**Sircol Dye**: Biocolor# S1005 ;

**Alkili reagent**: Biocolor#S0500.

## *C.9 Blyscan sGAG assay*

### C.9.1 Procedure

1. Digest tissue in pronase for overnight at 37$^o$C, stir vigorously during this period, pepsin: tissue (wet weight) ratio of 1:10;

2. Prepare regent blanks (100$\mu$l DI water), GAG standard (aliquots containing 1.0,2.0,3.0,4.0,5.0 $\mu$g) and test samples (10-100$\mu$l); adjust the contents of all tubes to 100$\mu$l with DI water; 3. Add 1 ml Blyscan Dye reagent and cap all tubes, mix;

4. Place tubes on a mechanical shaker for 30 min;

5. Transfer tubes to a micro centrifuge and spin at $>$ 10,000 xg for 10 min;

6. Invert the tubes to drain the unbound dye;

7. Add 1 ml dissociation reagent and mix;

8. Transfer 200 $\mu$l aliquots of samples from tubes to a 96-well multi-well plate;

9. Place the plate in a microplate reader, set using a red filter, read the absorbance at 656 nm.

#### *C.9.1.1 Reagents and solutions*

**Pronase**: Sigma #P6911

**Blyscan sGAG kit**: Biocolor, containing GAG standard (B1010), Blyscan dye (B1005), and dissociation reagents (B0500).

## *C.10 Sample preparation for Scanning Electron Microscopy*

### C.10.1 Procedure

1. Harvest tissue and rinse briefly in 0.2M sodium cacodylate buffer, pH 7.2;

2. Fix tissue in 2.5% glutaraldehyde in cacodylate buffer, pH 7.2 for 1-2 hours. Dilute the stock of 8% glutaraldehyde using 0.2M cacodylate buffer, pH 7.2 immediately before use;

3. Rinse in 0.2M cacodylate buffer, pH 7.2, 3 x 10 minutes;

4. Dehydrate tissue sample using the following schedule, each for 0.5-1 hour: 25% alcohol, 50%, 70%, 90% x 2, 100% x 2;

5. In place of critical point drying, dry the sample using hexamethyldisilazane. Use one of the following schedules (if the sample is of animal origin, use schedule a or b):

Ratio 100% ethanol:HMDS starting from 100% ethanol going to 100% HMDS, each step for 30 min:

a).100% Ethanol =>2:1, 1:1, 1:2 => 100% HMDS

b).100% Ethanol =>3:1, 1:1, 1:3 => 100% HMDS

6. Rinse in 3 changes of 100% HMDS;

7. Dry from the last 100% HMDS. The level of HMDS should just cover the tissue sample. Leave the tube containing the sample open in the fume hood and allow the HMDS to evaporate and thus dry the tissue. Depending on sample size, drying should occur overnight;

8. Adhere the sample to an aluminum stub using conductive, double sided carbon adhesive tape;

9. Sputter-coat the sample using gold to a thickness of approx. 100 Angstroms. Desiccate sample until ready to analyze (in MSE lab);

10. Keep tissue in desiccators (vacuum oven) before viewing under microscope.

### C.10.2 Reagents and supplies

**8% Glutaraldehyde**: Electron Microscopy Sciences #16019

**16% Paraformaldehyde**: Electron Microscopy Sciences #15710

**0.2M cacodylate buffer**, pH 7.4: Electron Microscopy Sciences # 11652

**Hexamethyldisilazane**: Electron Microscopy Sciences #16700

**Aluminum stubs** for the Hitachi S-800: SPI #01506-BA (table dia.12.7mm, pin dia. 3.2mm, pin

length 8.0mm)

**Conductive, double sided carbon adhesive tape**: SPI #05081-AB (6 mm x 20 feet)

# APPENDIX D

# ORIGINAL DATA

## *D.1 Constant static pressure: scintillation counting (cpm)*

| | duplicate 1 | duplicate 2 | vial | vial+tissue | dw (mg) | ave(cpm) | normalized (cpm/mg) | |
|---|---|---|---|---|---|---|---|---|
| C1 | 159794 | 190947 | 1512.4 | 1525 | 12.6 | 175370.5 | 13918.29365 | |
| C2 | 182599.5 | 170423.5 | 1515.5 | 1536.7 | 21.2 | 176511.5 | 8326.014151 | |
| C3 | 154025.5 | 159948 | 1517.7 | 1527.2 | 9.5 | 156986.8 | 16524.92105 | |
| C4 | 137829 | 142812 | 1524.2 | 1533.6 | 9.4 | 140320.5 | 14927.71277 | |
| C5 | 234327 | 190803 | 1506.2 | 1519.2 | 13 | 212565 | 16351.15385 | |
| C6 | 190897 | 217380.5 | 1505.1 | 1524.3 | 19.2 | 204138.8 | 10632.22656 | |
| C7 | 52607 | 51287 | 1528.81 | 1532.7 | 3.89 | 51947 | 13353.98458 | |
| C8 | 27826 | 26760.5 | 1542.49 | 1547.9 | 5.41 | 27293.25 | 5044.963031 | |
| C9 | 108846 | 92248.5 | 1532.23 | 1537.3 | 5.07 | 100547.3 | 19831.80473 | |
| C10 | 80557 | 78297.5 | 1517.67 | 1525.9 | 8.23 | 79427.25 | 9650.941677 | |
| C11 | 55184 | 51041.5 | 1517.9 | 1523.8 | 5.9 | 53112.75 | 9002.161017 | |
| C12 | 54775 | 51993.5 | 1525.59 | 1530.5 | 4.91 | 53384.25 | 10872.55601 | |
| P1 | 301299.5 | 217838.5 | 1522.1 | 1535.1 | 13 | 259569 | 19966.84615 | |
| P2 | 242110 | 256744.5 | 1529 | 1550 | 21 | 249427.3 | 11877.4881 | |
| P3 | 170729 | 182492 | 1517 | 1532.6 | 15.6 | 176610.5 | 11321.1859 | |
| P4 | 183949 | 186379.5 | 1506.7 | 1516.3 | 9.6 | 185164.3 | 19287.94271 | |
| P5 | 177672.5 | 179510 | 1523.2 | 1541.3 | 18.1 | 178591.3 | 9866.91989 | |
| P6 | 230172.5 | 250470 | 1506 | 1534.7 | 28.7 | 240321.3 | 8373.562718 | |
| P7 | 58505 | 55598.5 | 1532.91 | 1537.2 | 4.29 | 57051.75 | 28565.705 | |
| P8 | 35645.5 | 27601.5 | 1514.05 | 1518.4 | 4.35 | 31623.5 | 14557.775 | |
| P9 | 50167.5 | 43917 | 1527.78 | 1534.9 | 7.12 | 47042.25 | 22722.39 | |
| P10 | 80769.5 | 66586 | 1515.49 | 1522.2 | 6.71 | 73677.75 | 34050.745 | |
| P11 | 97451 | 82426.5 | 1536.23 | 1542.5 | 6.27 | 89938.75 | 41981.365 | |
| P12 | 101334.5 | 98738 | 1520.02 | 1526 | 5.98 | 100036.3 | 50129.01 | |

**Figure 81:** Collagen synthesis in scintillation counting (cpm), constant static pressure, 100 mmHg

| constant, 100 dna (cpm1), sGAG (cpm2) | | | | | |
|---|---|---|---|---|---|
| sample | cpm1 | cpm2 | dw(mg) | normalized cpm1 | normalized cpm2 |
| P1 | 37421.82 | 58610.91 | 2.70 | 90089. 57 | 21707. 74 |
| P2 | 44760.00 | 71742.22 | 2.50 | 116376. 00 | 28696. 89 |
| P3 | 48471.11 | 77044.44 | 2.60 | 121177. 78 | 29632. 48 |
| P4 | 53715.55 | 71591.11 | 4.20 | 83131. 21 | 17045. 50 |
| P5 | 42352.73 | 66072.73 | 2.20 | 125133. 07 | 30033. 06 |
| P6 | 46853.33 | 75328.88 | 2.50 | 121818. 66 | 30131. 55 |
| P7 | 41709.09 | 66443.63 | 2.80 | 96824. 67 | 23729. 87 |
| P8 | 70346.66 | 104913.33 | 4.30 | 106337. 97 | 24398. 45 |
| C1 | 71388.57 | 81262.85 | 2.50 | 185610. 28 | 32505. 14 |
| C2 | 63440.00 | 79531.42 | 3.70 | 111448. 65 | 21494. 98 |
| C3 | 36396.92 | 49227.69 | 1.20 | 197149. 98 | 41023. 08 |
| C4 | 47373.33 | 59053.33 | 1. 60 | 192454. 15 | 36908. 33 |
| C5 | 54217.78 | 70206.66 | 2.50 | 140966. 23 | 28082. 66 |
| C6 | 41807.27 | 55069.09 | 2.20 | 123521. 48 | 25031. 40 |
| C7 | 32800.00 | 51556.92 | 2.00 | 106600. 00 | 25778. 46 |
| C8 | 69171.42 | 101394.28 | 3.50 | 128461. 21 | 28969. 79 |

**Figure 82:** DNA and sGAG synthesis in scintillation counting (cpm),constant static pressure 100mmHg

## *D.2 Cyclic pressure-magnitude effects: scintillation counting (cpm)*

| constant static, 140, collagen | | | | | |
|---|---|---|---|---|---|
| sample | cpm (a) | cpm (b) | dw (mg) | cpm(ave) | normalized |
| C11 | 104186 | 115895.5 | 10.42 | 110040.75 | 10560.53263 |
| C12 | 65469.5 | 73100 | 11.33 | 69284.75 | 6115.15887 |
| C13 | 179043 | 145180.5 | 12.63 | 162111.75 | 12835.45131 |
| C21 | 91419.5 | 87564 | 8.45 | 89491.75 | 10590.73964 |
| C22 | 69185.5 | 76244.5 | 7.58 | 72715 | 9593.007916 |
| C23 | 133214 | 153657.5 | 13.82 | 143435.75 | 10378.85311 |
| C31 | 114513.5 | 123056 | 11.32 | 118784.75 | 10493.35247 |
| C32 | contaminated | | | | |
| C33 | contaminated | | | | |
| P11 | 166012.5 | 189167 | 13.29 | 177589.75 | 13362.65989 |
| P12 | 97029 | 109252.5 | 8.73 | 103140.75 | 11814.5189 |
| P13 | 107670.5 | 124742.5 | 19.39 | 116206.5 | 5993.115008 |
| P21 | 109597.5 | 124086.5 | 6.86 | 116842 | 17032.36152 |
| P22 | 152550.5 | 169156 | 12.44 | 160853.25 | 12930.32556 |
| P23 | 121604.5 | 135243 | 16.48 | 128423.75 | 7792.703277 |
| P31 | 216450 | 240121.5 | 12.98 | 228285.75 | 17587.5 |
| P32 | 174102 | 198031 | 10.48 | 186066.5 | 17754.43702 |
| P33 | 145687.5 | 171758 | 19.38 | 158722.75 | 8190.02838 |

**Figure 83:** Collagen synthesis in scintillation counting (cpm), constant static pressure, 140 mmHg

| constant, 140, dna (cpm1), sGAG (cpm2) | | | | | |
|---|---|---|---|---|---|
| sample | cpm1(ave) | cpm2(ave) | dw(mg) | normalized cpm1 | normalized cpm2 |
| P1 | 27525.92 | 39318.42 | 3.50 | 39322.74286 | 11233.83429 |
| P2 | 16901.29 | 19887.9 | 4.10 | 20611.32927 | 4850.707317 |
| P3 | 52396.22 | 56293.56 | 5.10 | 51368.84314 | 11037.95294 |
| P4 | 75334.28 | 76882.85 | 5.70 | 66082.70175 | 13488.2193 |
| P5 | 38814.55 | 48932.73 | 4.90 | 39606.68367 | 9986.271429 |
| P6 | 29045.98 | 35633.03 | 3.10 | 46848.35484 | 11494.52581 |
| P7 | 23572.63 | 22703.16 | 6.70 | 17591.51493 | 3388.531343 |
| P8 | 18959.13 | 18585.22 | 4.40 | 21544.46591 | 4223.913636 |
| C1 | 48180 | 49788.89 | 3.50 | 68828.57143 | 14225.39714 |
| C2 | 44718.18 | 61608.89 | 6.00 | 37265.15 | 10268.14833 |
| C3 | 108628 | 85460 | 4.20 | 129319.0476 | 20347.61905 |
| C4 | 90825.71 | 65971.43 | 4.90 | 92679.29592 | 13463.55714 |
| C5 | 45632.73 | 42943.64 | 3.40 | 67106.95588 | 12630.48235 |
| C6 | 51609.09 | 41054.55 | 3.40 | 75895.72059 | 12074.86765 |
| C7 | 22603.48 | 17815.65 | 7.40 | 15272.62162 | 2407.52027 |
| C8 | 26001.81 | 21987.31 | 8.00 | 16251.13125 | 2748.41375 |

**Figure 84:** DNA and sGAG synthesis in scintillation counting (cpm),constant static pressure, 140mmHg

| constant static, 170, collagen | | | | | |
|---|---|---|---|---|---|
| sample | dw (mg) | cpm(a) | cpm(b) | cpm(ave) | normalized |
| C1 | 9.28 | 38503.5 | 34556 | 36529.75 | 19681.97737 |
| C2 | 7.63 | 149155.5 | 134513 | 141834.25 | 92945.11796 |
| C3 | 9.42 | 148577 | 132741.5 | 140659.25 | 74659.89915 |
| C4 | 10.87 | 48405.5 | 43189.5 | 45797.5 | 21066.00736 |
| C5 | 11.72 | 121073 | 103757.5 | 112415.25 | 47958.7244 |
| C6 | 9.62 | 174166 | 156700 | 165433 | 85983.88773 |
| P1 | 4.08 | 106025 | 115945.5 | 110985.25 | 136011.3358 |
| P2 | 2.64 | 39988 | 44198 | 42093 | 79721.59091 |
| P3 | 8.58 | 52860 | 57357 | 55108.5 | 32114.51049 |
| P4 | 8.08 | 10739.5 | 12153 | 11446.25 | 7083.075495 |
| P5 | 6.42 | 187074.5 | 205412.5 | 196243.5 | 152837.6168 |
| P6 | 5.43 | 95885 | 103227 | 99556 | 91672.19153 |

**Figure 85:** Collagen synthesis in scintillation counting (cpm), constant static pressure, 170 mmHg

| constanr static, 170, dna (cpm1), sGAG (cpm2) | | | | | |
|---|---|---|---|---|---|
| sample | cpm1 | cpm2 | dw (mg) | normalized cpm1 | normalized cpm2 |
| P1 | 42225.45 | 58189.09 | 12.8 | 16494.31641 | 4546.022656 |
| P2 | 47555.55 | 66555.55 | 13.9 | 17106.31295 | 4788.169065 |
| P3 | 24832.94 | 35950.59 | 11.6 | 10703.85345 | 3099.188793 |
| P4 | 56444.44 | 74031.11 | 12.7 | 22222.22047 | 5829.22126 |
| P5 | 49404.44 | 68448.88 | 13.6 | 18163.39706 | 5033.005882 |
| P6 | 43516.36 | 55356.36 | 13.8 | 15766.7971 | 4011.330435 |
| P7 | 63948.57 | 75737.14 | 13.5 | 23684.65556 | 5610.158519 |
| P8 | 46426.66 | 60715.55 | 14.7 | 15791.38095 | 4130.309524 |
| C1 | 32698.46 | 41289.23 | 13.5 | 12110.54074 | 3058.461481 |
| C2 | 47915.55 | 56408.89 | 12.4 | 19320.78629 | 4549.104032 |
| C3 | 36347.69 | 45520.00 | 12.3 | 14775.48374 | 3700.813008 |
| C4 | 39945.45 | 44181.82 | 10 | 19972.725 | 4418.182 |
| C5 | 51425.00 | 58845.00 | 14.1 | 18235.8156 | 4173.404255 |
| C6 | 57244.44 | 66604.45 | 14.1 | 20299.44681 | 4723.719858 |
| C7 | 46093.33 | 63933.33 | 13 | 17728.20385 | 4917.948462 |
| C8 | 53195.55 | 71506.66 | 14.5 | 18343.2931 | 4931.493793 |

**Figure 86:** DNA and sGAG synthesis in scintillation counting (cpm),constant static pressure 170mmHg

| Cyclic pressure, 1.167 Hz, 140 mmHg,collagen synthesis | | | | | |
|---|---|---|---|---|---|
| sample | dw (mg) | cpm(a) | cpm(b) | cpm(ave) | normalized |
| c11 | 9.28 | 38503.5 | 34556 | 36529.75 | 19681.98 |
| c12 | 7.63 | 149155.5 | 134513 | 141834.3 | 92945.12 |
| c13 | 9.42 | 148577 | 132741.5 | 140659.3 | 74659.9 |
| c21 | 10.87 | 48405.5 | 43189.5 | 45797.5 | 21066.01 |
| c22 | 11.72 | 121073 | 103757.5 | 112415.3 | 47958.72 |
| c23 | 9.62 | 174166 | 156700 | 165433 | 85983.89 |
| p11 | 4.08 | 106025 | 115945.5 | 110985.3 | 136011.3 |
| p12 | 2.64 | 39988 | 44198 | 42093 | 79721.59 |
| p13 | 8.58 | 52860 | 57357 | 55108.5 | 32114.51 |
| p21 | 8.08 | 10739.5 | 12153 | 11446.25 | 7083.075 |
| p22 | 6.42 | 187074.5 | 205412.5 | 196243.5 | 152837.6 |
| p23 | 5.43 | 95885 | 103227 | 99556 | 91672.19 |

**Figure 87:** Collagen synthesis in scintillation counting (cpm), cyclic pressure: 1.167 Hz, 120-160 mmHg

## *D.3 Cyclic pressure-frequency effects: scintillation counting (cpm)*

| Cyclic pressure, 140, 1.167 Hz , dna (cpm1), sGAG (cpm2) | | | | | |
|---|---|---|---|---|---|
| sample | dw (mg) | cpm1(ave) | cpm2(ave) | normalized cpm1 | normalized cpm2 |
| C1 | 3.8 | 116845.8 | 32969.485 | 153744.4211 | 43380.90 |
| C2 | 4 | 82766.17 | 10368.02 | 103457.7125 | 12960.03 |
| C3 | 6.6 | 83227.37 | 19995.505 | 63051.03409 | 15148.11 |
| C4 | 2.5 | 71091.58 | 20452.38 | 142183.16 | 40904.76 |
| C5 | 3.3 | 42407.74 | 23119.75 | 64254.15152 | 35029.92 |
| C6 | 2.7 | 55396.47 | 25550.585 | 102586.0556 | 47315.90 |
| C7 | 1.8 | 262991.1 | 55010 | 730530.7222 | 152805.56 |
| C8 | 4.3 | 429428.5 | 65377.135 | 499335.5 | 76019.92 |
| P1 | 3.8 | 97609.31 | 7386.61 | 128433.3026 | 9719.22 |
| P2 | 6.3 | 230798.7 | 32608.33 | 183173.5437 | 25879.63 |
| P3 | 4.7 | 183373 | 13911.215 | 195077.7021 | 14799.16 |
| P4 | 3.7 | 98604.53 | 18235.905 | 133249.3581 | 24643.11 |
| P5 | 2.9 | 74276.19 | 12913.695 | 128062.3879 | 22264.99 |
| P6 | 3.1 | 93894.33 | 13705.57 | 151442.4597 | 22105.76 |
| P7 | 3 | 132091.9 | 17151.825 | 220153.1667 | 28586.38 |
| P8 | 4.6 | 221316.8 | 31480 | 240561.7011 | 34217.39 |

**Figure 88:** DNA and sGAG synthesis in scintillation counting (cpm),cyclic pressure: 1.167 Hz, 120-160 mmHg

| Cyclic pressure, 1.167 Hz, 170 mmHg,collagen synthesis | | | | | |
|---|---|---|---|---|---|
| sample | dw (mg) | cpm(a) | cpm(b) | cpm(ave) | normalized |
| c11 | 19.54 | 157554.5 | 187990 | 172772.3 | 8841.978 |
| c12 | 7.4 | 166217.5 | 185308.5 | 175763 | 23751.76 |
| c13 | 12.59 | 160598.5 | 170273 | 165435.8 | 13140.25 |
| c21 | 10.92 | 102052 | 115663.5 | 108857.8 | 9968.658 |
| c22 | 17.11 | 172424 | 185098.5 | 178761.3 | 10447.76 |
| c23 | 17.45 | 131944 | 142276 | 137110 | 7857.307 |
| p11 | 20.81 | 275001 | 289944 | 282472.5 | 13573.88 |
| p12 | 7.85 | 232247.5 | 259663 | 245955.3 | 31331.88 |
| p21 | 12.39 | 267512 | 306977 | 287244.5 | 23183.58 |
| p22 | 7.17 | 294600.5 | 331571 | 313085.8 | 43666.07 |
| p23 | 10.89 | 236250 | 253595.5 | 244922.8 | 22490.61 |

**Figure 89:** Collagen synthesis in scintillation counting (cpm),cyclic pressure: 1.167 Hz, 150-190 mmHg

| Cyclic pressure, 170, 1.167 Hz , dna (cpm1), sGAG (cpm2) | | | | | |
|---|---|---|---|---|---|
| sample | dw (mg) | cpm1(ave) | cpm2(ave) | normalized cpm1 | normalized cpm2 |
| C-1 | 3.6 | 85240 | 9428.75 | 118388.8889 | 13095.49 |
| C-2 | 2.4 | 75952.5 | 9380 | 158234.375 | 19541.67 |
| C-3 | 4.7 | 273151.6 | 65167.75 | 290586.8085 | 69327.39 |
| C-4 | 2.9 | 47487.5 | 5585 | 81875 | 9629.31 |
| C-5 | 5.2 | 37089.08 | 42280 | 35662.57212 | 40653.85 |
| C-6 | 2.5 | 23817.5 | 27625 | 47635 | 55250.00 |
| C-7 | 2.7 | 265447.2 | 4896.25 | 491568.9444 | 9067.13 |
| C-8 | 4 | 44874.7 | 44743.18 | 56093.375 | 55928.98 |
| P1 | 4.3 | 246227 | 66224.15 | 286310.4419 | 77004.83 |
| P2 | 4.1 | 368582.7 | 76367.85 | 449491.0732 | 93131.52 |
| P3 | 6.3 | 310630.2 | 80754.23 | 246531.9286 | 64090.66 |
| P4 | 3.4 | 40707.58 | 43574.4 | 59864.08088 | 64080.00 |
| P5 | 2.8 | 30978.33 | 37320.5 | 55318.4375 | 66643.75 |
| P6 | 1.8 | 32693.13 | 39856.1 | 90814.23611 | 110711.39 |
| P7 | 1.4 | 27451.08 | 16128.08 | 98039.55357 | 57600.29 |
| P8 | 4 | 54256.1 | 47208.3 | 67820.125 | 59010.38 |

**Figure 90:** DNA and sGAG synthesis in scintillation counting (cpm), cyclic pressure: 1.167 Hz, 150-190 mmHg

| Cyclic pressure, 0.5 hz, 100 mmHg, collagen(cpm1), sGAG (cpm2) | | | | | |
|---|---|---|---|---|---|
| | dw (mg) | cpm1 (ave) | cpm2(ave) | normalized cpm1 | normalized cpm2 |
| C1 | 4.7 | 273054.4 | 20592.34 | 290483.4468 | 21906.74 |
| C2 | 4 | 243667 | 17964.35 | 304583.7 | 22455.44 |
| C3 | 5.1 | 222495.9 | 16838.4 | 218133.2059 | 16508.24 |
| C4 | 4.3 | 289999.1 | 23233.81 | 337208.2093 | 27016.06 |
| C5 | 5.5 | 305443.5 | 27526.83 | 277675.9364 | 25024.39 |
| C6 | 5.5 | 313888.7 | 24119.48 | 285353.3364 | 21926.80 |
| C7 | 3.8 | 216466.8 | 17340.32 | 284824.7105 | 22816.21 |
| C8 | 6.2 | 291733 | 27449.09 | 235268.5484 | 22136.36 |
| C9 | 5.8 | 317554.7 | 28381.33 | 273754.0259 | 24466.66 |
| C10 | 3.8 | 206742.2 | 15408.15 | 272029.2368 | 20273.88 |
| C11 | 3.5 | 220683.7 | 15679.26 | 315262.4429 | 22398.94 |
| C12 | 3.4 | 170184.9 | 14163.87 | 250271.8529 | 20829.22 |
| P1 | 4.6 | 329053.8 | 18121.64 | 357667.1413 | 19697.43 |
| P2 | 3.6 | 248153.6 | 15019.16 | 344657.7361 | 20859.94 |
| P3 | 4.2 | 341343.5 | 17695.97 | 406361.3333 | 21066.63 |
| P4 | 5.6 | 362604.1 | 29845.54 | 323753.6607 | 26647.80 |
| P5 | 5.6 | 327876.6 | 26316.84 | 292746.9464 | 23497.18 |
| P6 | 4.8 | 340916.4 | 23944.31 | 355121.2396 | 24941.99 |
| P7 | 4.2 | 320315.3 | 25731.77 | 381327.7262 | 30633.06 |
| P8 | 5.8 | 316536 | 27921.33 | 272875.8621 | 24070.11 |
| P9 | 5.9 | 415934.7 | 36171.06 | 352487.0254 | 30653.44 |
| P10 | 3.1 | 250652.8 | 15308.92 | 404278.629 | 24691.81 |
| P11 | 3.4 | 242683.8 | 16868.86 | 356887.9706 | 24807.15 |
| P12 | 2.7 | 200054.9 | 11693.01 | 370472.0185 | 21653.72 |

**Figure 91:** Collagen and sGAG synthesis in scintillation counting (cpm), cyclic pressure: 0.5 Hz, 80-120 mmHg

## *D.4 Shear stress-intact leaflets*

| Cyclic pressure, 0.5 hz, 100 mmHg, dna(cpm1), sGAG (cpm2) | | | | | |
|---|---|---|---|---|---|
| sample | dw (mg) | cpm1 (ave) | cpm1(ave) | normalized cpm1 | normalized cpm2 |
| C1 | 4 | 151860 | 22636.84 | 189824.9875 | 28296.05 |
| C2 | 5.2 | 122089.6 | 18210.44 | 117393.8173 | 17510.03 |
| C3 | 4.8 | 109149 | 16362.46 | 113696.8542 | 17044.23 |
| C4 | 4.2 | 145552 | 21406.77 | 173276.1786 | 25484.24 |
| C5 | 6.4 | 142395.3 | 27806.92 | 111246.2891 | 21724.15 |
| C6 | 3.6 | 108024 | 16644.36 | 150033.3333 | 23117.16 |
| C7 | 4.9 | 167578.7 | 27785.33 | 170998.6429 | 28352.38 |
| C8 | 4.2 | 132964.6 | 22633.21 | 158291.2262 | 26944.30 |
| P1 | 3.3 | 173354.9 | 21223.18 | 262658.9697 | 32156.33 |
| P2 | 3.3 | 139166.1 | 16016.09 | 210857.6818 | 24266.80 |
| P3 | 4.4 | 118240.7 | 24159.67 | 134364.3864 | 27454.17 |
| P4 | 3.5 | 106995.8 | 21418.5 | 152851.1286 | 30597.85 |
| P5 | 4 | 165331.2 | 32325.64 | 206663.975 | 40407.05 |
| P6 | 5.3 | 94150.5 | 21131.63 | 88821.22642 | 19935.50 |
| P7 | 4 | 152097.6 | 27504.94 | 190121.9625 | 34381.18 |
| P8 | 6.1 | 158195.4 | 33584.61 | 129668.3443 | 27528.37 |

**Figure 92:** DNA and sGAG synthesis in scintillation counting (cpm),cyclic pressure: 0.5 Hz, 80-120 mmHg

| Cyclic pressure, 2 hz, 100 mmHg, dna(cpm1), sGAG (cpm2) | | | | | |
|---|---|---|---|---|---|
| sample | dw (mg) | cpm1 (ave) | cpm2 (ave) | normalized cpm1 | normalized cpm2 |
| C1 | 6.9 | 30471.39 | 32290.67 | 33121.07609 | 35098.54891 |
| C2 | 3.4 | 18674.66 | 20155.03 | 41194.10294 | 44459.625 |
| C3 | 3.5 | 18831.43 | 18248.73 | 40353.06429 | 39104.41071 |
| C4 | 5.6 | 25715.23 | 22936.84 | 34440.04018 | 30718.98214 |
| C5 | 4.5 | 22420.39 | 17855.38 | 37367.31667 | 29758.95833 |
| C6 | 5.6 | 31815.8 | 40016.41 | 42610.44643 | 53593.40625 |
| C7 | 4 | 23344.41 | 21546.52 | 43770.76875 | 40399.71563 |
| C8 | 4.2 | 23741.05 | 22103.04 | 42394.73214 | 39469.71429 |
| P1 | 6 | 74720 | 34263.08 | 93400 | 42828.84375 |
| P2 | 3.5 | 51752.77 | 20227.37 | 110898.7929 | 43344.36429 |
| P3 | 3 | 40145.97 | 19327.7 | 100364.925 | 48319.25 |
| P4 | 3.3 | 49483.16 | 22222.11 | 112461.7273 | 50504.78409 |
| P5 | 3.6 | 32071.8 | 18835.78 | 66816.25 | 39241.20833 |
| P6 | 5.9 | 70699.18 | 30784.72 | 89871.83898 | 39133.11864 |
| P7 | 4.7 | 33447.3 | 23411.77 | 53373.35106 | 37359.19947 |
| P8 | 4.4 | 25526.12 | 22121.11 | 43510.43182 | 37706.42898 |

**Figure 93:** DNA and sGAG synthesis in scintillation counting (cpm), cyclic pressure: 2 Hz, 80-120 mmHg

| | Cyclic pressure, 2 hz, 170 mmHg, collagen(cpm1), sGAG (cpm2) | | | | |
|---|---|---|---|---|---|
| sample | dw(mg) | cpm1-ave | cpm2-ave | normalized cpm1 | normalized cpm2 |
| C-1 | 6.80 | 191320.2 | 39867.54 | 211014.8713 | 43971.54596 |
| C-2 | 5.40 | 188940.6 | 38381.85 | 262417.5139 | 53308.11806 |
| C-3 | 6.20 | 192142.2 | 41915.55 | 232430.1048 | 50704.29435 |
| C-4 | 6.10 | 212865.3 | 40419.46 | 261719.6066 | 49696.05123 |
| C-5 | 4.90 | 181050.5 | 34730.64 | 277118.1276 | 53159.1352 |
| C-6 | 3.70 | 153005.6 | 27512.31 | 310146.4257 | 55768.18581 |
| C-7 | 4.40 | 187576.9 | 33820 | 319733.3864 | 57647.71875 |
| C-8 | 4.10 | 138164.1 | 27450.7 | 252739.1707 | 50214.69512 |
| P-1 | 5.10 | 234196.6 | 42671.27 | 344406.6912 | 62751.86765 |
| P-2 | 3.70 | 155222.2 | 23887 | 314639.5338 | 48419.58446 |
| P-3 | 3.00 | 175926.4 | 31306.67 | 439815.975 | 78266.6625 |
| P-4 | 5.70 | 345939.5 | 74066.66 | 455183.5526 | 97456.13158 |
| P-5 | 3.20 | 208776.9 | 32500 | 489320.9063 | 76171.86328 |
| P-6 | 3.40 | 230995.7 | 30655.34 | 509549.3824 | 67622.0625 |
| P-7 | 4.90 | 375190 | 66675.24 | 574270.3929 | 102053.9311 |
| P-8 | 4.10 | 315685 | 54167.5 | 577472.561 | 99086.89024 |

**Figure 94:** Collagen and sGAG synthesis in scintillation counting (cpm),cyclic pressure: 2 Hz, 150-190 mmHg

| Intact leaflets, 1 dyne/cm2 | | | Collagen synthesis | | | sGAG content | |
|---|---|---|---|---|---|---|---|
| | | Shear | Control | Ratio | Shear | Control | Ratio |
| | sample1 | 51.17966 | 60.18494 | 0.850373 | 38.45723 | 27.77159 | 1.384769 |
| | sample2 | 23.20532 | 24.25696 | 0.956646 | 42.87875 | 25.50202 | 1.681386 |
| | sample3 | 36.46382 | 87.76736 | 0.41546 | 20.14756 | 31.83357 | 0.632903 |
| | sample4 | 55.10118 | 43.79963 | 1.258028 | 27.6512 | 27.74547 | 0.996602 |
| | sample5 | 60.40913 | 29.45818 | 2.050674 | 28.28686 | 22.66536 | 1.248022 |
| | sample6 | 37.03323 | 37.80841 | 0.979497 | 22.71141 | N/A | N/A |
| | sample7 | 14.69069 | 17.85845 | 0.822618 | N/A | N/A | N/A |
| | sample8 | 13.0926 | 33.88757 | 0.386354 | N/A | N/A | N/A |
| | sample9 | 59.39133 | 38.14454 | 1.557007 | N/A | N/A | N/A |
| | sample10 | 39.60816 | 22.05772 | 1.79566 | N/A | N/A | N/A |
| | sample11 | 39.44253 | N/A | N/A | N/A | N/A | N/A |
| | sample12 | N/A | N/A | N/A | N/A | N/A | N/A |

**Figure 95:** Collagen synthesis ($\mu$g/mg) and sGAG content($\mu$g/mg) under steady laminar shear stress (1 dyne/cm$^2$): intact leaflets

| Intact leaflets, 9 dyne/cm2 | | | Collagen synthesis | | | sGAG content | |
|---|---|---|---|---|---|---|---|
| | | Shear | Control | Ratio | Shear | Control | Ratio |
| | sample1 | 25.49204 | 16.55915 | 1.539453 | 23.31538 | 28.80936 | 0.809299 |
| | sample2 | 25.04088 | 18.57641 | 1.347994 | 19.17992 | 22.70362 | 0.844796 |
| | sample3 | 38.66662 | 20.1757 | 1.916495 | 23.20906 | 25.52804 | 0.909159 |
| | sample4 | 28.31008 | 11.52674 | 2.456034 | 20.75464 | 21.89492 | 0.94792 |
| | sample5 | 20.46802 | 19.23797 | 1.063938 | 20.46104 | 22.94928 | 0.891577 |
| | sample6 | 23.00082 | 19.59507 | 1.173806 | 11.22498 | 6.457864 | 1.738188 |
| | sample7 | 56.52477 | 37.00127 | 1.527644 | 10.27075 | 10.58929 | 0.969919 |
| | sample8 | 26.61732 | 16.56456 | 1.606884 | 10.90792 | 11.595 | 0.940744 |
| | sample9 | 43.85317 | 39.01436 | 1.124026 | 15.69242 | 13.55649 | 1.157558 |
| | sample10 | 36.25886 | 22.17225 | 1.635327 | 19.956 | 29.60363 | 0.674106 |
| | sample11 | 31.65503 | 44.17035 | 0.716658 | N/A | N/A | N/A |
| | sample12 | N/A | N/A | N/A | N/A | N/A | N/A |

**Figure 96:** Collagen synthesis ($\mu$g/mg) and sGAG content($\mu$g/mg) under steady laminar shear stress (9 dyne/cm$^2$): intact leaflets

## *D.5 Shear stress-denuded leaflets*

| Intact leaflets, 25dyne/cm2 | | Collagen synthesis | | | sGAG content | | |
|---|---|---|---|---|---|---|---|
| | | Shear | Control | Ratio | Shear | Control | Ratio |
| | sample1 | 23.38136 | 20.92827 | 1.117214 | 22.77418 | 36.86292 | 0.617807 |
| | sample2 | 52.44641 | 38.86677 | 1.349389 | 18.36336 | 36.61758 | 0.50149 |
| | sample3 | 25.48126 | 46.57241 | 0.547132 | 22.20768 | 25.24758 | 0.879596 |
| | sample4 | 20.60904 | 56.82261 | 0.362691 | 18.7989 | 15.82879 | 1.18764 |
| | sample5 | 70.09037 | 49.17246 | 1.425399 | 24.76992 | 42.05458 | 0.588995 |
| | sample6 | 69.74708 | 44.20006 | 1.577986 | 21.94668 | 28.2112 | 0.777942 |
| | sample7 | 67.77969 | 55.88582 | 1.212825 | 21.28668 | 23.53298 | 0.904547 |
| | sample8 | 43.96192 | 12.51677 | 3.512242 | 21.03124 | 25.9965 | 0.809003 |
| | sample9 | 70.60915 | 37.57987 | 1.878909 | 25.99148 | 25.10872 | 1.035158 |
| | sample10 | 20.69023 | 12.42782 | 1.664833 | 21.14354 | 22.32206 | 0.947204 |
| | sample11 | 49.71383 | 44.15578 | 1.125874 | 18.26105 | 21.3158 | 0.856691 |
| | sample12 | 27.10292 | 13.7829 | 1.966416 | 22.32878 | 23.81414 | 0.937627 |

**Figure 97:** Collagen synthesis ($\mu$g/mg) and sGAG content($\mu$g/mg) under steady laminar shear stress (25 dyne/cm$^2$): intact leaflets

| Intact leaflets, 40 dyne/cm2 | | Collagen synthesis | | | sGAG content | | |
|---|---|---|---|---|---|---|---|
| | | Shear | Control | Ratio | Shear | Control | Ratio |
| | sample1 | 22.06041 | 12.92282 | 1.707089 | 24.8841 | 24.0938 | 1.032801 |
| | sample2 | 52.3195 | 6.388548 | 8.189576 | 36.2747 | 38.9728 | 0.93077 |
| | sample3 | 35.54911 | 9.713245 | 3.65986 | 26.724 | 40.7876 | 0.655199 |
| | sample4 | 10.89273 | 38.33929 | 0.284114 | 35.5264 | 33.108 | 1.073046 |
| | sample5 | 33.13105 | 16.7292 | 1.980433 | 33.5192 | 36.445 | 0.91972 |
| | sample6 | 27.20863 | 38.33056 | 0.709842 | 27.0929 | 58.7587 | 0.461087 |
| | sample7 | 43.22176 | 24.19694 | 1.786249 | 20.9898 | 30.77633 | 0.682011 |
| | sample8 | 17.76482 | 38.92026 | 0.456442 | 30.1425 | 27.8092 | 1.083904 |
| | sample9 | 28.29564 | 8.291665 | 3.41254 | 28.664 | 41.8985 | 0.68413 |
| | sample10 | 25.74152 | 30.54327 | 0.842789 | 21.6519 | 44.8973 | 0.482254 |
| | sample11 | 18.15497 | 17.58193 | 1.032593 | 35.0628 | 44.8859 | 0.781154 |
| | sample12 | N/A | N/A | N/A | 31.972 | 34.2553 | 0.933345 |

**Figure 98:** Collagen synthesis ($\mu$g/mg) and sGAG content($\mu$g/mg) under steady laminar shear stress (40 dyne/cm$^2$): intact leaflets

| Intact leaflets, 80 dyne/cm2 | | | Collagen synthesis | | | sGAG content | |
|---|---|---|---|---|---|---|---|
| | | Shear | Control | Ratio | Shear | Control | Ratio |
| | sample1 | 33.35625 | 6.7375 | 4.950835 | 28.446 | 31.24017 | 0.910559 |
| | sample2 | 38.245 | 8.56 | 4.467874 | 29.3965 | 30.999 | 0.948305 |
| | sample3 | 40.44286 | 3.935714 | 10.27586 | 35.35558 | 35.26333 | 1.002616 |
| | sample4 | 27.2375 | 11.15 | 2.442825 | 23.95717 | 39.61817 | 0.604702 |
| | sample5 | 24.3625 | 39.3 | 0.619911 | 20.488 | 14.86775 | 1.378016 |
| | sample6 | 32.81875 | 13.0625 | 2.51244 | 23.75358 | 17.7325 | 1.339551 |
| | sample7 | 42.65 | 24.3 | 1.755144 | 57.07733 | 42.10058 | 1.355737 |
| | sample8 | 28.5 | 27 | 1.055556 | 15.04133 | 38.08117 | 0.394981 |
| | sample9 | 53.05 | 9 | 5.894444 | 34.22333 | 18.41633 | 1.858314 |
| | sample10 | 19.56667 | 35.25 | 0.555083 | 29.57675 | 32.05325 | 0.922738 |
| | sample11 | N/A | N/A | N/A | 20.21783 | 25.70942 | 0.786398 |
| | sample12 | N/A | N/A | N/A | 38.49458 | 35.97825 | 1.06994 |

**Figure 99:** Collagen synthesis ($\mu$g/mg) and sGAG content($\mu$g/mg) under steady laminar shear stress (80 dyne/cm$^2$): intact leaflets

| Denuded leaflets, 1dyne/cm2 | | | Collagen synthesis | | | sGAG content | |
|---|---|---|---|---|---|---|---|
| | | Shear | Control | Ratio | Shear | Control | Ratio |
| | sample1 | 9.503943 | 8.274973 | 1.148516 | 15.0961 | 11.60071 | 1.301308 |
| | sample2 | 9.942911 | 7.863149 | 1.264495 | 16.21245 | 13.47866 | 1.202823 |
| | sample3 | 7.991501 | 8.005077 | 0.998304 | 10.59264 | 16.04465 | 0.660197 |
| | sample4 | 19.87693 | 19.68056 | 1.009978 | 13.26746 | 14.06027 | 0.943613 |
| | sample5 | 27.05304 | 15.51237 | 1.743966 | 12.42176 | 14.39411 | 0.862975 |
| | sample6 | 22.45633 | 18.12091 | 1.23925 | 14.34805 | 22.12729 | 0.648432 |
| | sample7 | 25.2942 | 24.29871 | 1.040969 | 12.73443 | 14.67874 | 0.867542 |
| | sample8 | 22.40877 | 21.43153 | 1.045599 | 11.00403 | 13.83606 | 0.795315 |
| | sample9 | 26.57931 | 22.98451 | 1.156401 | 9.664384 | 14.71381 | 0.656824 |
| | sample10 | 19.66585 | 19.94841 | 0.985835 | 7.996191 | 15.96074 | 0.500991 |
| | sample11 | 19.58568 | 20.31531 | 0.964085 | 11.194 | 13.80532 | 0.810847 |
| | sample12 | N/A | N/A | N/A | 13.65641 | 15.28428 | 0.893494 |

**Figure 100:** Collagen synthesis ($\mu$g/mg) and sGAG content($\mu$g/mg) under steady laminar shear stress (1 dyne/cm$^2$): denuded leaflets

| Denuded leaflets, 9dyne/cm2 | | | Collagen synthesis | | | sGAG content | |
|---|---|---|---|---|---|---|---|
| | | Shear | Control | Ratio | Shear | Control | Ratio |
| | sample1 | 9.5606 | 7.19011 | 1.329687 | 19.22177 | 0.773456 | 24.85179 |
| | sample2 | 14.7131 | 15.0767 | 0.975882 | 12.02231 | 1.260649 | 9.536599 |
| | sample3 | 10.6389 | 15.4258 | 0.689681 | 6.9263 | 2.607085 | 2.656722 |
| | sample4 | 10.9386 | 17.3111 | 0.631883 | 9.346 | 1.648113 | 5.670728 |
| | sample5 | 5.68085 | 2.17829 | 2.607936 | 15.6518 | 1.031412 | 15.17511 |
| | sample6 | N/A | 19.16 | N/A | 14.20547 | N/A | N/A |
| | sample7 | 5.839998 | 9.191631 | 0.63536 | 15.3614 | 1.224833 | 12.54163 |
| | sample8 | 23.29633 | 35.10054 | 0.663703 | 18.93947 | 1.032947 | 18.33537 |
| | sample9 | 16.596 | 20.27083 | 0.818713 | 14.6541 | 1.260391 | 11.62663 |
| | sample10 | 13.77854 | 24.93172 | 0.552651 | 16.40575 | 1.286374 | 12.75348 |
| | sample11 | 6.43095 | 19.362 | 0.332143 | 18.78972 | 1.041648 | 18.03844 |
| | sample12 | 23.98876 | 12.21466 | 1.963933 | 17.31442 | 1.027879 | 16.84479 |

**Figure 101:** Collagen synthesis ($\mu$g/mg) and sGAG content($\mu$g/mg) under steady laminar shear stress (9 dyne/cm$^2$): denuded leaflets

| Denuded leaflets, 25dyne/cm2 | | | Collagen synthesis | | | sGAG content | |
|---|---|---|---|---|---|---|---|
| | | Shear | Control | Ratio | Shear | Control | Ratio |
| | sample1 | 11.2083 | 1.673831 | 6.696196 | 11.0044 | 12.87515 | 0.854701 |
| | sample2 | 8.76719 | 1.490311 | 5.882791 | 10.24712 | 13.32655 | 0.768925 |
| | sample3 | 7.69566 | 0.42523 | 18.09766 | 14.30965 | 18.01283 | 0.794414 |
| | sample4 | 22.7219 | 1.210828 | 18.76558 | 18.68475 | 9.089395 | 2.055665 |
| | sample5 | 8.90674 | 0.87666 | 10.15985 | 15.97389 | 10.57958 | 1.509879 |
| | sample6 | 7.76569 | 0.956072 | 8.122495 | 14.03763 | 13.18877 | 1.064362 |
| | sample7 | 8.35346 | 1.908538 | 4.376886 | 10.90353 | 9.778738 | 1.115024 |
| | sample8 | 14.5243 | 0.799655 | 18.16318 | 18.12755 | 10.76171 | 1.684448 |
| | sample9 | 10.0184 | 0.827219 | 12.11095 | 21.65585 | 12.83145 | 1.687716 |
| | sample10 | 18.78 | 1.163625 | 16.13923 | 14.86875 | 11.27661 | 1.318547 |
| | sample11 | 10.8118 | 0.862893 | 12.52967 | 16.5066 | 5.823162 | 2.834646 |
| | sample12 | 12.627 | 0.712521 | 17.72165 | 14.71906 | 7.226796 | 2.036733 |

**Figure 102:** Collagen synthesis ($\mu$g/mg) and sGAG content($\mu$g/mg) under steady laminar shear stress (25 dyne/cm$^2$): denuded leaflets

| Denuded leaflets, 40dyne/cm2 | | | Collagen synthesis | | | sGAG content | |
|---|---|---|---|---|---|---|---|
| | | Shear | Control | Ratio | Shear | Control | Ratio |
| | sample1 | 21.16824 | 31.51647 | 0.671656 | 25.89113 | 20.85867 | 1.241265 |
| | sample2 | 39.47582 | 51.83536 | 0.761562 | 24.74977 | 23.354 | 1.059766 |
| | sample3 | 32.76337 | 25.21007 | 1.299615 | 34.68215 | 23.26706 | 1.490612 |
| | sample4 | 57.90194 | 51.48975 | 1.124533 | 38.00771 | 34.68422 | 1.095821 |
| | sample5 | 65.66079 | 39.07978 | 1.680173 | 32.84075 | 40.13937 | 0.818168 |
| | sample6 | 27.70528 | 20.64933 | 1.341704 | 34.45557 | 33.85679 | 1.017686 |
| | sample7 | 33.47582 | 72.929 | 0.459019 | 22.95801 | 49.39809 | 0.464755 |
| | sample8 | 23.0512 | 38.37431 | 0.600694 | 29.58545 | 24.72395 | 1.196631 |
| | sample9 | 73.963 | 62.54169 | 1.182619 | 42.10184 | 40.89668 | 1.029468 |
| | sample10 | 56.118 | 36.86006 | 1.522461 | 33.91318 | 22.19877 | 1.527705 |
| | sample11 | 60.35621 | 44.62165 | 1.352622 | 32.70379 | 27.95742 | 1.169771 |
| | sample12 | 13.85808 | 16.19768 | 0.85556 | 34.89425 | 53.41737 | 0.653238 |

**Figure 103:** Collagen synthesis ($\mu$g/mg) and sGAG content($\mu$g/mg) under steady laminar shear stress (40 dyne/cm$^2$): denuded leaflets

| Denuded leaflets, 80dyne/cm2 | | | Collagen synthesis | | | sGAG content | |
|---|---|---|---|---|---|---|---|
| | | Shear | Control | Ratio | Shear | Control | Ratio |
| | sample1 | 20.11689 | 15.59102 | 1.290287 | 8.589455 | 10.11202 | 0.84943 |
| | sample2 | 20.45349 | 13.97304 | 1.463782 | 11.01662 | 9.896479 | 1.113185 |
| | sample3 | 18.18675 | 16.2237 | 1.120999 | 4.547931 | 9.16994 | 0.495961 |
| | sample4 | 13.2095 | 18.78819 | 0.703074 | 8.708805 | 7.864902 | 1.1073 |
| | sample5 | 17.39229 | 18.26547 | 0.952195 | 8.102135 | 9.478231 | 0.854815 |
| | sample6 | 16.6456 | 15.09472 | 1.102743 | 8.289431 | 8.905612 | 0.93081 |
| | sample7 | 13.62791 | 18.56955 | 0.733885 | 16.72248 | 13.54071 | 1.234978 |
| | sample8 | 15.18193 | 18.90055 | 0.803254 | 10.47667 | 12.92963 | 0.810284 |
| | sample9 | 17.4521 | 18.83644 | 0.926507 | 10.00728 | 13.76715 | 0.726896 |
| | sample10 | 7.640583 | 9.318321 | 0.819953 | 9.844017 | 7.501303 | 1.312308 |
| | sample11 | 8.631087 | 9.275251 | 0.93055 | 7.850373 | 7.218259 | 1.087572 |
| | sample12 | 7.866874 | 7.268524 | 1.082321 | 10.82565 | 10.621 | 1.019269 |

**Figure 104:** Collagen synthesis ($\mu$g/mg) and sGAG content ($\mu$g/mg) under steady laminar shear stress (80 dyne/cm$^2$): denuded leaflets

# APPENDIX E

## MOVAT'S PENTACHROME STAINING

The movat's staining results did not show very good consistency from experiment to experiment; therefore the images were not included in the results chapter. Variations can be caused by the freshness of the reagents, who did the experiment etc. Showing below are some staining images from the various experiments.

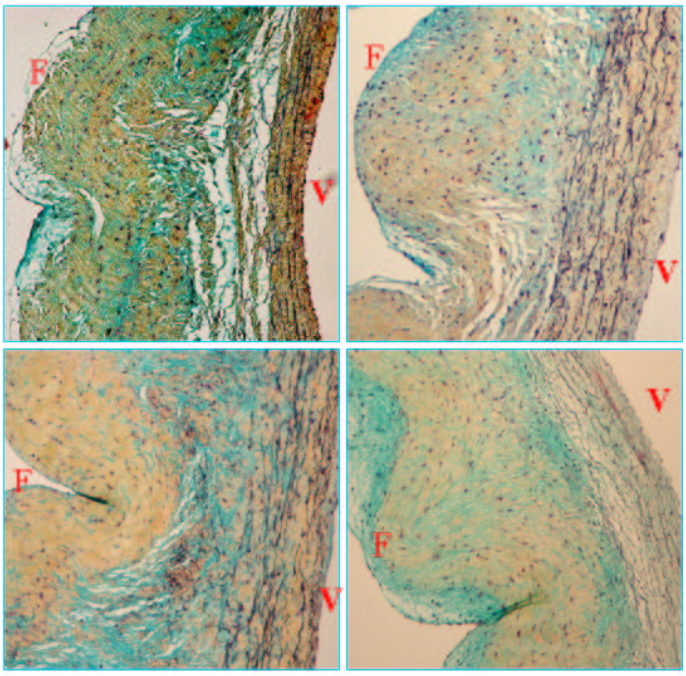


**Figure 105:** Movat staining of fresh porcine aortic valve leaflets collected from different experiments: collagen-yellow, elastic fibers and cell nuclei-black, sGAG - light blue, F indicates the fibrosa side and V indicates ventricular side

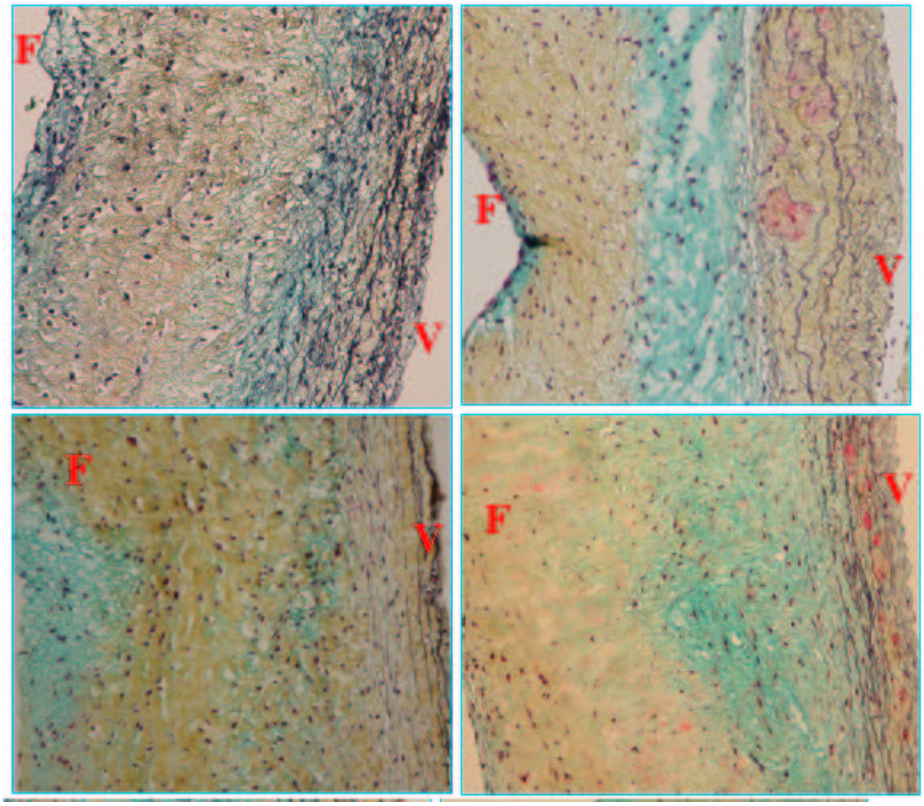


**Figure 106:** Movat staining of porcine aortic valve leaflets incubated for 48 hrs in DMEM: collagen-yellow, elastic fibers and cell nuclei-black, sGAG - light blue, F indicates the fibrosa side and V indicates the ventricular side

# APPENDIX F

# BIOLOGICAL VARIABILITY BETWEEN VALVES AND LEAFLETS WITHIN THE SAME VALVE

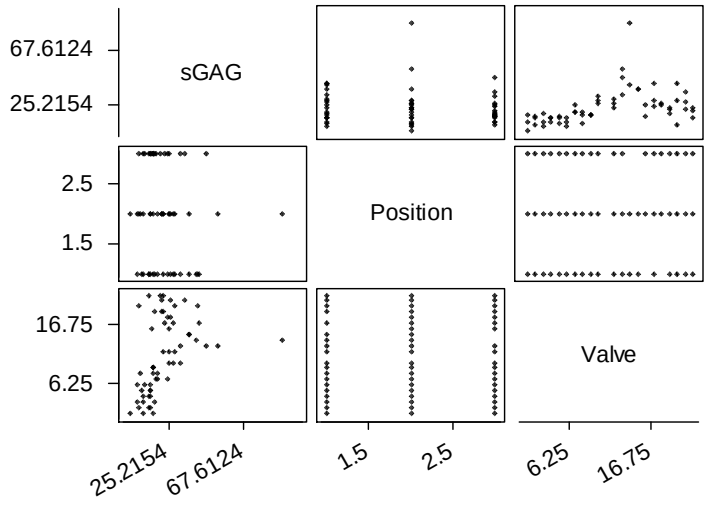


**Figure 107:** Matrix plot with variables of sGAG content, leaflet position and different valves. Of particular interests are the plots with sGAG content in the y-axis and leaflet position and valve ID in the x-axis respectively; note that the sGAG content varied from valve to valve, but the variations among the three different leaflets positions were relatively insignificant.

**General Linear Model**

| Factor | Type | Levels | Values |
|---|---|---|---|
| Position | fixed | 3 | 1 2 3 |
| Valve | fixed | 21 | 1 2 3 4 5 6 7 8 9 10 12 13 14 15 16 17 18 19 20 21 22 |

**Analysis of Variance for sGAG, using Adjusted SS for Tests**

| Source | DF | Seq SS | Adj SS | Adj MS | F | P |
|---|---|---|---|---|---|---|
| Position | 2 | 166.92 | 9.11 | 4.55 | 0.06 | 0.939 |
| Valve | 20 | 7900.70 | 7900.70 | 395.04 | 5.45 | 0.000 |
| Error | 36 | 2607.20 | 2607.20 | 72.42 | | |
| Total | 58 | 10674.82 | | | | |

**Figure 108:** ANOVA of sGAG synthesis with respect to leaflet position and valves

# REFERENCES


[1] *http://www.mayoclinic.org/heartvalvedisease-rst/.*

[2] *http://www.ctsnet.org/edmunds/Chapter28section2.html*.

[3] *Heart disease and stroke statistics - 2004 update.*, p. 17, 2004,American Heart Association and American Stoke Association.

[4] ACEVEDO, A., BOWSER, S., GERRITSEN, M., and BIZIOS, R., "Morphological and proliferative responses of endothelial cells to hydrostatic pressure: role of fibroblast growth factor.," *J Cell Physiol.*, vol. 157, no. 3, pp. 603–14, 1993.

[5] AGRAWAL, C. and RAY, R., "Biodegadable polymeric scaffolds for musculoskeletal tissue engineering.," *Journal of Biomedical Materials Research*, vol. 55, pp. 141–150, 2001.

[6] APENBERG, S., FREYBERG, M., and FRIEDL, P., "Shear stress induces apoptosis in vascular smooth muscle cells via an autocrine fas/fasl pathway.," *Biochem Biophys Res Commun.*, vol. 310, no. 2, pp. 355–9, 2003.

[7] ASANUMA, K., MAGID, R., JOHNSON, C., NEREM, R., and GALIS, Z., "Uniaxial strain upregulates matrix-degrading enzymes produced by human vascular smooth muscle cells," *Am J Physiol Heart Circ Physiol*, vol. 284, no. 5, pp. H1778–84, 2003.

[8] BAJPAI, P., "Immunological aspects of treated natural tissue prostheses.," *Biocompatibility of Tissue Analogs. Ed. DF Williams.*, vol. CRC,, pp. 5–25, 1985.

[9] BARTLETT, D., WRIGHT, M., YAYANOS, A., and SILVERMAN, M., "Interstital cells of the heart valves posess characteristics similar to smooth muscle cells," *Nature*, vol. 342, pp. 572–574, 1989.

[10] BASSIOUNY, H., SONG, R., HONG, X., SINGH, A., KOCHARYAN, H., and GLAGOV, S., "Floe regulation of 72-kd collagenase iv (mmp-2) after experimental arterial injury," *Circulation*, vol. 98, pp. 157–163, 1998.

[11] BATTEN, P., MCCORMACK, A., ROSE, M., and YACOUB, M., "Valve interstitial cells induce donor-specific t cell allergy.," *Journal of Thoracic Cardiovascular Surgery*, vol. 122, pp. 129–135, 2001.

[12] BLANN, A., BURROWS, G., and MCCOLLUM, C., "Oxidised and native low-density lipoproteins induce the release of von willebrand factor from human endothelial cells in vitro.," *Br J Biomed Sci.*, vol. 60, no. 3, pp. 155–60, 2003.

[13] BOTNEY, M., LIPTAY, M., KAISER, L., COOPER, J., PARKS, W., and MECHAM, R., "Active collagen synthesis by pulmonary arteries in human primary pulmonary hypertension," *American Journal of Pathology*, vol. 143, no. 1, pp. 121–9, 1993.

[14] BROCKBANK, K. and BANK, H., "Measurement of postcryopreservation viability.," *J Cardiac Surg.*, vol. 2 [Suppl], pp. 145–151, 1987.

[15] BROWN, T., "Techniques for mechanical stimulation of cells in vitro: a review," *Journal of Biomechanics*, vol. 33, pp. 3–14, 2000.

[16] BUCK, R., "Reorientation response of cells to repeated stretch and recoil of the substratum.," *Exp Cell Res.*, vol. 127, no. 2, pp. 470–4., 1980.

[17] BUTANYA, J., AHLUWALIAA, M., MUNROEA, C., FAYETA, C., AHNA, C., BLITA, P., KEPRONA, C., CUSIMANOB, R., and LEASKA, R., "Mechanical heart valve prostheses: identification and evaluation (erratum).," *Cardiovascuar Pathology.*, vol. 12, pp. 322–344, 2003.

[18] BUTCHER, J., PENROD, A., GARCIA, A., and NEREM, R., "Unique morphology and focal adhesion development of valvular endothelial cells in static and fluid flow environments.," *Arterioscler Thromb Vasc Biol*, vol. 24, no. 8, pp. 1429–34, 2004.

[19] CAMP, T., SMILEY, L., HAYDEN, M., and TYAGI, S., "Mechanism of matrix accumulation and glomerulosclerosis in spontaneously hypertensive rats," *Journal of Hypertension*, vol. 21, no. 9, pp. 1719–27, 2003.

[20] CANVER, C., GREGORY, R., COOLER, S., and VOYTOVICH, M., "Association of osteopontin with calcification in human mitral valves.," *J Cardiovasc Surg.*, vol. 41, no. 2, pp. 171–4, 2000.

[21] CARVER, W., NAGPAL, M., NACHTIGAL, M., BORG, T., and TERRACIO, L., "Collagen expression in mechanically stimulated cardiac fibroblasts," *Circulation Research*, vol. 69, pp. 116–122, 1991.

[22] CHESLER, N., KU, D., and GALLIS, Z., "Transmural pressure induces matrix-degrading activity in porcine arteries ex vivo," *Am J Physiol Heart Circ Physiol*, vol. 277, pp. H2002–H2009, 1999.

[23] CHESTER, A., MIFIELD, M., and YACOUB, M., "Receptor-mediated contraction of aortic valve leaflets.," *Journal of Heart Valve Disease*, vol. 9, pp. 250–255, 2000.

[24] CHIEN, S., "Effects of mechanical forces on signal transduction and gene expression in endothelial cells.," *Hypertension.*, vol. 31, pp. 162–169, 1998.

[25] CHIU, J., CHEN, L., LEE, P., and LEE, C., "A model for studying the effect of shear stress on interactions between vascular endothelial cells and smooth muscle cells.," *Journal of Biomechanics*, vol. 37, no. 4, pp. 531–9, 2004.

[26] CHIU, J., CHEN, L., LEE, P., LEE, C., LO, L., USAMI, S., and CHIEN, S., "Shear stress inhibits adhesion molecule expression in vascular endothelial cells induced by coculture with smooth muscle cells.," *Blood.*, vol. 101, no. 7, pp. 2667–74, 2003.

[27] CHRISTIE, G., "Anatomy of aortic heart valve leaflets: the influence of glutaraldehyde fixation on function.," *Eur J. Cardio-thorac Surg.*, vol. 6[suppl 1], pp. S25–33, 1992.

[28] CHRISTIE, G., "Computer modelling of bioprosthetic heart valves.," *Eur J Cardiothorac Surg.*, vol. 6, no. Suppl 1, pp. S95–100, 1992.

[29] CORDEN, J., DAVID, T., and FISHER, J., "Determination of the curvatures and bending strains in open trileaflet heart valves.," *Proc Instn Mech Engrs H.*, vol. 209, no. 2, pp. 121–128, 1995.

[30] CORDEN, J., DAVID, T., and FISHER, J., "In vitro determination of the curvatures and bending strains acting on the leaflets of polyurethane trileaflet heart valves during leaflet motion.," *Proc Instn Mech Engrs H.*, vol. 209, no. 4, pp. 243–53, 1995.

[31] DAVIES, P., "Mechanisms involved in endothelial responses to hemadynamic forces," *Atheroslerosis*, vol. 131, no. Suppl, pp. S15–S17, 1997.

[32] DAVIES, P., PASSERINI, A., and SIMMONS, C., "Aortic valve: turning over a new leaf(let) in endothelial phenotypic heterogeneity.," *Arterioscler Thromb Vasc Biol*, vol. 24, no. 8, pp. 1331–3, 2004.

[33] DAVIES, P. and TRIPATHI, S., "Mechanical stress mechanisms and the cell. an endothelial paradigm.," *Circulation Research*, vol. 72, pp. 239–245, 1993.

[34] DECK, J., "Endothelial cell orientation on aortic valve leaflets.," *Cardiovasc Res.*, vol. 20, pp. 760–767, 1986.

[35] DECK, J., "Structure, stress and tissue repair in aortic valve leaflets.," *Cardiovasc Res.*, vol. 22, pp. 7–16, 1988.

[36] DELVIN, A., CLARK, J., REID, J., and DOMINICZAK, A., "Dna synthesis and apoptosis in smooth muscle cells from a model of generic hypertension," *Hypertension*, vol. 36, pp. 110–115, 2000.

[37] DEWEY, C., "The dynamic response of vascular endothelial cells to fluid shear stress.," *Jounal of Biomechanical Engineering.*, vol. 103, pp. 177–185, 1981.

[38] DEWITT, M., HANDLEY, C., OAKES, B., and LOWTHER, D., "In vitro response of chondrocytes to mechanical loading: the effect of short term mechanical tension.," *Connective Tissue Res.*, vol. 12, pp. 97–109, 1984.

[39] DI-LUOZZO, G., BHARGAVA, J., and POWELL, R., "Vascular smooth muscle cell effect on endothelial cell endothelin-1 production.," *J Vasc Surg.*, vol. 31, no. 4, pp. 781–9, 2000.

[40] DOHERTY, T. and DETRANO, R., "Coronary arterial calcification as an active process: a new perspective on an old problem," *Calcif Tissue Int.*, vol. 54, pp. 224–30, 1994.

[41] DREGER, S., TAYLOR, P., ALLEN, S., and YACOUB, M., "Profiles and localization of matrix metalloprotenases (mmps) and their inhibitors (timps) in human heart valves," *Journal of Heart Valve Disease*, vol. 11, pp. 875–880, 2002.

[42] DUMONT, K., YPERMAN, J., VERBEKEN, E., SEGERS, P., MEURIS, B., VANDENBERGHE, S., FLAMENG, W., and VERDONCK, P., "Design of a new pulsatile bioreactor for tissue engineered aortic heart valve formation.," *Artif Organs.*, vol. 26, no. 8, pp. 710–4, 2002.

[43] DURBIN, A. and GOTLIEB, A., "Advances towards understanding heart valve responses to injury," *Cardiovascular Pathology*, vol. 11, no. 2, pp. 69–77, 2002.

[44] DUWEL, P., JUNGLING, E., WESTHOFEN, M., and LUCKHOFF, A., "Potassium currents in vestibular type II hair cells activated by hydrostatic pressure.," *Neuroscience.*, vol. 116, no. 4, pp. 963–972, 2003.

[45] ENGELMAYR, G., HILDEBRAND, D., SUTHERLAND, F., MAYER, J., and SACKS, M., "A novel bioreactor for the dynamic flexural stimulation of tissue engineered heart valve biomaterials.," *Biomaterials.*, vol. 24, no. 14, pp. 2523–32, 2003.

[46] FERRANS, V. and BUTANY, J., "Ultrastructural pathology of the heart," *Diagnostic electron microscopy. Ed. BF Trump and RT Jones, Toronto:John Wiley & Sons*, pp. 319–474, 1983.

[47] FERRARO, J., DANESHMAND, M., BIZIOS, R., and RIZZO, V., "Depletion of plasma membrane cholesterol dampens hydrostatic pressure and shear stress-induced mechanotransduction pathways in osteoblast cultures.," *Am J Physiol Cell Physiol.*, vol. 286, no. 4, pp. C831–9, 2004.

[48] FISCHER, M., KAECH, S., KNUTTI, D., and MATUS, A., "Rapid actinbased plasticity in dendritic spines.," *Neuron.*, vol. 20, pp. 847–854, 1998.

[49] FRATER, R., "Endothelial covering of biological artificial heart valves.," *Annals of Thoracic Surgery*, vol. 134, pp. 1142–1149, 1992.

[50] FUKUDA, S. and SCHMID-SCHONBEIN, G., "Regulation of cd18 expression on neutrophils in response to fluid shear stress," *PNAS*, vol. 100, no. 11, pp. 13152–13157, 2003.

[51] GALIS, Z. and KHATRI, J., "Matrix metalloproteinases in vascular remodeling and atherogenesis: the good, the bad, and the ugly.," *Circulation Research*, vol. 90, no. 3, pp. 251–62, 2002.

[52] GARVER, D., KACZMAREK, R., SILVERMAN, B., GROSS, T., and HAMILTON, P., "The epidemiology of prosthetic heart valves in the united states," *Tex Heart Inst J*, vol. 22, pp. 86–91, 1995.

[53] GARVEY, W., FATHI, A., BIGELOW, F., CARPENTER, B., and JIMENEZ, C., "Improved movat pentachrome stain.," *Stain Technol*, vol. 61, no. 1, pp. 60–2, 1986.

[54] GOLDSTEIN, S., CLARKE, D., WALSH, S., BLACK, K., and O'BRIEN, M., "Transpecies heart valve transplant: advanced studies of a bioengineered xeno-autograft," *Annals of Thoracic Surgery*, vol. 70, no. 6, pp. 1962–9, 1999.

[55] GRANDE, K., "Stress variations in the human aortic root and valve: the role of anatomic asymmetry.," *Annals of Biomedical Engineering*, vol. 26, pp. 534–545, 1998.

[56] GRANDE-ALLEN, K., MAKO, W., CALABRO, A., SHI, Y., RATLIFF, N., and VESELY, I., "Loss of chondroitin 6-sulfate and hyaluronan from failed porcine bioprosthetic valves," *Journal of Biomedical Materials Research*, vol. 65A, pp. 251–259, 2002.

[57] GUYTON, A., "Textbook of medical physiology," *8th ed, Saunders*, Philadephia, PA, 1991.

[58] HAN, H. and KU, D., "Contractile responses in arteries to hypertensive pressure in seven-day organ culture.," *Annals of Biomedical Engineering*, vol. 29, pp. 467–475, 2001.

[59] HELMKE, B. and DAVIES, P., "The cytoskeleton under esternal fluid mechanical forces: hemodynamic forces acting on the endothelium.," *Annals of Biomedical Engineering*, vol. 30, pp. 284–296, 2002.

[60] HILBERT, S., FERRANS, V., and JONES, M., "Tissue-derived biomaterials and their use in cardiovascular prosthetic devices.," *Med Prog Technol.*, vol. 14, no. 3-4, pp. 115–63, 1988-89.

[61] HISHIKAWA, K., NAKAKI, T., MARUMO, T., HAYASHI, M., SUZUKI, H., KATO, R., and SARUTA, T., "Pressure promotes dna synthesis in rat cultured vascular smooth muscle cells.," *J.Clin.Invest.*, vol. 93, pp. 1975–1980, 1994.

[62] HOERSTRUP, S., SODIAN, R., DAEBRITZ, S., WANG, J., BACHA, E., MARTIN, D., MORAN, A., GULESERIAN, K., SPERLING, J., KAUSHAL, S., VACANTI, J., SCHOEN, F., and MAYER, J., "Functional living trileaflet heart valves grown in vitro," *Circulation*, vol. 102, no. suppl III, pp. III44–49, 2000.

[63] HUNTER, C., IMLER, S., MALAVIYA, P., NEREM, R., and LEVENSTON, M., "Mechanical compression alters gene expression and extracellular matrix synthesis by chondrocytes cultured in collagen I gels.," *Biomaterials.*, vol. 23, no. 4, pp. 1249–59, 2002.

[64] HUTTON, W., ELMER, W., BODEN, S., HYON, S., TORIBATAKE, Y., TOMITA, K., and HAIR., G., "The effect of hydrostatic pressure on intervertebral disc metabolism," *Spine.*, vol. 24, pp. 1507–1515, 1999.

[65] HWANG, J., ING, M., SALAZAR, A., LASSEGUE, B., GRIENDLING, K., NAVAB, M., SEVANIAN, A., and HSIAI, T., "Pulsatile versus oscillatory shear stress regulates nadph oxidase subunit expression: implication for native ldl oxidation.," *Circulation Research*, vol. 93, no. 12, pp. 1225–32, 2003.

[66] IIZUKA, K., MORITA, N., MURAKAMI, T., and KAWAGUCHI, H., "Nipradilol inhibits atmospheric pressure-induced cell proliferation in human aortic smooth muscle cells.," *Pharmacol Res.*, vol. 49, no. 3, pp. 217–25, 2004.

[67] IVES, C., "Mechanical effects on endothelial cell morphology: in vitro assessment.," *In Vitro Cell Dev Biol.*, vol. 22, pp. 500–507, 1986.

[68] JOCKENHOEVEL, S., ZUND, G., HOERSTRUP, S., CHALABI, K., SACHWEH, J., DEMIRCAN, L., MESSMER, B., and MTURINA, "Fibrin gel – advantages of a new scaffold in cardiovascular tissue engineering.," *Eur J Cardiothorac Surg.*, vol. 19, no. 4, pp. 424–30, 2001.

[69] JOURET, C., "Effects of matrix and phenotype on human dermal fibroblast attachment under laminar shear stress: implications for the development of tissue-engineered heart valves.," *Master Thesis, Georgia Institute of Technology*, 1997.

[70] KATWA, L., RATAJSKA, A., CLEUTJENS, J., SUN, Y., ZHOU, G., LEE, S., and WEBER, K., "Angiotensin converting enzyme and kinase-II-like activities in cultured valvular interstitial cells of rat heart," *Cardiovasc. Res.*, vol. 29, pp. 57–64, 1995.

[71] KATWA, L., TYAGI, S., CAMPBELL, S., LEE, S., CICILA, G., and WEBER, K., "Valbular interstitial cells express angiotensinogen and cathepsin d, and generate angiotensin peptides," *Int. J. Biochem. Cell Biol.*, vol. 28, no. 7, pp. 807–821, 1996.

[72] KU, C., JOHNSON, P., CHAMBERS, R., CHESTER, A., TAYLOR, P., and YACOUB, M., "Up-regulation of total collagen production and deposition by aortic valve interstitial cells (AVICs) in responses to stretch," *ISACB, 9th Biennial Meeting Proceedings, page 19*, 2004.

[73] KU, D., NELSON, J., CAUFIELD, J., and WINN, M., "Release of endothelium-derived relaxing factors from cardiac valves," *J Cardiovasc Pharmacol.*, vol. 16, pp. 212–8, 1990.

[74] LAMMI, M., INKINEN, R., PARKKINEN, J., HAKKINEN, T., JORTIKKA, M., NELIMARKKA, L., JARVELAINEN, H., and TAMMI, M., "Expression of reduced amounts of structurally altered aggrecan in articular cartilage chondrocytes exposed to high hydrostatic pressure.," *Biochem J.*, vol. 304, no. Pt 3, pp. 723–30, 1994.

[75] LEE, R., RICH, J., KELLEY, K., WEIMAN, D., and MATHEWS, M., "A comparison of in vitro cellular responses to mechanical and electrical stimulation.," *Am Surg.*, vol. 48, no. 11, pp. 567–74, 1982.

[76] LEE, Y. and CHOU, Y., "Endothelial alterations and senile calcific aortic stenosis: an electron microscopic observation.," *Proc Natl Sci Counc Repub China.*, vol. 21, no. 4, pp. 137–43, 1997.

[77] LEHOUX, S., LEMARIÉ, C., ESPOSITO, B., LIJNEN, H., and TEDGUI, A., "Pressure-induced matrix metalloproteinase-9 contributes to early hypertensive remodeling," *Circulation*, vol. 109, pp. 1041–1047, 2004.

[78] LEVESQUE, M. and NEREM, R., "The elongation and orientation of cultured endothelial cells in response to shear stress.," *J. Biomech Eng.*, vol. 107, pp. 341–347, 1985.

[79] LIPKE, D. and COUCHMAN, J., "Increased proteoglycan synthesis by the cardiovascular system of coarctation hypertensive rats.," *J.Cell Physiol.*, vol. 147, pp. 479–486, 1991.

[80] LUPINETTI, F., KNEEBONE, J., REKHTER, M., BROCKBANK, K., and GORDON, D., "Procollagen production in fresh and cryopreserved aortic valve grafts.," *J Thorac Cardiovasc Surg.*, vol. 113, pp. 102–107, 1997.

[81] MACDONALD, A., "Ion channels under high pressure.," *Comp Biochem Physiol A Mol Integr Physiol.*, vol. 131, no. 3, pp. 587–93, 2002.

[82] MAGID, R., , MURPHY, T., and GALIS, Z., "Expression of matrix metalloproteinase-9 in endothelial cells is differentially regulated by shear stress. role of c-myc.," *J. Biol. Chem.*, vol. 278, no. 35, pp. 32994–9, 2003.

[83] MARRON, K., YACOUB, M., POLAK, J., SHEPPARD, M., FAGAN, D., DE LEVAL, B. W. M., ANDERSON, R., and WHARTON, J., "Innervation of human atrioventricular and arterial valves," *Circulation*, vol. 94, pp. 368–375, 1995.

[84] MCGIFFIN, D., "Invited letter concerning leaflet viability and the durability of the allograft aortic valve.," *J Thorac Cardiovasc Surg.*, vol. 108, pp. 988–990, 1994.

[85] MCINTIRE, L., "Bioengineering and vascular biology.," *Annals of Biomedical Engineering*, vol. 22, pp. 2–13, 1994.

[86] MEHRABIAN, M., DEMER, L., and LUSIS, A., "Differential accumulation of intimal monocyte-macrophages relative to lipoproteins and lipofuscin corresponds to hemodynamic forces on cardiac valves in mice," *Arteriosclerosis and Thrombosis*, vol. 11, pp. 947–957, 1991.

[87] MITCHELL, R., JONAS, R., and SCHOEN, F., "Pathology of explanted cryopreserved allograft heart valves: comparison with aortic valves from orthotopic heart transplants.," *J Thorac Cardiovasc Surg.*, vol. 115, pp. 118–127, 1998.

[88] MIZUNO, S., TATEISHI, T., USHIDA, T., and GLOWACKI, J., "Hydrostatic fluid pressure enhances matrix synthesis and accumulation by bovinechondrocytes in three-dimensional culture," *Cell Physio*, vol. 193, pp. 319–327, 2002.

[89] MOHLER, E., CHAWLA, M., CHANG, A., VYAVAHARE, N., LEVY, R., GRAHAM, L., and GANNON, F., "Identification and characterization of calcifying valve cells from human and canine aortic valves.," *Journal of Heart Valve Disease*, vol. 8, pp. 254–260, 1999.

[90] MOHLER, E., GANNON, F., REYNOLDS, C., ZIMMERMAN, R., KEANE, M., and KAPLAN, F., "Bone formation and inflammation in cardiac valves," *Circulation*, vol. 103, pp. 1522–1528, 2001.

[91] MOL, A., BOUTEN, C., BAAIJENS, F., ZUND, G., TURINA, M., and HOERSTRUP, S., "Review article: Tissue engineering of semilunar heart valves: Current status and future development," *Journal of Heart Valve Disease*, vol. 13, pp. 272–280, 2004.

[92] MORITA, N., IIZUKA, K., MURAKAMI, T., and KAWAGUCHI, H., "N-terminal kinase, and c-src are activated in human aortic smooth muscle cells by pressure stress.," *Mol Cell Biochem.*, vol. 262, no. 1-2, pp. 71–8, 2004.

[93] MOVAT, H., "Demonstration of all connective tissue elements in a single section.," *Pathology*, vol. 60, no. 4, pp. 289–295, 1955.

[94] NACKMAN, G., FILLINGER, M., SHAFRITZ, R., WEI, T., and GRAHAM, A., "Flow modulates endothelial regulation of smooth muscle cell proliferation: a new model.," *Surgery.*, vol. 124, no. 2, pp. 353–60, 1998.

[95] NAGATOMI, J., ARULANANDAM, B., METZGER, D., MEUNIER, A., and ., R. B., "Frequency- and duration-dependent effects of cyclic pressure on select bone cell functions.," *Tissue Engineering*, vol. 7, no. 6, pp. 717–28, 2001.

[96] NIKLASON, L., GAO, J., ABBOTT, W., HIRSCHI, K., S, S. H., MARINI, R., and LANGER, R., "Functional arteries grown in vitro.," *Science*, vol. 284, no. 5413, pp. 489–93, 1999.

[97] NORIA, S., XU, F., MCCUE, S., JONES, M., AI, A. G., and LANGILLE, B., "Assembly and reorientation of stress fibers drives morphological changes to endothelial cells exposed to shear stress.," *American Journal of Pathology*, vol. 164, no. 4, pp. 1211–23, 2004.

[98] OZAWA, H., IMAMURA, K., ABE, E., TAKAHASHI, N., HIRAIDE, T., SHIBASAKI, Y., FUKUHARA, T., and SUDA, T., "Effect of a continuously applied compressive pressure on mouse osteoblast-like cells (mc3t3-e1) in vitro.," *J Cell Physiol.*, vol. 142, no. 1, pp. 177–85, 1990.

[99] PACZEK, L., TESCHNER, M., SCHAEFER, R., KOVAR, J., ROMEN, W., and HEIDLAND, A., "Proteinase activity in isolated glomeruli of goldblatt hypertensive rats.," *Clin Exp Hypertens A.*, vol. 13, no. 3, pp. 339–56, 1991.

[100] PALUMBO, R., GAETANO, C., MELILLO, G., TOSCHI, E., REMUZZI, A., and CAPOGROSSI, M., "Shear stress downregulation of platelet-derived growth factor receptor-$\beta$ and matrix mettaloproteinase-2 is associated with inhibition of smppth muscle cell invasion and migration," *Circulation*, vol. 102, pp. 225–230, 2000.

[101] PAPADAKI, M. and ESKIN, S., "Effects of fluid shear stress on gene regulation of vascular cells.," *Biotechnol Prog.*, vol. 13, no. 3, pp. 209–21, 1997.

[102] PATRICK, C. and MCINTIRE, L., "Shear stress and cyclic strain modulation of gene expression in vascular endothelial cells.," *Blood Purif.*, vol. 13, no. 3-4, pp. 112–24, 1995.

[103] PEARSON, R., BHANDARI, R., QUIRK, R., and SHAKESHEFF, K., "Recent advances in tissue engineering: an invited review.," *J Long Term Eff Med Implants.*, vol. 12, no. 1, pp. 1–33, 2002.

[104] POWELL, R., CRONENWETT, J., FILLINGER, M., WAGNER, R., and SAMPSON, L., "Endothelial cell modulation of smooth muscle cell morphology and organizational growth pattern.," *Ann Vasc Surg.*, vol. 10, no. 1, pp. 4–10, 1996.

[105] POWELL, R., HYDOWSKI, J., FRANK, O., BHARGAVA, J., and SUMPIO, B., "Endothelial cell effect on smooth muscle cell collagen synthesis.," *J Surg Res.*, vol. 69, no. 1, pp. 113–8, 1997.

[106] QUICK, D., KUNZELMAN, K., KNEEBONE, J., and COCHRAN, R., "Collagen synthesis is upregulated in mitral valves subjected to altered stress," *ASAIO J.*, vol. 43, pp. 181–186, 1997.

[107] RABKIN, E., AIKAWA, M., STONE, J., FUKUMOTO, Y., LIBBY, P., and SCHOEN, F., "Activated interstitial myofibroblasts express catabolic enzymes and mediate matrix remodeling in myxomatous heart valves," *Circulation*, vol. 104, pp. 2525–2532, 2001.

[108] RABKIN, E., HOERSTRUP, S., AIKAWA, M., MAYER, J., and SCHOEN, F., "Evolution of cell phenotype and ecm in tissue-engineered heart valves during in vitro and in vivo remodeling.," *Journal of Heart Valve Disease*, vol. 11, pp. 308–314, 2002.

[109] RABKIN-AIKAWA, E., FARBER, M., AIKAWA, M., and SCHOEN, F., "Dynamic and reversible changes of interstitial cell phenotype during remodeling of cardiac valves.," *Journal of Heart Valve Disease*, vol. 13, no. 5, pp. 841–7, 2004.

[110] RADOSEVICH, J., HAINES, G., ELSETH, K., SHAMBAUGH, G., and MAKER, V., "A new method for the detection of viable cells in tissue sections using 3-[4,5-dimethylthiazol-2-yl]-2,5-diphenyltetrazolium bromide (MTT): an application in the assessment of tissue damage by surgical instruments.," *Virchows Archiv B Cell Pathol.*, vol. 63, pp. 345–350, 1993.

[111] RESNICK, N., COLLINS, T., ATKINSON, W., BONTHRON, D., DEWEY, C., and GIMBRONE, M., "Platelet-derived growth factor b chain promoter contains a cis-acting fluid shear-stress-responsive element.," *Proceedings of National Academy of Science*, vol. 90, no. 10, pp. 4591–5, 1993.

[112] REUSCH, H., CHAN, G., IVES, H., and NEMENOFF, R., "Activation of jnk/sapk and erk by mechanical strain in vascular smooth muscle cells depends on extracellular matrix composition," *Biochem Biophys Res Commun.*, vol. 237, pp. 239–244, 1997.

[113] RIVAS-GOTZ, C., CENTRELLA, M., and SUMPIO, B., "Stretch stimulates human keratinocyte but not dermal fibroblast proliferation.," *Surg Forum.*, vol. 46, pp. 740–742, 1995.

[114] RIZZO, V., SUNG, A., OH, P., and SCHNITZER, J., "Rapid mechanotransduction in situ at the luminal cell surface of vascular endothelium and its caveolae.," *J. Biol. Chem.*, vol. 273, p. 26323, 1998.

[115] ROELOFSEN, J., KLEIN-NULEND, J., and BURGER, E., "Mechanical stimulation by intermittent hydrostatic compression promotes bone-specific gene expression in vitro," *Journal of Biomechanics*, vol. 28, no. 12, pp. 1493–1503, 1995.

[116] ROTHENBURGER, M., VOLKER, W., VISCHER, J., BERENDES, E., GLASMACHER, B., SCHELD, H., and DEIWICK, M., "Tissue engineering of heart valves: formation of a three-dimensional tissue using porcine heart valve cells.," *ASAIO J.*, vol. 48, no. 6, pp. 586–91, 2002.

[117] ROZEK, R., KUO, T., GIACOMELLI, F., and WIENER, J., "Proteolytic activities in hypertensive cardiomyopathy of rats.," *J Mol Cell Cardiol.*, vol. 15, no. 3, pp. 173–87, 1983.

[118] SACKS, M., SMITH, D., and HIESTER, E., "The aortic valve microstructure: Effects of transvavular pressure," *Journal of Biomedical Materials Research*, vol. 41, pp. 131–141, 1998.

[119] SALWEN, S., SZAROWSKI, D., TURNER, J., and BIZIOS, R., "Three-dimentional changes of the cytoskeleton of vascular endothelial cells exposed to sustained hydrostatic pressure," *Transplant Proceedings*, vol. 33, pp. 66–68, 2001.

[120] SASAHARA, M., HAZAMA, F., AMANO, S., HAYASE, Y., YUKIOKA, N., KAWAI, J., and KATAOKA, H., "Effect of hypertension on lysosomal enzyme activities in aortic endothelial cells.," *Atherosclerosis*, vol. 70, no. 1-2, pp. 53–62, 1988.

[121] SCHMIDT, A., GRUNWALD, J., and BUDDECKE, E., "[35s] proteoglycan metabolism of arterial smooth muscle cells cultured from normotensive and hypertensive rats.," *Atherosclerosis.*, vol. 45, pp. 299–310, 1982.

[122] SCHNEIDER, P. and DECK, J., "Tissue and cell renewal in the natural aortic valve of rats: an autoradiographic study," *Cardiovasc.Res.*, vol. 15, pp. 181–189, 1981.

[123] SCHNEIDER, P. and DECK, J., "Tissue and cell renewal in the natural aortic valve of rats: an autoradiographic study," *Cardiovasc.Res.*, vol. 15, pp. 181–189, 1984.

[124] SCHOEN, F., FERNANDEZ, J., GONZALEZ-LAVIN, L., and CERNAIANU, A., "Causes of failure and pathologic findings in surgically removed ionecu-shiley standard bovine pericardial heart valve bioprostheses: emphasis on progressive structural deterioration.," *Circulation*, vol. 76, no. 3, pp. 618–627, 1987.

[125] SCHOEN, F. and LEVY, R., "Tissue heart valves: Current challenges and future research perspectives," *Journal of Biomedical Materials Research*, vol. 47, pp. 439–465, 1999.

[126] SCHWARTZ, E., BIZIOS, R., MEDOW, M., and GERRITSEN, M., "Exposure of human vascular endothelial cells to sustained hydrostatic pressure stimulates proliferation: Involvement of the $\alpha$ -v integrins," *Circulation Research*, vol. 84, pp. 315–322, 1999.

[127] SHIN, H., GARRITSEN, M., and BIZIOS, R., "Regulation of endothelial cell proliferation and apoptosis by cyclic pressure.," *Annals of Biomedical Engineering*, vol. 30, no. 3, pp. 297–304, 2002.

[128] SHIN, H., SMITH, M., TOY, K., WILLIAMS, P., BIZIOS, R., and GERRITSEN, M., "VEGF-C mediates cyclic pressure-induced endothelial cell proliferation.," *Physiol Genomics.*, vol. 11, no. 3, pp. 245–51, 2002.

[129] SHINOKA, T., MA, P., SHUM-TIM, D., BREUER, C., CUSICK, R., ZUND, G., LANGER, R., VACANTI, J., and MAYER, J., "Tissue-engineered heart valves. autologous valve leaflet replacement study in a lamb model.," *Circulation*, vol. 94, no. 9 Suppl, pp. II164–8, 1996.

[130] SHIU, Y., LI, S., MARGANSKI, W., SCHWARTZ, S. U. M., WANG, Y., DEMBO, M., and CHIEN, S., "Rho mediates the shear-enhancement of endothelial cell migration and traction force generation.," *Biophys J.*, vol. 86, no. 4, pp. 2558–65, 2004.

[131] SHYY, J. and CHIEN, S., "Role of integrins in endothelial mechanosensing of shear stress," *Circulation Research*, vol. 91, pp. 769–75, 2002.

[132] SIMMONS, C., ZILBERBERG, J., and DAVIES, P., "A rapid, reliable method to isolate high quality endohtelial ena from small spatially-defined locations.," *Annals of Biomedical Engineering*, vol. 32, no. 10, pp. 1453–1459, 2004.

[133] SINEY, L. and LEWIS, M., "Nitric oxide release from porcine mitral valves," *Cardiovasc Res.*, vol. 27, pp. 1657–1661, 1993.

[134] SODIAN, R., HOERSTRUP, S., SPERLING, J., DAEBRITZ, S., MARTIN, D., MORAN, A., KIM, B., SCHOEN, F., VACANTI, J., and MAYER, J., "Early in vivo experience with tissue-engineered trileaflet heart valves," *Circulation*, vol. 102, no. suppl III, pp. III22–29, 2000.

[135] SOMERO, G., "Environmental and metabolic animal physiology.," *C.L. Prosser (Ed), Wiley Liss, New York*, pp. 167–204, 1991.

[136] SONG, Y., YAO, L., KNEEBONE, J., and LUPINETTI, F., "Effect of cryopreservation and histocompatibility on type I procollagen gene expression in aortic valve grafts.," *J Thorac Cardiovasc Surg.*, vol. 114, pp. 421–427, 1997.

[137] SOTOUDEH, M., JALALI, S., USAMI, S., SHYY, J., and CHIEN, S., "A strain device imposing dynamic and uniform equi-biaxial strain to cultured cells.," *Annals of Biomedical Engineering*, vol. 26, no. 2, pp. 181–9, 1998.

[138] STAMATAS, G. and MCINTIRE, L., "Rapid flow-induced responses in endothelial cells.," *Biotechnol Prog.*, vol. 17, pp. 383–402, 2001.

[139] STEVENS, R., BHARGAVA, J., and POWELL, R., "Endothelial cells inhibit smooth muscle cell secretion of hyaluronanic acid.," *J Vasc Surg.*, vol. 28, no. 2, pp. 319–25, 1998.

[140] STEWART, B., SISCOVICK, D., LIND, B., GARDIN, J., GOTTDIENER, J., SMITH, V., KITZMAN, D., and OTTO, C., "Clinical factors associated with calcific aortic valve disease. cardiovascular health study.," *J Am Coll Cardiol.*, vol. 29, no. 3, pp. 630–4, 1997.

[141] STYPMANN, J., GLASER, K., ROTH, W., TOBIN, D., PETERMANN, I., MATTHIAS, R., MONNIG, G., HAVERKAMP, W., BREITHARDT, G., SCHMAHL, W., and PETERS, C., "Dilated cadiomyopathy in mice deficient for the lysosomal cycteine peptidase cathepsin l," *Proceedings of National Academy of Science*, vol. 99, no. 9, pp. 6234–6239, 2002.

[142] SUMPIO, B., WIDMANN, M., RICOTTA, J., AWOLESI, M., and WATASE, M., "Increased ambient pressure stimulates proliferation and morphologic changes in cultured endothelial cells.," *J Cell Physiol.*, vol. 158, no. 1, pp. 133–9, 1994.

[143] SUN, H., NALIM, R., and YOKOTA, H., "Expression and activities of matrix metaaloproteinases under oscillatory shear in il-1-stimulated synovial cells," *Connective Tissue Research*, vol. 44, pp. 42–49, 2003.

[144] SUN, Y., CHEUNG, J., MARTEL-PELLETIER, J., PELLETIER, J., WENGER, L., ALTMAN, R., HOWELL, D., and CHEUNG, H., "Wild type and mutant p53 differentially regulate the gene expression of human collagenase-3 (hmmp-13).," *J. Biol. Chem.*, vol. 275, no. 15, pp. 11327–32, 2000.

[145] SUN, Y. and WEBER, K., "Ras and connective tissue in the heart.," *Int. J. Biochem. Cell Biol.*, vol. 35, pp. 919–931, 2003.

[146] SUZUKI, H., SCHAEFER, L., LING, H., SCHAEFER, R., J, J. D., TESCHNER, M., and HEIDLAND, A., "Prevention of cardiac hypertrophy in experimental chronic renal failure by long-term ace inhibitor administration: potential role of lysosomal proteinases.," *Am J Nephrol.*, vol. 15, no. 2, pp. 129–36, 1995.

[147] TANAKA, S., LI, J., DUNCAN, R., YOKOTA, H., BURR, D., and TURNER, C., "Effects of broad frequency vibration on cultured osteoblasts," *Journal of Biomechanics*, vol. 36, pp. 73–80, 2003.

[148] TANCK, E., VAN DRIEL, W., HAGEN, J., BURGER, E., LANKEVOORT, L., and HUISKES, R., "Why does intermittent hydrostatic pressure enhance the mineralization process in fetal cartilage ?," *Journal of Biomechanics*, vol. 32, pp. 153–161, 1999.

[149] TANIMURA, A., MCGREGOR, D., and ANDERSON, H., "Matrix vesicles in atheroslerotic calcification.," *Proc Soc Exp Biol Med.*, vol. 172, pp. 173–7, 1983.

[150] TAYLOR, P., ALLEN, S., DREGER, S., and YACOUB, M., "Human cardiac valve interstitial cells in collagen sponge: a biological three-dimensional matrix for tissue engineering.," *Journal of Heart Valve Disease*, vol. 11, no. 3, pp. 298–306, 2002.

[151] TAYLOR, P., BATTEN, P., BRAND, N., THOMAS, P., and YACOUB, M., "The cardiac valve interstitial cell," *Int. J. Biochem. Cell Biol.*, vol. 35, pp. 113–118, 2003.

[152] THUBRIKAR, M., "The aortic valve," *CRC press*, p. 112, 1990.

[153] THUBRIKAR, M., PIEPGRASS, W., DECK, J., and NOLAN, S., "Stresses of natural versus prosthetic aortic valve leaflets in vivo.," *Annals of Thoracic Surgery*, vol. 30, p. 230, 1980.

[154] THUBRIKAR, M., DECK, J., AOUAD, J., and NOLAN, S., "Role of mechanical stress in calcification of aortic bioprosthetic valves.," *J Thorac Cardiovasc Surg.*, vol. 86, no. 1, pp. 115–25, 1983.

[155] TOKUNAGA, O., FAN, J., and WATANABE, T., "Atherosclerosis and endothelium part ii. properties of aortic endothelial and smooth muscle cells cultured at various ambient pressures," *Acta Pathology of Japan*, vol. 39, pp. 356–362, 1989.

[156] TOKUNAGA, O. and WATANABE, T., "Properties of endothelial cell and smooth muscle cell cultured in ambient pressure," *In vitro Cellular & Development Biology*, vol. 23, pp. 528–534, 1987.

[157] VANDENBURGH, H., "Mechanical forces and their second messengers in stimulating cell growth in vitro.," *American Journal of Physiology*, vol. 262, pp. R350–R355, 1992.

[158] VANHEE, C., "Influence of shear stress on cell proliferation and on protein kinase c localization in an anchorage-dependent mammalian cell line.," *MS Thesis, Georgia Institute of Technology*, 1991.

[159] VOUYOUKA, A., JIANG, Y., and BASSON, M., "Pressure alters endothelial effects upon vascular smooth muscle cells by decreasing smooth muscle cell proliferation and increasing smooth muscle cell apoptosis.," *Surgery*, vol. 136, no. 2, pp. 282–90, 2004.

[160] VOUYOUKA, A., POWELL, R., RICOTTA, J., CHEN, H., DUDRICK, D., SAWMILLER, C., DUDRICK, S., and SUMPIO, B., "Ambient pulsatile pressure modulates endothelial cell proliferation," *Journal of Molecular and Cellular Cardiology*, vol. 30, pp. 609–615, 1998.

[161] VOUYOUKA, A., SALIB, S., CALA, S., MARSH, J., and BASSON, B., "Chronic high pressure potentiates the antiproliferative effect and abolishes contractile phenotypic changes caused by endothelial cells in cocultured smooth muscle cells.," *J Surg Res.*, vol. 110, no. 2, pp. 344–51, 2003.

[162] WANG, B., CHANG, H., LIN, S., KUAN, P., and SHYU, K., "Induction of matrix metalloproteinases-14 and -2 by cyclical mechanical stretch is mediated by tumor necrosis factor-alpha in cultured human umbilical vein endothelial cells," *Cardiovasc Res.*, vol. 59, no. 2, pp. 460–9, 2003.

[163] WATASE, M., AWOLESI, M., RICOTTA, J., and SUMPIO, B., "Effect of pressure on cultured smooth muscle cells," *Life Science*, vol. 61, no. 10, pp. 987–996, 1997.

[164] WEBER, K., JANICKI, J., SHROFF, S., PICK, R., CHEN, R., and BASHEY, R., "Collagen remodeling of the pressure-overloaded, hypertrophied non-human primate myocardium," *Circulation Research*, vol. 62, pp. 757–765, 1988.

[165] WEBER, K., SUN, Y., KATWA, L., CLEUTJENS, J., and ZHOU, G., "Connective tissue and repair in the heart. potential regulatory mechanisms," *Ann N Y Acad Sci.*, vol. 752, pp. 286–99, 1995.

[166] WEBER, K., SWAMYNATHAN, S., GUNTAKA, R., and SUN, Y., "Angiotensin II and extracellular matrix homeostasis," *The International Journal of Biochemistry & Cell Biology.*, vol. 31, pp. 395–403, 1999.

[167] WEIND, K., ELLIS, C., and BOUGHNER, D., "The aortic valve blood supply.," *Journal of Heart Valve Disease*, vol. 9, no. 1, pp. 1–7, 2000.

[168] WESTON, M., "Effects of shear stress on the biosynthetic activity of porcine aortic valve leaflets.," *Doctoral Thesis, Georgia Institute of Technology*, 2000.

[169] WESTON, M. and YOGANATHAN, A., "Biosynthetic activity in heart valve leaflets in response to in vitro flow environments.," *Annals of Biomedical Engineering*, vol. 29, pp. 752–763, 2001.

[170] WILLIAMS, P., KYBERD, P., SIMPSON, H., KENWRIGHT, J., and GOLDSPINK, G., "The morphological basis of increased stiffness of rabbit tibialis anterior muscles during surgical limb-lengthening.," *Journal of Anatomy.*, vol. 193, no. Pt 1, pp. 131–8, 1998.

[171] WILLIEM, I., HAVENITH, M., SMITS, J., and DAEMEN, M., "Structural alterations in heart valves during left ventricular pressure overload in the rat," *Lab Invest.*, vol. 71, pp. 127–133, 1994.

[172] WILSON, G., COURTMAN, D., KLEMENT, P., LEE, J., and YEGER, H., "Accellular matrix: A biomaterials approach for coronary artery bypass and heart valve replacement," *Annals of Thoracic Surgery*, vol. 60, pp. S353–8, 1995.

[173] WONG, A., POLLARD, T., and HERMAN, I., "Actin filament stress fibers in vascular endothelial cells in vivo.," *Science.*, vol. 219, pp. 867–869, 1983.

[174] YACOUB, M., KILNER, P., BIRKS, E., and MISFELD, M., "The aortic outflow and root: a tale of dynanism and crosstalk," *Annals of Thoracic Surgery*, vol. 68(Suppl), pp. S37–S43, 1999.

[175] YE, Q., ZUND, G., JOCKENHOEVEL, S., SCHOEBERLEIN, A., HOERSTRUP, S., GRUNENFELDER, J., BENEDIKT, P., and TURINA, M., "Scaffold precoating with human autologous extracellular matrix for improved cell attachment in cardiovascular tissue engineering.," *ASAIO J.*, vol. 46, no. 6, pp. 730–3, 2000.

[176] YOGANATHAN, A., LEO, H., TRAVIS, B., and TEOH, S., "Heart valve bioengineering.," *Encyclopedia of Comprehensive Structural Integrity (CSI). Elsevier Science*, pp. 795–796, 2003.

[177] YOUNG, S. and LIN, S., "A possible relation between pressure loading and thickened leaflets of the aortic valve: a model simulation.," *Med Eng Phys.*, vol. 16, no. 6, pp. 465–9, 1994.

[178] ZERVOUDAKI, A., ECONOMOU, E., STEFANADIS, C., PITSAVOS, C., TSIOUFIS, K., AGGELI, C., VASILIADOU, K., TOUTOUZA, M., and TOUTOUZAS, P., "Plasma levels of active extracellular matrix metalloproteinases 2 and 9 in patients with essential hypertension before and after antihypertensive treatment," *J Hum Hypertens*, vol. 17, no. 2, pp. 119–24, 2003.

[179] ZUND, G., YE, Q., HOERSTRUP, S., SCHOEBERLEIN, A., SCHMID, A., GRUNENFELDER, J., VOGT, P., and TURINA, M., "MTT, a rapid and reliable quantitative method to assess the optimal human cell seeding on polymeric meshes.," *Eur J Cardiothorac Surg .*, vol. 15, pp. 519–524, 1999.